NANOFABRICATION OF TWO- AND THREE-DIMENSIONAL STRUCTURES BY MULTIVALENT SUPRAMOLECULAR INTERACTIONS

Nanofabrication of Two- and Three-Dimensional Structures by Multivalent Supramolecular Interactions

Olga Crespo Biel

This research has been financially supported by the Council for Chemical Sciences of the Netherlands Organization for Scientific Research (NWO-CW) in the Young Chemists programme (grant 700.50.522). The research was carried out at the Supramolecular Chemistry and Technology group (SMCT), MESA$^+$ Institute for Nanotechnology, University of Twente.

Publisher: Wöhrmann Print Service, Zutphen, The Netherlands

Cover design by Vincent Steenbrink, Manon Ludden and Olga Crespo.

University of Twente, Enschede, The Netherlands.
ISBN 90-365-2304-4

NANOFABRICATION OF TWO- AND THREE-DIMENSIONAL STRUCTURES BY MULTIVALENT SUPRAMOLECULAR INTERACTIONS

PROEFSCHRIFT

ter verkrijging van
de graad van doctor aan de Universiteit Twente,
op gezag van de rector magnificus,
prof. dr. W.H.M. Zijm,
volgens besluit van het College voor Promoties
in het openbaar te verdedigen
op vrijdag 10 februari 2006 om 13.15 uur

door

Olga Crespo Biel

geboren op 14 februari 1978
te Sabadell, Spanje

Dit proefschrift is goedgekeurd door:

Promotoren:	prof. dr. ir. D. N. Reinhoudt
	prof. dr. ir. J. Huskens
Assistent-promotor:	dr. B. J. Ravoo

The important thing is not to stop questioning

Albert Einstein

A mis padres y Natalia

Contents

Chapter 3

Multivalent Host-Guest Interactions between Cyclodextrin Self-Assembled Monolayers and Poly(isobutene-alt-maleic acid)s Modified with Hydrophobic Guest Molecules

Chapter 4

Multivalent Aggregation of Cyclodextrin Gold Nanoparticles and Adamantyl-terminated Guest Molecules

Chapter 5

Supramolecular Layer-by-Layer Assembly: Alternating Adsorptions of Guest- and Host-Functionalized Molecules and Particles Using Multivalent Supramolecular Interactions

Chapter 6

Patterned, Hybrid, Multilayer 3D Nanostructures Based on Multivalent Supramolecular Interactions

Chapter 7

Surface Enhancement of Supramolecular Complexes at Interfaces by Multivalent, Orthogonal Interaction Motifs

Chapter 1

General Introduction

Nanotechnology is at first sight nothing more than the logical extension of microtechnology,[1] a step further toward miniaturization.[2] Nanotechnology is the manipulation of individual objects with dimensions from 1 to 100 nm. In physics these are considered to be small, in chemistry to be large, while for biologists this is the usual size of individual biomacromolecules. However, nanotechnology has emerged not only to reduce the dimensions of existing microdevices, but also to design new nanostructured materials or new types of architectures with novel properties for use in computation and information storage and transmission.[3] The expectations of what nanotechnology will achieve in the future range from quantum computers, ultrastrong materials, information storage and retrieval, and self-cleaning fabrics to implantable biosensors and drug delivery to individual cells and.[4]

Nanofabrication is the subdiscipline of nanotechnology that deals with the development of general fabrication methodologies for the preparation of nanostructures (in three dimensions) as well as of patterned substrates (in two dimensions), and of assembly methods for the anchoring of the structures to the patterned areas. There are two fundamental ways of fabricating nanostructures: top-down and bottom-up. The top-down techniques are the most widely explored approach to achieve miniaturization of devices, which are usually an extrapolation of existing physical methods, such as lithography and photolithography.[5] Surprisingly, technologies that are familiar to

chemistry such as printing, molding, and embossing, have emerged (in the form of soft lithography) as potential competitors.[6,7]

Self-assembly[8] is the alternative, bottom-up approach. It starts from the smallest building blocks, atoms and molecules, and assembles these into larger and complex structures. This is where the discipline of supramolecular chemistry plays a unique role.[9] Thus, supramolecular chemistry may expect to have a strong impact on materials science by means of the explicit manipulation of the noncovalent forces that hold the constituents together. These interactions and the recognition processes which they govern will allow the design of new materials and the precise control of their structure and composition. Indeed, self-assembly has started to appear as a potential tool for the fabrication of microelectronic[10] and photonic[11] devices since it is an easy and interesting route to assemble components larger than molecules.

An especially powerful and versatile self-assembly pathway exploits multivalency, which offers unique thermodynamic and kinetic properties to supramolecular complexes. Multivalency denotes the use of multiple interactions between two molecules, which results in a stronger binding than the monovalent parent.[12] Supramolecular multivalency will be a key issue in nanofabrication schemes due to its potential use for the assembly of kinetically and thermodynamically stable nanostructures, especially in combination with surfaces.[13] Besides, multivalency could also be employed to construct more sophisticated structures generated by layer-by-layer (LBL) deposition techniques, or for the creation of organized two- (2D) and three-dimensional (3D) structures at surfaces in which multiple interactions are combined.

The research described in this thesis is aimed at the use of multivalent host-guest interactions for the construction of 2D and 3D nanostructures. Self-assembled monolayers (SAMs)[14] on flat surfaces and on nanoparticle surfaces have been employed as a basis for the organization and construction of these functional structures governed by multiple host-guest interactions. More specifically, the host-guest binding motif between β-cyclodextrin (CD) and adamantyl-functionalized guest molecules is at the core of the study. The application of molecules that allow multiple supramolecular interactions provides a tool to tune adsorption and desorption because the thermodynamic and kinetic parameters are related to the number of interactions as well as the strength and the

kinetics of an individual interaction. This paradigm of multivalent supramolecular interactions has been applied to nanofabrication schemes.

Chapter 2 contains a literature overview on 2D and 3D nanostructures on surfaces where assembly takes place through noncovalent interactions. Particular attention is devoted to the positioning of molecules and nanoparticles on surfaces, and to the assembly of those nanoparticles into larger aggregates.

In Chapter 3, the molecular recognition by CD SAMs of poly(isobutene-*alt*-maleic acid)s modified with hydrophobic groups is described. The mechanism of the assembly of such polymers at the surface is investigated as a function of the nature and the number of hydrophobic groups that interact with the CD surface and the intramolecular interactions within the polymer. Furthermore, a quantitative interpretation of the binding events using the effective concentration (C_{eff}) concept is presented.

In Chapter 4, a method to control nanoparticle assembly in solution by multiple supramolecular interactions is described. The assembly of gold nanoparticles bearing surface-immobilized CD hosts is driven by adamantyl-terminated guest molecules, acting as noncovalent molecular linkers between the nanoparticles. The intra- and intermolecular binding as a function of the number of interactions and the geometry of the guest molecules is the focus of this study.

In Chapter 5, the stepwise construction of a novel kind of self-assembled organic/inorganic multilayers based on multivalent supramolecular interactions between guest-functionalized dendrimers and CD-modified gold nanoparticles is described. Layer-LBL assembly is used as a method for the fabrication of such structures. The growth process as well as the resulting multilayer thickness of the assembly is studied.

Chapter 6 introduces the readily accessible soft lithographic techniques microcontact printing (μCP) and nanoimprint lithography (NIL) to create patterns of supramolecular LBL assemblies. Directed LBL assembly on μCP- and NIL-patterned SAMs is performed. Furthermore, a modification of the nanotransfer printing (nTP) approach is employed to transfer complete LBL assemblies, whereas NIL provides topographical masks for LBL assembly. The emphasis of the chapter relies on the interfacial supramolecular specificity and on the layer growth characteristics.

In Chapter 7, a new concept which involves multivalent, heterotropic, orthogonal interactions is described. The multivalent binding of a supramolecular complex at a multivalent host surface involving the orthogonal cyclodextrin host-guest and metal ion-ethylenediamine coordination interaction motifs is studied. The binding of the supramolecular complex with CD is studied in solution and at the surface. A heterotropic multivalency model at interfaces is presented to quantify the species present in solution and at the surface at different pH.

1.1 References

1. General introduction to microfabrication: (a) Menz, W.; Mohr, J.; Paul, O. *Microsystem Technology*, 2nd ed., Wiley-VCH, Weinheim, Germany **2001**. (b) Madou, M. J. *Fundamentals of Microfabrication: The Science of Miniaturization*, 2nd ed., CRC Press, Boca Raton, U.S.A. **2001**.
2. Service, R. F. *Science* **2004**, *304*, 1732-1734.
3. For a general review on nanostructures see: *Chem. Rev.* **2005,** *105*, vol. 4.
4. Whitesides, G. M. *Small* **2005**, *1*, 172-179.
5. Geissler, M.; Xia, Y. N. *Adv. Mater.* **2004**, *16*, 1249-1269.
6. Xia, Y. N.; Whitesides, G. M. *Angew. Chem. Int. Ed.* **1998**, *37*, 551-575.
7. Gates, B. D.; Xu, Q. B.; Love, J. C.; Wolfe, D. B.; Whitesides, G. M. *Annu. Rev. Mater. Res.* **2004**, *34*, 339-372.
8. Whitesides, G. M.; Grzybowski, B. *Science* **2002**, *295*, 2418-2421.
9. Lehn, J. M. S*upramolecular Chemistry: Concepts and Perspectives*, VCH, Weinheim, Germany **1995**.
10. Sirringhaus, H.; Kawase, T.; Friend, R. H.; Shimoda, T.; Inbasekaran, M.; Wu, W.; Woo, E. P. *Science* **2000**, *290*, 2123-2126.
11. Xia, Y. N.; Gates, B.; Yin, Y. D.; Lu, Y. *Adv. Mater.* **2000**, *12*, 693-713.
12. Mammen, M.; Choi, S. K.; Whitesides, G. M. *Angew. Chem. Int. Ed.* **1998**, *37*, 2755-2794.
13. Mulder, A.; Huskens, J.; Reinhoudt, D. N. *Org. Biomol. Chem.* **2004**, *2*, 3409-3424.
14. Ulman, A. *An Introduction to Ultrathin Organic Films: From Langmuir-Blodgett to Self-Assembly*; Academic Press: Boston, U.S.A. **1991**.

Chapter 2

Noncovalent Nanoarchitectures on Surfaces: From 2D to 3D

Nanofabrication requires new methodologies for the assembly of molecular- to micrometer-scale objects onto substrates in predetermined arrangements for the fabrication of two- and three-dimensional nanostructures. The positioning and the organization of such structures into spatially well-defined arrays provides a powerful tool for the creation of materials structured at the molecular level, and to extend the preferred properties of these materials to the macroscopic level. Self-assembly is the pathway that enables the formation of such structures, and the formation of multiple supramolecular interactions provides a tool to control the thermodynamics and kinetics of such assemblies. This chapter is devoted to some representative examples to assemble molecules and nanoparticles in solution and at surfaces based on noncovalent interactions as a potential tool for the construction of two- and three-dimensional systems.

2.1 Introduction

Molecular self-assembly is the spontaneous association of molecules under equilibrium conditions into stable, structurally well-defined aggregates joined by noncovalent interactions. Self-assembly based on selective control of non-covalent interactions provides a powerful tool for the creation of structured systems at a molecular level, and application of this methodology to molecular systems provides a means for extending such structures to macroscopic length scale. Therefore, molecular self-assembly has appeared as a useful tool for the fabrication of materials with characteristic lengthscales of 1-100 nm, thus facilitating the chemical "bottom-up" approach.[1] A single ordered layer of molecules anchored on a surface can be used as a platform because, in principle, its orientation and positioning can be controlled, producing well-defined structural motifs organized over large areas in two dimensions (2D), or volumes in three dimensions (3D). Self-assembled monolayers (SAMs)[2] are ordered molecular assemblies formed by the adsorption of an adsorbate on a solid surface. The order of these SAMs relies on the spontaneous chemisorption at the interface, as the system approaches equilibrium. A considerable number of self-assembling systems have been investigated in the last years, both on flat substrates[3] and nanoparticle surfaces.[4] The versatility and flexibility, both at individual molecular and at materials levels, make SAMs valuable substrates for the investigation of specific interactions at interfaces and platforms for the production of 2D and 3D assemblies.

Multivalent interactions involve the simultaneous binding of multiple ligand sites on one entity to multiple receptor sites on another, and can result in the formation of numerous simultaneous complexes that afford a high functional affinity.[5] The selectivity and the number of interactions involved in the binding of multivalent species makes multivalency useful for creating stable and complex molecular assemblies. Thus, multivalency has started to emerge as a powerful self-assembly tool in supramolecular chemistry and in nanofabrication schemes.[6]

Nanotechnology requires new methodologies for the assembly of molecular- to micrometer-scale objects onto substrates in predetermined arrangements for the fabrication of 3D nanostructures. Such nanostructures will have controllable sizes in all

three directions. However, self-assembly by itself is still unable to produce such devices and the requirement of top-down surface patterning methods, such as soft-lithography, is entailed. The combination of a top-down surface patterning method, to achieve x,y control, with a self-assembly method to shape the z direction will lead to well-defined, high-resolution 3D nanostructures of a large variety of materials.

The first part of this chapter highlights examples of self-assembled systems in which complementary recognition functionalities are arranged in a 2D plane, and demonstrates how these systems can be employed towards the construction of multilayered 3D nanostructures. The second part is devoted to examples of 3D assemblies where the recognition motif is anchored on a nanoparticle surface, and the multivalent binding events result in the controlled aggregation of these nanoparticles.

2.2 2D Nanoarchitectures: Self-Assembly on Surfaces

One of the key challenges in nanofabrication is the positioning of individual units, such as small molecular ligands, larger molecules, proteins and nanoparticles with nanometer precision. Supramolecular interactions, such as those observed in host-guest complexes, are specific and directional, and a wealth of information is usually available on their binding strengths and kinetics. Moreover, the application of molecules that allow the formation of multiple supramolecular interactions provides a tool to tune adsorption and desorption because the thermodynamics and kinetics parameters are related to the number of interactions, and the strength and kinetics of an individual interaction.

This section is devoted to different systems and methodologies that have been used in order to attach molecules and nanoparticles onto surfaces through specific and selective noncovalent interactions. Moreover, some examples of layer-by-layer systems will be described as a potential platform for the construction of three-dimensional (3D) systems.

2.2.1 Self-assembly of molecules on SAMs

There are many examples in literature of molecular recognition of small molecules on SAMs formed from complex synthetic receptors, such as cyclodextrins and calix[n]arene derivatives. These "hosts" contain a molecular cavity for the recognition of "guest" molecules. The challenge has been to understand the role of molecular structure, organization, and interactions in the recognition process and thereby improving selectivity. Therefore, a detailed understanding of molecular recognition of small molecules at interfaces is required.

Calix[n]arene-based adsorbates were shown to give well-packed, ordered monolayers[7,8] capable of interacting with small guests such as tetrachloroethylene and toluene in the vapor phase,[9] and steroids[10] or other neutral molecules[11,12] in aqueous solution. In a recent study, Gupta and co-workers demonstrated that thiolated calix[4]arene molecules assembled on gold surfaces could discriminate between two structural isomers. The authors postulated that the combination of factors such as hydrogen bonding, hydrophobic interactions and steric match permitted such discrimination.[13]

Cyclodextrins (CDs) are a different type of receptor molecules. They contain hydrophobic cavities lined by the glycosidic oxygen bonds, which are responsible for the ability of CDs to include hydrophobic molecules. Such a hydrophobic cavity makes them ideal hosts for molecular recognition in aqueous solution.[14] Several routes for the immobilization of cyclodextrins on surfaces have been developed, mainly on gold[15] and recently on other types of surfaces such as silicon oxide.[16] The most common CD SAMs are prepared from *per*-6-functionalized cyclodextrins, first reported by Kaifer *et al.* in 1995,[17] in which the CD cavities are immobilized upwards with their secondary face towards the solution readily available for complexation of guest molecules. Binding studies at such SAMs have been performed with a variety of small hydrophobic guest molecules. Ferrocene derivatives,[17,18] dopamine,[19] coumarin,[20] azo compounds[21,22] steroids,[23] phenyls,[21,23] adamantyls,[23] bisphenols,[24] and charged guests[25,26] among others, have been studied by means of surface plasmon resonance (SPR) spectroscopy, electrochemical methods, Raman spectroscopy, and single molecule force spectroscopy.

In the last method, the rupture force of an individual host-guest complex is determined by pulling a guest-modified AFM tip off the host SAM.[27] Thus, CDs on surfaces are suitable host molecules showing similar binding properties as in solution. Since CDs are chiral, it is also possible for CDs to recognize the chirality of guest molecules. The group of Kitano *et al.* took advantage of the chiral recognition properties of CDs and investigated the regio- and stereoselective complexation of optically active azo dyes, showing that the enantioselectivity of CD was preserved after immobilization onto a solid surface.[22]

In our group, a wide range of molecules (calix[4]arenes, dendritic wedges and dendrimers) functionalized with multiple adamantyl and ferrocenyl units have been immobilized onto CD SAMs on gold and silicon oxide surfaces.[28-32] Stable positioning and patterning of such molecules was achieved by means of multivalent supramolecular interactions between the hydrophobic moieties at the guest molecules and the CD cavities at the surface. These host surfaces serve as "molecular printboards" for the positioning of guest molecules.[29,31] Besides developing a thermodynamic model for studying the interactions at interfaces,[33] our group has also been able to determine experimentally the number of interactions of these hydrophobically modified molecules towards the CD SAM, enabling the tuning of adsorption and desorption processes at surfaces using the number of interactions.[31,32] Moreover, it has been able to electrochemically induce desorption at CD SAMs by using ferrocene-terminated dendrimers, revealing the possibility to intentionally adsorb and desorb molecules to and from surfaces (Figure 2.1A).[34] Furthermore, molecular patterns of guest-functionalized calix[n]arene molecules, dendritic wedges labeled with fluorescent groups, and dendrimers have been prepared on these molecular printboards by using the readily accessible (soft) lithographic techniques such as microcontact printing (μCP) and dip-pen nanolithography (DPN).[29,30,35]

Myles and co-workers have described the immobilization of barbituric acid derivatives on mixed monolayers of alkanethiols and bis(2,6-diaminopyridine) amide of isophthalic acid-functionalized decanethiol on gold films. The immobilization of the barbiturate derivatives to the receptor-functionalized SAM involved the use of multiple hydrogen bonds to achieve a stable assembly on the surface, showing equal 1:1 stoichiometry in solution and on surfaces.[36] A more complex system, also involving barbituric acid derivatives, was reported by our group where individual synthetic

hydrogen-bonded assemblies were grown on SAMs on gold surfaces.[37] The approach used is based on the spontaneous formation of stable hydrogen-bonded assemblies in apolar solvents between calix[4]arene dimelamines and barbituric/cyanuric acid derivatives, where 9 molecules are held together by 36 hydrogen bonds. The growth of the assemblies at the surface was performed by embedding the thioether-modified calix[4]arene dimelamines into a thiolate SAM. Subsequently, the monolayers containing one of the building blocks were immersed in a solution of the already formed hydrogen-bonded assembly, resulting in stable hydrogen-bonded assemblies at the surface.

Functionalized nanotubes, which can recognize specific complementary molecules, have become increasingly important in the design of nanometer-sized functional materials. The group of Matsui *et al.* functionalized a peptide nanotube, which specifically and selectively binds a well-defined region on a complementary ligand-patterned substrate. They have employed azobenzene[38] and ferrocene[39] groups as a linking unit for the immobilization of nanotubes at CD SAMs on gold surfaces. Hydrogen bonding interactions between the hydroxy azobenzene carboxylic acid and the amide functionalities on the *trans*-form of the azobenzene moieties were employed to assemble the azobenzene-functionalized peptide nanotubes onto α-CD SAMs in an ethanol-water mixture. Upon UV-irradiation the azobenzene moieties switched to the *cis*-form, which has a lower affinity for α-cyclodextrin, and thus resulted in desorption of the nanotubes from the surface (Figure 2.1D).[38] In the case of the ferrocene-functionalized peptide nanotubes, desorption from a β-CD SAM took place by tuning electrochemically the redox states of ferrocene moieties.[39] Only in the latter case, control experiments were performed on α-CD SAMs showing the size specificity of the host-guest recognition of the ferrocene-nanotubes towards the β-CD SAM. In another example, molecular nanotubes formed by the one-dimensional linkages of α-CDs, were immobilized through a monovalent inclusion complex formation with dodecanethiol onto self-assembled monolayers of inclusion complexes between dodecanethiol and β-CD. Surface plasmon resonance (SPR) measurements showed a lower thickness of the molecular tubes after immobilization, which can be related to a partial adsorption or domain formation of the molecular tubes on the dodecanethiol-β-CD SAM.[40]

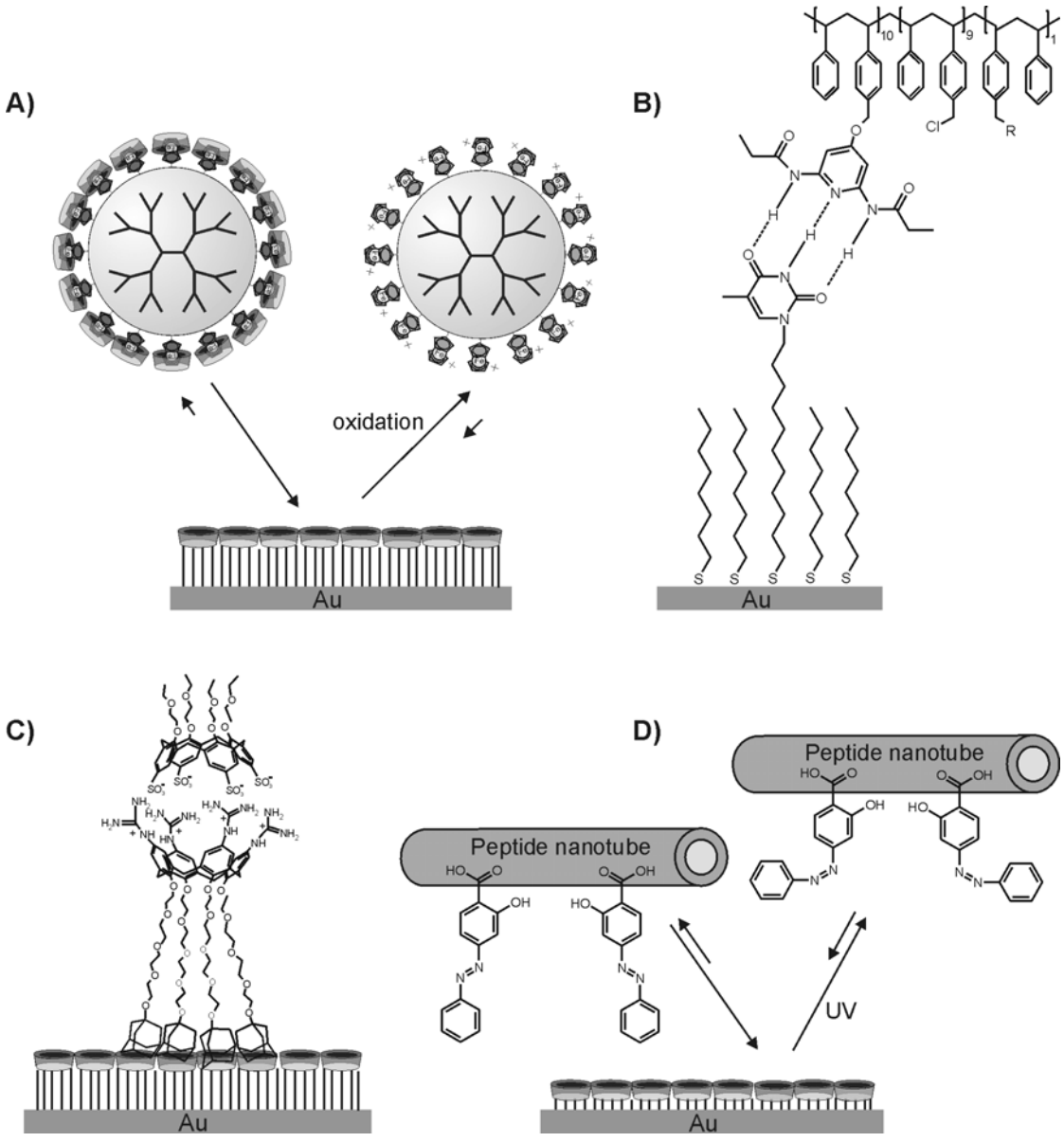

Figure 2.1*: Molecules on SAMs: electrochemically induced desorption at CD SAMs by using ferrocene-terminated dendrimers (A),[34] polymers tethered to surfaces using hydrogen bond interactions (B),[41] positioning of molecular capsules at CD SAMs (C),[42] and attachment of peptide nanotubes on CD SAMs (D).[38]*

Polymers tethered onto surfaces have been subject of attention owing to their potential use in many surface-based devices and technologies such as switchable membranes, sensors, cell growth, and biomimetic materials.[43-46] Some examples of polymers modified with molecular recognition sites assembled onto functionalized SAMs

with complementary sites have been described. A study of particular interest by Whitesides and co-workers employed a bifunctional polymer presenting vancomycin (Van) and fluorescein groups for the detection of anti-fluorescein antibodies to SAMs containing D-alanine-D-alanine (DADA) moieties.[47] These polymers were shown to bind specifically to these SAMs via multiple interactions between DADA and Van groups. SPR was used to study the binding of the polymer to the SAM and, subsequently, the binding of antibodies to the surface comprising the SAM and a film of adsorbed polymer. The SPR sensograms showed the strong adsorption of the bifunctional polymer to the SAM due to the multiple interactions available for binding. Desorption was possible by adding a competitor in solution, while inhibition of binding between the anti-fluorescein antibody and the polymer tethered on the surface was achieved by using a soluble fluorescein derivative. Rotello and co-workers used complementary three-point hydrogen-bonding interactions between modified SAMs and complementary functionalized mono- and di-block copolymers to direct the adsorption process onto surfaces.[41,48,49] The thymine-diamidopyridine (Thy-DAP) hydrogen-bonding motif provided a highly selective adsorption of the DAP-containing mono- and di-block copolymers onto the Thy-decorated gold surface under controlled deposition conditions. In spite of the multiple binding moieties, desorption of the polymer from the surface could be induced by increasing polarity of the solvent and by rinsing the temperature, due to the nature of the hydrogen-bonding interactions, and thus creating renewable surfaces (Figure 2.1B). Using similar hydrogen-bonding interactions, the group of Yoon and co-workers were able to organize microcrystals on glass consisting of thymine and 3-methylthymine modified-zeolite crystals tethered on an adenine-modified glass surface.[50]

An interesting supramolecular assembly on flat surfaces towards the construction of 3D nanostructures is the assembly of supramolecular containers on functionalized SAMs. The group of Shinkai reported the formation and subsequent immobilization of a hexacationic homooxacalix[3]arene-[60]fullerene 2:1 complex on anion-coated SAMs on gold and studied their photelectrochemical response under UV-irradiation.[51] Our group reported the formation of a resorcin[4]arene–based carceplex onto a SAM on gold,[52] and the formation of a molecular cage based on metal-ligand coordination at surfaces, with one of the components directly anchored to a gold surface.[53,54] Furthermore, our group

also reported the stepwise formation of a supramolecular capsule on the surface by using the noncovalent attachment of one component of the molecular capsule onto a β-CD SAM followed by the electrostatic self-assembly of the second component at the interface (Figure 2.1C).[42] The positioning and the stepwise assembly of the molecular capsule on the surface was monitored by SPR, showing a 1:1 complex with an association constant comparable to the complex in solution ($7.5 \pm 1.2 \times 10^5$ M^{-1}). The stable binding of one of the components onto the surface, ensured by multiple host-guest interactions, enabled the reversible capsule formation in two steps: first the disruption of the electrostatic interactions, and in a second step of the host-guest interactions.

2.2.2 Self-assembly of nanoparticles on SAMs

Particles typically ranging in size from 1 nm to several μm play a major role in the development of nanoscience and nanotechnology.[55] Nanoparticles (NPs) are promising candidates for the construction of new nanomaterials. The controlled organization and precise positioning of NPs on 2D surfaces, as well as their hierarchical self-organization, are essential for the development of new functional materials that can be applied in numerous sensing, electronic, optoelectronic, and photoelectronic applications.[56]

A variety of methodologies such as colloidal epitaxy, capillary forces, the application of an external electric field, or covalent attachment have been employed to induce NP self-assembly on surfaces.[57] However, this section will be devoted to an overview of different examples of immobilization of NPs on chemically-modified solid supports, where colloidal self-assembly takes place via specific noncovalent interactions. Some weak interactions to form ordered 2D particle arrays will be discussed followed by the use of biological molecules and their molecular-recognition properties to guide the assembly.

Among the different immobilization approaches, electrostatic self-assembly has been most widely used to direct NP assembly on surfaces. Electrostatic forces, which are mediated by a protective organic layer and by a linker molecule, are strong enough to

ensure a sufficient stability of the assembly, but nevertheless weak enough to allow a reaction of the system to environmental changes, such as ionic strength or pH.[58,59]

An example of electrostatic assembly of NPs on solid supports involves the interaction between positively charged amine groups and negatively charged carboxylate groups. For example, the group of Auer *et al.* studied the formation of gold NP assemblies on planar gold surfaces modified with mercaptohexadecanoic acid using bis-benzamidines as a linker group between two negatively charged gold surfaces.[60] In this three-step process, the different quality and order on the bis-benzamidine linker resulted in variations of the layer thickness and density of the charged NPs. The versatility of the electrostatic assembly has been applied in other systems such as the assembly of silver NPs[61] and gold nanorods.[62] This protocol requires the formation of a SAM on a substrate, followed by immersion of the substrate in a colloidal solution. The first step determines the surface coverage of NPs at the surface.[63] Adsorption of particles by this method results in only monolayer and submonolayer coverages since further adsorption on the surface is prevented by electrostatic repulsion between the charged particles.

The group of Maoz and Sagiv developed a versatile self-assembly approach for the in-situ chemical surface generation of spatially defined nanostructures, based on a non-destructive patterning process that allows the further functionalization on the surface of a highly ordered long-tail organosilane SAM on silicon oxide (Figure 2.2).[64,65] The approach, called “constructive nanolithography”, is based on applying an electrical bias to a conducting AFM tip to induce an electrochemical surface transformation affecting the outer exposed functional groups of a SAM, while preserving the overall monolayer structural integrity. The AFM tip induces oxidation of the surface-exposed vinyl[64] and methyl[65] groups to hydroxyl-containing functionalities, which can participate in further self-assembly and chemical modification. Particularly, this method has been employed to produce organic film patterns (monolayers and thicker layered assemblies) for precise control of the self-assembly pattern of selected inorganic materials such as metals and semiconductors (CdS).[66] This methodology was also applied in different routes for the template-guided assembly of gold NPs.[67,68] Synthesized Au_{55} clusters were successfully organized ex-situ by guided self-assembly on such tip-modified bilayer template patterns, by ligand exchange mechanism of the Au_{55} to the thiolated surface sites.[67] In a different

route negatively charged gold NPs were self-assembled on positively charged bilayer template patterns with top $–NH_2$ functionalities.[68]

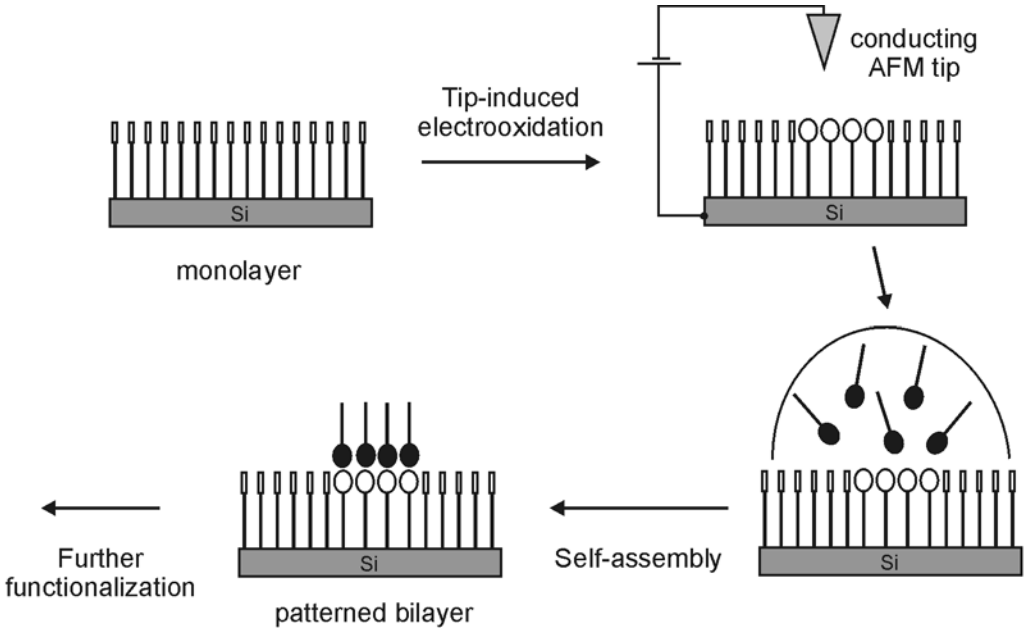

Figure 2.2: *Schematic representation of constructive nanolithography as a generic method for directed surface self-assembly of nanostructures.*[64,65]

The group of Schubert utilized the constructive nanolithography approach for the controlled assembly of differently sized particles to a surface. The tip-modified surface exhibited negatively charged carboxylate groups, that were used as templates for the site-selective binding of cationic gold NPs and amine-terminated CdSe/ZnS core-shell NPs.[69] In this approach the first tip-induced oxidation allowed the first assembly of particles, while the application of a second oxidation in close proximity to the already present NPs, resulted in complex nanostructures decorated with a range of different NPs. The same procedure was applied in the fabrication of nanosized magnetic structures.[70]

Polymers tethered on surfaces have also been used as a template for ordering nanoparticles through multiple electrostatic interactions. Miyashita and co-workers employed polymer nanosheets, which were transferred onto a solid support by the Langmuir-Blodgett method, where negatively charged gold NPs could be adsorbed

effectively onto the positively charged polymer nanosheet containing 4-vinyl-pyridine, yielding an adsorbed gold NP monolayer.[71] In addition, a patterned gold NP monolayer was obtained with photopatterned polymer nanosheets. In another approach using polymers for NP assembly, Bhat *et al.* described the use of surface-bounded polymer brushes to create different density gradients of NPs depending on the polymer chain length (Figure 2.3).[72] Polyelectrolytes have also been used to assemble NPs on surfaces in a multilayer fashion using the well-known layer-by-layer (LBL) technique (Section 2.2.3.2).

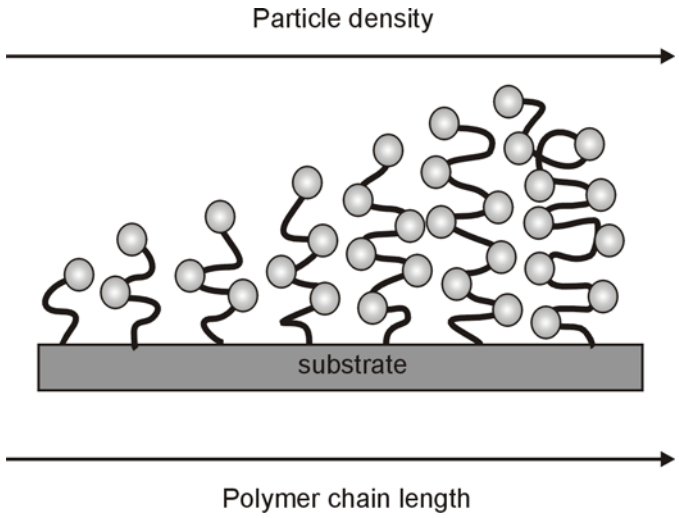

Figure 2.3: *Schematic drawing representing the spatial distribution of dispersed gold NPs adsorbed along a surface-anchored poly(acryl amide) brush with a molecular weight gradient.*[72]

To advance from micro- to nanometer size patterns, our group used nanoimprint lithography (NIL) to create NIL-patterned SAM substrates to electrostatically direct NP adsorption.[73] In this case the endgroup functionality of the NIL-patterned SAM was used to direct the deposition of functionalized particles. NP deposition was achieved on samples where the polymer was still present or on samples where a second SAM was assembled after polymer removal. This second SAM can be used to tune the selectivity for NP adsorption.

Related approaches for the immobilization of NPs using hydrophobic interactions have also been described. A straight forward mechanism was described by Dong and co-

workers where two different kinds of hydrophobic surfaces promoted NP assembly.[74] Hydrophobically-modified NPs were assembled on two different kinds of hydrophobic surfaces, 1-decanethiol (DT) and 2-mercapto-3-*n*-octylthiophene (MOT). The NPs showed a higher affinity for the MOT SAM compared to the DT SAM, which was attributed to an enhanced hydrophobic effect due to a more loosely packed MOT monolayer.

A more sophisticated approach to immobilize NPs on solid supports was developed by Fitzmaurice and co-workers by using a pseudorotaxane formation, between an electron-rich crown ether (dibenzocrown-8) and an electron-poor cation (dibenzyl-ammonium), as the driving force for the assembly.[75] They prepared a silicon wafer modified with the precursor of the dibenzylammonium cation moiety. The cation precursor was converted to the corresponding cation by exposure to blue light. After immersion of the substrate in a solution containing the crown-modified NPs, SEM images showed that these NPs were adsorbed predominantly at the cation-modified regions.

Our group exploited the multiple hydrophobic interactions presented between adamantyl-terminated poly(propyleneimine) (PPI) dendrimers and cyclodextrin-modified silica NPs to create stable and dense monolayers of these particles onto a cyclodextrin surface. Control experiments with glucosamine-functionalized silica particles resulted in a very low coverage, thus confirming the supramolecular specificity needed for efficient adsorption.[76]

Recently, Binder and co-workers developed a new methodology for NP immobilization on flat surfaces through specific hydrogen bond interactions.[77] They based their approach on the multiple hydrogen bond interactions of the “Hamilton-type” receptor (Figure 2.4). Two gold NP sizes were used in the study, 5 and 20 nm respectively. It was found that the surface coverage of NPs could be adjusted by the receptor in the mixed SAM. Additionally, the authors estimated the number of receptor molecules that could participate in the NP binding to 45 for the 20 nm NPs and 3-4 for the 5 nm NPs. The stability of the NP assembly was proven by repetitive imaging of the same area, whereas the specificity of the assembly was established by the absence of binding of octadecyl-modified gold NPs to the receptor-modified surface.

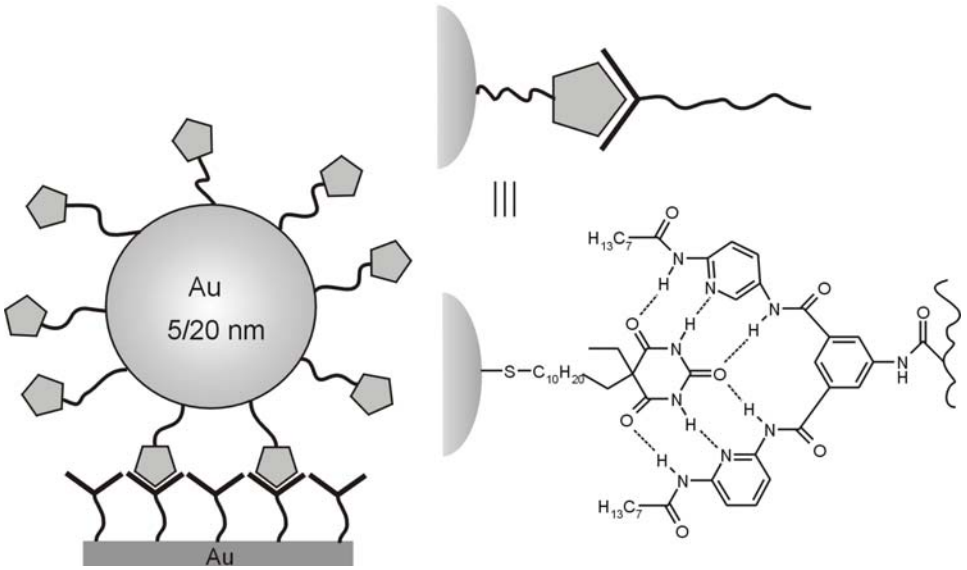

Figure 2.4: *Concept of NP binding mediated by the "Hamilton-type" receptor.*[77]

The immobilization of biomolecule-nanoparticle hybrid systems on surfaces provides unique features for the generation of ordered NPs arrays. Biomaterials, such as nucleic acids, streptavidin-biotin, or antigen-antibody complexes provide interesting templates for the immobilization of NPs. Additionally, hybrid biomolecule-NP composites on surfaces provide functional interfaces that can be employed for sensor, photoelectrochemical, and electronic circuitry applications.[78] However, these subjects will not be discussed in this section because they have been reviewed by others.[78,79]

Nucleic acids can serve as templates to bind DNA-functionalized nanoparticles at complementary segments. When DNA templates are fixed at a surface of a solid support, the resulting assemblies of NPs can yield a pattern that is dependent on either the shape produced by the DNA template itself or on the pattern produced upon its immobilization.

Niemeyer and co-workers prepared oligofunctionalized gold NPs containing different DNA sequences and varying the number of DNA sequences attached to the NPs, ranging from one up to seven.[80] Biotinylated oligomers were immobilized on streptavidin-coated microplates, and saturated with complementary linker oligonucleotides providing the specific sequence complementary to the gold particle-bound oligonucleotides (Figure 2.5). Hybridization of the complementary oligonucleotide sequences, resulted in the immobilization of DNA-gold NPs, and furthermore led to the

formation of a silver precipitate that was quantified by absorbance measurements. In a following study, gold NPs functionalized with two different oligonucleotides were used as building blocks that contained two independently addressable DNA sequences: one of the sequences was utilized for attaching the gold NPs at the solid support, while the other sequence was used to establish lateral cross-links between the adjacently immobilized NPs.[81] A similar approach was applied by Mirkin *et al.* to construct mono- and multilayered DNA-gold NP structures on a glass support.[82] In a another study, Niemeyer and co-workers used the linkage of an antibody/antigen complex to create NP assemblies.[83]

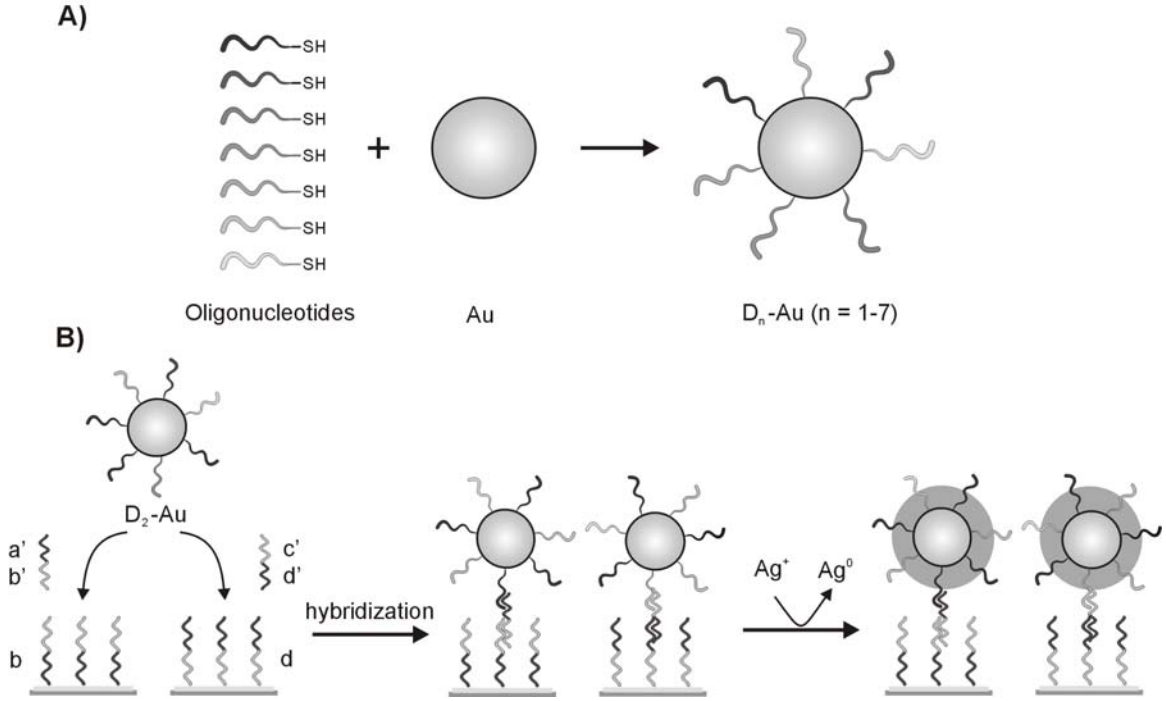

Figure 2.5: *A) Schematic drawing of the preparation of the oligofunctionalized DNA-gold NPs (D_n-Au) containing different DNA sequences. B) DNA-directed immobilization of D_2-Au and subsequent silver enhancement step.*[80]

Self-assembly of metallic NPs into high density 2D arrays has been obtained by a process in which DNA-gold NPs were hybridized to a pre-assembled 2D DNA scaffold deposited onto a mica surface.[84] The latter was designed to form rows of hybridization

sites with a 4 nm spacing between sites and a 64 nm separation between rows. The DNA-gold NPs functionalized with multiple complementary DNA strands were hybridized to the pre-assembled 2D DNA scaffold. AFM images of samples taken after the NP hybridization step revealed an assembly of closely-packed particles along the lines on the scaffold. This methodology could be interesting for the assembly of 2D nanoelectronic components arrays and their further application in nanodevices and circuits. Similar approaches based on DNA-hybridization driven self-assembly have been used for the immobilization of nanowires.[85]

Another approach to the directed placement of NPs on solid supports by means of DNA hybridization is based on the micro- and nanopatterning of a surface with DNA molecules followed by hybridization with complementary-DNA functionalized NPs. This approach provides the specific immobilization of NPs at target domains of the pattern. Micropatterns of DNA-functionalized NPs were obtained by depositing an amine derivative of an oligonucleotide in a pattern onto a chemically modified glass surface using a nanoliter dispensing device. Gold NP patterns were formed by hybridization of the patterned DNA regions with the complementary DNA-modified NPs.[86] A more direct and precise placement of gold NPs was demonstrated by dip-pen nanolithography (DPN), which was applied to the patterning of the primary DNA on the surface followed by hybridization with complementary DNA-functionalized NPs.[87,88] A similar approach was used to pattern surfaces with functionalized gold NPs by DPN based on antigen-antibody interactions.[89]

2.2.3 Multilayer thin films

2.2.3.1 General aspects of layer-by-layer assembly

In the previous sections we have discussed several methodologies to assemble monomolecular films ranging from small to larger molecules such as polymers and nanoparticles. These approaches can be extended to multilayer films that can enhance the properties of monomolecular films and at the same time create a new class of materials possessing functional groups at controlled sites in three-dimensional arrangements. Such structures require control of molecular orientation and organization at the nanometer

scale, and therefore it is essential to study and develop methods for the controlled assembly of multicomponent nanostructures.

Layer-by-layer (LBL) assembly[90] has emerged as a promising method for fabricating structured and functional thin films on solid supports. LBL assembly is an approach based on the alternate adsorption of materials containing complementary charged or functional groups to form multicomponent ultrathin films as illustrated schematically in Figure 2.6. LBL assembly has been defined as a versatile, universal and simple method for constructing building blocks of different compositions into ultrathin multilayer films with controlled thickness and molecular structure on arbitrary solid substrates. Some interesting properties and possible applications of LBL films will be discussed in this section. The references hereby described are intended only to give some introductory information about selected recent developments of LBL assembly, which has been well covered by recent books and reviews.[91,92]

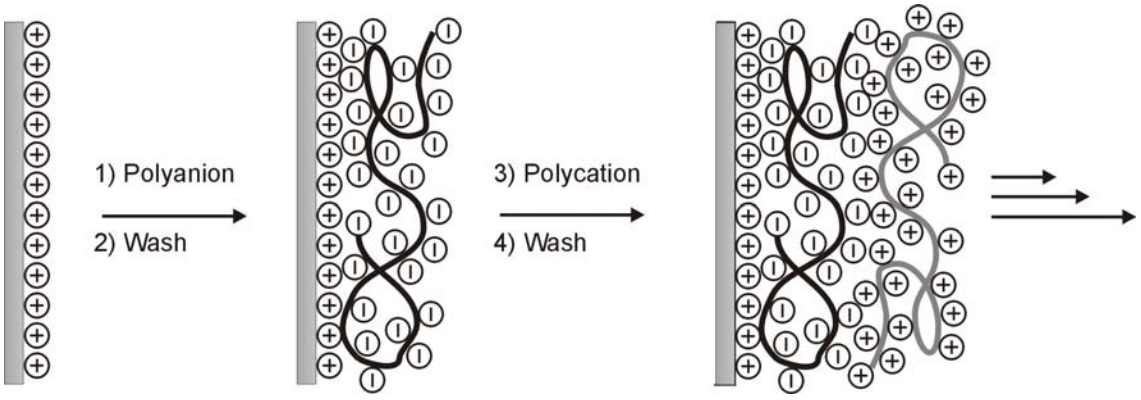

Figure 2.6: *Concept of layer-by-layer assembly, depicting film deposition of two complementary polyelectrolyte species.*

The LBL method has been most often manifested in the alternation of oppositely charged species.[92] However, it has been successfully extended to various other driving forces such as hydrogen-bonding,[93] charge transfer,[94] acid base pairs,[95] metal-ion coordination,[96] inter- or intramolecular interactions in the dried state,[97] covalent bonds,[98] biospecific interactions (e.g.; sugar-lectin interactions),[99] and host-guest interactions between cyclodextrin dimers and ferrocene-appended poly(allylamine) polymers[100] (more

examples can be found in Chapter 5). In general, one can use any interaction (this may be one or several different interactions) between two species in order to incorporate them into a multilayer film. For example, Rubner and co-workers introduced for the first time hydrogen-bonding interactions between two conjugated polymers as a driving force for LBL assembly.[93] The LBL assembly was demonstrated with polyaniline, which can form strong hydrogen bonds at both the amine and imine sites along its polymer backbone, and a variety of different nonionic water-soluble polymers. Rubinstein and co-workers described the use of coordination chemistry in the multilayer assembly on gold surfaces.[96] In this approach a bifunctional ligand was used as the base layer, bearing a cyclic disulfide group for attachment to the gold surface and a bishydroxamate group capable of ion binding (Zr^{4+} or Ce^{4+}). The chelated metal ion was then used for coordination of a second ligand possessing four hydroxamate groups. Successive addition of metal ions and tetrahydroxamate led to the formation of a well-defined multilayer. The biospecific interactions between the lectin protein Concanavalin A (Con A) and a mannose-labeled enzyme were exploited also in LBL assembly, and it showed that the Con A-sugar complexation was a useful tool for constructing multilayer thin films of proteins.[99]

What is unique for LBL assembly in comparison with other film deposition techniques is the broad range of materials that is available for incorporation in a multilayer thin film, and the versatility of the number of interactions available for such assemblies. Some of these materials include polymers,[92] inorganic nanoparticles (Section 2.2.3.2), clay,[101] organic components,[102] carbon nanotubes,[103] dendrimers,[104] and biological macromolecules such as proteins[105] and DNA.[106] LBL assembly is therefore emerging as an inexpensive and versatile technique to create electro-optical, conducting sensors and perm-selective, luminescent films.[92]

In general, multilayer films show a linear growth of mass and thickness, although a second class of films have been reported in which mass and thickness grow exponentially with the number of deposition steps.[107]

2.2.3.2 Nanoparticle multilayer films

Of special interest is the multilayer assembly of inorganic NPs. The incorporation of inorganic NPs or their precursors through direct adsorption into the multilayer thin films has been demonstrated to yield closely packed layers of NPs homogeneously distributed throughout the multilayer film[91,92]. NP multilayer films are of great importance for sensing and electronic applications.

One of the most simple and versatile methods for the construction of ultrathin organized NP multilayers is the electrostatic LBL assembly of NPs and polyelectrolytes.[56] The driving force for the assembly are the electrostatic interactions between the charged groups in the outer layer of the film and the charged groups at the particle surface, enabling the creation of 2D structures in a stepwise fashion. One of the advantages of using polymers for NP assembly is the possibility of fabricating hybrid materials that incorporate not only metal and semiconductor NPs, but also different polymers with different properties, such as conducting [108,109] or redox active polymers.[110] Moreover, electrostatic NP arrays can be constructed from any charged NP and any oppositely charged crosslinker with the same protocol as in the polymer-colloid multilayers. The crosslinker can be any type of molecule, the only requisite is the presence of multiple charges, so that it can simultaneously interact with several colloidal layers. For example, thin films of silver NPs were incorporated into generation 1 and 5 PPI dendrimers, giving different optical properties depending on the generation and concentration of dendrimer used.[111] Moreover, dendrimers with higher generations can also be used to encapsulate NPs, therefore metal-dendrimer nanocomposites can be prepared using dendrimers with various terminal groups able to interact with each other. Esumi and co-workers studied the LBL formation using a positively charged gold-dendrimer nanocomposite and a negatively charged silver-dendrimer nanocomposite. The dendrimer carrier used for the assembly was a generation 5 polyamidoamine (PAMAM) dendrimer (Figure 2.7).[112]

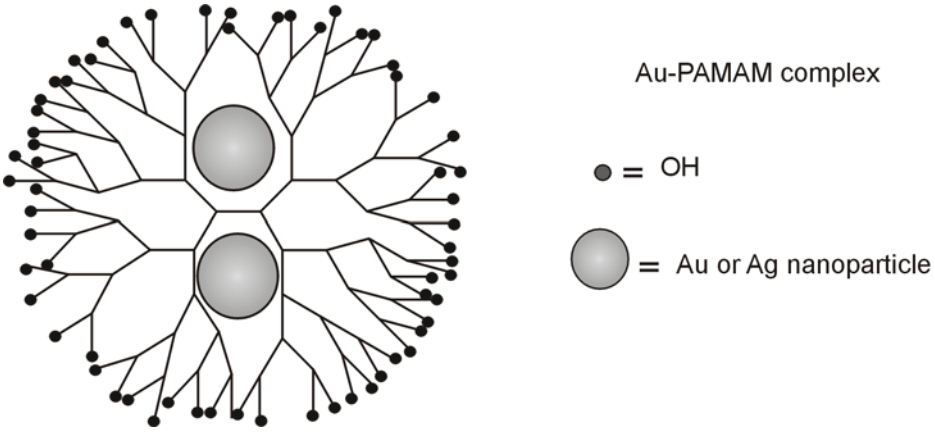

Figure 2.7: *Schematic picture of a PAMAM dendrimer encapsulating NPs.*[112]

Multilayers of particles can be also produced by alternate immersion into a functional crosslinker and a NP solutions, which produce random arrays of NPs of controllable thickness. For example, this has been accomplished by the use of bisthiol crosslinkers for gold.[113] If the gold NP monolayer is exposed to a solution of a bisthiol, then the crosslinker assembles on the gold surface, which leaves thiol moieties at the nanostructure-solution interface. The assembly of a second colloidal layer is thereby possible and the construction can continue in the same way. The versatility of the method, depending on the type of functional groups used as crosslinker, allowed the construction of multilayers of different nanoparticle composition.[114]

Coordination chemistry offers stable bonding and metal-ligand specificity, so that ligand-bearing NPs can be assembled at surfaces using the appropriate metals ions. This approach is particularly compatible with different molecule construction systems since binding of the metal ions activates the surface toward NP-ligand binding, and vice versa. The use of different building blocks containing similar ligand functionalities provides a general method to assemble NP arrays and NP multilayer films on surfaces. The first example of coordinated NP films was described by Murray and co-workers. The procedure consists of the repetitive adsorption of carboxylate-modified gold NPs and divalent metal ions (Cu^{2+}, Zn^{2+}, Pb^{2+}) on two different types of anchoring surfaces, gold and silicon oxide with carboxylate-terminated SAMs.[115-117] Repeated dipping cycles resulted in the formation of network NP films. This NP network exhibited electrical

conductivities that could be varied by both the number of methylene segments in the ligands and the medium.[118] However, in this type of coordination-based NP networks, the interparticle distance was shown to be lower than expected for a coordinative carboxylate-metal ion binding (and also the absorbance changes were much larger that those expected for a LBL film growth). Chen and co-workers obtained similar results with pyridine-functionalized gold NPs and Cu^{2+} ions, studied by quartz crystal microbalance (QCM) measurements.[119] These observations suggested that the excess surface-coordinated Cu^{2+} could migrate out toward the NP solution resulting in a poorly controlled NP network growth. In an attempt to achieve controlled growth of NP films, Rubinstein and co-workers reported the construction of monolayer and multilayer NP architectures on surfaces by coordination chemistry with Zr^{4+} ions (Figure 2.8).[120]

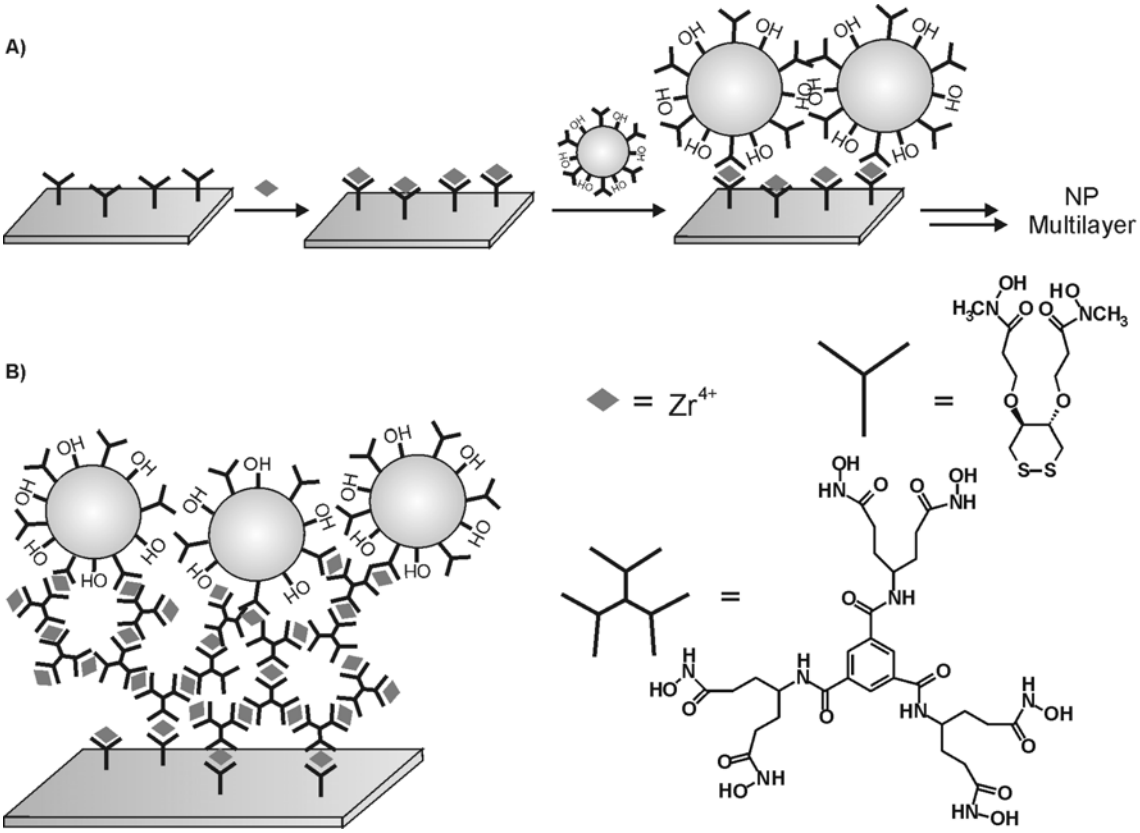

Figure 2.8: *Schematic representation of: (A) Stepwise assembly of bishydroxamate gold NPs onto a bishydroxamate disulfide SAM on a gold surface through the coordination of Zr^{4+} ions. (B) Spacing of a NP monolayer from the gold surface using a similar metal-coordination approach.*

In this study hydroxyl-functionalized gold NPs were prepared and derivatized with a disulfide bishydroxamate ligand by partial displacement of the hydroxyl groups. A monolayer of the ligand-modified gold NPs was assembled via coordination of the Zr^{4+} ions onto a bishydroxamate disulfide SAM on a gold surface. Controlled spacing of NP layers from the surface was achieved by binding the gold NPs onto a thick organic multilayer, where the NPs and spacer layer were assembled using the same coordination chemistry. Furthermore, using the same binding approach, construction of NPs nanostructures was attained showing a similar NP density in successive layers and a gradual roughness increase.

The incorporation of semiconductor quantum dots (QDs) into the multilayer thin films has been of interest for the use in fluorescence and luminescent detections methods. For example Kotov and co-workers demonstrated that LBL methods can be used to build graded semiconductor composite films of highly luminescent CdTe.[121] Four different CdTe NPs were used; these particles displayed green, yellow, orange, and red luminescence spectra due to their differences in particle size and were alternately dispersed with a strong polycation and deposited on glass and plastic supports. After adsorption of 10 layers, the resulting film exhibited a clear gradient in nanoparticle size and therefore density across the thickness of the film, thus, yielding a “rainbow” of colors resulting from each of the individual particles. The purpose of the study relied on the construction of multilayer nanoparticle films to exhibit energy transfer effects across the gradient films, which could be useful for photovoltaic applications.

2.2.3.3 Multilayer templating on particle surfaces

Most of the approaches discussed in the previous sections address the formation of structures build up from 2D surfaces. However, uniform multilayers can also be formed on a number of 3D objects. The most common system type of LBL assembly on colloidal particles is the electrostatic deposition of polyelectrolytes (Figure 2.9). This capability was first demonstrated by Donath, Caruso, Möhwald and co-workers.[122,123] The approach is based on the consecutive adsorption of polyelectrolytes on the surface of negatively charged polystyrene and melamine formaldehyde latex particles. Although it seems an easy procedure some requirements have to be met to avoid flocculation induced

by the added polyelectrolytes. It was found that by properly adjusting polyelectrolyte and colloid concentration and by providing sufficient charges on the polylectrolyte in order to avoid partial removal upon adsorption of the next polyelectrolyte layer, continuous layer growth could be obtained avoiding colloidal aggregation. Besides the use of different polyelectrolytes, a number of other synthetic components ranging from inorganic nanoparticles,[124-128] DNA,[106] lipid bilayers,[129] and proteins[130] have been used to fabricate new LBL colloidal type nanostructures with controllable thickness and composition at the interfacial region. Thus, this methodology permits remarkable control over the coating uniformity and thickness, and the high level of flexibility allows the design, structure and properties of the resulting particles to be varied tremendously. This area of the field has been expanding rapidly and it has been well covered by several reviews.[124,131] Nevertheless, some examples as well as some interesting applications will be discussed here.

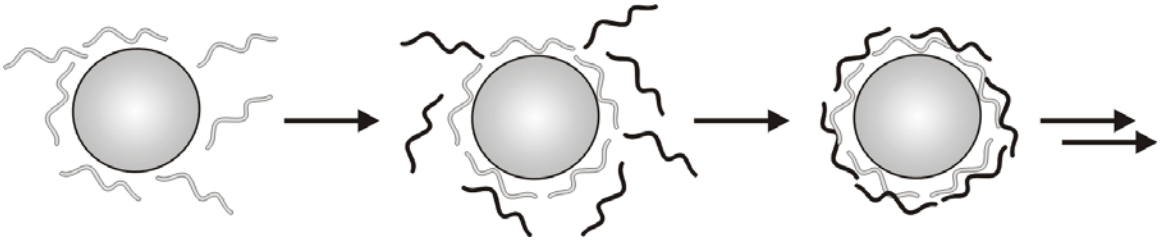

Figure 2.9: *Schematic illustration of the polyelectrolyte deposition process in colloid-templated electrostatic layer-by-layer assembly.*

Individual layers of inorganic nanoparticles can be incorporated into the multilayers, including silica, gold, silver, and iron oxide.[124-128] The assembly of a dense layer of nanoparticles on colloidal particles includes the use of electrolyte or other synthetic material shielding, to prevent repulsive interactions and to enable the dense packing of nanoparticles enabling the formation of shells on the colloid surface. Depending on the nature of the nanoparticle, the LBL colloidal nanocomposite can lead to materials with magnetic properties,[128] or different optical response depending on the morphology of the building blocks;[126] besides they can also be used as sites for further electroless deposition.[125]

Additionally, it was found that decomposition or dissolution of the templating core could yield hollow microcapsule shells consisting of the free LBL assembled films in the form of the original NP shape.[122,124] This process required the dissolution in organic solvents or calcination of the polystyrene particles or the dissolution of melamine formaldehyde particles in acidic solution. The two different processes can lead to different morphologies of hollow spheres (Figure 2.10).[124] The nanoscale morphology was reported by Decher *et al.* who used gold NPs to create hollow nanospheres. Dissolution of the gold core was achieved under vigorous stirring of the particle suspension in a solution containing an excess of KCN.[132] The tickness of the hollow sphere walls can be controlled with the number of layers deposited, size, shape and composition of the spheres, which can be easily determined by the templating colloid employed and the incorporation of different materials. Because of the versatility of the system and the generally flexible membrane, these hollow structures have interesting potential applications as micro- and nanocarriers for molecules and nanoparticles, as well as biological species for the controlled release and targeting of drugs, catalytic nanoreactors, and photonic materials.[131,133,134]

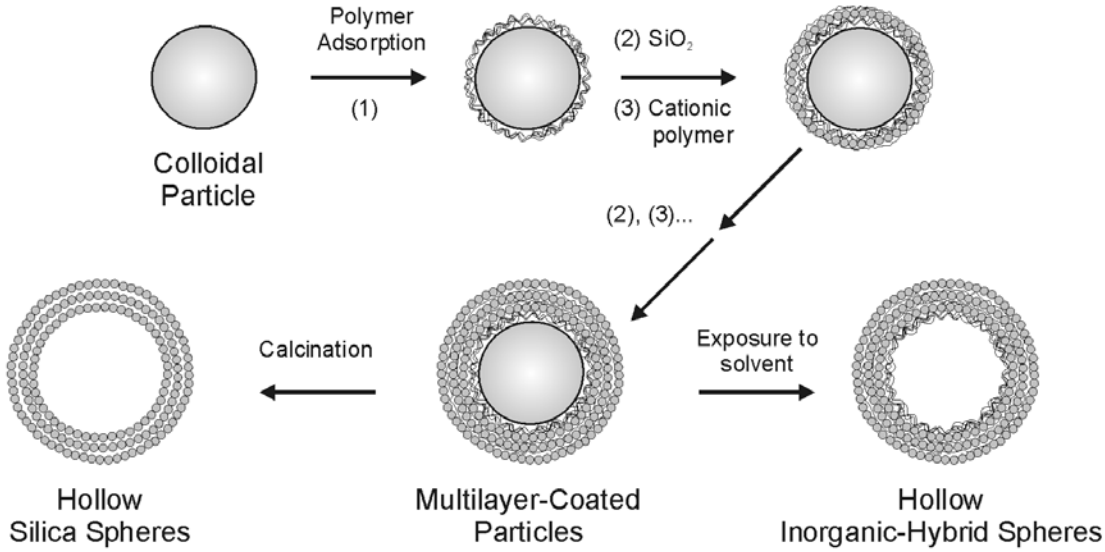

Figure 2.10: *Illustration of procedures for preparing hollow inorganic silica and inorganic-hybrid spheres through the colloid-templated electrostatic LBL assembly of silica NP polymer multilayers, followed by the removal of the templating core and, optionally, the polymer.*[124]

Similarly to the LBL assemblies on flat surfaces, the incorporation of quantum dots (QDs) in the interior of these templated colloids has also been attained. Li and co-workers described an example in which magnetic luminescent nanocomposites composed of Fe_3O_4 and CdTe were prepared. Fe_3O_4 nanoparticles were used as a template for the deposition of three polyelectrolyte/CdTe QD multilayers. It was found that the photoluminescence properties of the magnetic luminescent nanocomposites could be tuned by controlling the distance of the polyelectrolyte interlayer between the magnetic nanoparticles and QDs and the CdTe QD loading of the nanocomposites.[135] Additionally, the authors used magnetic fields for the separation and redispersion process of the nanocomposites.

Spherical particles are not the only ones which can act as templates. Multilayers on coated cells have been prepared, on which a perfect, ultrathin membrane was formed around an individual cell.[136] Other geometries such as nanotubes from human serum albumin (HSA) were prepared by the alternate adsorption of the respective positively and negatively charged species on the inner walls of an alumina template membrane. After subsequent removal of the template, free-standing HSA nanotubes were obtained.[137] Highly porous materials such as porous calcium carbonate particles can be used as template materials as well. The use of these types of templates results in the formation of thin films on the exterior surfaces as well as on the interior pores of these particles.[138]

2.2.3.4 Methods to pattern multilayer thin films

LBL allows the tuning of the thin films composition at the nanometer scale and, when combined with inexpensive patterning routes, provides a powerful tool for patterning nanometer- to micrometer-scale assemblies.[92]

The first micropatterning approach was reported by Hammond and co-workers in which they utilized the concept of selective deposition on chemically patterned surfaces.[139-142] The driving force of the approach is the use of secondary or nonspecific interactions, in combination with steric repulsion and electrostatic interactions, to chemically direct the deposition of polyelectrolytes on chemically patterned substrates. Thus, one surface region supports the build-up of the LBL assembly, whereas the alternate region acts as a resist to deposition. The approach described by Hammond's

group employed microcontact printing techniques to create SAMs of micrometer-scale features on surfaces of the desired functional groups. Carboxylic acid-functionalized SAMs, alternating with an oligo(ethylene glycol) (EG) SAMs were immersed in solutions of the respective polyelectrolytes to build up patterned multilayer films. Oligomers of EG are known to act as hydrated brushes in aqueous solution, thus preventing the adsorption of polyions due to repulsive forces and enthalpic penalties for disruption of the hydrogen bonds EG forms with water. However, the region of preferred deposition on chemically patterned surface can be influenced by hydrogen-bonding and hydrophobic interactions, as well as electrostatic interactions, between the charged polymer and the surface. For example, certain polyamines consistently adsorbed to the EG region of the surface due to non-electrostatic interactions, resulting in some cases in preferential build-up of multilayer films on the EG region. This behavior was observed in the adsorption of weak polyelectrolytes for which the degree of ionization is dependent on pH, and secondary interactions may prevail over given pH range.[141] Similar studies by the same group showed that at very high salt concentrations, polyelectrolyte deposition can be reversed creating a negative of the original positive structure.[140] So far, this method has only been applied to micrometer features, but the ability of this methodology to gain smaller feature sizes at a nanometer lengthscale was recently demonstrated by Jonas an co-workers.[143] Electron beam lithography followed by gas-phase silanation was utilized to create chemical patterns to direct LBL assembly with features down to 150 nm dots. The selective deposition is easily achieved when systems of different compositions are being assembled on a surface. However, when thin film compositions are similar in nature, it is challenging to create patterned surfaces onto which such systems will adsorb selectively.

The selective deposition described above provides the advantage of soft-lithographic methods; however, multilayer thin films can also be patterned using photopatterning techniques. The most common approach uses a photo-crosslinkable polyion in the multilayer thin film. This was demonstrated through the use of diazoresins to create multilayers in which photocrosslinking stabilizes specific regions of the film.[144-148] After the LBL assembly, the substrate is exposed to UV irradiation through a photomask, causing crosslinking in the polyelectrolyte regions exposed to UV light. The films were then exposed to a surfactant solution containing sodium dodecyl sulfate,

which caused the dissolution of the unexposed film areas. Despite the variety of the procedure, it requires the introduction of a photo-crosslinkable monomer into the LBL assembly (Figure 2.11).

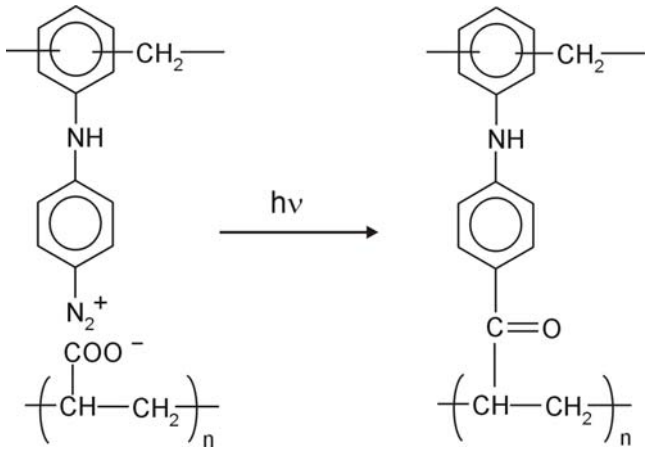

Figure 2.11: *Schematic representation of the reaction between diazo-resins and poly(acrylic acid) in a multilayer assembly upon UV irradiation.*

A different technique was introduced by Lvov and co-workers, who used a metal mask in combination with a lift-off approach to pattern LBL assemblies of more than one type of NPs.[149,150] A silicon substrate was coated with a multilayer film of polystyrene particles on top of which aluminum and photoresist layers were deposited subsequently. After UV irradiation through a photomask and exposure to an aluminum etchant, a layer of different silica particles was deposited on top. After lift-off of the photoresist and aluminum, a pattern with two types of particles was obtained (Figure 2.12).

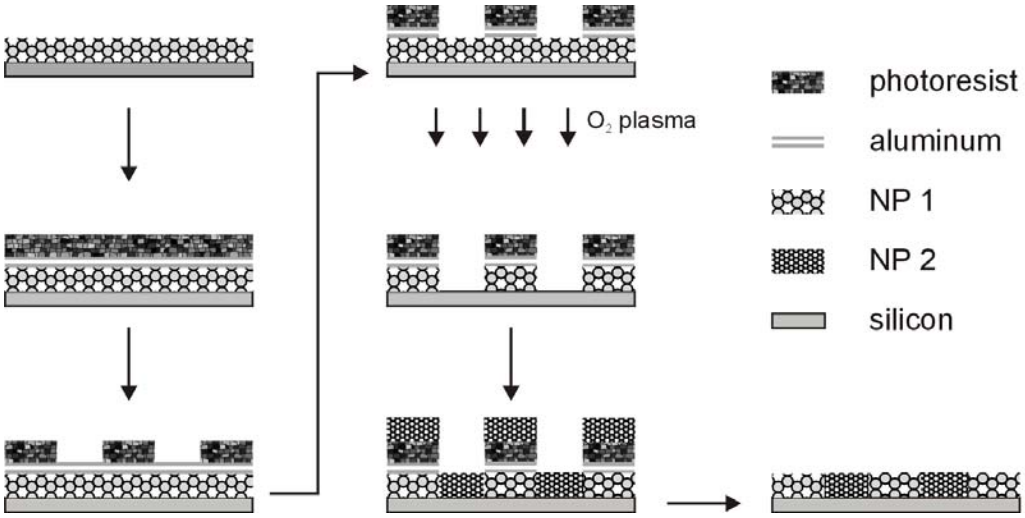

Figure 2.12: *Schematic representation of the combination of a metal mask with a lift-off approach to pattern multilayers of two types of NPs.*[150]

Moving towards the construction of more complex, 3D structures, Hammond's group developed a technique consisting of LBL assembly on a PDMS relief stamp which allowed subsequent transfer of the LBL structures onto a substrate in the contact areas.[151] This approach resembles nanotransfer printing (nTP) developed by Rogers *et al.*[152] This technique will be described in detail in Chapter 6.

So far, the above methodologies described the patterning of multilayers onto substrates. However, it would be desirable to pattern a single layer of a chemical functionality on top of an existing layer. Therefore, Hammond and co-workers developed the so-called polymer-on-polymer stamping (POPS) technique (Figure 2.13).[153] In this approach chemical patterns were obtained by the direct stamping of functional polymers onto a surface containing complementary functional groups. The resulting pattern was then used as a template for the deposition of materials on the surface. The versatility of this method allows the functionalization of surfaces with a number of different functional groups. POPS has been used as a template for the attachment of inorganic NPs,[59,154-156] cells,[157,158] microcapsules,[159] and to generate electroless plated metal patterns.[160]

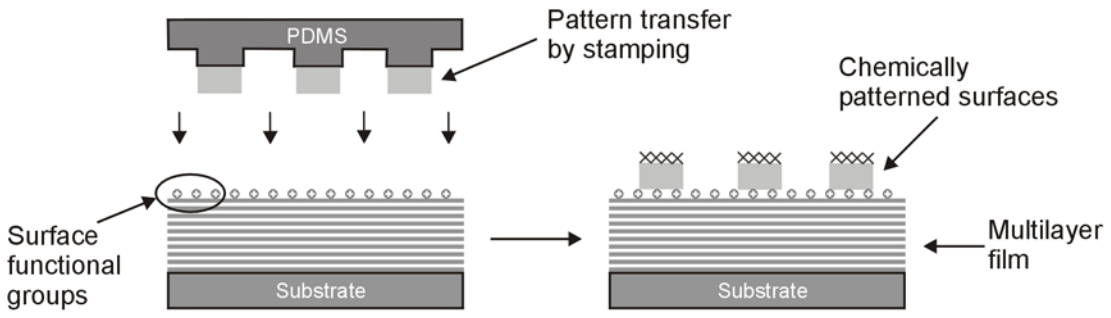

Figure 2.13: *Schematic illustration of the transfer of a functional polymer to a surface with complementary functionality using polymer-on-polymer stamping (POPS).*[153]

2.3 3D Nanoarchitectures: Templated Nanoparticle Assembly

During the last decade substantial research has been focused on metal (Au, Ag, Pt, Cu) and semiconductor (PbS, Ag_2S, CdS, CdSe, TiO_2) NPs, partially as a consequence of the development of methods to control particle size and also to stabilize the particles in solution.[4,161] One possible approach is to passivate the surface of the NPs with an organic monolayer that protects them from aggregation and provides functional and specific chemical properties.[162,163] The versatility of physical and chemical properties of metal and semiconductor NPs makes them promising as miniature devices, with potential applications ranging from optoelectronics[164] and sensing[56] to catalysis[165] and biology.[78,166] They also provide building blocks for more complex systems. Organization of functional NPs into spatially well-defined arrays provides a powerful tool for the creation of materials structured at the nanometer level, and to extend the prefered properties of these materials to the macroscopic level.

This section is focused on the different methodologies to create and control NP assembly into well-defined nanoarchitectures based on non-covalent interactions. One-dimensional (1D) assemblies are described in other reviews.[167] First, NP assembly that is based on supramolecular recognition and the different non-covalent interactions that have been used for NP assembly will be described. In the last section NP assemblies induced

by specific biological interactions will described, highlighting some representative examples found in literature.

2.3.1 Nanoparticle assembly by molecular recognition

The controlled assembly of NPs in solution based on noncovalent bonding is a general strategy that leads to organized NP materials. Various approaches have been reported using hydrogen-bonding, host-guest, metal coordination, electrostatic, charge-transfer, and π-π interactions. This section is dedicated to recent examples of the use of these interactions to assemble NPs into well-ordered 3D nanostructures.

2.3.1.1 Hydrogen-bonding-directed nanoparticle assembly

Molecular recognition through multiple hydrogen-bonding interactions has been widely used to create complex 3D structures in solution. The use of multiple hydrogen-bonding interactions allows assembly at near-equilibrium conditions, which facilitates control over the thermodynamic parameters of the assembly.

Fitzmaurice and co-workers have described an example of a three-point hydrogen-bonding interaction for NP assembly. In this approach, gold NPs were prepared by a chemisorbed mixture of dodecanethiol and a uracil receptor. Addition of a molecule incorporating a diaminopyridine substrate resulted in the formation of a 1:1 complex associated by a triple array of complementary hydrogen bonds.[168]

Rotello and co-workers have developed a polymer-mediated “bricks and mortar” strategy for NP assembly. They have utilized a polymer scaffold and NPs that are functionalized with complementary recognition units[169] and have reported their use for different applications such as chemical sensing and catalysis.[170] Diaminotriazine-thymine three-point hydrogen-bonding interactions were employed to obtain complementarity between thymine-functionalized gold NPs (Thy-Au) and diaminotrazine-functionalized polystyrene (poly-Triaz).[171] Addition of poly-Triaz to a concentrated solution of Thy-Au in nonpolar solvents resulted in the formation of spherical aggregates (Figure 2.14). In contrast, no precipitation was observed when the control MeThy-Au NPs were used, demonstrating the role of specific three-point hydrogen bonding for the formation of

poly-Triaz/Thy-Au aggregates. The temperature at which the assembly process was performed had a tremendous effect on the diameter and the morphology of these aggregates. At room temperature TEM images showed the formation of large spherical clusters comprising 3000-7000 individual gold NPs. Performing the assembly at –20 °C yielded to 5-10 times larger clusters.[169]

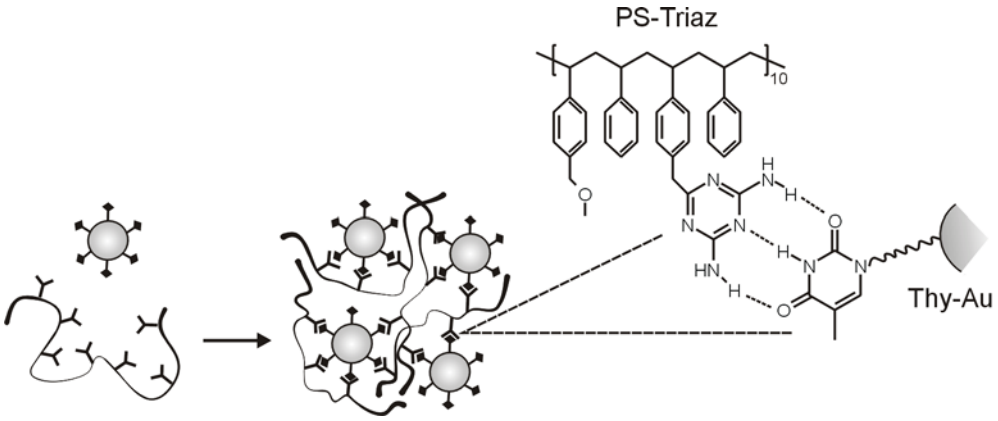

Figure 2.14: *NP-polymer assembly through a three-point hydrogen bonding between thymine-functionalized gold NPs and triazine functionalities attached to a polystyrene backbone.*[169]

In an effort to provide a component-based mechanism of control over aggregate size, Rotello and co-workers replaced the functionalized polystyrene random copolymer with diblock copolymers, where one block that was analogous to the previous poly-Triaz was covalently linked to an "inert" polystyrene block.[172] Three symmetric diblock copolymers of different lengths were used as the 'mortar'. The NP assembly resulted in spherical aggregates with diameters that directly correlated with the length of the functionalized block copolymer. Combined measurements of average core size (from TEM) and overall aggregate size (from DLS) indicated that the polystyrene chains decorating the exterior made up for less than half of the overall aggregate radius, suggesting that the polymer chains within the core are somewhat extended relative to the polystyrene corona.

Rotello and co-workers extended the repertoire of aggregate compositions by preparing a novel type of large-scale assemblies composed of diaminopyridine-functionalized polyoligosilsequioxane (POSS) and thymine-functionalized NPs

assembled through three-point hydrogen bonding (Figure 2.15).[173] The same group reported the use of polymer-mediated self-assembly to modulate the physical and functional properties of γ-Fe_2O_3 NPs aggregates while retaining the magnetic properties in the assembly.[174] Additionally, gold NPs capped with a thiolate shell and alkanethiols terminated with carboxylic acid groups were employed to construct network architectures via hydrogen-bonding linkages at the carboxylic acid shell.[175]

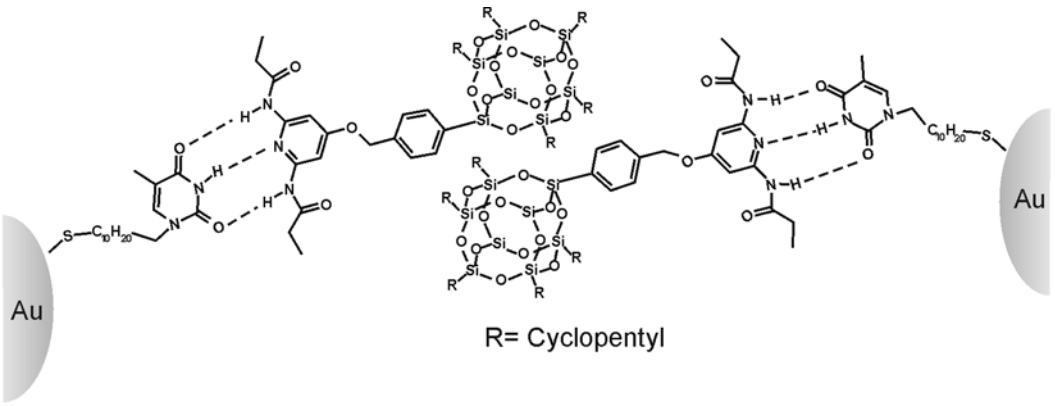

Figure 2.15*: Thymine-functionalized NPs and diaminopyridine-functionalized POSS showing three-point hydrogen bonding.*[173]

Not only different methodologies and different compositions of hydrogen-bonded NPs assemblies have been studied, also the structure and dynamics[176] as well the kinetics[177] of the assembly have been investigated carefully. Rotello *et al.* found that both structure and dynamics of the assembly can be controlled by the incorporation of internal, intramonolayer hydrogen-bonding elements (amide-functionalized NPs). Thus, when the distance between the amide functionality and the core increases, the disorder of the monolayer increases, making the intramonolayer interactions more entropically disfavored. Additionally, NPs with an amide functionality near the exterior of the monolayer bind intermolecularly to other NPs creating large amorphous self-assembled network NPs.[176] The aggregation kinetics of the assembly was also studied by Fitzmaurice *et al.* who found that the kinetics of NP aggregation, and as a consequence the structure of the resulting NP aggregates, depends on the number of receptor sites at the surface of the NPs.[177]

2.3.1.2 Nanoparticle assembly by inclusion (interaction)

NP assembly has been performed using host-guest inclusion (interaction) as the driving force for the assembly, resulting in the formation of 3D nanostructures. Cyclodextrins can be incorporated into the monolayer of the NPs to provide a motif for molecular recognition. Kaifer and co-workers developed a modified CD system that was immobilized on the surface of platinum,[178] palladium,[179,180] silver,[181] and gold.[182] The same group studied the formation of supramolecular aggregates between β-cyclodextrin functionalized NPs and a divalent bis(ferrocene).[182]. The addition of the bis(ferrocene) to a solution of β-cyclodextrin NPs resulted in the formation of large network aggregates, which eventually precipitated. Addition of a competitor in solution, either ferrocene methanol or free β-cyclodextrin, did not lead to any precipitation or flocculation of the NPs. Additionally, decrease of concentration and increase of temperature slowed down the kinetics of precipitation. The same behavior was observed for γ-cyclodextrin-modified gold NPs in combination with C_{60} fullerene molecules.[183]

Another approach to incorporate inclusion-based host-guest recognition is through the use of pseudorotaxane assemblies. To integrate this motif into NP systems, the groups of Fitzmaurice and Stoddart have synthesized gold NPs featuring dibenzo[24]crown-8 ether moieties on the surface.[184] Through NMR experiments it was shown that these NPs formed pseudorotaxanes on the surface by binding dibenzylammonium cations. The same groups studied the possibility to form NP assemblies based on the same pseudorotaxane formation.[185] In this study silver NPs were stabilized by chemisorption of an alkanethiol/dibenzo-24-crown-8 adsorbate mixture. Addition of a stochiometric amount of a bis-dibenzylammonium dication initiated the aggregation of the dibenzo-24-crown-8 silver NPs, leading to the formation of larger aggregates through [3]pseudorotaxane complexes (Figure 2.16). Like Kaifer *et al.* reported for the cyclodextrin-modified NPs,[182,183] control over the NP assembly was demonstrated by the addition of an excess of the receptor or of the substrate which inhibited aggregation.

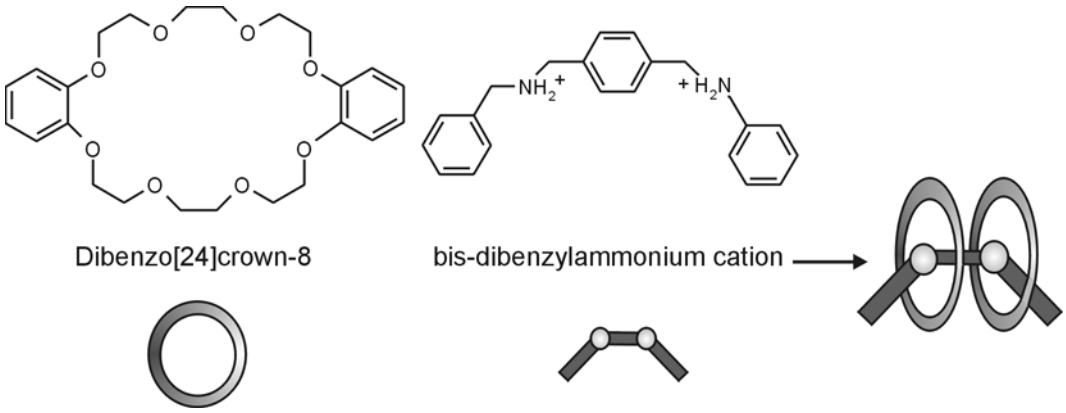

Figure 2.16: *[3]Pseudorotaxane formation induced-NP assembly is due to the recognition and selective binding of dibenzo[24]crown-8 and bis-dibenzylammonium cation.*[185]

Pseudorotaxane recognition was applied to binary NP structures assembled in solution from silver NPs surrounding silica NPs.[186] The assembly consisted of dibenzo[24]crown-8-modified silver NPs and dibenzylammonium-modified silica NPs, where the cation was generated in situ at the surface of the silica NPs by photolysis and subsequent protonation. The recognition of the silica NPs by silver NPs led to the pseudorotaxane formation at the surface of the NPs and subsequent aggregation. Thermal annealing led to an irreversible coating of silver around the silica beads.

2.3.1.3 Metal ion-directed nanoparticle assembly

Metal-ligand systems provide a means of expanding the structural diversity of self-assembly processes.[187] To explore the application of this methodology to nanocomposite fabrication, Rotello's group has synthesized NPs bearing terpyridine (terpy) ligands and studied their self-assembly using a variety of transition metals.[48] Metal-induced aggregation of NPs was obtained with Fe, Ag, Zn, and Cu ions. Aggregates formed by the addition of the weaker tetracoordinate complexes (Ag, Cu) appeared to be more dense as a result of a thermodynamically controlled assembly process, which allows for reorganization and optimization of coordination interactions within the assembly. The stronger hexacoordinated terpy complexes formed very rapidly and resulted in aggregates filled with many voids and cavities. The overall strength of the assemblies could be controlled through the choice of bridging metal ions. In a similar

experiment, Murray and co-workers controlled the formation of aggregates of thiopronin-modified NPs by the addition of Cu^{2+}. The amount of Cu^{2+} required to induce NP assembly was strongly dependent on pH and increased at lower pH, where the thiopronin acid groups were protonated making them no longer available to chelate the Cu^{2+} ions.[116]

One characteristic of gold NPs is the relatively high extinction coefficient that makes them very attractive as colorimetric reporters for particular metal ions. Hupp and co-workers prepared 11-mercaptoundecanoic acid-capped gold NPs that aggregated in solution in the presence of divalent metal ions like Pb, Cd, and Hg by an ion-templated chelation process.[188] The aggregation process was monitored through changes in the adsorption spectrum of the particles. The process could be reversed by the addition of a strong metal ion chelator such as EDTA.

One of the limitations of developing organic chromophores for practical Li^+ detection is their lack of solubility in aqueous media. To overcome that problem, Murphy and co-workers designed a detection system based on NP aggregation.[189] Gold NPs were functionalized with 1,10-phenanthroline derivatives, which are particularly selective for Li^+. Addition of Li^+ to the NP solution resulted in a color change of the solution followed by precipitation. The sensitivity for Li^+ was tested as a function of NP size, showing that smaller NPs have lower detection limits.

In contrast to the previous studies, Chen and co-workers developed a more specific method for metal-ion sensing with gold colloids.[190] They attached crown ether receptors onto a gold NP in order to detect the presence of K^+ over Li^+, Cs^+, NH_4^+, Ca^{2+}, and Na^+. Upon addition of Na^+ to the modified 15-crown-5 gold NPs, stable complexes were obtained. However, the addition of K^+ to the Na^+-NP complexes resulted in the formation of aggregates composed of a "sandwich complex" of 2:1 15-crown-5 and K^+.

2.3.1.4 Nanoparticle assembly by electrostatic interactions

Rotello and co-workers described the assembly of two different types of NPs that through electrostatic interactions.[191] Their strategy involved the functionalization of one type of colloidal building block (SiO_2 NPs) with a primary amine, and a counterpart (gold NPs) with a carboxylic acid derivative. By combining the two systems, acid-base chemistry followed by immediate charge-pairing resulted in the spontaneous formation of

electrostatically bound mixed-colloid constructs. The shape and size of these ensembles was controlled by variation of particle size of the two components and their stoichiometry. A more elegant multi-component electrostatic self-assembly protocol was proposed by the same group a making use of the "bricks-and-mortar" system with a polymer serving as a matrix for the controlled assembly of nanoparticles.[170] Carboxylic acid-terminated gold and silica NPs were employed together with an amine-functionalized polystyrene random copolymer. In this three-component system, electrostatic interactions between the basic polymer and the acid-functionalized NPs resulted in the formation of diverse structures. Control over the assembly process was provided through the order of the component addition. For example, when the polymer was added to a mixture of the two NPs, well-integrated nanocomposites were obtained. However, premixing of the silica NPs with the polymer followed by addition of the gold NPs led to segregated clusters, where the gold NPs were exposed at the surface of the supporting silica aggregates.[192]

Weller and co-workers studied the self-organization of positively and negatively charged CdS NPs, and negatively charged gold NPs in order to obtain 3D ordered NP systems.[193] Mixing of the two different nanoparticle solutions led to different superlattices depending on the ratio of the positive to negative charges. The particles were stable in solution if one of the components was in excess, while precipitation occurred if the ratio was close to 1. NP aggregates could be redissolved or precipitated by changing the ionic strength of the solution. Using similar methodologies, hybrid inorganic/organic composite materials composed of gold colloids and polyhedral oligomeric silsesquioxane (POSS) were prepared by the groups of Rotello[194] and Chujo.[195] These assemblies feature uniform and rigid interparticle spacings consistent with the POSS diameter.

Another approach for NP assembly has focused on the use of amino acids (which bind to gold NPs with their amino groups) as binding agents. Their control of aggregation depends on the reactivity of the α-amine, which is found to be pH-dependent. Linking via the α-amine is activated at low pH but suppressed at intermediate and high pH due to electrostatic repulsive forces between the gold surface and the charged carboxylate groups or even the (formally neutral) polar carbonyl groups in amides. However, dibasic

amino acids can still be used to crosslink gold colloids at high pH.[196] Two different aminoacids have been used for such an approach, cysteine (Cys)[197] and lysine (Lys).[198,199] In the case of Cys, the two functional groups (SH and NH_2) are able to bind gold with different abilities, the SH group binds readily, whereas the α-amino group displays pH-dependent behavior. In the case of Lys two chemically distinct amino groups determined the ability to bind gold and organize the NPs into supramolecular aggregates. By adjusting the pH, starting concentrations and surface charge (by way of the Au:aminoacid ratio), the aggregation process could be manipulated to produce a structure of desired size and shape. In the case of Cys, a pH range of 7-10 and Au:Cys molar ratios of 1:0.5-1:2 resulted in the formation of spherical aggregates.[197] For Lys, at a pH range between 8-10 and a molar ratio of 0.5, linear gold aggregates were obtained.[198] Additionally, NP assemblies could be adjusted from spherical-like to chain-like by mixing Cys and Lys in various ratios.

Several factors can influence the stability and morphology of NP aggregates. The pH and the ionic strength have a huge influence on electrostatically induced NP assembly due to the presence of ionizable groups on the particle surface.[200] However, also charge density and concentration of crosslinkers affect the formation of such assemblies (Figure 2.17).[201] Crosslinkers with a high charge or high concentration can neutralize the particle's zeta potential, facilitating the formation of tightly bound aggregates. On the other hand, crosslinkers with a low concentration or charge do not allow the full neutralization of the zeta potential, so they are ineffective at bridging the NPs together into stringlike aggregates. The elimination of excess free ions results in a appropriate balance of repulsion and attraction among colloids which leads to their self-assembly into 3D cluster-type aggregates.[202]

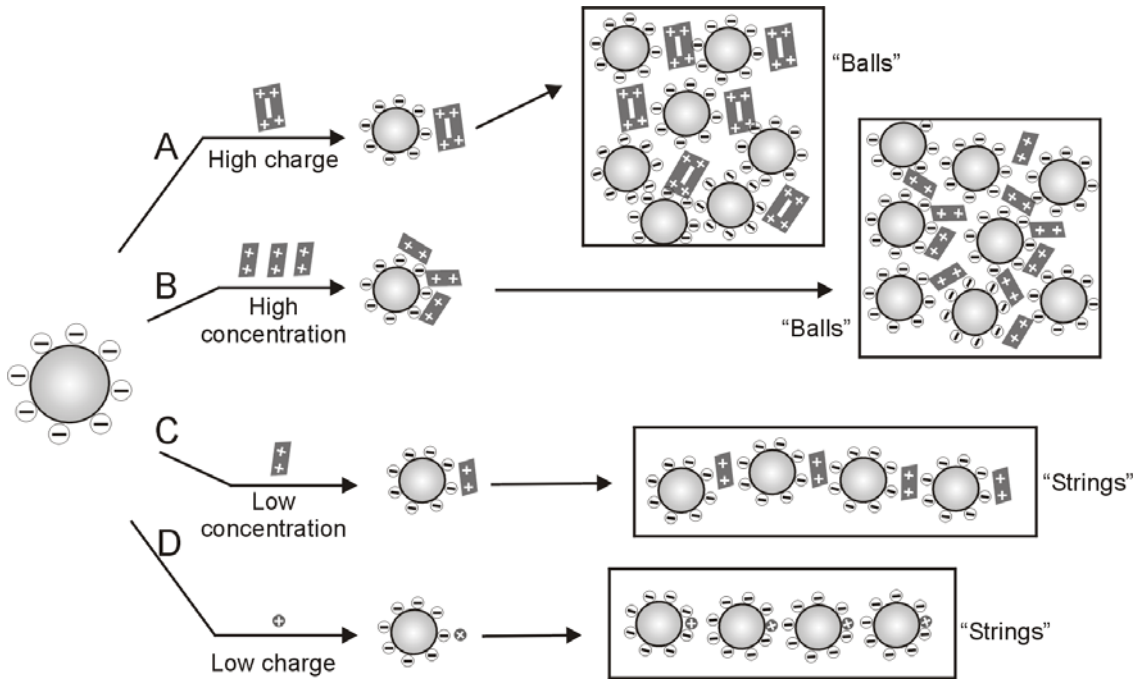

Figure 2.17: *Possible mechanisms for the formation of "string-like" and "ball-like" aggregates of gold NPs based on crosslinker charge and concentration.*[201]

As mentioned before, the physical properties of NPs are affected by neighboring particles in a strongly distance-dependent interaction.[203] Controlling interparticle distance has been achieved through hydrogen-bonding (see section 2.3.1.1) and electrostatic interactions by means of using separate entities such as polymers or dendrimers to regulate the interparticle distance. The group of Rotello employed PAMAM dendrimers of different generations (0-4) to assemble gold NPs and control the separation distance between them (Figure 2.18).[204] In this approach, direct control of interparticle separation was provided through the choice of dendrimer generation. Gold NPs were functionalized with carboxylic acid groups. Salt-bridge formation between the dendrimer amino groups and the NP peripheral carboxylic acid groups led to electrostatic self-assembly between the dendrimer and NP components resulting in well-controlled aggregates. Interparticle distance in the aggregates formed was quantified by using small angle X-ray scattering (SAXS). It was observed that the sharp Bragg reflections shifted towards lower angles (larger interparticle distances) as the dendrimer generation increased. Control of interparticle spacing also provided a method for systematically shifting the surface

plasmon resonance (SPR) of the particles, therefore having functional control over the NP aggregates.[205] In addition, these dendrimer-mediated NP assemblies open the door to create tailored magnetic NP structures.[206]

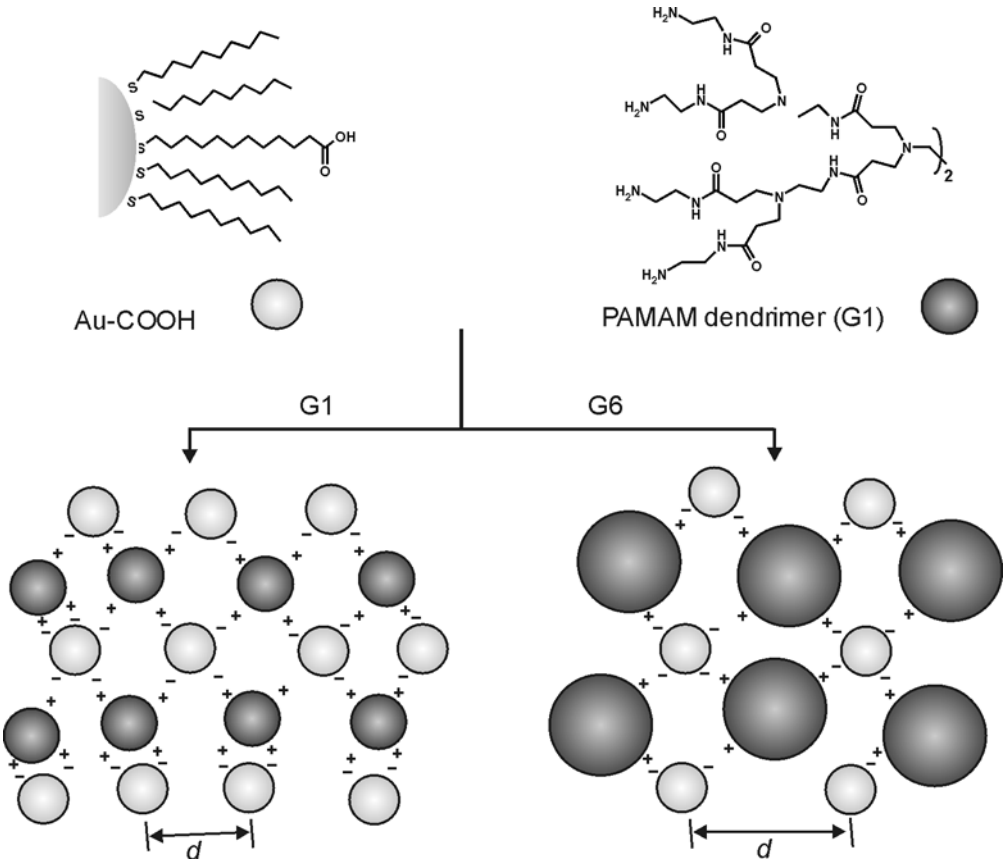

Figure 2.18: *Schematic representation of electrostatic self-assembly of carboxylic acid-terminated gold nanoparticles and PAMAM dendrimers, illustrating the control over average interparticle spacing, d, through dendrimer size.*[204]

2.3.1.5 Charge transfer-directed nanoparticle assembly

Electron transfer interactions involve the partial transfer of a single electron from one molecular entity to another, or between two localized sites in the same molecular entity. This section will be focused on charge transfer (CT) interactions, that occur between an electron-donor and an electron-acceptor, and furthermore on the π-π interactions, that hold molecules together due to a sharing of electrons of sp^2 orbitals.

The strategy employed by Chujo and co-workers to program self-assembly of colloidal gold NPs into macroscopic 3D aggregates involved the charge transfer interaction between pyrenyl units, as an electron donor, immobilized on the surface of the gold NPs and a bivalent linker containing two dinitrophenyl units as an electron acceptor (Figure 2.19).[207] The addition of the bivalent linker to the pyrenyl-modified NP solution resulted in the formation of large, spherical aggregates with a diameter of 1 ± 0.7 μm, composed of individual gold NPs. The degree of colloidal association could be controlled by adjusting the concentration of the linker group in solution. Reversibility of the aggregated state was demonstrated by heating the solution to 50 °C and was found to be reproducible for several cycles. Recently, the same group described the formation of spherical aggregates induced by a charge transfer between the bis(dinitrophenyl) linker and 9-carbazolyl-modified gold NPs (Figure 2.19).[208]

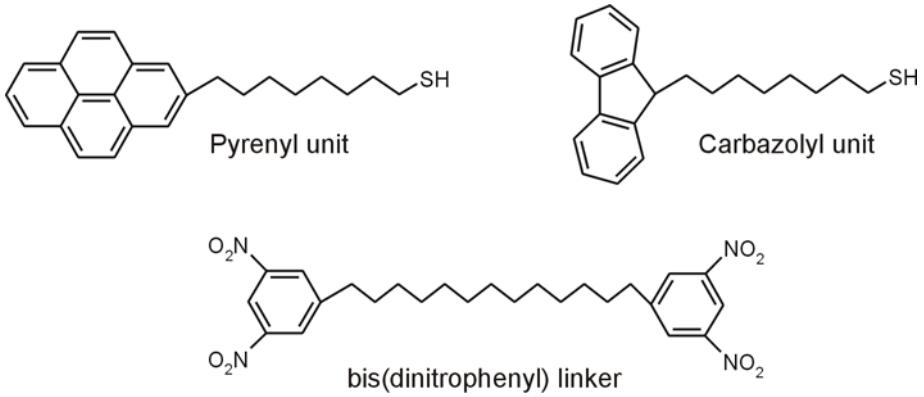

Figure 2.19: *Molecules used for charge transfer NP assembly.*

Photoinduced electron transfer and energy transfer in a number of donor-acceptor systems have been extensively studied with the aim to mimic natural photosynthesis by converting the charge-separated state into chemical or electrical energy. This concept has been successfully demonstrated using fullerenes (C_{60}) for the construction of two- and three- dimensional nanoassemblies of photoactive molecules with colloidal metal particles. Brust and co-workers described the first NP assembly consisting of gold NPs and fullerenes.[209] In this study tetraoctylammonium bromide-stabilized gold particles in toluene were assembled into aggregates by the addition of C_{60} molecules. After the

addition of the fullerenes, the ruby-colored solution slowly changed color to blueish violet, and it entirely precipitated after 3 weeks. TEM images showed the formation of strings of non-ordered 3D aggregates composed of gold nanoparticles. High resolution images showed that these particles were not in direct contact with each other but were apparently "glued" together by a shell of fullerene molecules.

With a focus on the preparation of organic solar cells, Fukumozi and co-workers reported the quaternary organization of porphyrin (donor) and fullerene (acceptor) dye units by clustering with gold NPs (Figure 2.20).[210]

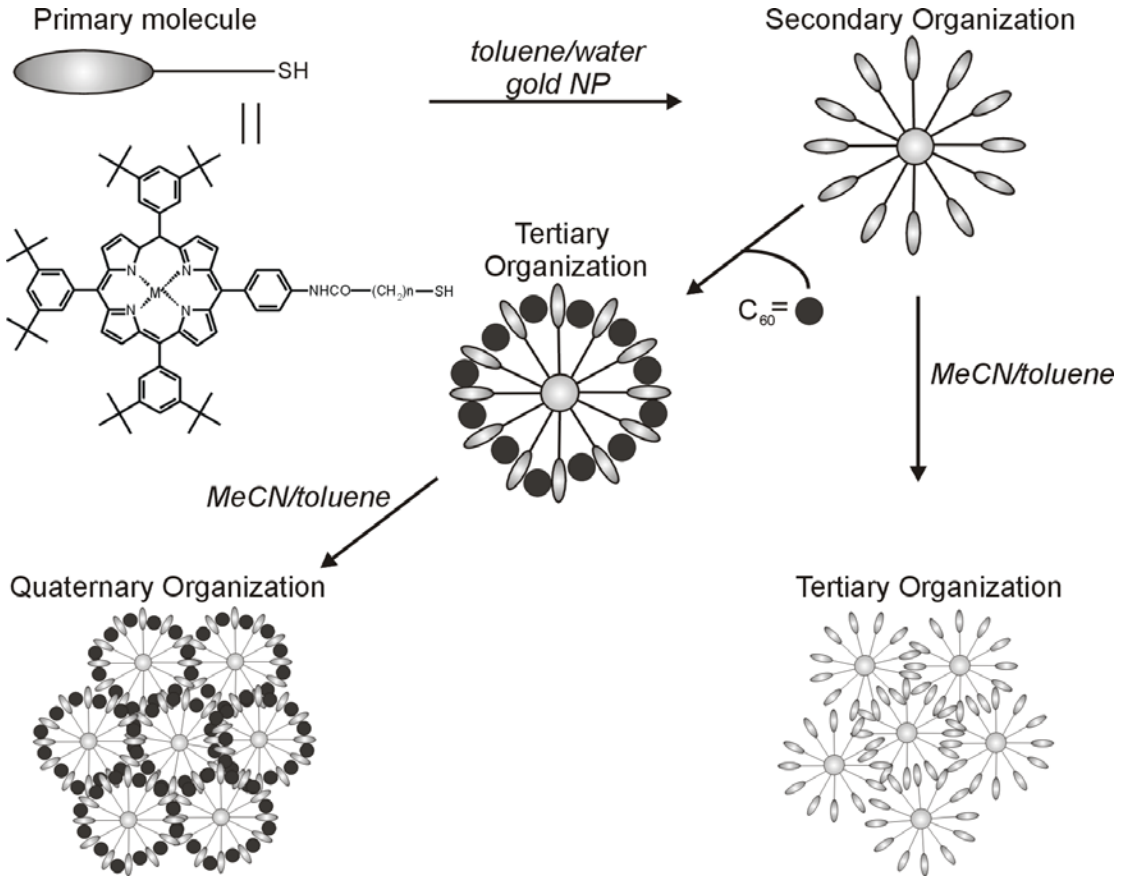

Figure 2.20: *Illustration of higher order organization of porphyrin and C_{60} units with gold NPs.*

First, porphyrin-alkanethiolate gold NPs with well-defined sizes (8-9 nm) and spherical shape were prepared (secondary organization) from the primary components. After this, these NPs formed complexes with fullerene molecules (tertiary organization),

and they were clustered in an acetonitrile/toluene mixed solvent (quaternary organization). TEM images of the quaternary organization displayed well-controlled size and shape of larger nanoclusters with a diameter of 300-400 nm. Control experiments of the porphyrin-modified NPs without C_{60} exhibited irregular and smaller clusters. From these experiments and from the diameter of the porphyrin-NPs in the quaternary organization (8-9 nm) the authors concluded that specific donor-acceptor interactions were needed to yield well-defined nanoclusters with an interpenetrating network (Figure 2.20).

In a different strategy directed by π-π interactions, self-assembly of individual 2-carboxyterthiophene magnetic NPs was performed by Jin *et al.*[211] The individual NPs aggregated through weak π-π interactions forming spherical aggregates consisting of thousands of NPs, which could be easily redissolved by sonication. In order to analyze the magnetic characteristics of the aggregates, a superconducting quantum interference device (SQUID) magnetometer was employed. The field- and temperature-dependent magnetization data for the aggregates showed that at lower temperatures (5 K) the magnetization of the aggregates increased and exhibited a symmetrical hysteresis loop, consistent with superparamagnetic behavior.

2.3.2 Biomolecule-directed nanoparticle assembly

The aggregation of NPs induced by specific biological interactions has attracted huge interest in the assembly of nanoscale components into controlled and sophisticated nanostructures in order to develop methods that mimic or exploit the recognition capabilities and interactions found in biology.[78,166,212] For the generation of biomolecule-crosslinked NPs, two types of complementary units should participate in the assembly process. Biomaterials utilized in the fabrication of such biomolecule-NP aggregates include complementary oligonucleotides, and protein pairs such as biotin-streptavidin and antigen-antibody. Besides the assembly into 3D nanostructures, the aggregation properties of biomolecule-modified NPs have been used in medicine for diagnostic assays,[79] such as immunoassays,[213] detection of polyvalent proteins,[214] and detection of a

virus in solution,[215] among others. This section is devoted to recent examples of these biological interactions for directing NP assembly.

2.3.2.1 Protein-directed nanoparticle assembly

Proteins can be used to organize NPs into well-structured aggregates. The most frequently used protein-ligand system for such assemblies has been the biotin-streptavidin couple. The recognition between biotin and the homotetrameric streptavidin (SAv) is characterized by one of the highest stability constants known for noncovalent binding of a protein and a small ligand in aqueous solution, $K_a > 10^{14}$ M^{-1}.[216]

The first example of NP assembly based on protein binding was described by Connolly and Fitzmaurice in 1999.[217] Gold NPs were assembled in solution via two different routes. The first one consisted of the modification of gold NPs by chemisorption of a biotin-modified disulfide, followed by the addition of SAv; the second route involved the binding of the biotin adsorbate to SAv before the attachment onto the gold surface (Figure 2.21).

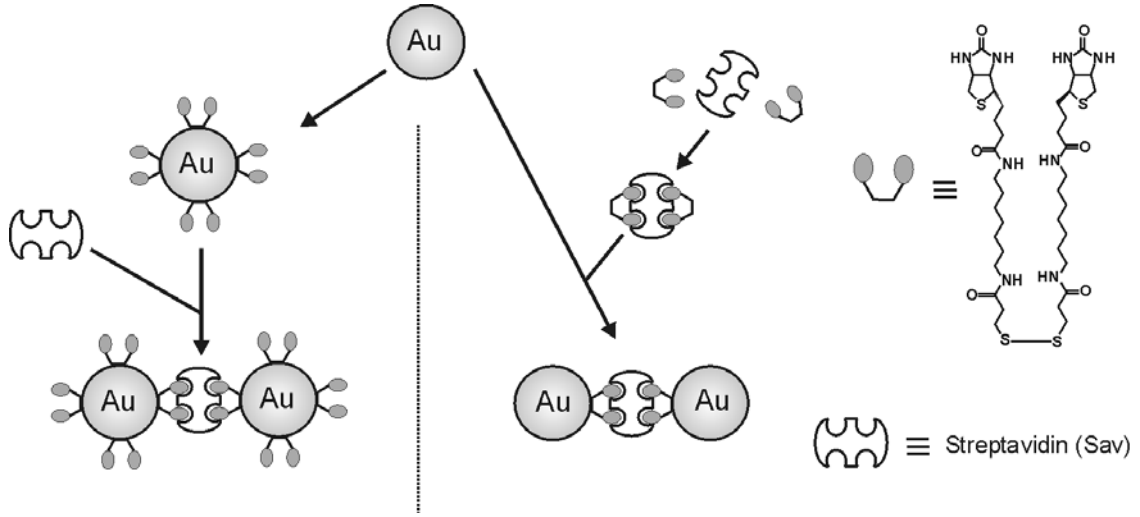

***Figure 2.21**: Two routes for the aggregation of gold nanoparticles using streptavidin and a disulfide-biotin adsorbate.*[217]

The assembly of gold NPs was monitored by dynamic light scattering (DLS) showing a rapid increase in the average hydrodynamic radius upon addition of SAv

accompanied by a color change of the solution from red to blue. TEM showed a homogeneous distribution of the unmodified gold NPs, while in the case of the biotin-modified NPs aggregated by addition of SAv, isolated particles were absent and larger aggregates with and interparticle distance of approx. 5 nm, corresponding to an interspersed SAv, were observed.

The SAv-biotin induced aggregation has also been used to assemble other systems like nanorods[218] and protein-encapsulated Fe_2O_3 NPs,[219] the latter with important applications in magnetic storage and nanoelectronic devices (Figure 2.22).

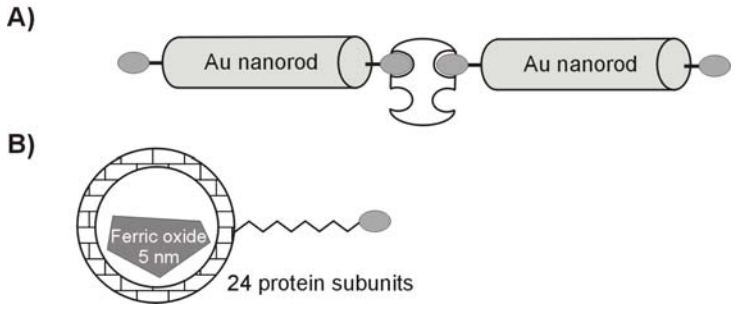

Figure 2.22: *(A) End-to-end assembly of biotin-functionalized gold nanorods that are crosslinked by SAv.[218] (B) Biotin-functionalized ferritin.[219]*

Mann *et al.* have reported different strategies that involve the surface attachment of IgE or IgG antibodies to metal NPs followed by addition and subsequent crosslinking of a divalent antigen with appropriate double-headed functionalities.[220] The formation of specific antibody-antigen NP assemblies resulted in the formation of differently structured 3D network aggregates. Anti-dinitrophenyl (anti-DNP) IgE antibodies were chemisorbed onto 12 nm gold NPs and then bis-*N*-2,4-dinitrophenyloctamethylene diamine was added at a molar equivalence. No aggregation was observed but leaving the colloid dispersion at 4 °C gave a macroscopic purple precipitate, for which TEM revealed large disordered 3D networks of discrete gold NPs. Alternatively, two different antibody-modified NPs, anti-DNP IgE and anti-biotin IgG, were prepared. Equimolar mixtures of these antibody-coated NPs could be specifically aggregated by the addition of a synthetic "Janus" antigen, which consists of DNP and biotin haptens separated by a flexible linker.

TEM showed structures of macroscopic filaments consisting of spatially separated gold NPs. Bimetallic nanoparticle aggregates comprising gold and silver were also obtained by using the DNP-biotin antigen biomolecular recognition.

Kotov and co-workers used a different antibody-antigen system to assemble luminescent CdTe NPs into ordered supramolecular aggregates.[221] Thiol-stabilized green- and red-emitting CdTe NPs were modified with bovine serum albumin (BSA) and the corresponding antibody (anti-BSA). When the IgG NPs (anti-BSA) with green luminescence were combined in a 1:1 molar ratio with BSA-labeled NPs with red-luminescence, an enhancement of the red-emission at 611 nm of the BSA NPs and a quenching of the green emission at 555 nm of the IgG NPs were observed. Apparently, the highly specific affinity of the antigen-antibody complex brought the NPs close enough to allow the resonance dipole-dipole coupling required for fluorescence resonance energy transfer (FRET). These results showed that well-organized assemblies of luminescent NPs could be obtained as well as an enhancement of the luminescent quantum yield in the bioconjugate, which is important for protein sensing.

Also carbohydrate-carbohydrate interactions have been shown to be specific and directional and have been used to drive NP assembly. Penadés and co-workers prepared oligosaccharide-functionalized gold NPs with a 3D polyvalent carbohydrate network,[222,223] and studied how carbohydrate-carbohydrate interactions can be used to guide the assembly of the gold clusters.[224] They prepared gold NPs functionalized with two biologically significant oligosaccharides: the lactose dissacharide (Lac-Au) and the trisaccharide Le^x antigen (Le^x-Au). In the presence of Ca^{2+} ions, specific carbohydrate-carbohydrate interactions between the Le^x antigen molecules in the Le^x-Au provoked the aggregation of the gold NPs, which could be reversed by the addition of EDTA. Addition of $CaCl_2$ to a Lac-Au NP solution did not cause any aggregation of the clusters. The authors also reported the functionalization of the gold NPs with fluorescein molecules together with Lac or Le^x oligosaccharides. These hybrid NPs showed self-organization onto a copper grid in a two-dimensional hexagonal structure defined by the gold centers.[224]

2.3.2.2 DNA-directed nanoparticle assembly

The specific recognition embedded in the DNA sequence double helix is being used more and more in nanoscience and nanotechnology, particularly as a versatile construction material specially due to its high specificity, and also its flexible length and the chemically programmable duplex structure.[79,225,226] The specificity of the adenine-thymine (A-T) and guanine-cytosine (G-C) Watson-Crick hydrogen bonding allows the construction of ordered systems with predictable structure. During the last few years, it has been demonstrated that one can use DNA to control the assembly of NPs in solution in the form of aggregates and small clusters and on substrates in the form of multilayered structures (section 2.2.3.2). In all these nanomaterials, DNA is used mainly as a structuring element to drive the assembly of molecules that would not interact by themselves, or would do so in a disordered fashion.

Besides being used as a molecular template for the self-assembly of nanostructures, DNA has also been used to develop a variety of biomolecule detection schemes based on their collective optical, catalytic, or electrical properties.[227] Mirkin reported a highly selective colorimetric detection technology for the detection of complementary DNA based on red-to-purple color changes resulting from the formation of a network of gold NPs.[227-229] The high sensitivity and selectivity of the DNA-NP assemblies for detection purposes often rival with fluorescent detection owing to the strong distance-dependent optical properties,[230] the melting temperatures,[231] and the electrical properties[232] of these DNA-NP assemblies. Moreover, Mirkin's colorimetric detection strategy has been expanded to the detection of other systems such as adenosine[233] and metal ions,[234] among others.

DNA has been extensively used as a building block for assembling NPs into network aggregates. The group of Mirkin,[235,236] Alivisatos,[237] and Brust[238] have provided examples where oligonucleotides were used to order aggregates of gold NPs in solution. Mirkin and co-workers have developed many techniques for arranging NPs exploiting the code of oligonucleotides that are attached to them. The first strategy consisted of the introduction of a single-strand DNA to a solution of NPs modified with partially complementary DNA, where the single-strand DNA served as the "glue" to assemble the DNA NPs but only if the two halves are complementary to the DNA anchored on the

NPs.[235] This approach has also helped them to assembly binary network materials comprising two differently sized, DNA-functionalized NPs.[236] The structural characterization of such assemblies was performed with SAXS. In this study issues like particle spacing depending upon different number of bases in the DNA interconnect, size of the NP building blocks and interparticle interactions are discussed in detail.[239]

Alivisatos and co-workers have used an analogous approach to fabricate multiple trimer and tetramer architectures of DNA-gold NPs.[237,240] The authors reported a procedure where branched DNA scaffolds were hybridized in different positions to produce a three-armed dendritic structure comprised of one unique and two duplicate sequences. To generate well-defined assemblies, gold NPs functionalized with single strands of thiolated linear DNA were utilized. Following the same procedure, asymmetric structures were also produced in which 5 and 10 nm gold NPs were assembled on the DNA branched scaffolds. By using electrophoresis it was possible to isolate Au/DNA structures.[241]

A similar method of nanostructure manipulation was demonstrated by Brust and co-workers, in which biocatalyzed transformations of functionalized DNA assemblies were used to perform the controlled association of NPs and to provide stabilization of the aggregates.[238] 15 nm gold NPs were modified with thiolated single-strand DNA. The DNA-modified NPs were then converted to the double-strand form by hybridization with the complementary single-strand DNA. A restriction enzyme was used to cleave the double strands on the particles at specific sites. This resulted in cohesive ends of single-strand DNA, which can bind by hybridization to complementary sequences present in the system resulting in the formation of weak and small aggregates. More stable, larger aggregates were obtained in a second ligation step (Figure 2.23).

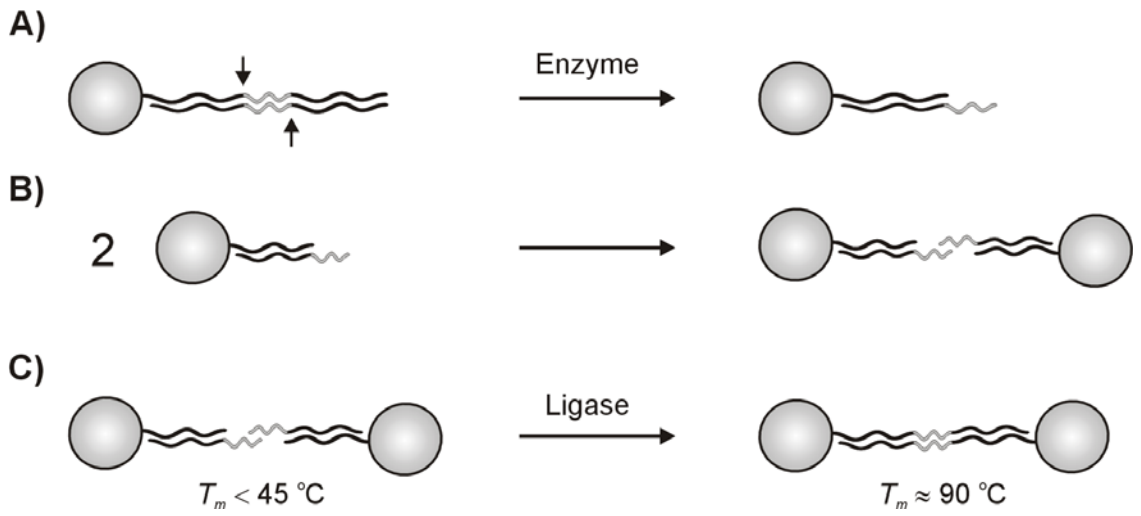

Figure 2.23: *Schematic representation of the method used by Brust and co-workers. (A) Gold NPs derivatized with double-strand DNA are treated with a restriction enzyme, which cleaves the DNA to yield cohesive ends. (B) Two cohesive ends hybridize, which leads to weak association of NPs. (C) The DNA backbones are covalently joined at the hybridized site by DNA ligase to yield a stable DNA double-strand link between the particles.*[238]

A similar strategy, using DNA as a structuring element, has been used to create ordered aggregates composed of other types of NPs. For example, Mann and co-workers have used DNA to induce the programmed assembly of gold NPs onto silica NPs.[242] The field of semiconductor quantum dots (QDs) passivated with DNA has been explored by Mirkin and co-workers.[243] Modification of QDs with single-strand DNA generated DNA-linked QD assemblies through specific binding between complementary DNA strands. Moreover, the versatility of the system allowed the construction of hybrid metal/semiconductor nanostructures composed of DNA-modified gold NPs and DNA-modified QDs.

Fitzmaurice *et al.* were able to control NP aggregation in solution by attachment of complementary protein-DNA conjugates.[244] Gold NPs were modified with disulfide-biotin derivatives that were able to recognize and bind selectively SAv-DNA conjugates, resulting in NP assembly. The driving force for the assembly was the formation of a DNA duplex between the two complementary DNA oligomers bound to the individual NPs. The advantage of this methodology is that the aggregation rate can be controlled by

the addition of single-strand DNA oligomers to a dispersion of NPs protein-DNA conjugates. The single-strand DNA immediately formed duplexes with the immobilized DNA and the aggregation process was terminated (Figure 2.24).

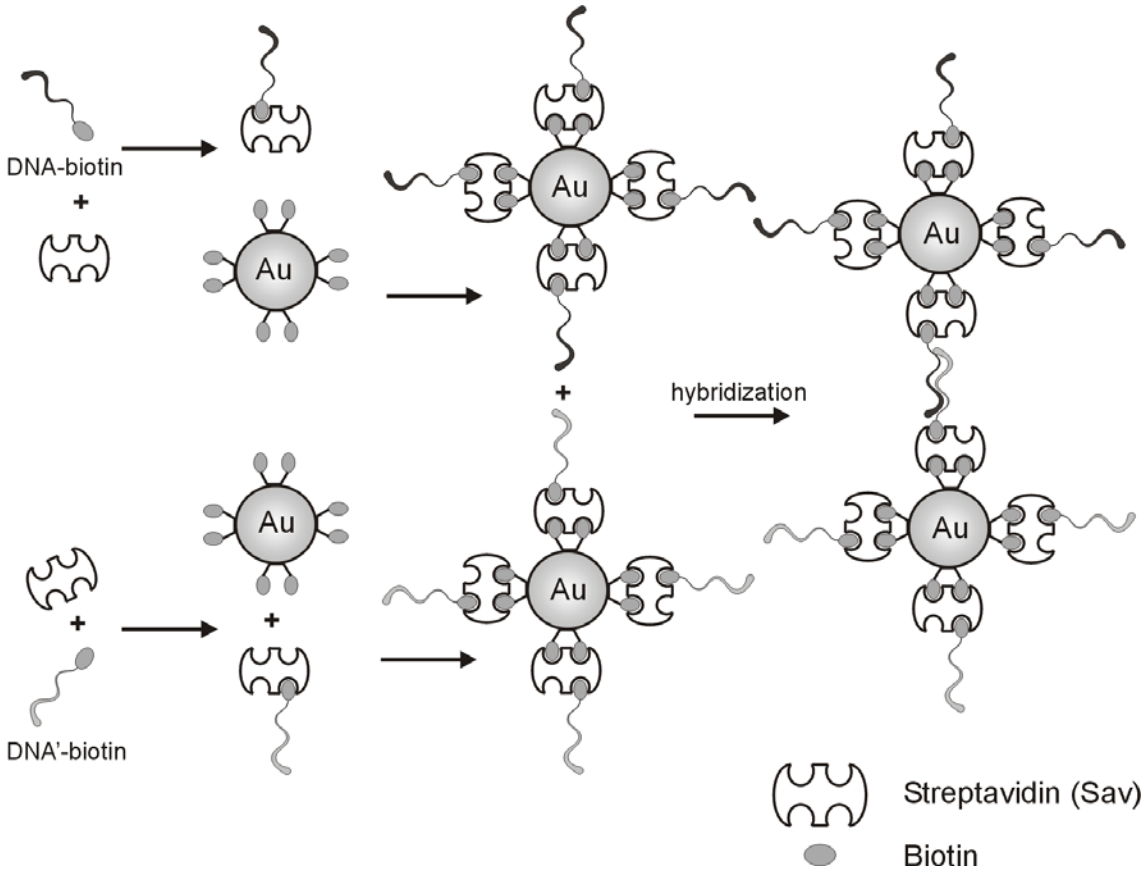

Figure 2.24: *Illustration of the biotin-modified NP assembly induced by attachment of complementary SAv-DNA conjugates.*[244]

Moreover, the kinetics of the aggregation process could be changed by varying the salt and particle concentrations. The strong biotin-SAv interactions and the specific hybridization capabilities of DNA-SAv conjugates have also been used to organize gold NPs. Niemeyer and co-workers[245] modified 1.4 nm gold clusters with a single biotin group, where the biotin moiety was used to organize the nanoclusters into the tetrahedral superstructure, defined by the geometry of the biotin-binding sites. Furthermore, the nanocluster-loaded proteins self-assembled in the presence of the complementary single-

strand DNA, therefore generating novel biometallic nanostructures. Introduction of a functional immunoglobulin, allowed the targeting of the biometallic nanostructures to specific tissues.

As explained in Section 2.2.2, proteins have been used to drive NP assemblies through specific interactions. However, since proteins and protein receptors can be functionalized with oligonucleotides, it is possible to immobilize such molecules onto oligonucleotide-modified NPs and to generate new classes of hybrid particles exhibiting the high stability of the oligonucleotide-modified particles but at the same time having the molecular recognition properties of the protein. Taking advantage of that approach, Mirkin and co-workers designed three-building-block NP/protein assemblies: SAv complexed to four biotinylated oligonucleotides, oligonucleotide-modified gold NPs, and a linker oligonucleotide complementary to the other two groups. Addition of the three components and increasing the temperature of the solution to a few degrees below the melting temperature of the DNA interconnects resulted in the growth of micrometer-sized aggregates.[246]

Peptide nucleic acids (PNAs), which are DNA analogues in which the entire sugar-phosphate backbone is replaced by a polypeptide backbone, have also been used to drive NP aggregation.[247,248] The use of PNA complexes offers greater advantages for nanofabrication over the analogous DNA: (1) greater stability, and (2) greater mismatch sensitivity, which leads to an improved selectivity and makes them better suitable for biosensing.

2.4 Conclusions and Outlook

In this chapter some examples of self-assembly at flat and nanoparticle surfaces have been discussed. Self-assembly has been shown to be a tool for the fabrication of 2D and 3D nanostructures. It has been demonstrated that it is possible to assemble molecules and nanometer-scale components, such as nanoparticles, polymers or biomolecules, into ordered arrays with dimensions larger than 100 nm. Such ordered arrays are difficult to achieve with a process other than self-assembly. Furthermore, the fundamental concept of

self-assembly for the preparation of nanomaterials has been extended to integrate functional molecular components into ordered assemblies with well-defined architectures. The combination of such approaches with top-down methodologies will lead to well-defined functional 3D nanostructures and devices.

However, self-assembly as a nanofabrication tool is still in its infancy and a lot of effort still needs to be made in order to make self-assembly a more valuable and versatile instrument for nanofabrication schemes. Although self-assembly has been employed to produce nanostructures with a wide range of components, nonetheless the precise spatial positioning of components, the controlled shapes and size, and the elimination of defects of such nanostructures are still open questions that will need to be solved. Thus, self-assembly as a bottom-up chemical approach as yet requires the spatial confinement of conventional surface patterning techniques (top-down), such as soft-lithography, in order to produce functional materials with long range order. The combination of bottom-up and top-down approaches will lead to functional and well-defined 3D nanostructures.

This thesis describes how self-assembly based on multiple supramolecular interactions between host-modified surfaces (CD SAMs and CD-modified NPs) and guest-modified molecules can be used to assemble 2D and 3D nanostructures at surfaces and in solution. The specificity and stability of multivalent supramolecular interactions can be used to obtain various supramolecular architectures at surfaces. The combination of those interactions with self-assembly techniques such as LBL deposition can be used to assemble larger architectures on flat surfaces, while retaining the interfacial supramolecular specificity. By employing top-down surface patterning strategies such as soft lithography, control over the *x*, *y*, and *z* directions can be achieved leading to 3D nanofabrication schemes.

2.5 References and Notes

1. Whitesides, G. M.; Grzybowski, B. *Science* **2002**, *295*, 2418-2421.
2. Ulman, A. *An Introduction to Ultrathin Organic Films: From Langmuir-Blodgett to Self-Assembly*; Academic Press: Boston, U.S.A. **1991**.
3. Ulman, A. *Chem. Rev.* **1996**, *96*, 1533-1554.

4. Burda, C.; Chen, X. B.; Narayanan, R.; El-Sayed, M. A. *Chem. Rev.* **2005**, *105*, 1025-1102.
5. Mammen, M.; Choi, S. K.; Whitesides, G. M. *Angew. Chem. Int. Ed.* **1998**, *37*, 2755-2794.
6. Mulder, A.; Huskens, J.; Reinhoudt, D. N. *Org. Biomol. Chem.* **2004**, *2*, 3409-3424.
7. Thoden van Velzen, E. U.; Engbersen, J. F. J.; Delange, P. J.; Mahy, J. W. G.; Reinhoudt, D. N. *J. Am. Chem. Soc.* **1995**, *117*, 6853-6862.
8. Schönherr, H.; Vancso, G. J.; Huisman, B. H.; Van Veggel, F. C. J. M.; Reinhoudt, D. N. *Langmuir* **1997**, *13*, 1567-1570.
9. Huisman, B. H.; Kooyman, R. P. H.; Van Veggel, F. C. J. M.; Reinhoudt, D. N. *Adv. Mater.* **1996**, *8*, 561-564.
10. Friggeri, A.; Van Veggel, F. C. J. M.; Reinhoudt, D. N. *Chem. Eur. J.* **1999**, *5*, 3595-3602.
11. Friggeri, A.; Van Veggel, F. C. J. M.; Reinhoudt, D. N.; Kooyman, R. P. H. *Langmuir* **1998**, *14*, 5457-5463.
12. Faull, J. D.; Gupta, V. K. *Langmuir* **2002**, *18*, 6584-6592.
13. Faull, J. D.; Gupta, V. K. *Langmuir* **2001**, *17*, 1470-1476.
14. For comprehensive reviews on cyclodextrin chemistry see: *Chem. Rev*. **1998**, *98*.
15. A. Mulder, PhD thesis, University of Twente **2004** and references therein.
16. Onclin, S.; Mulder, A.; Huskens, J.; Ravoo, B. J.; Reinhoudt, D. N. *Langmuir* **2004**, *20*, 5460-5466.
17. Rojas, M. T.; Königer, R.; Stoddart, J. F.; Kaifer, A. E. *J. Am. Chem. Soc.* **1995**, *117*, 336-343.
18. Wang, Y.; Kaifer, A. E. *J. Phys. Chem. B* **1998**, *102*, 9922-9927.
19. Fragoso, A.; Almirall, E.; Cao, R.; Echegoyen, L.; González-Jonte, R. *Chem. Commun.* **2004**, 2230-2231.
20. Velic, D.; Kohler, G. *Chem. Phys. Lett.* **2003**, *371*, 483-489.
21. Maeda, Y.; Fukuda, T.; Yamamoto, H.; Kitano, H. *Langmuir* **1997**, *13*, 4187-4189.
22. Yamamoto, H.; Maeda, Y.; Kitano, H. *J. Phys. Chem. B* **1997**, *101*, 6855-6860.
23. De Jong, M. R.; Huskens, J.; Reinhoudt, D. N. *Chem. Eur. J.* **2001**, *7*, 4164-4170.
24. Endo, H.; Nakaji-Hirabayashi, T.; Morokoshi, S.; Gemmei-Ide, M.; Kitano, H. *Langmuir* **2005**, *21*, 1314-1321.
25. Michalke, A.; Janshoff, A.; Steinem, C.; Henke, C.; Sieber, M.; Galla, H. J. *Anal. Chem.* **1999**, *71*, 2528-2533.
26. Beulen, M. W. J.; Bügler, J.; De Jong, M. R.; Lammerink, B.; Huskens, J.; Schönherr, H.; Vancso, G. J.; Boukamp, B. A.; Wieder, H.; Offenhauser, A.; Knoll, W.; Van Veggel, F. C. J. M.; Reinhoudt, D. N. *Chem. Eur. J.* **2000**, *6*, 1176-1183.

27. Auletta, T.; De Jong, M. R.; Mulder, A.; Van Veggel, F. C. J. M.; Huskens, J.; Reinhoudt, D. N.; Zou, S.; Zapotoczny, S.; Schönherr, H.; Vancso, G. J.; Kuipers, L. *J. Am. Chem. Soc.* **2004**, *126*, 1577-1584.
28. Mulder, A.; Auletta, T.; Sartori, A.; Del Ciotto, S.; Casnati, A.; Ungaro, R.; Huskens, J.; Reinhoudt, D. N. *J. Am. Chem. Soc.* **2004**, *126*, 6627-6636.
29. Auletta, T.; Dordi, B.; Mulder, A.; Sartori, A.; Onclin, S.; Bruinink, C. M.; Péter, M.; Nijhuis, C. A.; Beijleveld, H.; Schönherr, H.; Vancso, G. J.; Casnati, A.; Ungaro, R.; Ravoo, B. J.; Huskens, J.; Reinhoudt, D. N. *Angew. Chem. Int. Ed.* **2004**, *43*, 369-373.
30. Mulder, A.; Onclin, S.; Péter, M.; Hoogenboom, J. P.; Beijleveld, H.; Ter Maat, J.; García-Parajó, M. F.; Ravoo, B. J.; Huskens, J.; Van Hulst, N. F.; Reinhoudt, D. N. *Small* **2005**, *1*, 242-253.
31. Huskens, J.; Deij, M. A.; Reinhoudt, D. N. *Angew. Chem. Int. Ed.* **2002**, *41*, 4467-4471.
32. Nijhuis, C. A.; Yu, F.; Knoll, W.; Huskens, J.; Reinhoudt, D. N. *Langmuir* **2005**, *21*, 7866-7876.
33. Huskens, J.; Mulder, A.; Auletta, T.; Nijhuis, C. A.; Ludden, M. J. W.; Reinhoudt, D. N. *J. Am. Chem. Soc.* **2004**, *126*, 6784-6797.
34. Nijhuis, C. A.; Huskens, J.; Reinhoudt, D. N. *J. Am. Chem. Soc.* **2004**, *126*, 12266-12267.
35. Bruinink, C. M.; Nijhuis, C. A.; Péter, M.; Dordi, B.; Crespo-Biel, O.; Auletta, T.; Mulder, A.; Schönherr, H.; Vancso, G. J.; Huskens, J.; Reinhoudt, D. N. *Chem. Eur. J.* **2005**, *11*, 3988-3996.
36. Motesharei, K.; Myles, D. C. *J. Am. Chem. Soc.* **1998**, *120*, 7328-7336.
37. García-López, J. J.; Zapotoczny, S.; Timmerman, P.; Van Veggel, F. C. J. M.; Vancso, G. J. ; Crego-Calama, M.; Reinhoudt, D. N. *Chem. Commun.* **2003**, 352-353.
38. Banerjee, I. A.; Yu, L. T.; Matsui, H. *J. Am. Chem. Soc.* **2003**, *125*, 9542-9543.
39. Chen, Y. F.; Banerjee, I. A.; Yu, L.; Djalali, R.; Matsui, H. *Langmuir* **2004**, *20*, 8409-8413.
40. Samitsu, S.; Shimomura, T.; Ito, K.; Hara, M. *Appl. Phys. Lett.* **2004**, *85*, 3875-3877.
41. Norsten, T. B.; Jeoung, E.; Thibault, R. J.; Rotello, V. M. *Langmuir* **2003**, *19*, 7089-7093.
42. Corbellini, F.; Mulder, A.; Sartori, A.; Ludden, M. J. W.; Casnati, A.; Ungaro, R.; Huskens, J.; Crego-Calama, M.; Reinhoudt, D. N. *J. Am. Chem. Soc.* **2004**, *126*, 17050-17058.
43. Ito, Y.; Park, Y. S.; Imanishi, Y. *J. Am. Chem. Soc.* **1997**, *119*, 2739-2740.
44. Chen, C. S.; Mrksich, M.; Huang, S.; Whitesides, G. M.; Ingber, D. E. *Science* **1997**, *276*, 1425-1428.
45. Haupt, K.; Mosbach, K. *Chem. Rev.* **2000**, *100*, 2495-2504.
46. Chen, G. P.; Ushida, T.; Tateishi, T. *Macromol. Biosci.* **2002**, *2*, 67-77.

47. Metallo, S. J.; Kane, R. S.; Holmlin, R. E.; Whitesides, G. M. *J. Am. Chem. Soc.* **2003**, *125*, 4534-4540.
48. Norsten, T. B.; Frankamp, B. L.; Rotello, V. M. *Nano Lett.* **2002**, *2*, 1345-1348.
49. Sanyal, A.; Norsten, T. B.; Uzun, O.; Rotello, V. M. *Langmuir* **2004**, *20*, 5958-5964.
50. Park, J. S.; Lee, G. S.; Lee, Y. J.; Park, Y. S.; Yoon, K. B. *J. Am. Chem. Soc.* **2002**, *124*, 13366-13367.
51. Hatano, T.; Ikeda, A.; Akiyama, T.; Yamada, S.; Sano, M.; Kanekiyo, Y.; Shinkai, S. *J. Chem. Soc., Perkin Trans. 2* **2000**, *5*, 909-912.
52. Huisman, B. H.; Rudkevich, D. M.; Van Veggel, F. C. J. M.; Reinhoudt, D. N. *J. Am. Chem. Soc.* **1996**, *118*, 3523-3524.
53. Levi, S. A.; Guatteri, P.; Van Veggel, F. C. J. M.; Vancso, G. J.; Dalcanale, E.; Reinhoudt, D. N. *Angew. Chem. Int. Ed.* **2001**, *40*, 1892-1896.
54. Menozzi, E.; Pinalli, R.; Speets, E. A.; Ravoo, B. J.; Dalcanale, E.; Reinhoudt, D. N. *Chem. Eur. J.* **2004**, *10*, 2199-2206.
55. Fendler, J. H. *Nanoparticles and Nanostructured Films: Preparation, Characterization and Applications*; Wiley-VCH: Weinheim, Germany, **1998**.
56. Shipway, A. N.; Katz, E.; Willner, I. *ChemPhysChem* **2000**, *1*, 18-52.
57. Wang, D. Y.; Möhwald, H. *J. Mater. Chem.* **2004**, *14*, 459-468.
58. Zhu, T.; Fu, X. Y.; Mu, T.; Wang, J.; Liu, Z. F. *Langmuir* **1999**, *15*, 5197-5199.
59. Chen, K. M.; Jiang, X. P.; Kimerling, L. C.; Hammond, P. T. *Langmuir* **2000**, *16*, 7825-7834.
60. Auer, F.; Scotti, M.; Ulman, A.; Jordan, R.; Sellergren, B.; Garno, J.; Liu, G. Y. *Langmuir* **2000**, *16*, 7554-7557.
61. Gole, A.; Sainkar, S. R.; Sastry, M. *Chem. Mater.* **2000**, *12*, 1234-1239.
62. Gole, A.; Orendorff, C. J.; Murphy, C. J. *Langmuir* **2004**, *20*, 7117-7122.
63. Bhat, R. R.; Fischer, D. A.; Genzer, J. *Langmuir* **2002**, *18*, 5640-5643.
64. Maoz, R.; Cohen, S. R.; Sagiv, J. *Adv. Mater.* **1999**, *11*, 55-61.
65. Maoz, R.; Frydman, E.; Cohen, S. R.; Sagiv, J. *Adv. Mater.* **2000**, *12*, 725-731.
66. Hoeppener, S.; Maoz, R.; Cohen, S. R.; Chi, L. F.; Fuchs, H.; Sagiv, J. *Adv. Mater.* **2002**, *14*, 1036-1041.
67. Liu, S. T.; Maoz, R.; Schmid, G.; Sagiv, J. *Nano Lett.* **2002**, *2*, 1055-1060.
68. Liu, S. T.; Maoz, R.; Sagiv, J. *Nano Lett.* **2004**, *4*, 845-851.
69. Wouters, D.; Schubert, U. S. *J. Mater. Chem.* **2005**, *15*, 2353-2355.
70. Hoeppener, S.; Schubert, U. S. *Small* **2005**, *1*, 628-632.

71. Tanaka, H.; Mitsuishi, M.; Miyashita, T. *Langmuir* **2003**, *19*, 3103-3105.
72. Bhat, R. R.; Genzer, J.; Chaney, B. N.; Sugg, H. W.; Liebmann-Vinson, A. *Nanotechnology* **2003**, *14*, 1145-1152.
73. Maury, P.; Péter, M.; Mahalingam, V.; Reinhoudt, D. N.; Huskens, J. *Adv. Funct. Mater.* **2005**, *15*, 451-457.
74. Peng, Z. Q.; Qu, X. H.; Dong, S. J. *Langmuir* **2004**, *20*, 5-10.
75. Ryan, D.; Nagle, L.; Fitzmaurice, D. *Nano Lett.* **2004**, *4*, 573-575.
76. Mahalingam, V.; Onclin, S.; Péter, M.; Ravoo, B. J.; Huskens, J.; Reinhoudt, D. N. *Langmuir* **2004**, *20*, 11756-11762.
77. Zirbs, R.; Kienberger, F.; Hinterdorfer, P.; Binder, W. H. *Langmuir* **2005**, *21*, 8414-8421.
78. Katz, E.; Willner, I. *Angew. Chem. Int. Ed.* **2004**, *43*, 6042-6108.
79. Rosi, N. L.; Mirkin, C. A. *Chem. Rev.* **2005**, *105*, 1547-1562.
80. Niemeyer, C. M.; Ceyhan, B.; Hazarika, P. *Angew. Chem. Int. Ed.* **2003**, *42*, 5766-5770.
81. Niemeyer, C. M.; Ceyhan, B.; Noyong, M.; Simon, U. *Biochem. Biophys. Res. Commun.* **2003**, *311*, 995-999.
82. Taton, T. A.; Mucic, R. C.; Mirkin, C. A.; Letsinger, R. L. *J. Am. Chem. Soc.* **2000**, *122*, 6305-6306.
83. Niemeyer, C. M.; Ceyhan, B. *Angew. Chem. Int. Ed.* **2001**, *40*, 3685-3688.
84. Le, J. D.; Pinto, Y.; Seeman, N. C.; Musier-Forsyth, K.; Taton, T. A.; Kiehl, R. A. *Nano Lett.* **2004**, *4*, 2343-2347.
85. Mbindyo, J. K. N.; Reiss, B. D.; Martin, B. R.; Keating, C. D.; Natan, M. J.; Mallouk, T. E. *Adv. Mater.* **2001**, *13*, 249-254.
86. Niemeyer, C. M.; Ceyhan, B.; Gao, S.; Chi, L.; Peschel, S.; Simon, U. *Colloid Polym. Sci.* **2001**, *279*, 68-72.
87. Demers, L. M.; Park, S. J.; Taton, T. A.; Li, Z.; Mirkin, C. A. *Angew. Chem. Int. Ed.* **2001**, *40*, 3071-3073.
88. Demers, L. M.; Ginger, D. S.; Park, S. J.; Li, Z.; Chung, S. W.; Mirkin, C. A. *Science* **2002**, *296*, 1836-1838.
89. Lee, K. B.; Lim, J. H.; Mirkin, C. A. *J. Am. Chem. Soc.* **2003**, *125*, 5588-5589.
90. Decher, G. *Science* **1997**, *277*, 1232-1237.
91. Decher, G.; Schlenoff, J. B. *Multilayer Thin Films*; Wiley: Weinheim, Germany, 2003.
92. Hammond, P. T. *Adv. Mater.* **2004**, *16*, 1271-1293.
93. Stockton, W. B.; Rubner, M. F. *Macromolecules* **1997**, *30*, 2717-2725.
94. Wang, X. Q.; Naka, K.; Itoh, H.; Uemura, T.; Chujo, Y. *Macromolecules* **2003**, *36*, 533-

535.

95. Li, D.; Jiang, Y. D.; Wu, Z. M.; Chen, X. D.; Li, Y. R. *Thin Solid Films* **2000**, *360*, 24-27.
96. Hatzor, A.; Moav, T.; Cohen, H.; Matlis, S.; Libman, J.; Vaskevich, A.; Shanzer, A.; Rubinstein, I. *J. Am. Chem. Soc.* **1998**, *120*, 13469-13477.
97. Serizawa, T.; Hashiguchi, S.; Akashi, M. *Langmuir* **1999**, *15*, 5363-5368.
98. Kohli, P.; Blanchard, G. J. *Langmuir* **2000**, *16*, 8518-8524.
99. Anzai, J.; Kobayashi, Y. *Langmuir* **2000**, *16*, 2851-2856.
100. Suzuki, I.; Egawa, Y.; Mizukawa, Y.; Hoshi, T.; Anzai, J. *Chem. Commun.* **2002**, 164-165.
101. Zhou, Y. L.; Li, Z.; Hu, N. F.; Zeng, Y. H.; Rusling, J. F. *Langmuir* **2002**, *18*, 8573-8579.
102. Shen, Y.; Liu, J. Y.; Jiang, J. G.; Liu, B. F.; Dong, S. J. *J. Phys. Chem. B* **2003**, *107*, 9744-9748.
103. Olek, M.; Ostrander, J.; Jurga, S.; Möhwald, H.; Kotov, N.; Kempa, K.; Giersig, M. *Nano Lett.* **2004**, *4*, 1889-1895.
104. Dan, N. *Nano Lett.* **2003**, *3*, 823-827.
105. Panchagnula, V.; Kumar, C. V.; Rusling, J. F. *J. Am. Chem. Soc.* **2002**, *124*, 12515-12521.
106. Johnston, A. P. R.; Read, E. S.; Caruso, F. *Nano Lett.* **2005**, *5*, 953-956.
107. Picart, C.; Lavalle, P.; Hubert, P.; Cuisinier, F. J. G.; Decher, G.; Schaaf, P.; Voegel, J. C. *Langmuir* **2001**, *17*, 7414-7424.
108. Tian, S. J.; Liu, J. Y.; Zhu, T.; Knoll, W. *Chem. Mater.* **2004**, *16*, 4103-4108.
109. Kulesza, P. J.; Chojak, M.; Karnicka, K.; Miecznikowski, K.; Palys, B.; Lewera, A.; Wieckowski, A. *Chem. Mater.* **2004**, *16*, 4128-4134.
110. Ferreyra, N.; Coche-Guerente, L.; Fatisson, J.; Teijelo, M. L.; Labbe, P. *Chem. Commun.* **2003**, 2056-2057.
111. Goulet, P. J. G.; Dos Santos, D. S.; Álvarez-Puebla, R. A.; Oliveira, O. N.; Aroca, R. F. *Langmuir* **2005**, *21*, 5576-5581.
112. Esumi, K.; Akiyama, S.; Yoshimura, T. *Langmuir* **2003**, *19*, 7679-7681.
113. Baum, T.; Bethell, D.; Brust, M.; Schiffrin, D. J. *Langmuir* **1999**, *15*, 866-871.
114. Musick, M. D.; Keating, C. D.; Lyon, L. A.; Botsko, S. L.; Pena, D. J.; Holliway, W. D.; Mcevoy, T. M.; Richardson, J. N.; Natan, M. J. *Chem. Mater.* **2000**, *12*, 2869-2881.
115. Zamborini, F. P.; Hicks, J. F.; Murray, R. W. *J. Am. Chem. Soc.* **2000**, *122*, 4514-4515.
116. Templeton, A. C.; Zamborini, F. P.; Wuelfing, W. P.; Murray, R. W. *Langmuir* **2000**, *16*, 6682-6688.
117. Wuelfing, W. P.; Zamborini, F. P.; Templeton, A. C.; Wen, X. G.; Yoon, H.; Murray, R. W. *Chem. Mater.* **2001**, *13*, 87-95.

118. Zamborini, F. P.; Leopold, M. C.; Hicks, J. F.; Kulesza, P. J.; Malik, M. A.; Murray, R. W. *J. Am. Chem. Soc.* **2002**, *124*, 8958-8964.
119. Chen, S. W.; Pei, R. J.; Zhao, T. F.; Dyer, D. J. *J. Phys. Chem. B* **2002**, *106*, 1903-1908.
120. Wanunu, M.; Popovitz-Biro, R.; Cohen, H.; Vaskevich, A.; Rubinstein, I. *J. Am. Chem. Soc.* **2005**, *127*, 9207-9215.
121. Mamedov, A. A.; Belov, A.; Giersig, M.; Mamedova, N. N.; Kotov, N. A. *J. Am. Chem. Soc.* **2001**, *123*, 7738-7739.
122. Donath, E.; Sukhorukov, G. B.; Caruso, F.; Davis, S. A.; Möhwald, H. *Angew. Chem. Int. Ed.* **1998**, *37*, 2202-2205.
123. Sukhorukov, G. B. ; Donath, E.; Davis, S.; Lichtenfeld, H.; Caruso, F.; Popov, V. I.; Möhwald, H. *Polym. Adv. Technol.* **1998**, *9*, 759-767.
124. Caruso, F.; Caruso, R. A.; Möhwald, H. *Science* **1998**, *282*, 1111-1114.
125. Kaltenpoth, G.; Himmelhaus, M.; Slansky, L.; Caruso, F.; Grunze, M. *Adv. Mater.* **2003**, *15*, 1113-1118.
126. Salgueiriño-Maceira, V.; Caruso, F.; Liz-Marzán, L. M. *J. Phys. Chem. B* **2003**, *107*, 10990-10994.
127. Caruso, F.; Caruso, R. A.; Möhwald, H. *Chem. Mater.* **1999**, *11*, 3309-3314.
128. Aliev, F. G.; Correa-Duarte, M. A.; Mamedov, A.; Ostrander, J. W.; Giersig, M.; Liz-Marzán, L. M.; Kotov, N. A. *Adv. Mater.* **1999**, *11*, 1006-1010.
129. Khopade, A. J.; Möhwald, H. *Adv. Funct. Mater.* **2005**, *15*, 1088-1094.
130. Caruso, F.; Möhwald, H. *J. Am. Chem. Soc.* **1999**, *121*, 6039-6046.
131. Caruso, F. *Adv. Mater.* **2001**, *13*, 11-22.
132. Schneider, G.; Decher, G. *Nano Lett.* **2004**, *4*, 1833-1839.
133. Yu, A. M.; Wang, Y. J.; Barlow, E.; Caruso, F. *Adv. Mater.* **2005**, *17*, 1737-1741.
134. Rogach, A.; Susha, A.; Caruso, F.; Sukhorukov, G.; Kornowski, A.; Kershaw, S.; Möhwald, H.; Eychmuller, A.; Weller, H. *Adv. Mater.* **2000**, *12*, 333-337.
135. Hong, X.; Li, J.; Wang, M. J.; Xu, J. J.; Guo, W.; Li, J. H.; Bai, Y. B.; Li, T. J. *Chem. Mater.* **2004**, *16*, 4022-4027.
136. Georgieva, R.; Moya, S.; Donath, E.; Baümler, H. *Langmuir* **2004**, *20*, 1895-1900.
137. Lu, G.; Ai, S.; Li, J. B. *Langmuir* **2005**, *21*, 1679-1682.
138. Volodkin, D. V.; Petrov, A. I.; Prevot, M.; Sukhorukov, G. B. *Langmuir* **2004**, *20*, 3398-3406.
139. Clark, S. L.; Montague, M.; Hammond, P. T. *Supramol. Sci.* **1997**, *4*, 141-146.
140. Clark, S. L.; Montague, M. F.; Hammond, P. T. *Macromolecules* **1997**, *30*, 7237-7244.

141. Jiang, X. P.; Clark, S. L.; Hammond, P. T. *Adv. Mater.* **2001**, *13*, 1669-1673.
142. Clark, S. L.; Hammond, P. T. *Adv. Mater.* **1998**, *10*, 1515-1519.
143. Pallandre, A.; Glinel, K.; Jonas, A. M.; Nysten, B. *Nano Lett.* **2004**, *4*, 365-371.
144. Shi, F.; Dong, B.; Qiu, D. L.; Sun, J. Q.; Wu, T.; Zhang, X. *Adv. Mater.* **2002**, *14*, 805-809.
145. Li, Q.; Ouyang, J. H.; Chen, J. Y.; Zhao, X. S.; Cao, W. X. *J. Polym. Sci., Part A: Polym. Chem.* **2002**, *40*, 222-228.
146. Shi, F.; Wang, Z. Q.; Zhao, N.; Zhang, X. *Langmuir* **2005**, *21*, 1599-1602.
147. Lu, C. H.; Wu, N. Z.; Wei, F.; Zhao, X. S.; Jiao, X. M.; Xu, J.; Luo, C. Q.; Cao, W. X. *Adv. Funct. Mater.* **2003**, *13*, 548-552.
148. Cao, T. B.; Wei, F.; Jiao, X. M.; Chen, J. Y.; Liao, W.; Zhao, X.; Cao, W. X. *Langmuir* **2003**, *19*, 8127-8129.
149. Hua, F.; Cui, T. H.; Lvov, Y. *Langmuir* **2002**, *18*, 6712-6715.
150. Hua, F.; Shi, J.; Lvov, Y.; Cui, T. *Nano Lett.* **2002**, *2*, 1219-1222.
151. Park, J.; Hammond, P. T. *Adv. Mater.* **2004**, *16*, 520-525.
152. Menard, E.; Bilhaut, L.; Zaumseil, J.; Rogers, J. A. *Langmuir* **2004**, *20*, 6871-6878.
153. Jiang, X. P.; Zheng, H. P.; Gourdin, S.; Hammond, P. T. *Langmuir* **2002**, *18*, 2607-2615.
154. Zheng, H. P.; Rubner, M. F.; Hammond, P. T. *Langmuir* **2002**, *18*, 4505-4510.
155. Zheng, H. P.; Lee, I.; Rubner, M. F.; Hammond, P. T. *Adv. Mater.* **2002**, *14*, 569-572.
156. Lee, I.; Zheng, H. P.; Rubner, M. F.; Hammond, P. T. *Adv. Mater.* **2002**, *14*, 572-577.
157. Kim, H.; Doh, J.; Irvine, D. J.; Cohen, R. E.; Hammond, P. T. *Biomacromolecules* **2004**, *5*, 822-827.
158. Zheng, H. P.; Berg, M. C.; Rubner, M. F.; Hammond, P. T. *Langmuir* **2004**, *20*, 7215-7222.
159. Feng, J.; Wang, B.; Gao, C. Y.; Shen, J. C. *Adv. Mater.* **2004**, *16*, 1940-1944.
160. Lee, I. S.; Hammond, P. T.; Rubner, M. F. *Chem. Mater.* **2003**, *15*, 4583-4589.
161. Templeton, A. C.; Wuelfing, M. P.; Murray, R. W. *Acc. Chem. Res.* **2000**, *33*, 27-36.
162. Shenhar, R.; Rotello, V. M. *Acc. Chem. Res.* **2003**, *36*, 549-561.
163. Daniel, M. C.; Astruc, D. *Chem. Rev.* **2004**, *104*, 293-346.
164. Trindade, T.; O'Brien, P.; Pickett, N. L. *Chem. Mater.* **2001**, *13*, 3843-3858.
165. Raimondi, F.; Scherer, G. G.; Kotz, R.; Wokaun, A. *Angew. Chem. Int. Ed.* **2005**, *44*, 2190-2209.
166. Niemeyer, C. M. *Angew. Chem. Int. Ed.* **2001**, *40*, 4128-4158.
167. Tang, Z. Y.; Kotov, N. A. *Adv. Mater.* **2005**, *17*, 951-962.
168. Aherne, D.; Rao, S. N.; Fitzmaurice, D. *J. Phys. Chem. B* **1999**, *103*, 1821-1825.
169. Boal, A. K.; Ilhan, F.; Derouchey, J. E.; Thurn-Albrecht, T.; Russell, T. P.; Rotello, V. M.

Nature **2000**, *404*, 746-748.

170. Shenhar, R.; Norsten, T. B.; Rotello, V. M. *Adv. Mater.* **2005**, *17*, 657-669.
171. Deans, R.; Ilhan, F.; Rotello, V. M. *Macromolecules* **1999**, *32*, 4956-4960.
172. Frankamp, B. L.; Uzun, O.; Ilhan, F.; Boal, A. K.; Rotello, V. M. *J. Am. Chem. Soc.* **2002**, *124*, 892-893.
173. Carroll, J. B.; Frankamp, B. L.; Rotello, V. M. *Chem. Commun.* **2002**, 1892-1893.
174. Boal, A. K.; Frankamp, B. L.; Uzun, O.; Tuominen, M. T.; Rotello, V. M. *Chem. Mater.* **2004**, *16*, 3252-3256.
175. Zheng, W. X.; Maye, M. M.; Leibowitz, F. L.; Zhong, C. J. *Anal. Chem.* **2000**, *72*, 2190-2199.
176. Boal, A. K.; Rotello, V. M. *Langmuir* **2000**, *16*, 9527-9532.
177. Fullam, S.; Rao, S. N.; Fitzmaurice, D. *J. Phys. Chem. B* **2000**, *104*, 6164-6173.
178. Álvarez, J.; Liu, J.; Román, E.; Kaifer, A. E. *Chem. Commun.* **2000**, 1151-1152.
179. Liu, J.; Álvarez, J.; Ong, W.; Román, E.; Kaifer, A. E. *Langmuir* **2001**, *17*, 6762-6764.
180. Strimbu, L.; Liu, J.; Kaifer, A. E. *Langmuir* **2003**, *19*, 483-485.
181. Liu, J.; Ong, W.; Kaifer, A. E.; Peinador, C. *Langmuir* **2002**, *18*, 5981-5983.
182. Liu, J.; Mendoza, S.; Román, E.; Lynn, M. J.; Xu, R. L.; Kaifer, A. E. *J. Am. Chem. Soc.* **1999**, *121*, 4304-4305.
183. Liu, J.; Álvarez, J.; Ong, W.; Kaifer, A. E. *Nano Lett.* **2001**, *1*, 57-60.
184. Fitzmaurice, D.; Rao, S. N.; Preece, J. A.; Stoddart, J. F.; Wenger, S.; Zaccheroni, N. *Angew. Chem. Int. Ed.* **1999**, *38*, 1147-1150.
185. Ryan, D.; Rao, S. N.; Rensmo, H.; Fitzmaurice, D.; Preece, J. A.; Wenger, S.; Stoddart, J. F.; Zaccheroni, N. *J. Am. Chem. Soc.* **2000**, *122*, 6252-6257.
186. Ryan, D.; Nagle, L.; Rensmo, H.; Fitzmaurice, D. *J. Phys. Chem. B* **2002**, *106*, 5371-5377.
187. Leininger, S.; Olenyuk, B.; Stang, P. J. *Chem. Rev.* **2000**, *100*, 853-907.
188. Kim, Y. J.; Johnson, R. C.; Hupp, J. T. *Nano Lett.* **2001**, *1*, 165-167.
189. Obare, S. O.; Hollowell, R. E.; Murphy, C. J. *Langmuir* **2002**, *18*, 10407-10410.
190. Lin, S. Y.; Liu, S. W.; Lin, C. M.; Chen, C. H. *Anal. Chem.* **2002**, *74*, 330-335.
191. Galow, T. H.; Boal, A. K.; Rotello, V. M. *Adv. Mater.* **2000**, *12*, 576-579.
192. Boal, A. K.; Galow, T. H.; Ilhan, F.; Rotello, V. M. *Adv. Funct. Mater.* **2001**, *11*, 461-465.
193. Kolny, J.; Kornowski, A.; Weller, H. *Nano Lett.* **2002**, *2*, 361-364.
194. Carroll, J. B.; Frankamp, B. L.; Srivastava, S.; Rotello, V. M. *J. Mater. Chem.* **2004**, *14*, 690-694.
195. Wang, X. Q.; Naka, K.; Itoh, H.; Chujo, Y. *Chem. Lett.* **2004**, *33*, 216-217.

196. Zhong, Z. Y.; Patskovskyy, S.; Bouvrette, P.; Luong, J. H. T.; Gedanken, A. *J. Phys. Chem. B* **2004**, *108*, 4046-4052.
197. Zhong, Z. Y.; Subramanian, A. S.; Highfield, J.; Carpenter, K.; Gedanken, A. *Chem. Eur. J.* **2005**, *11*, 1473-1478.
198. Zhong, Z. Y.; Luo, J. Z.; Ang, T. P.; Highfield, J.; Lin, J. Y.; Gedanken, A. *J. Phys. Chem. B* **2004**, *108*, 18119-18123.
199. Selvakannan, P. R.; Mandal, S.; Phadtare, S.; Pasricha, R.; Sastry, M. *Langmuir* **2003**, *19*, 3545-3549.
200. Hiramatsu, H.; Osterloh, F. E. *Langmuir* **2003**, *19*, 7003-7011.
201. Shipway, A. N.; Lahav, M.; Gabai, R.; Willner, I. *Langmuir* **2000**, *16*, 8789-8795.
202. Adachi, E. *Langmuir* **2000**, *16*, 6460-6463.
203. Murray, C. B.; Kagan, C. R.; Bawendi, M. G. *Annu. Rev. Mater. Sci.* **2000**, *30*, 545-610.
204. Frankamp, B. L.; Boal, A. K.; Rotello, V. M. *J. Am. Chem. Soc.* **2002**, *124*, 15146-15147.
205. Srivastava, S.; Frankamp, B. L.; Rotello, V. M. *Chem. Mater.* **2005**, *17*, 487-490.
206. Frankamp, B. L.; Boal, A. K.; Tuominen, M. T.; Rotello, V. M. *J. Am. Chem. Soc.* **2005**, *127*, 9731-9735.
207. Naka, K.; Itoh, H.; Chujo, Y. *Langmuir* **2003**, *19*, 5496-5501.
208. Naka, K.; Itoh, H.; Chujo, Y. *Bull. Chem. Soc. Jpn.* **2005**, *78*, 501-505.
209. Brust, M.; Kiely, C. J.; Bethell, D.; Schiffrin, D. J. *J. Am. Chem. Soc.* **1998**, *120*, 12367-12368.
210. Hasobe, T.; Imahori, H.; Kamat, P. V.; Fukuzumi, S. *J. Am. Chem. Soc.* **2003**, *125*, 14962-14963.
211. Jin, J.; Iyoda, T.; Cao, C. S.; Song, Y. L.; Jiang, L.; Li, T. J.; Ben Zhu, D. *Angew. Chem. Int. Ed.* **2001**, *40*, 2135-2138.
212. Mann, S.; Shenton, W.; Li, M.; Connolly, S.; Fitzmaurice, D. *Adv. Mater.* **2000**, *12*, 147-150.
213. Hirsch, L. R.; Jackson, J. B.; Lee, A.; Halas, N. J.; West, J. *Anal. Chem.* **2003**, *75*, 2377-2381.
214. Nam, J. M.; Park, S. J.; Mirkin, C. A. *J. Am. Chem. Soc.* **2002**, *124*, 3820-3821.
215. Perez, J. M.; Simeone, F. J.; Saeki, Y.; Josephson, L.; Weissleder, R. *J. Am. Chem. Soc.* **2003**, *125*, 10192-10193.
216. Weber, P. C.; Ohlendorf, D. H.; Wendoloski, J. J.; Salemme, F. R. *Science* **1989**, *243*, 85-88.
217. Connolly, S.; Fitzmaurice, D. *Adv. Mater.* **1999**, *11*, 1202-1205.

218. Caswell, K. K.; Wilson, J. N.; Bunz, U. H. F.; Murphy, C. J. *J. Am. Chem. Soc.* **2003**, *125*, 13914-13915.
219. Li, M.; Wong, K. K. W.; Mann, S. *Chem. Mater.* **1999**, *11*, 23-26.
220. Shenton, W.; Davis, S. A.; Mann, S. *Adv. Mater.* **1999**, *11*, 449-452.
221. Wang, S. P.; Mamedova, N.; Kotov, N. A.; Chen, W.; Studer, J. *Nano Lett.* **2002**, *2*, 817-822.
222. De La Fuente, J. M.; Barrientos, A. G.; Rojas, T. C.; Rojo, J.; Canada, J.; Fernández, A.; Penadés, S. *Angew. Chem. Int. Ed.* **2001**, *40*, 2257-2261.
223. Barrientos, A. G.; De La Fuente, J. M.; Rojas, T. C.; Fernández, A.; Penadés, S. *Chem. Eur. J.* **2003**, *9*, 1909-1921.
224. Rojas, T. C.; De La Fuente, J. M.; Barrientos, A. G.; Penadés, S.; Ponsonnet, L.; Fernández, A. *Adv. Mater.* **2002**, *14*, 585-588.
225. Samori, B.; Zuccheri, G. *Angew. Chem. Int. Ed.* **2005**, *44*, 1166-1181.
226. Storhoff, J. J.; Mirkin, C. A. *Chem. Rev.* **1999**, *99*, 1849-1862.
227. Elghanian, R.; Storhoff, J. J.; Mucic, R. C.; Letsinger, R. L.; Mirkin, C. A. *Science* **1997**, *277*, 1078-1081.
228. Storhoff, J. J.; Elghanian, R.; Mucic, R. C.; Mirkin, C. A.; Letsinger, R. L. *J. Am. Chem. Soc.* **1998**, *120*, 1959-1964.
229. Reynolds, R. A.; Mirkin, C. A.; Letsinger, R. L. *J. Am. Chem. Soc.* **2000**, *122*, 3795-3796.
230. Storhoff, J. J.; Lazarides, A. A.; Mucic, R. C.; Mirkin, C. A.; Letsinger, R. L.; Schatz, G. C. *J. Am. Chem. Soc.* **2000**, *122*, 4640-4650.
231. Jin, R. C.; Wu, G. S.; Li, Z.; Mirkin, C. A.; Schatz, G. C. *J. Am. Chem. Soc.* **2003**, *125*, 1643-1654.
232. Park, S. J.; Lazarides, A. A.; Mirkin, C. A.; Brazis, P. W.; Kannewurf, C. R.; Letsinger, R. L. *Angew. Chem. Int. Ed.* **2000**, *39*, 3845-3848.
233. Liu, J. W.; Lu, Y. *Anal. Chem.* **2004**, *76*, 1627-1632.
234. Liu, J. W.; Lu, Y. *J. Am. Chem. Soc.* **2003**, *125*, 6642-6643.
235. Mirkin, C. A.; Letsinger, R. L.; Mucic, R. C.; Storhoff, J. J. *Nature* **1996**, *382*, 607-609.
236. Mucic, R. C.; Storhoff, J. J.; Mirkin, C. A.; Letsinger, R. L. *J. Am. Chem. Soc.* **1998**, *120*, 12674-12675.
237. Claridge, S. A.; Goh, S. L.; Frechet, J. M. J.; Williams, S. C.; Micheel, C. M.; Alivisatos, A. P. *Chem. Mater.* **2005**, *17*, 1628-1635.
238. Kanaras, A. G.; Wang, Z. X.; Bates, A. D.; Cosstick, R.; Brust, M. *Angew. Chem. Int. Ed.* **2003**, *42*, 191-194.

239. Park, S. J.; Lazarides, A. A.; Storhoff, J. J.; Pesce, L.; Mirkin, C. A. *J. Phys. Chem. B* **2004**, *108*, 12375-12380.
240. Alivisatos, A. P.; Johnsson, K. P.; Peng, X. G.; Wilson, T. E.; Loweth, C. J.; Bruchez, M. P.; Schultz, P. G. *Nature* **1996**, *382*, 609-611.
241. Zanchet, D.; Micheel, C. M.; Parak, W. J.; Gerion, D.; Williams, S. C.; Alivisatos, A. P. *J. Phys. Chem. B* **2002**, *106*, 11758-11763.
242. Sadasivan, S.; Dujardin, E.; Li, M.; Johnson, C. J.; Mann, S. *Small* **2005**, *1* , 103-106.
243. Mitchell, G. P.; Mirkin, C. A.; Letsinger, R. L. *J. Am. Chem. Soc.* **1999**, *121*, 8122-8123.
244. Cobbe, S.; Connolly, S.; Ryan, D.; Nagle, L.; Eritja, R.; Fitzmaurice, D. *J. Phys. Chem. B* **2003**, *107*, 470-477.
245. Niemeyer, C. M.; Burger, W.; Peplies, J. *Angew. Chem. Int. Ed.* **1998**, *37*, 2265-2268.
246. Park, S. J.; Lazarides, A. A.; Mirkin, C. A.; Letsinger, R. L. *Angew. Chem. Int. Ed.* **2001**, *40*, 2909-2912.
247. Chakrabarti, R.; Klibanov, A. M. *J. Am. Chem. Soc.* **2003**, *125*, 12531-12540.
248. Levy, R.; Thanh, N. T. K.; Doty, R. C.; Hussain, I.; Nichols, R. J.; Schiffrin, D. J.; Brust, M.; Fernig, D. G. *J. Am. Chem. Soc.* **2004**, *126*, 10076-10084.

Chapter 3

Multivalent Host-Guest Interactions between Cyclodextrin Self-Assembled Monolayers and Poly(isobutene-*alt*-maleic acid)s Modified with Hydrophobic Guest Molecules*

The interaction of poly(isobutene-alt-maleic acid)s modified with p-tert-butylphenyl or adamantyl groups onto cyclodextrin self-assembled monolayers (CD SAMs) was studied. The adsorption was shown to be strong, specific and irreversible. Even with monovalent competitor in solution, adsorption to the CD SAMs was observed, and desorption proved impossible. The polymer adsorbed onto the CD surface as a very thin layer as evidenced by surface plasmon resonance and AFM. Apparently, all or most hydrophobic groups were employed efficiently in the multivalent binding. Supramolecular microcontact printing of the polymers onto the CD SAMs led to assembly formation in the targeted areas of the substrates.

* Part of this chapter has been published in: Crespo-Biel, O.; Péter, M.; Bruinink, C. M.; Ravoo, B. J.; Reinhoudt, D. N.; Huskens, J. *Chem. Eur. J.* **2005**, *11*, 2426-2432.

3.1 Introduction

Multivalent interactions involve the simultaneous binding of multiple ligand sites on one entity to multiple receptor sites on another,[1] and can result in the formation of numerous simultaneous complexation events that afford a high functional affinity. These interactions occur throughout biology.[2] For example, processes such as cell-cell recognition often depend on the formation of multiple receptor-ligand complexes at the cell surface.[3] Multivalent ligands, in contrast to monovalent ligands, can interact with receptors via different mechanisms.[4] [5]Therefore, a conception of these mechanisms in well-defined synthetic systems will help to understand how natural systems function. The nature of the binding elements, structure of the scaffold,[6,7] number of binding groups, and density of binding elements[8-10] are some of the parameters that influence the mechanisms by which a multivalent synthetic ligand acts.[11]

Polymer systems are currently the most extensively studied[12-17] of all multivalent ligands, and serve as the prototypical system for the design of reagents for biochemistry and biology. Polymers tethered onto surfaces have been a subject of attention owing to their potential use in many surface-based devices phenomena and technologies such as switchable membranes, sensors, cell growth control, and biomimetic materials.[18-20] For example, Ravoo and co-workers studied the interaction between polymers modified with hydrophobic groups and β-cyclodextrin-modified bilayer vesicles[21-24] by means of capillary electrophoresis.[25]

Self-assembled monolayers (SAMs) of a β-cyclodextrin (CD) heptathioether adsorbate have been prepared on gold substrates[26,27] for the formation of densely packed, well-ordered SAMs,[28] the hexagonal packing of which has been visualized by atomic force microscopy (AFM).[29] The stable positioning and patterning of molecules on these SAMs by means of multiple hydrophobic interactions has been achieved. Thus, these SAMs constitute molecular printboards for the binding, organization, and local functionalization of polyvalent systems.[30,31] Moreover, the thermodynamic and kinetic stabilities of the resulting patterns can be tuned, and this has led to, for example, electrochemically induced desorption.[31]

In this chapter, the molecular recognition by CD SAMs of poly(isobutene-*alt*-maleic acid)s modified with hydrophobic *p-tert*-butylphenyl or adamantyl groups (guest polymers) is described. The multivalent noncovalent interactions of the guest polymers with the CD SAMs were investigated as a function of the nature and number of hydrophobic groups that interact with the CD surface and the intramolecular interactions within the polymer.

3.2 Results and Discussion

3.2.1 Interactions of guest polymers with CD SAMs

The guest polymers with hydrophobic *p-tert*-butylphenyl groups, BAN09 and BAN42, and adamantyl groups, ADA10 and ADA20 are shown in Chart 3.1, as well as the reference compound, poly(isobutene-*alt*-maleic acid) (PiBMA), which lacks such hydrophobic groups. Note that throughout this chapter, the concentration of guest polymers is expressed as the concentration of hydrophobic substituents.[21] CD SAMs of a CD heptathioether adsorbate (Chart 3.1) were prepared as described before.[26]

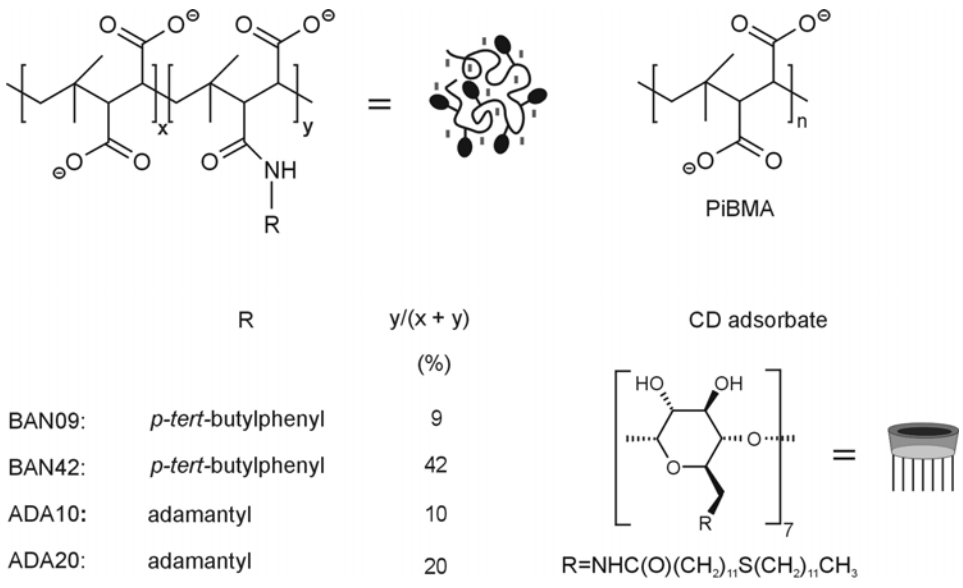

Chart 3.1: *Chemical structures of guest polymers and host adsorbate used in this study.*

Binding of the guest polymers to CD SAMs was studied by surface plasmon resonance (SPR) spectroscopy.[32] SPR titrations were performed in the presence of 10 mM phosphate buffer. As illustrated in Figure 3.1, an SPR angle change was observed after injection of an aqueous solution of BAN09 (A), indicative of adsorption. The adsorption was followed for 30 min showing an increase of 0.11°. Rinsing with a 10 mM phosphate buffer solution (B) reduced the angle change to about 0.05°. Extensive rinsing of the cell with buffer (B) and with 8 mM β-CD (C) did not completely restore the signal to the baseline. Subsequent polymer additions showed smaller angle changes, and extensive rinsing always led back to the ~0.05° angle change obtained during the first addition.

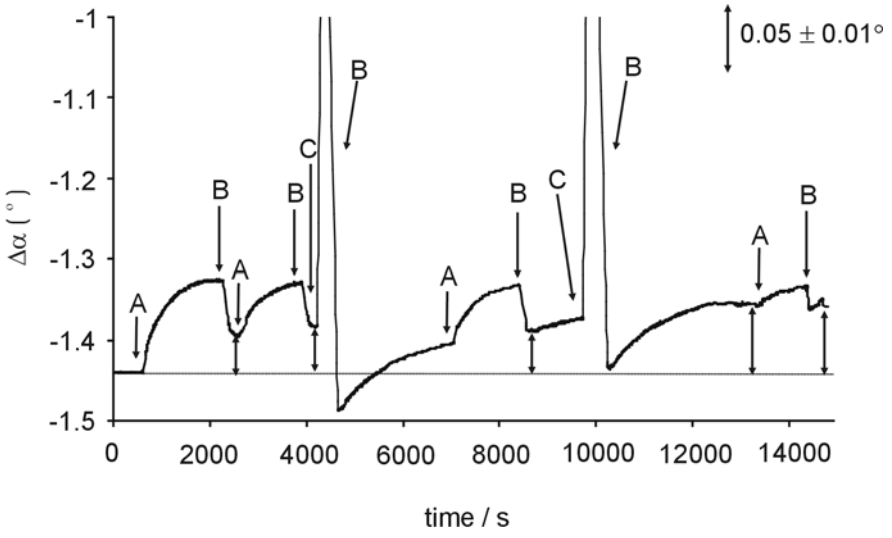

Figure 3.1: *Surface plasmon resonance (SPR) spectroscopy time traces of the adsorption and attempted desorption of BAN09 (0.025 mM in hydrophobic moieties) onto a CD SAM; solutions (all in phosphate buffer 10 mM, pH 7): A) BAN09, B) buffer, C) 8 mM CD.*

A possible interpretation is that the 0.05° angle change reflects the strong, irreversible adsorption of polymer through specific, multivalent interactions, whereas the remainder of the angle change of the first addition and the entire angle change of subsequent additions is due to non-specific adsorption. When compared to a maximal angle change of 0.09° observed for small guests such as acetamidoadamantane,[26] the

angle change of 0.05° observed here suggests that a thin layer of polymer is adsorbed with efficient use of all or most of the hydrophobic groups (upper right sketch in Figure 3.2). Similar SPR titrations were performed with the other guest polymers, ADA10, ADA20, and BAN42, and the same behavior was observed for all polymers (data not shown) suggesting a strong affinity for the CD SAMs.

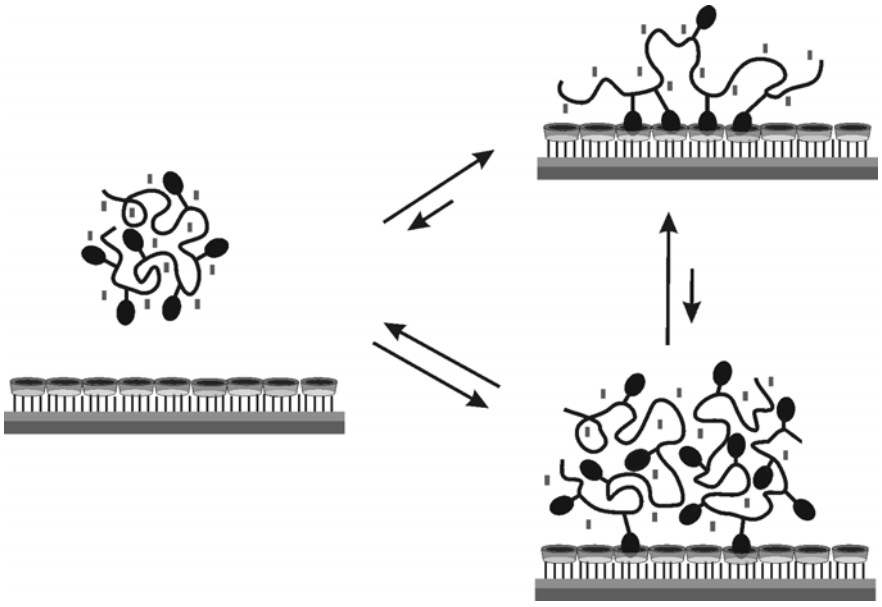

Figure 3.2: *Schematical representation of possible binding modes of guest polymers onto CD SAMs.*

Titrations performed with ADA10 on 11-mercapto-1-undecanol reference SAMs (OH SAMs) (lacking the host sites) and with PiBMA (lacking the guest sites) on CD SAMs only exhibited a small refractive index effect on the SPR signal, which could be instantaneously restored by rinsing the SAMs with the solutions indicated above. No clear adsorption or desorption traces could be recorded, thus indicating the need for specific interactions between guest polymers and CD SAMs in order to form stable assemblies.

From these results, it was concluded that the binding of guest polymers to CD-coated gold surfaces was due to the formation of inclusion complexes between adamantyl

or *p-tert*-butylphenyl groups of the guest polymers and CD sites immobilized on the SAMs, and that the binding between polymer and surface was irreversible.

The adsorption of ADA10 on CD SAMs was also studied by electrochemical impedance spectroscopy (EIS). The initial value of the charge-transfer resistance (R_{CT}) of the CD SAM using $Fe(CN)_6^{3-}/Fe(CN)_6^{4-}$ as a redox couple was 110 ± 10 kΩ, indicating a highly ordered monolayer that blocks the redox current effectively (see Table 3.1).[33] Adsorption of ADA10 from solution (0.1 mM in adamantyl moieties) resulted in an increase of R_{CT} up to 300 ± 50 kΩ due to the electrostatic repulsion between the carboxylate anions of the polymer and the redox couple. When using the positively charged $Ru(NH_3)_6^{2+}/Ru(NH_3)_6^{3+}$ as the reporter redox couple, EIS showed a decrease of the charge-transfer resistance upon adsorption of ADA10 from 47 to 24 (± 15) kΩ resulting from the electrostatic attraction between the negatively charged polymer and the positively charged redox pair. Thus, EIS confirmed the adsorption of ADA10 on the CD SAMs.

Table 3.1: *Charge-transfer resistance (R_{CT}) values for the adsorption of ADA10 onto CD SAMs as determined by electrochemical impedance spectroscopy.*

Substrate	redox couple $Fe(CN)_6^{3-}/Fe(CN)_6^{4-}$ (kΩ)	redox couple $Ru(NH_3)_6^{2+}/Ru(NH_3)_6^{3+}$ (kΩ)
CD SAM	110 ± 10	47 ± 15
CD SAM + ADA10	300 ± 50	24 ± 15

AFM was used for a direct determination of the thickness of the guest polymer film.[34,35] Adsorption of the polymer was achieved by immersion of a CD SAM in an ADA10 solution (1 mM in adamantyl functionalities), followed by rinsing with a 10 mM phosphate buffer solution. The AFM tip was used to create a scratch down to the gold, and the thickness was determined by scanning across the scratch with the AFM tip. The thickness (1.77 ± 0.03 nm) was compared to the thickness of a bare CD SAM (1.34 ± 0.03 nm). Thus, an estimate of the polymer thickness of 0.44 ± 0.06 nm was obtained. In addition, the thickness of the absorbed guest polymer layer was also estimated from

microcontact printed substrates (see below) to be about 0.50 nm, corroborating the scratching experiments.

From the diffusion coefficients of the polymers,[21] the hydrodynamic radii of the polymers in solution were estimated to be about 10 nm using the Stokes-Einstein equation. It should be emphasized that this equation assumes a spherical conformation of the polymer chains. Nevertheless, the comparison between these radii and the values for the thickness of adsorbed polymers clearly indicates that the strong binding observed in the latter case, using efficiently all or most hydrophobic groups, leads to strong stretching and flattening of the polymers when adsorbing to the β-CD SAMs (Figure 3.2, top right).

In order to evaluate the effect of the polymer concentration on the adsorption process onto the CD surface, the interaction of ADA10 with CD SAMs was studied at 1 μM, 0.1 mM, and 1 mM in adamantyl moieties. SPR titrations were performed under the same conditions as described above. For the titration at 1 μM, adsorption appeared to be very slow probably due to severe diffusion limitation. As a consequence, an exact value for the SPR angle change was difficult to determine. In contrast, titration of 0.1 mM ADA10 showed a maximum SPR angle change of 0.05°. After thorough rinsing with 10 mM phosphate buffer and 8 mM CD solution, an angle change of 0.03° remained. Similarly, titration of 1 mM ADA10 showed a maximum SPR angle change of 0.08°, indicating more non-specific adsorption at this concentration. After rinsing, a residual SPR angle change of 0.03° was observed. These experiments led to the conclusion that the mode in which guest polymers bind to the molecular printboard is not concentration dependent in this concentration range. Combined with the thickness measurements discussed above, it is concluded that the polymers bind under all conditions employed here as a thin layer, making efficient use of the hydrophobic groups, (Figure 3.2, top right), and that a more spherical adsorption (Figure 3.2, bottom right) is not observed, although it can not be excluded that this is a rapidly progressing intermediate state.

In order to verify the absence of free, uncomplexed guest moieties in adsorbed guest polymers, the binding of CD-covered gold nanoparticles (CD Au NPs) was attempted. A CD SAM was saturated with a 0.1 mM solution of ADA10. After thoroughly rinsing with phosphate buffer, the surface was exposed to a solution of 0.1 mM CD Au NPs.[36] An SPR angle change of 0.25° was observed, but after copious

rinsing with water, the SPR angle change was restored to the baseline (data not shown). It was shown before that a divalent adamantyl-CD interaction is already strong enough to prohibit dissociation by rinsing with water;[31,37,38] only upon rinsing with competing CD in solution, significant dissociation can occur. Therefore, the results shown here demonstrate that the binding of the gold nanoparticles has occurred by physisorption and/or maximally one host-guest interaction per particle.[39] In conclusion, the surface concentration of free guest sites for a substrate with ADA10 adsorbed is significantly lower than the surface concentration of adamantyl-CD complexes between the CD SAM and the polymer, which confirms that the binding of the guest polymer to the molecular printboard is efficient using most or all hydrophobic groups.

3.2.2 Competition experiments with monovalent hosts and guests

ADA10 and BAN42 were dissolved in a 10 mM phosphate buffer solution containing a high concentration of competing monovalent host (8 mM CD). In SPR titrations, SPR angle changes of 0.08° and 0.20° for ADA10 and BAN42, respectively, were observed after injection of the aqueous solution of the respective guest polymer (0.025 mM in hydrophobic moieties) (Figure 3.3). The adsorptions of ADA10 and BAN42 showed rapid kinetics (about 80% of binding after 5 min). After thorough rinsing with 8 mM CD in 10 mM phosphate buffer, approximately 0.06° and 0.12° remained, in agreement with the experiments described above. Consecutive additions of polymer did not lead to specific adsorption. These experiments confirmed our earlier statement that guest polymers are bound to CD SAMs in a strong and irreversible fashion, probably using nearly all hydrophobic groups available. The resulting assemblies even formed and remained stable at high concentrations of competing monovalent CD in solution.

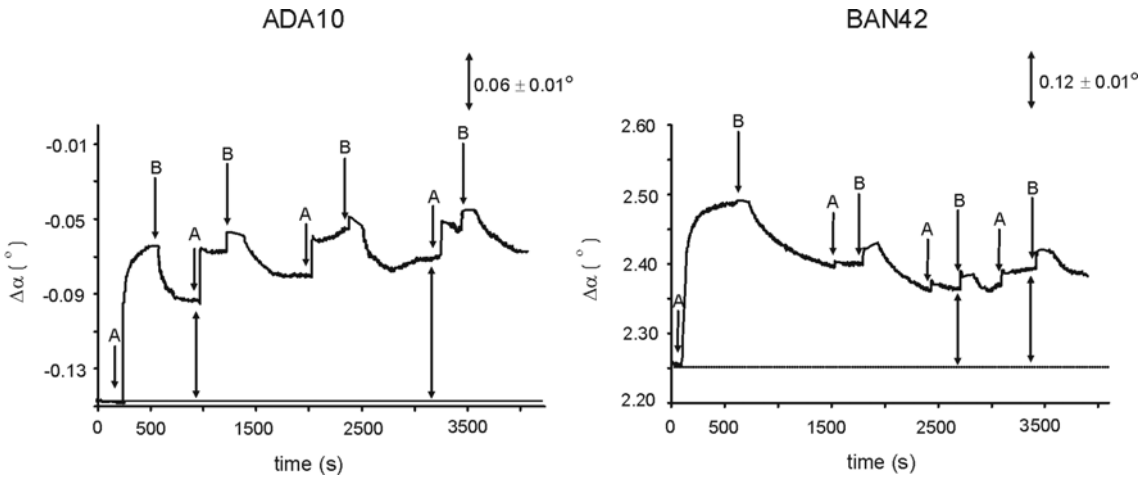

Figure 3.3: *SPR spectroscopy time traces of the adsorption and attempted desorption of ADA10 (left) and BAN42 (right) (0.025 mM in hydrophobic moieties) onto a CD SAM in competition with monovalent host in solution; solutions (all in 10 mM phosphate buffer and 8 mM CD): A) guest polymer, B) buffer with 8 mM CD.*

BAN09 was chosen to carry out SPR titrations in competition with monovalent guest in solution due its lowest number of hydrophobic groups and weakest type of interaction.[40] After adsorption of BAN09 (0.1 mM in hydrophobic moieties) to the CD SAM and rinsing with 5 mM 1-adamantylamine, an SPR angle change of 0.06° was observed (Figure 3.4). This value is comparable to the values obtained for ADA10 and BAN42 in competition with monovalent host in solution. Again, these results confirm that competition with a monovalent competitor only leads to partial desorption of material from the CD surface, but that specifically and strongly bound guest polymer remains. The material that is removed is most likely physisorbed material, but the removal of a small fraction of specifically, but weakly, bound polymer cannot be excluded.

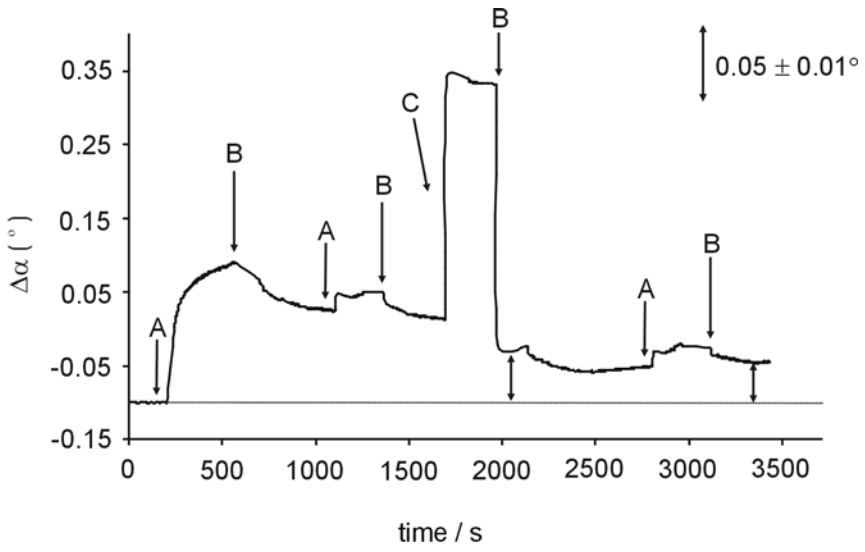

Figure 3.4: *SPR spectroscopy time traces of the adsorption and attempted desorption of BAN09 (0.025 mM in hydrophobic moieties) onto a CD SAM in competition with monovalent guest in solution; solutions (all in 10 mM phosphate buffer): A) BAN09, B) buffer, C) 5 mM 1-adamantylamine.*

In order to estimate the binding strength of the polymers to the surface quantitatively, a recently developed model for multivalent interactions at interfaces was applied.[37,38] This model employs an effective concentration parameter, C_{eff}, which represents the concentration of free, uncomplexed surface host sites experienced by a non-complexed guest site connected to a surface-bound guest site by a linker. Thus, C_{eff} is surface coverage-dependent, and is assumed to be independent of the number of binding sites of the guest but only dependent on its molecular geometry (linker length, stiffness, etc.) and the number of host sites that a non-attached guest site can reach at the surface.

Table 3.2 gives estimates of the maximal C_{eff} values (reached at low surface coverages) as determined from the linker lengths,[37] which were assumed equal to the average distances between hydrophobic groups in the guest polymers based on the extended conformation of the polymer backbone (see Figure 3.5). In our case the $C_{eff,max}$ for the different polymers was calculated to be 0.15 - 0.35 M. Thus it can be clearly seen that this value is always higher than can be reached by a monovalent competitor in solution (ca. 15 mM for CD and ca. 50 mM for hydrophobic guest), thus the adsorption

of polymer is always favored. The absolute stability constant *K* of the polymer on the CD SAMs, can be estimated using Equation 3.1.[37]

$$K = K_{i,s}^{\ n}\ C_{eff,\,max}^{\ n-1} \qquad \text{(Equation 3.1)}$$

Assuming that the known intrinsic binding constants of the guest polymers in solution[21] are equal to the intrinsic binding constants at the surface, $K_{i,s}$, it can be estimated that for all polymers $K > 5 \times 10^{87}$ M^{-1}.[41] This supports the observed stabilities and irreversibility of the polymer assembly formation.

Table 3.2: *Degree of substitution, average spacing of substituents, and effective concentrations of the hydrophobic group-modified guest polymers*

Polymer	average number of groups per polymer chain	average distance between groups (nm)	$C_{eff,max}$ [a] (M)
BAN09	35	5.4	0.15
BAN42	164	1.6	0.34
ADA20	78	2.6	0.28
ADA10	39	5.4	0.15

[a] effective concentration employed in the multivalency model (see text and ref. 40)

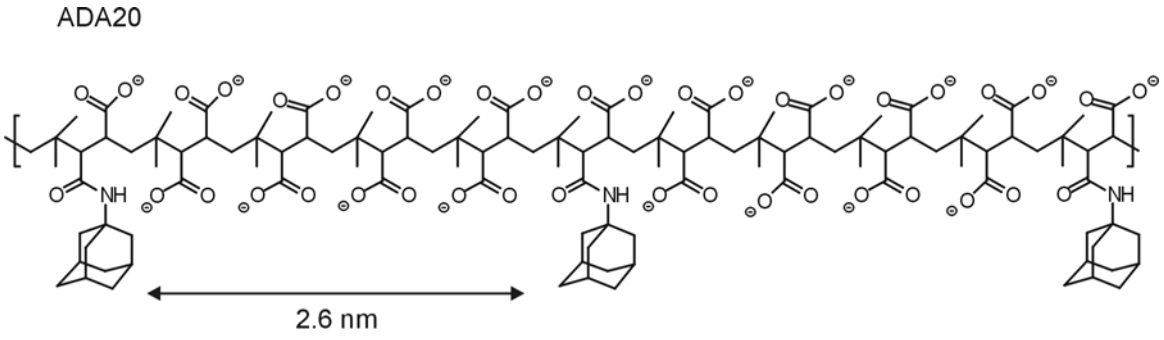

Figure 3.5: *Extended conformation of the polymer backbone, in this case ADA20.*

These conclusions are in marked contrast to the observations made for the inclusion of the guest polymers with vesicles composed of modified cyclodextrin.[21] The guest polymers bind to these vesicles in a brush- or mushroom-type conformation (Figure 3.2, bottom right) with an affinity of 2×10^6 M^{-1} at most. It is likely that the oligo(ethylene glycol) residues protruding from the surface of the vesicles prevent optimal multivalent interaction with the guest polymers. This type of steric repulsion is well known for colloids and surfaces decorated with poly(ethylene glycol).[42]

3.2.3 Supramolecular microcontact printing

Supramolecular microcontact printing[31,43,44] (μCP) was used to transfer the guest polymers onto the CD SAMs. Owing to the hydrophilicity of the ink, oxidation of the PDMS stamp by mild UV/ozone (UVO) treatment for 30 min was required to ink the stamp.[45,46] After immersing the hydrophilic stamps in an ADA10 solution (1 mM in adamantyl moieties), they were applied by hand onto the molecular printboard for 60 s. As seen from Figure 3.6 (top, left), a pattern was observed in height, but more clearly in friction, confirming the transfer of polymer onto the substrate. The darker lines in the latter image represent the CD SAM areas, while the brighter ones are the areas printed with ADA10.

As described before for small guest molecules,[31] the printed substrates were rinsed with copious amounts of 8 mM CD in 10 mM phosphate buffer. AFM friction images (Figure 3.6, top) confirmed the SPR results, as it can be clearly seen that the transferred pattern is still present even after competitive rinsing.

A similar printing experiment was applied on a 11-mercapto-1-undecanol SAM (OH SAM). These layers have a polarity comparable to the CD layers, but lack the possibility to form specific host-guest complexes. Patterns after printing were observed similar to the patterns on the CD SAMs. However, exposing the printed pattern to the CD rinsing procedure led to the complete removal of the pattern, proving physisorption in this case (Figure 3.6, bottom).

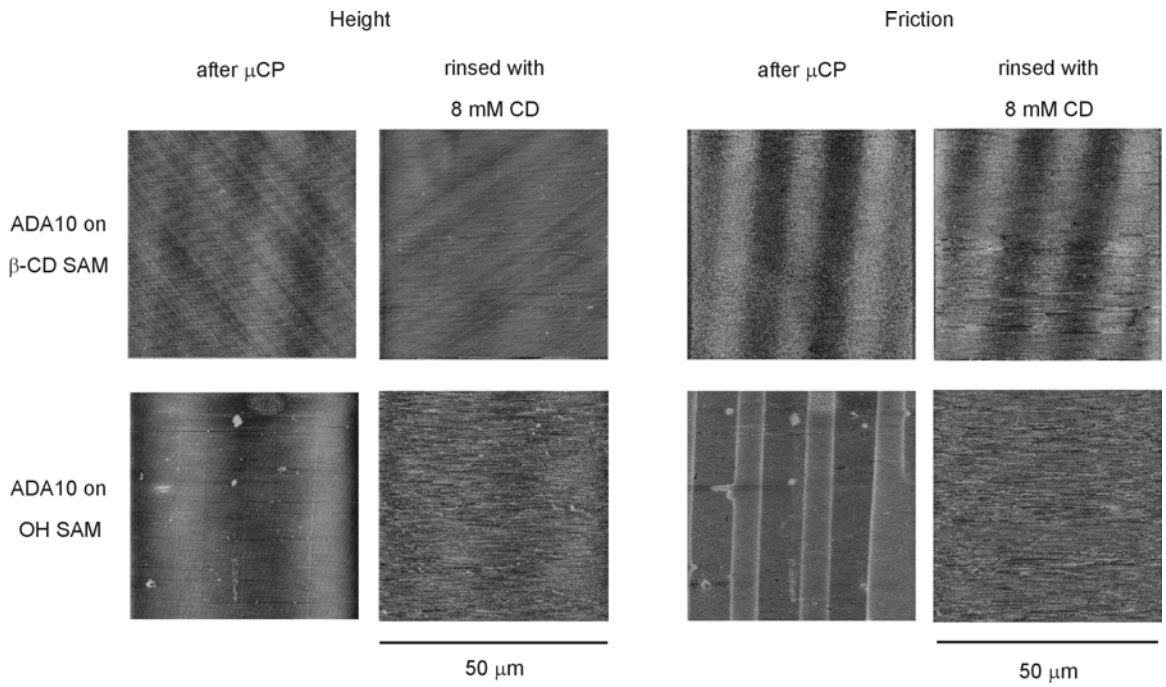

Figure 3.6: *Contact mode-AFM height (left, z range 5μm) and friction (right, z range 0.1 - 0.2 V) images in air of patterns obtained by μCP of ADA10 (0.1 mM in adamantyl moieties) on CD (top) and OH SAMs (bottom): before and after rinsing with 10 mM phosphate buffer containing 8 mM CD, respectively (image size: 50 × 50 μm^2).*

3.3 Conclusions

The binding of hydrophobic guest-functionalized poly(isobutene-*alt*-maleic acid)s and CD SAMs through multiple inclusion of the guest substituents of the polymers into the cavities of the CDs was shown to be very strong and irreversible. The polymer adsorption led to very thin polymer films on the surface, apparently using all or many of the hydrophobic groups, even though the polymers in solution are known to be spherical and to have strong intramolecular hydrophobic interactions leading to reduced affinity for CD in solution.[21] Variations of the nature and number of hydrophobic groups in the polymer, and the polymer concentration in solution did not lead to significant differences in adsorption behavior. Even competition with a monovalent host and guest in solution

did not lead to measurable polymer desorption, even though competition is known to enhance multivalent dissociation kinetics.[47] This behavior is attributed to the large number of hydrophobic groups present in the polymer and to the close-to-optimal linker lengths (1.6–5.4 nm) between the hydrophobic groups relative to the periodicity of the CD lattice (approx. 2 nm)[29,37] leading to high effective concentrations at the CD SAMs. These aspects cause the guest polymers-CD SAM assemblies to reach huge stability constants and concomitantly immeasurably long lifetimes, even under competitive conditions. Thus we have proven that multivalent polymer assemblies can be thermodynamically and kinetically stable, even though intrinsically weak and rapidly reversible supramolecular interactions are employed. This paradigm can be of value for nanofabrication.

3.4 Experimental Section

Materials

Guest polymers BAN09, BAN42, ADA10 and ADA20, were kindly donated by Prof. Gerhard Wenz (Saarland University, Germany) or prepared as described[48] by amidation of poly(isobutene-*alt*-maleic anhydride) (PiBM) of MW = 60 kD with varying amounts of *p*-*tert*-butylaniline or adamantylamine, respectively, followed by hydrolysis of the remaining anhydride groups. Throughout this chapter, the concentration of guest polymers is expressed as the concentration of hydrophobic substituents.[21] Poly(isobutene-*alt*-maleic acid) (PiBMA) was obtained by hydrolysis of PiBM using aqueous NaOH. *p*-*tert*-Butylbenzoic acid was obtained from Aldrich and converted to the sodium salt by addition of 1 equivalent of aqueous NaOH. Synthesis of the β-cyclodextrin heptathioether adsorbate was reported previously.[26]

CD-coated gold nanoparticles (CD Au NPs) were synthesized according to a literature procedure[36] by reduction of $AuCl_4^-$ in DMSO solution containing perthiolated β-CD[49] in a ratio [β-CD]/[$AuCl_4^-$] = 0.30. The reaction mixture became deep-brown immediately upon the addition of the reducing agent, $NaBH_4$. The CD-modified gold

particles were isolated by precipitation from CH_3CN and characterized by UV/vis spectroscopy, ^1H NMR, and transmission electron microscopy (TEM). Using TEM, a mean particle size of 2.5 ± 0.6 nm was found.

Substrate and monolayer preparation

All glassware used to prepare monolayers was immersed in piraña (conc. H_2SO_4 and 33% H_2O_2 in a 3:1 ratio, warning! piraña should be handled with caution; it can detonate unexpectedly). The glassware was rinsed with large amounts of high purity water (Millipore). All adsorbate solutions were prepared freshly prior to use. Round glass-supported gold substrates for SPR (2.54 cm diameter; 47.5 nm Au) and gold substrates for μCP (20 nm of gold on a 3'' silicon wafer with a 2 nm titanium adhesion layer) were obtained from Ssens BV (Hengelo, The Netherlands). Prior to use the substrates (20 nm gold) were cut to the preferred shape and size. Substrates were cleaned by immersing the substrates in piraña for 5 s and leaving the substrates for 5 min in absolute EtOH.[50] The substrates were subsequently immersed into a 0.1 mM CD heptathioether adsorbate solution in EtOH and $CHCl_3$ (1:2 v/v) for 16 h at 60 °C. The samples were removed from the solution and rinsed with substantial amounts of chloroform, ethanol, and Milli-Q water. 11-Mercapto-1-undecanol was purchased from Aldrich, and cleaned gold substrates were immersed with minimal delay into a 0.1 mM adsorbate solution in EtOH for 24 h. Subsequently, the substrates were removed from the solution and rinsed repeatedly with chloroform or dichloromethane, ethanol, and water to remove any physisorbed material. Gold substrates (200 nm on quartz, Metallhandel Schroer GmbH., Lienen, Germany) for the direct determination of the thickness of the guest polymer films were flame-annealed in a H_2 flame. After the annealing procedure, the substrates were immersed into a 0.1 mM CD heptathioether adsorbate solution in EtOH and $CHCl_3$ (1:2 v/v) for 16 h at 60 °C. The same rinsing procedures were applied as described above. All solvents used in monolayer preparation were of p.a. grade.

Monolayer characterization

Advancing and receding contact angles were measured on a Krüss G10 Contact Angle Measuring Instrument equipped with a CCD camera during the growth and shrinkage of a water droplet, respectively. Electrochemical measurements (cyclic voltammetry and impedance spectroscopy) were performed using an Autolab PGSTAT10 (ECOCHEMIE, Utrecht, The Netherlands) in a three-electrode configuration consisting of a gold working electrode (clamped to the bottom of the cell, exposing a geometric area of 0.44 cm^2 to the electrolyte solution), a platinum counter electrode, and a mercury/mercurous sulfate reference electrode (+0.61 V_{NHE}). Cyclic voltammetric capacitance measurements were conducted in 0.1 M K_2SO_4 between –0.35 V_{MSE} and –0.25 V_{MSE} at scan rates ranging from 0.1 to 2.0 Vs^{-1}. Impedance spectroscopy measurements were performed in aqueous $K_3Fe(CN)_6/K_4Fe(CN)_6$ (both 1 mM) containing 0.1 M K_2SO_4 at –0.2 V_{MSE} with an amplitude of 5 mV using a frequency range from 50 kHz to 0.1 Hz. The charge transfer resistance of the monolayer was obtained by fitting the experimental data to an equivalent circuit consisting of the monolayer resistance parallel to the monolayer capacitance, in series with the solution resistance.[51]

Microcontact printed substrates

Microcontact printed substrates were prepared according to literature procedures.[43,52,53] Stamps were prepared by casting a 10:1 (v/v) mixture of poly(dimethylsiloxane) (PDMS) and curing agent (Sylgard 184, Dow Corning) against a patterned silicon master. After curing, the stamps were mildly oxidized by UV/ozone (UVO) treatment in an ozone plasma reactor for 30 min and then inked by soaking them in the polymer solution (1 mM in hydrophobic groups) for 30-45 min. The master employed to prepare the PDMS stamp had 10 μm line features with 5 μm gaps, but the ozone treatment of the stamp decreased the features to about 8 ± 1 μm. Before printing, the stamps were blown dry in a stream of N_2. The stamps were applied manually (without pressure control) for 60 s on preformed SAMs (CD or 11-mercapto-1-undecanol) on gold and then carefully removed. After each printing step the inking procedure was repeated. Microcontact printed substrates were

thoroughly rinsed with 200 ml of aqueous solutions of either CD (8 mM in 10 mM phosphate buffer pH 7) or phosphate buffer (10 mM pH 7).

Surface plasmon resonance (SPR) spectroscopy

SPR measurements were performed in a two-channel vibrating mirror angle scan set-up based on the Kretschmann configuration, described by Kooyman *et al.*[54] Light from a 2 mW HeNe laser was directed onto a prism surface by means of a vibrating mirror. The intensity of the light was measured using of a large-area photodiode. This set-up allows the determination of changes in plasmon angle with an accuracy of 0.002°. The gold substrates with the monolayer were optically matched to the prism using an index matching oil. A Teflon cell was placed on a monolayer via an O-ring, to avoid leakage, and filled with 800 μl of 10 mM phosphate buffer solution. After stabilization of the SPR signal, titrations were performed by removing an amount of the buffer solution from the cell and adding the same amount of stock solution of guest polymers in phosphate buffer at different hydrophobic group concentrations (1 μM, 0.1 mM, or 1 mM). After each addition, the cell was thoroughly washed with 10 mM phosphate buffer pH 7 (5 times 700 μl) or 8 mM CD in 10 mM phosphate buffer pH 7. SPR time traces shown in the figures are corrected for baseline drifts by subtraction of the reference channel intensities.

Atomic force microscopy (AFM)

AFM experiments were carried out with a NanoScope IIIa Multimode AFM (Digital Instruments, Veeco Metrology Group, USA) in contact mode using V-shaped Si_3N_4 cantilevers (Nanoprobes, Veeco) with a nominal spring constant of 0.32 $N \cdot m^{-1}$. The AFM was equipped with a J scanner. Before thickness determination the scanner was calibrated in the z direction. The error was about 2%. Gold coated AFM tips were functionalized with 1H,1H,2H,2H-perfluorodecanethiol (purchased from Fluorochem) in order to avoid the adhesion of polymer chains to the AFM tip during imaging. The fluorinated AFM tips were immersed into a 0.1 mM 1H,1H,2H,2H-perfluorodecanethiol solution in CH_2Cl_2 overnight. The AFM tips were removed from the solution and rinsed with substantial

amounts of dichloromethane, ethanol, and Milli-Q water. Images were captured in ambient atmosphere (25 °C).

3.4 References and Notes

1. Mammen, M.; Choi, S. K.; Whitesides, G. M. *Angew. Chem. Int. Ed.* **1998**, *37*, 2755-2794.
2. Kiessling, L. L.; Pohl, N. L. *Chem. Biol.* **1996**, *3*, 71-77.
3. Gordon, E. J.; Gestwicki, J. E.; Strong, L. E.; Kiessling, L. L. *Chem. Biol.* **2000**, *7*, 9-16.
4. Gestwicki, J. E.; Cairo, C. W.; Strong, L. E.; Oetjen, K. A.; Kiessling, L. L. *J. Am. Chem. Soc.* **2002**, *124*, 14922-14933.
5. Kiessling, L. L.; Strong, L. E.; Gestwicki, J. E. *Ann. Rep. Med. Chem.* **2000**, *35*, 321-330.
6. Kanai, M.; Mortell, K. H.; Kiessling, L. L. *J. Am. Chem. Soc.* **1997**, *119*, 9931-9932.
7. Lynn, D. M.; Anderson, D. G.; Putnam, D.; Langer, R. *J. Am. Chem. Soc.* **2001**, *123*, 8155-8156.
8. Cairo, C. W.; Gestwicki, J. E.; Kanai, M.; Kiessling, L. L. *J. Am. Chem. Soc.* **2002**, *124*, 1615-1619.
9. Allen, J. R.; Harris, C. R.; Danishefsky, S. J. *J. Am. Chem. Soc.* **2001**, *123*, 1890-1897.
10. Maheshwari, G.; Brown, G.; Lauffenburger, D. A.; Wells, A.; Griffith, L. G. *J. Cell Sci.* **2000**, *113*, 1677-1686.
11. Kiessling, L. L.; Gestwicki, J. E.; Strong, L. E. *Curr. Opin. Chem. Biol.* **2000**, *4*, 696-703.
12. Sigal, G. B.; Mammen, M.; Dahmann, G.; Whitesides, G. M. *J. Am. Chem. Soc.* **1996**, *118*, 3789-3800.
13. Spaltenstein, A.; Whitesides, G. M. *J. Am. Chem. Soc.* **1991**, *113*, 686-687.
14. Choi, S. K.; Mammen, M.; Whitesides, G. M. *J. Am. Chem. Soc.* **1997**, *119*, 4103-4111.
15. Metallo, S. J.; Kane, R. S.; Holmlin, R. E.; Whitesides, G. M. *J. Am. Chem. Soc.* **2003**, *125*, 4534-4540.
16. Matrosovich, M.; Klenk, H. D. *Rev. Med. Virol.* **2003**, *13*, 85-97.
17. Matrosovich, M. N.; Mochalova, L. V.; Marinina, V. P.; Byramova, N. E.; Bovin, N. V. *FEBS Lett.* **1990**, *272*, 209-212.
18. Yang, X. G.; Shi, J. X.; Johnson, S.; Swanson, B. *Langmuir* **1998**, *14*, 1505-1507.
19. Ito, Y.; Ochiai, Y.; Park, Y. S.; Imanishi, Y. *J. Am. Chem. Soc.* **1997**, *119*, 1619-1623.
20. Chen, C. S.; Mrksich, M.; Huang, S.; Whitesides, G. M.; Ingber, D. E. *Science* **1997**, *276*, 1425-1428.

21. Ravoo, B. J.; Jacquier, J. C. *Macromolecules* **2002**, *35*, 6412-6416.
22. Ravoo, B. J.; Jacquier, J. C.; Wenz, G. *Angew. Chem. Int. Ed.* **2003**, *42*, 2066-2070.
23. Nolan, D.; Darcy, R.; Ravoo, B. J. *Langmuir* **2003**, *19*, 4469-4472.
24. Ravoo, B. J.; Darcy, R. *Angew. Chem. Int. Ed.* **2000**, *39*, 4324-4326.
25. Colton, I. J.; Carbeck, J. D.; Rao, J.; Whitesides, G. M. *Electrophoresis* **1998**, *19*, 367-382.
26. De Jong, M. R.; Huskens, J.; Reinhoudt, D. N. *Chem. Eur. J.* **2001**, *7*, 4164-4170.
27. Beulen, M. W. J.; Bügler, J.; Lammerink, B.; Geurts, F. A. J.; Biemond, E. M. E. F.; Van Leerdam, K. G. C.; Van Veggel, F. C. J. M.; Engbersen, J. F. J.; Reinhoudt, D. N. *Langmuir* **1998**, *14*, 6424-6429.
28. Ulman, A. *An Introduction to Ultrathin Films: From Langmuir-Blodgett to Self-Assembly*, Academic Press, Boston, U.S.A. **1991**.
29. Schönherr, H.; Beulen, M. W. J.; Bügler, J.; Huskens, J.; Van Veggel, F. C. C. J.; Reinhoudt, D. N.; Vancso, G. J. *J. Am. Chem. Soc.* **2000**, *122*, 4963-4967.
30. Huskens, J.; Deij, M. A.; Reinhoudt, D. N. *Angew. Chem. Int. Ed.* **2002**, *41*, 4467-4471.
31. Auletta, T.; Dordi, B.; Mulder, A.; Sartori, A.; Onclin, S.; Bruinink, C. M.; Péter, M.; Nijhuis, C. A.; Beijleveld, H.; Schönherr, H.; Vancso, G. J.; Casnati, A.; Ungaro, R.; Ravoo, B. J.; Huskens, J.; Reinhoudt, D. N. *Angew. Chem. Int. Ed.* **2004** , *43*, 369-373.
32. Knoll, W. *Annu. Rev. Phys. Chem.* **1998**, *49*, 569-638.
33. Beulen, M. W. J.; Kastenberg, M. I.; Van Veggel, F. C. J. M.; Reinhoudt, D. N. *Langmuir* **1998**, *14*, 7463-7467.
34. Lobo, R. F. M.; Pereira-Da-Silva, M. A.; Raposo, M.; Faria, R. M.; Oliveira, O. N. *Nanotechnology* **1999**, *10*, 389-393.
35. Thickness increases upon polymer adsorption determined by ellipsometry were significantly low (< 1 nm). Higher accuracies can not be obtained for these substrates which require fitting of the optical parameters using the silicon substrate, the gold and titanium layers, and the organic layer.
36. Liu, J.; Ong, W.; Roman, E.; Lynn, M. J.; Kaifer, A. E. *Langmuir* **2000**, *16*, 3000-3002.
37. Huskens, J.; Mulder, A.; Auletta, T.; Nijhuis, C. A.; Ludden, M. J. W.; Reinhoudt, D. N. *J. Am. Chem. Soc.* **2004**, *126*, 6784-6797.
38. Mulder, A.; Auletta, T.; Sartori, A.; Del Ciotto, S.; Casnati, A.; Ungaro, R.; Huskens, J.; Reinhoudt, D. N. *J. Am. Chem. Soc.* **2004**, *126*, 6627-6636.
39. In contrast, when adamantyl-terminated dendrimers are adsorbed on a β–CD SAM, the adsorption of CD-modified gold nanoparticles becomes very strong, owing to multivalent binding; see: Chapter 5.

40. Rekharsky, M. V.; Inoue, Y. *Chem. Rev.* **1998**, *98*, 1875-1917.
41. Calculated $K_{i,s}$ = 3 x 10^3 M^{-1}, $C_{eff,max}$ = 0.1 M and n = 35.
42. Lasic, D. D. *Angew. Chem. Int. Ed. Engl.* **1994**, *33*, 1685-1698.
43. Xia, Y. N.; Whitesides, G. M. *Angew. Chem. Int. Ed.* **1998**, *37*, 551-575.
44. Biebuyck, H. A.; Larsen, N. B.; Delamarche, E.; Michel, B. *IBM J. Res. Dev.* **1997**, *41*, 159-170.
45. Martin, B. D.; Brandow, S. L.; Dressick, W. J.; Schull, T. L. *Langmuir* **2000**, *16*, 9944-9946.
46. Yan, L.; Huck, W. T. S.; Zhao, X. M.; Whitesides, G. M. *Langmuir* **1999**, *15*, 1208-1214.
47. Rao, J. H.; Lahiri, J.; Isaacs, L.; Weis, R. M.; Whitesides, G. M. *Science* **1998**, *280*, 708-711.
48. Weickenmeier, M.; Wenz, G.; Huff, J. *Macromol. Rapid. Commun.* **1997**, *18*, 1117-1123.
49. Rojas, M. T.; Königer, R.; Stoddart, J. F.; Kaifer, A. E. *J. Am. Chem. Soc.* **1995**, *117*, 336-343.
50. Ron, H.; Rubinstein, I. *Langmuir* **1994**, *10*, 4566-4573.
51. a) Boukamp, B. A. *Solid State Ionics* **1986**, *18-19*, 136-140. b) Boukamp, B. A. *Solid State Ionics* **1986**, *20*, 31-44.
52. Kumar, A.; Biebuyck, H. A.; Whitesides, G. M. *Langmuir* **1994**, *10*, 1498-1511.
53. Xia, Y. N.; Whitesides, G. M. *Adv. Mater.* **1995**, *7*, 471-473.
54. Lenferink, A. T. M.; Kooyman, R. P. H.; Greve, J. *Sens. Actuators, B* **1991**, *3*, 261-265.

Chapter 4

Multivalent Aggregation of Cyclodextrin Gold Nanoparticles and Adamantyl-terminated Guest Molecules*

*The formation of large network aggregates composed of gold nanoparticles bearing surface-immobilized β-cyclodextrin (CD) hosts, whose assembly is driven by adamantyl-terminated guest molecules, was studied as a function of the number of interactions and the geometry of the guest molecules. The assembly was shown to be strong, specific, and irreversible by addition of an adamantyl-terminated dendrimer leading to strong aggregation of the CD gold nanoparticles and consequently to the formation of an insoluble precipitate. The bis-adamantane guest molecule **3** allowed more control over the self-assembly of such aggregates. In this case intramolecular interactions were favored over the intermolecular interactions, and the aggregation process of this guest could be inhibited by a monovalent competitor in solution.*

* Part of this chapter has been published in: Crespo-Biel, O.; Juković, A.; Karlsson, M.; Reinhoudt, D. N.; Huskens, J. *Isr. J. Chem.* **2005**, *45*, 353-362, 'Special Issue on Supramolecular assemblies'.

4.1 Introduction

The combination of multiple interactions between non-covalently interacting species can result in an overall interaction strength that is much higher than that of a monovalent one. This effect is generally recognized as multivalency and gives rise to enhanced binding affinities and specificities that lack in monovalent interactions.[1,2] Multivalency in ligand-receptor interactions is widely used in nature and plays an important role in events that determine interactions between cell surface receptors and carbohydrates in processes including fertilization, proliferation, viral/bacterial infection, and the inflammatory response.[1,2] For that reason multivalent protein-carbohydrate interactions have been an important topic in scientific research during the last years.[3-7] A number of diverse scaffolds has been generated in order to mimic natural systems, such as low molecular weight displays,[8] copolymers,[9] dendrimers,[10] nanoparticles,[11-15] and liposomes.[16,17]

As it has been shown in Chapter 3, guest polymers modified with multiple hydrophobic groups can bind in an intramolecular fashion to a multivalent host surface. However, a multivalent guest can also bind to a multivalent host in an intermolecular fashion. It is not always straightforward to discriminate between intra- and intermolecular binding, and great care should be taken when interpreting multivalent binding studies since a lot of factors such as the architecture, the size and shape of the multivalent entities, the tether length between the binding functionalities, and the concentration of the two entities are involved. Intramolecular binding typically leads to relatively high association constants with respect to monovalent binding and to the formation of well-defined complexes.[4] In contrast, intermolecular binding potentially leads to the formation of large aggregates that often precipitate from solution.[18] Binding shows association constants comparable to those of the corresponding monovalent interactions while irreversible precipitation and aggregation lead to decreased dissociation rates and consequently to an apparent binding enhancement.

Multivalent interactions at interfaces are particularly important since such interfaces, when modified with monovalent ligands or receptors, can act as multivalent systems in complexing multivalent counterparts. Concentrations of these agents, either

ligands or receptors, at the interface can differ[19-22] and the distribution may be uneven and could alter upon binding with a multivalent counterpart (clustering).[19,23]

Gold nanoparticles (Au NPs)[28] have a well-developed surface chemistry,[29] a constant shape and size in solution, are rigid and chemically stable,[30] which makes them ideal model systems to study and understand multivalency. Recently, several groups have modified metal nanoparticles with synthetic receptors or substrates in order to use well-known molecular recognition to drive and control particle assembly.[31-49] Mirkin and co-workers have functionalized nanoparticles with DNA for detection of target sequences through complementary hybridization.[33] Other groups have prepared multivalent glycoconjugates on gold nanoparticles to employ them as useful tools to investigate carbohydrate recognition processes.[12,14,15] Kaifer and co-workers have taken advantage of the host properties of cyclodextrins[50] (CDs) as molecular receptors, and they have prepared per-6-thio-cyclodextrin-covered nanoparticles.[51,52] They studied the interactions with divalent bis(ferrocene)[34] and with C_{60} fullerene molecules,[35] where the addition of the guest molecules led to the formation of a red precipitate, which is due to the intermolecular binding between the guest units and the cyclodextrin nanoparticles.

In this chapter a method to control nanoparticle assembly in solution by multiple supramolecular interactions, leading to the formation of large network aggregates is described. The assembly of gold nanoparticles bearing surface-immobilized β-cyclodextrin hosts (CD Au NPs)[52] is driven by adamantyl-terminated guest molecules, acting as noncovalent molecular linkers between the nanoparticles. Multivalent aggregation, employing guest systems that can give intra- and intermolecular binding, is studied as a function of the number of interactions available for the assembly, and of the geometry of the guests.

4.2 Results and Discussion

4.2.1 Synthesis and characterization of the modified gold nanoparticles

Scheme 4.1 illustrates the synthesis of the CD Au NPs (**1a**). CD Au NPs **1a** were prepared following a literature procedure[51] by reduction of $AuCl_4^-$ with $NaBH_4$ in DMSO

solution containing perthiolated CD (CD/Au = 0.3/1). The reaction mixture colored deep brown immediately after addition of the reducing agent. This one-phase procedure is similar to that reported by Brust and co-workers for the preparation of gold clusters protected with *p*-mercaptophenol.[53] The CD Au NPs **1a** were isolated by precipitation from CH_3CN and collected by centrifugation. Tetra(ethylene glycol)-functionalized gold nanoparticles (**1b**) were prepared analogously.[54,55]

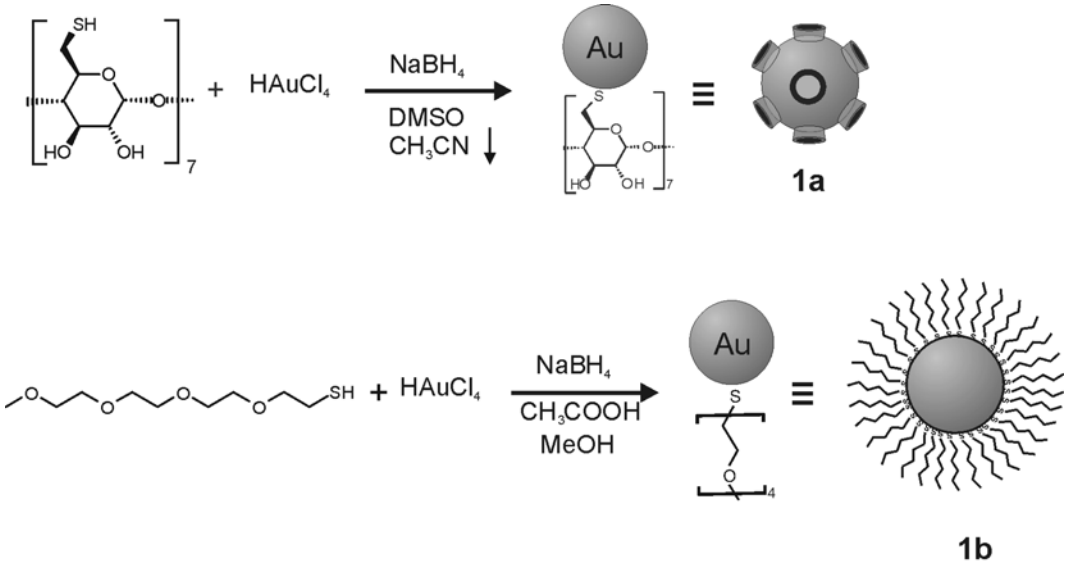

Scheme 4.1: *Preparation of CD-functionalized (**1a**) and tetra(ethylene glycol)-modified gold nanoparticles (**1b**).*

The ^{1}H NMR spectrum (D_2O) of **1a** showed broad peaks that couldd be assigned to immobilized thiolated CDs. TEM images (Figure 4.1A) showed unaggregated particles while the histogram (Figure 4.1B) showed the relatively narrow particle size distribution of 2.8 ± 0.6 nm. UV-vis spectroscopy (Figure 4.1C) showed the commonly observed plasmon absorption band at around 530 nm, again indicating the absence of aggregation. From batch to batch, the exact position of the plasmon band varied (between 528-534 nm), but for measurements performed with the same batch the reproducibility of determinations of λ_{max} was found to be about ±1 nm. Thermogravimetric analysis (TGA) (Figure 4.1D) displayed two distinct weight losses. Until about 220°C, the mass slowly

decreased (~13% w/w loss) attributed to the removal of physisorbed water. Between 220-300°C, the TGA curve displays a more prominent weight loss (~ 25% w/w) attributed to the elimination of the organic layer. In principle, the TGA results allow estimation of the concentration of CDs upon dissolution of a known amount of **1a** in a given volume. Apart from the physisorbed water (13% w/w), the CD Au NPs **1a** consist of approx. 62% w/w Au and of 25% w/w perthiolated CD.

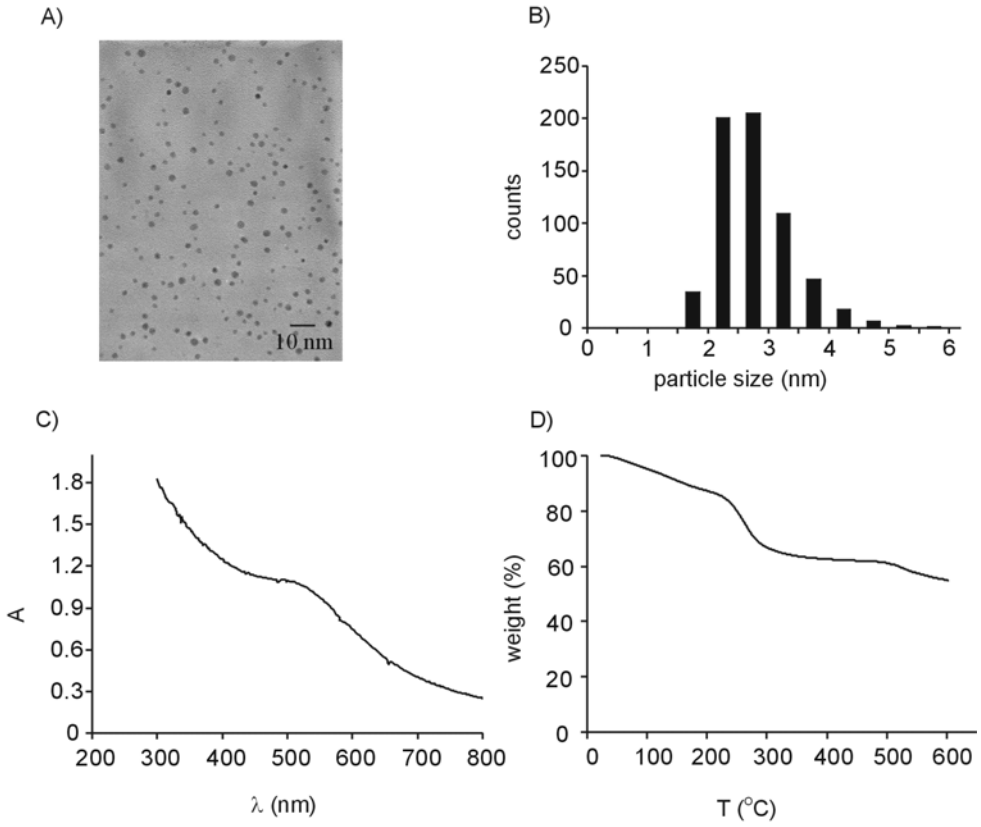

Figure 4.1: *Characterization of the CD Au NPs* ***1a****. (A) TEM image, (B) Histogram showing the size distribution of* ***1a*** *(average diameter 2.8 ± 0.6 nm), (C) UV-vis spectrum of an aqueous solution of* ***1a****. (D) thermogravimetric analysis of* ***1a****.*

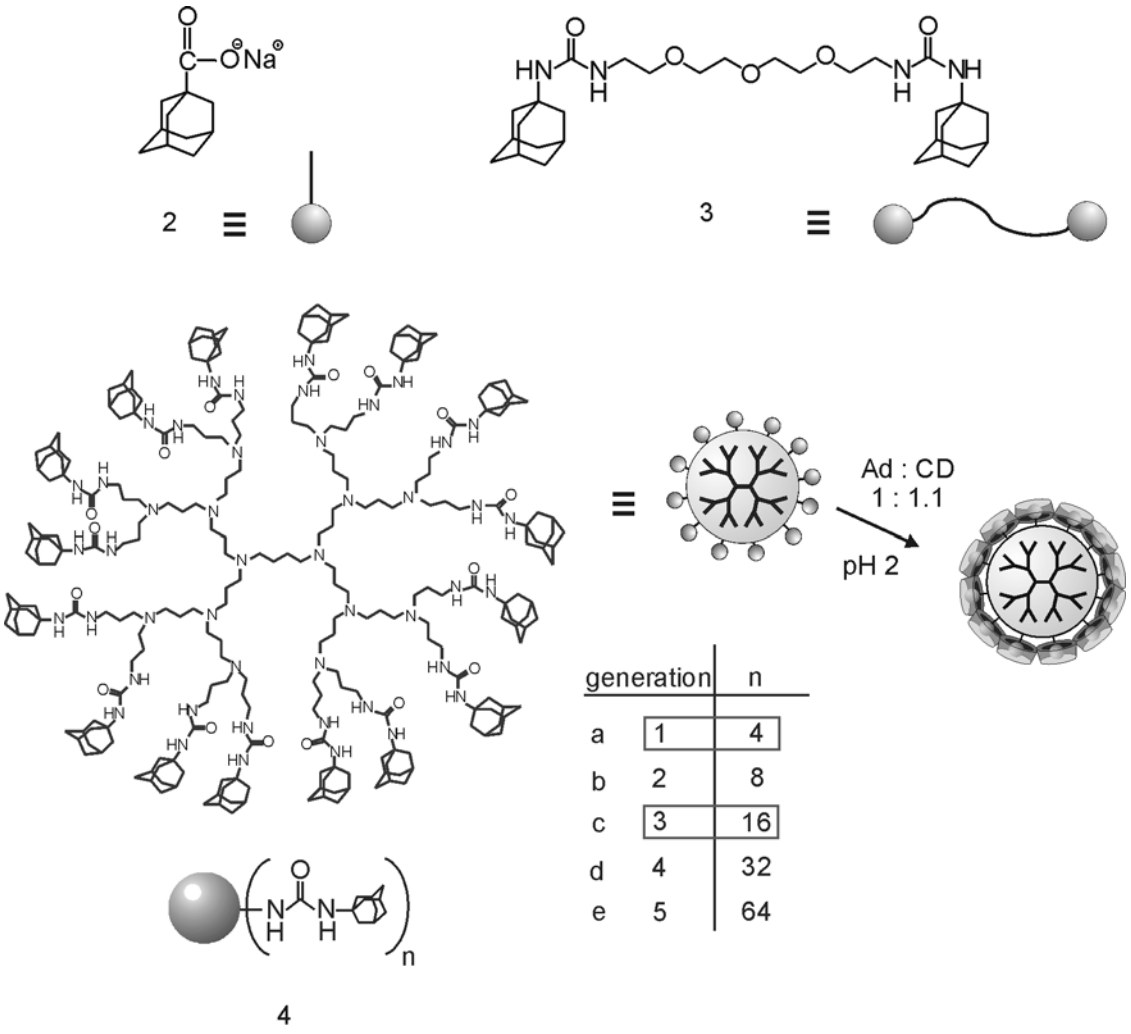

Chart 4.1: *Chemical structures of adamantane carboxylate (**2**), the bis-adamantyl guest molecule (**3**), and the adamantyl-terminated PPI dendrimers (**4**).*

To confirm the CD concentration of a solution of **1a**, isothermal titration microcalorimetry (ITC) measurements were performed by titrating an adamantane carboxylate solution (**2,** see Chart 4.1) to a **1a** solution (Figure 4.2). The enthalpogram was fitted to a 1:1 binding model using the association constant, *K*, the binding enthalpy, ΔH°, and the CD concentration, as independent fitting parameters. The binding constant *K* (2.31×10^4 M^{-1}) and the enthalpy of binding (-6.8 kcal·mol^{-1}) are typical of a CD-adamantane interaction.[50] The calculated CD concentration was found to correspond to

25% w/w of CD present on the CD Au NPs **1a**. Thus, the ITC results are in excellent agreement with the TGA results discussed above.

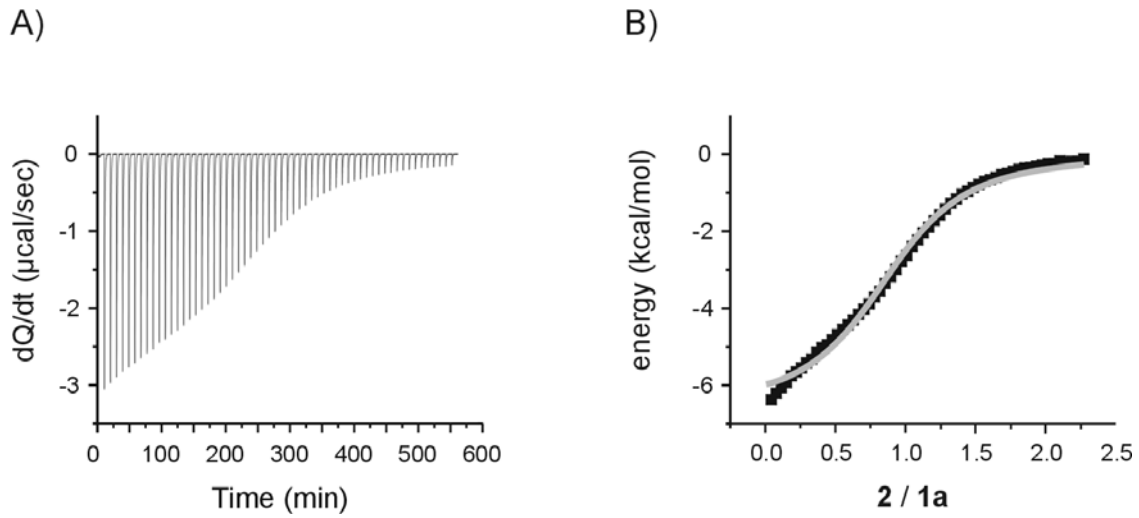

Figure 4.2: *ITC titration of CD Au NPs **1a** (CD concentration approx. 0.05 mM; measurement cell) with 5 mM adamantane carboxylate **2** (burette); A) data of heat evolution with injection of **2**, B) resulting binding curve (markers) and best fit to a 1:1 model (line).*

4.2.2 Host-guest complexation abilities in solution

The host-guest complexation abilities of **1a** in solution were further investigated by studying the complexation-induced aggregation of **1a** in the presence of multivalent guest molecules (see Chart 4.1) as schematically shown in Scheme 4.2.

The number of hydrophobic moieties present in the guest molecules as well as the geometry, can either prevent or provoke aggregation and possibly subsequent flocculation/precipitation of the gold nanoparticles. The multivalent noncovalent interactions of the guest molecules with the CD Au NPs **1a** were investigated as a function of the number of guest moieties available to induce cross-linking between particles and of their concentration in solution. Throughout this chapter, concentrations of the guest molecules and of **1a** will be given as concentrations of the monovalent, functional groups, *i.e.* adamantyl and CD moieties, respectively. The aggregation process

was studied by UV-vis spectroscopy as aggregation is known to lead to a red-shift of the plasmon absorption band.[56]

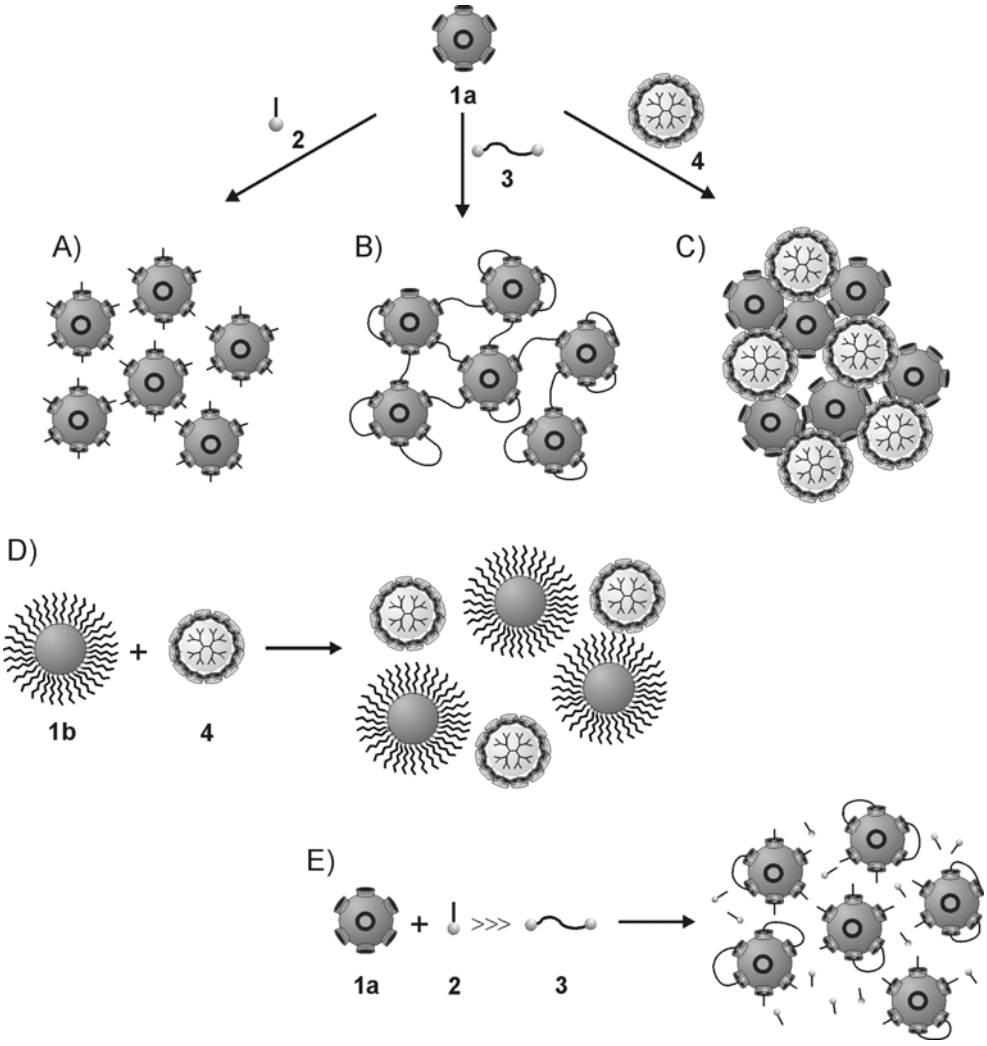

Scheme 4.2: *Schematic representation of the aggregation phenomena of CD Au NPs* ***1a*** *with adamantyl-terminated guest molecules: (A) addition of* ***2*** *to a solution of* ***1a****, (B) addition of* ***3*** *to a solution of* ***1a****, (C) addition of* ***4*** *to a solution of* ***1a****, (D) control experiment for the addition of* ***4*** *to a solution of Au NPs* ***1b****, (E) competition experiment for the addition of* ***3*** *to a solution of* ***1a*** *and* ***2****.*

Gold nanoparticles have a tendency to be negatively charged, making them unstable at low pH solutions.[57] On the other hand adamantyl-terminated poly(propylene

imine) (PPI) dendrimers[58] (**4**) are only soluble in acidic media, causing protonation of the core amines, in the presence of an excess of CD.[59] Therefore, experimental conditions were chosen such that both species were stable in aqueous solution for prolonged periods of times, *i.e.* in phosphate buffer at pH 5.7 with an excess of CD.

Changes in the plasmon absorption band of the particle solutions were followed by UV-vis spectroscopy as a function of the concentration of adamantane carboxylate (**2**) added. Increasing amounts of a 2.5 mM solution of **2** to 0.6 ml of a 0.104 mM solution of **1a**, did not cause any decrease of the intensity nor a red-shift of the plasmon absorption band (data not shown). Thus, addition of a monovalent guest to a solution of **1a** does not induce precipitation or flocculation, and results in stable assemblies (see scheme 4.2A). This was confirmed by the ITC experiments discussed above.

Similar experiments were performed with bis-adamantyl guest molecule **3** in order to investigate intra- *vs*. intermolecular binding. The guest molecule was prepared by linking two adamantyl moieties to an oligo(ethylene glycol) chain allowing flexibility, while also introducing water solubility and preventing nonspecific interactions. The tether length between the two adamantyl functionalities is sufficient to allow intramolecular binding on the surface of the CD Au NPs **1a**.

UV-vis titrations were carried out varying the concentrations of the bis-adamantane guest molecule (0.65 - 5 mM in adamantyl moieties) and of the CD Au NPs **1a** (0.04 - 0.16 mM in CD entities). UV-vis titrations were carried out under the same conditions as described above for **2**. Figure 4.3A shows the plasmon absorption band for each addition of **3** plotted *vs.* the molar ratio of adamantyl to CD. Addition of **3** causes a red-shift of the plasmon absorption band with a $\Delta\lambda_{max}$ of approximately 4 nm, indicating the presence of aggregated particles, which was not observed in the case of **2**. Furthermore, the absorbance of **3** decreases down to 85% of the original value due to flocculation (Figure 4.3B). Nevertheless, these minor changes suggest a large number of nanoparticles of the complex **3**/**1a** remain stable in solution. Similar experiments were performed at three different concentrations of **1a**, but all showed the same behavior. These observations suggest that for the bis-adamantane molecule **3** intramolecular interactions are predominant over intermolecular interactions (see scheme 4.2B). Nevertheless, intermolecular interactions are also present as can be observed from the

decrease in absorbance and the red-shift of λ_{max}. Although the ratio between intra- and intermolecular binding should be concentration-dependent, this was not observed for the concentration range assessed here.

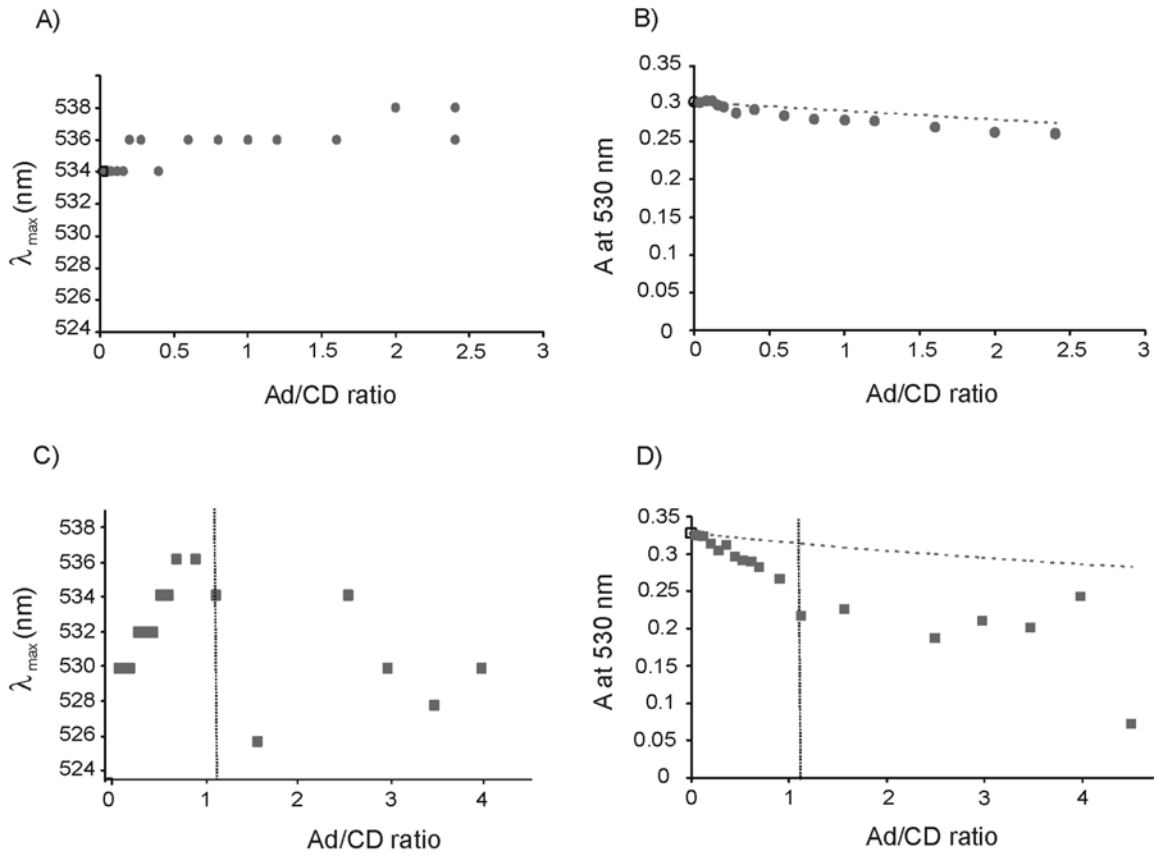

Figure 4.3: *Changes of λ_{max} (A, C) and absorbance at 530 nm (B, D) (dashed curve: expected absorbance when taking dilution into account only) of UV-vis spectra plotted against the molar adamantyl/CD ratio (present on guest molecules and **1a**, respectively) for titrations of **3** (A, B) and **4c** (C, D) (both 2.5 mM in adamantyl moieties) to 0.6 ml of CD Au NPs **1a** (0.104 mM in CD concentration); the vertical dotted lines at a molar Ad/CD ratio of 1 represents the onset of visible precipitation; solutions all in phosphate buffer pH 5.7, also containing 7.5 mM excess free cyclodextrin.*

A model recently developed for predicting the thermodynamics of binding of multivalent guest molecules to hosts immobilized at interfaces,[60] provides insight into the here observed predominance of intramolecular binding. From the geometries of the guest

3 and the CD Au NPs **1a**, it can be estimated that the effective CD concentration, which reflects the concentration of free host sites on the same particle experienced by a noncomplexed guest site of a multivalent guest which is bound monovalently to the particle, is about 0.1 M or larger. Thus, it becomes evident that the intramolecular binding prevails as long as the overall CD concentration in solution remains below this value.

Figure 4.3C shows the changes in λ_{max} for the plasmon absorption band of the CD Au NPs **1a** as a function of the dendrimer concentration **4c**. Up to an adamantyl/CD ratio of about one, addition of a 2.5 mM solution of dendrimer **4c** to a CD Au NPs **1a** solution (0.1 mM) caused a decrease of the plasmon absorption band (see Figure 4.3D) and a red-shift of λ_{max} from 530 to 536 nm (Figure 4.3C). Both changes confirm the occurrence of aggregation as depicted in Scheme 4.2C. Above an adamantyl/CD ratio of about one, λ_{max} started to fluctuate, while the absorbance continued to decrease and flocculation became apparent to the naked eye. The precipitation became complete within a few min after the last addition. It was evident that an insoluble complex between the nanoparticles and the dendrimer had formed. Titrations with the dendrimer **4a** showed a very similar behavior (data not shown), and the onset of visible precipitation and fluctuation of λ_{max} also started at an adamantyl/CD ratio of one.

Aggregation caused by **4a** and **4c** was more severe than aggregation caused by the divalent, flexible linker **3** and led to larger, macroscopically visible, precipitates. This is caused by the fact that the dendrimers, unlike **3**, have redundant guest moieties for binding CD Au NPs **1a**. It is known from analogues ferrocene-terminated dendrimers[61] that **4a** can use two interactions at an interface, and **4c** up to four. This still leaves two and twelve interacting sites, respectively, free for binding additional particles, leading to efficient cross-linking.

Furthermore, the dynamics of such multivalent interactions becomes progressively slower, explaining the irreversibility of the precipitation, which could not be counteracted by additions of larger excesses of dendrimers, nor of monovalent **2** (see below). The Ad/CD ratio of about 1 at which visible flocculation occurs for both dendrimers, seems to indicate the point at which the concentration of the participating host and guest sites are close to equal, and thus that both are used efficiently in the aggregation process. The fluctuation of λ_{max} is attributed to more rapid growth of the

larger assemblies which then precipitate, leading to, on average, smaller aggregates remaining in solution with a concomitant lower λ_{max}, which then get the chance to grow, etc.

Further evidence for the aggregation of the nanoparticles was obtained from TEM experiments. TEM images of the CD Au NPs **1a** (Figure 4.1A) show unaggregated, well-dispersed CD Au NPs, verifying the absence of aggregates in solution. However, a TEM image of the system after the addition of **4c** (see Figure 4.4) shows extended aggregation as expected for linkages generated by multivalent interactions between **1a** and **4c**.

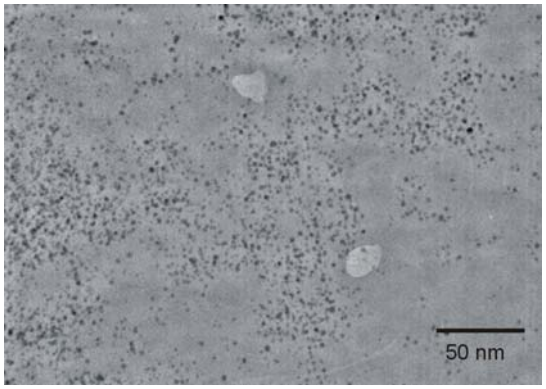

Figure 4.4: *TEM image obtained after the addition of adamantyl-terminated PPI dendrimer* ***4c*** *to Au NP* ***1a.***

In contrast to the experiments using CD Au NPs **1a**, the addition of **4c** to a solution of oligo(ethylene glycol)-functionalized Au NPs **1b**[54,55] (see Scheme 4.2D) did not lead to precipitation nor to changes of the plasmon absorption band (data not shown).[62] This is attributed to the lack of CD receptor sites for **1b**, and, in addition, to the absence of non-specific adsorption of the dendrimers. This clearly shows the need of specific host-guest interactions for aggregation to occur.

4.2.3 Competition experiments in solution

In order to test the effect of competition between guests on the aggregation behavior, the bis-adamantyl guest **3** (2.5 mM) was added to a solution containing CD Au

NPs **1a** (0.104 mM) and a large excess of **2** (25 mM). The peak position and intensity of the plasmon absorption band remained unchanged and no flocculation was observed (see Figures 4.5A and 4.5B). This suggest that the monovalent guest **2** competes efficiently with intermolecular binding of **3** (see Scheme 4.2E), which would lead to aggregation (see above). Most likely, *intramolecular* binding is *not* inhibited by the addition of **2**, since the intramolecularly bound divalent **3** is expected to have a significantly higher binding constant.

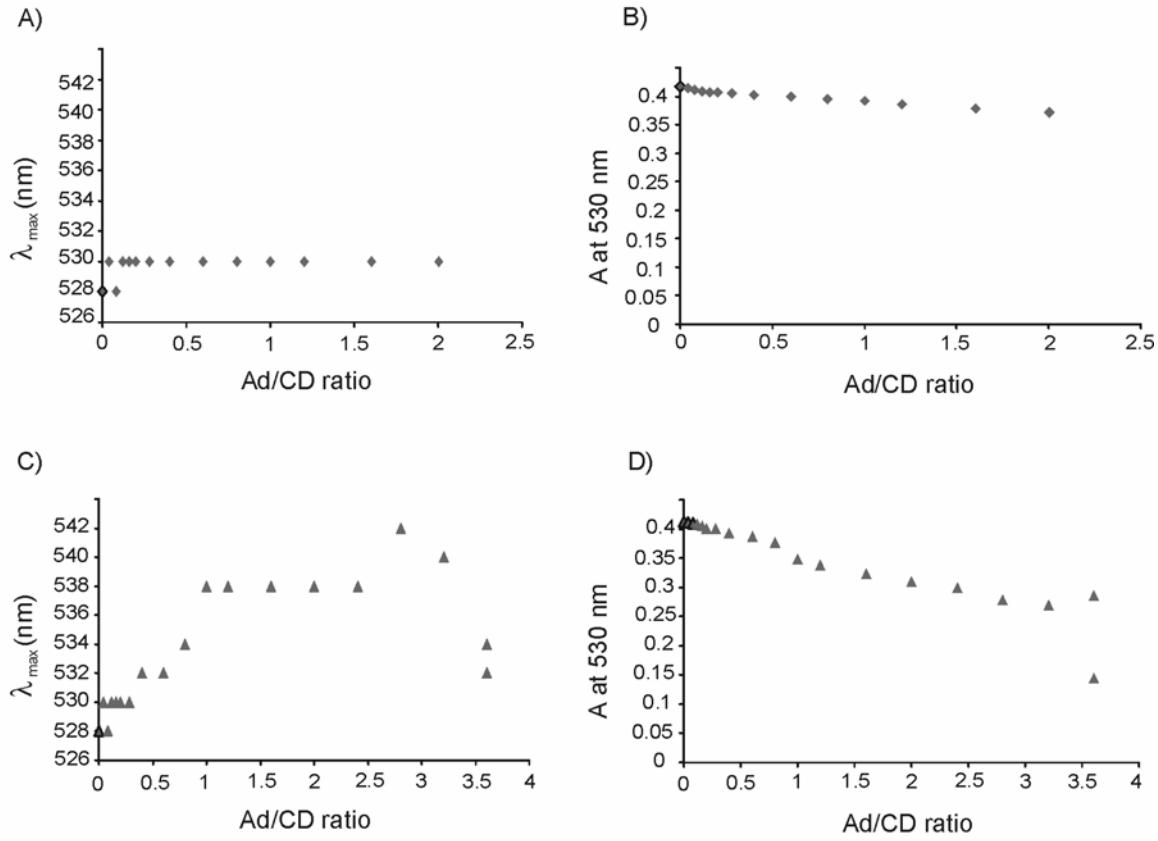

Figure 4.5: *Changes of λ_{max} (A, C) and absorbance at 530 nm (B, D) of UV-vis spectra plotted against the molar adamantyl/CD ratio (present on **3** or **4a** and on **1a**, respectively) for titrations of **3** (A, B) and **4a** (C, D) (both 2.5 mM in adamantyl moieties) to 0.6 ml of CD Au NPs **1a** (0.104 mM in CD concentration) and **2** (25 mM); solutions all in phosphate buffer pH 5.7, also containing 7.5 mM excess free cyclodextrin.*

In contrast, the addition of **4a** to a solution of CD Au NPs **1a** and **2** (25 mM) led to visible precipitation as also reflected in a decrease of the intensity and a red-shift of λ_{max} of the plasmon absorption band (see Figure 4.5C and 4.5D), comparable to the results obtained without adding a competitor in solution (see above). Thus, it is clear that both the valency and the geometry of the guest molecules play an important role in tuning the interactions between CD-functionalized nanoparticles and guest molecules and thus provide a means to control the formation of large aggregates.

4.3 Conclusions

In conclusion, it has been shown that adamantyl-terminated guest molecules mediated the aggregation of CD Au NPs in aqueous solution by employing strong, specific, and multivalent host-guest interactions. This process can be controlled by the number of interactions available for the assembly, the geometry of the molecules, and by adding a competitor in solution to prevent aggregation. Adamantyl-terminated dendrimers, owing to their globular shape and high number of interactions, lead to the formation of insoluble nanoparticle aggregates without a long-range order. Conversely, the bis-adamantyl molecule **3**, with two possible interactions and a flexible linker did not show the formation of an insoluble complex, which is attributed to predominant intramolecular binding. The aggregation process for the bis-adamantyl guest **3** can be controlled by adding a monovalent competitor (**2**) in solution. We expect that such aggregation schemes can be used to assemble larger architectures on flat surfaces, employing for example layer-by-layer (LbL) techniques, as shown in Chapter 5.

4.4 Experimental Section

Materials

Chemicals were obtained from commercial sources and used as such. β-Cyclodextrin (CD) was dried in vacuum at 80 °C in the presence of P_2O_5 for at least 5 h before use.

Solvents were purified according to standard laboratory methods.[63] Tetra(ethylene glycol) thiol (EG_4-SH) was prepared as described by bromination of tetra(ethylene glycol) monomethyl ether followed by a bromo-thiol exchange, and purified by distillation[54,55]. Perthiolated β-CD was synthesized according to a literature procedure.[64] Millipore water with a resistivity larger than 18 MΩ·cm was used in all our experiments. Generation one (**4a**) and three (**4c**) adamantyl-terminated poly(propylene imine) (PPI) dendrimers (with 4 and 16 adamantyl groups, respectively) were synthesized as reported before.[58] NMR spectra were recorded on Bruker AC300 and AMX400 spectrometers. FAB-MS spectra were recorded with a Finnigan MAT 90 spectrometer using *m*-nitrobenzylalcohol as the matrix.

Cyclodextrin-functionalized gold nanoparticles (1a)

CD Au NPs were synthesized according to literature procedure.[51] $HAuCl_4$ (180 mg, 0.53 mmol) was dissolved in DMSO (20 ml). This solution was mixed quickly with a solution of $NaBH_4$ (246 mg, 6.50 mmol) and *per*-6-thio-cyclodextrin[64] (200 mg, 0.16 mmol) in DMSO (20 ml). The reaction mixture turned deep-brown immediately, and was allowed to continue for 24 h. At this point, CH_3CN (40 ml) was added to precipitate the nanoparticles, which were collected and purified by centrifugation, followed by washing with CH_3CN:DMSO (1:1 v/v, 60 ml) and ethanol (60 ml), dissolution in water, and freeze-drying.

Tetra(ethylene glycol)-modified gold nanoparticles (1b)

EG_4 Au NPs were synthesized according to a literature procedure.[54,55] $HAuCl_4$ (88.5 mg, 0.225 mmol) was dissolved in MeOH (30 ml) and acetic acid (5 ml). After stirring for 5 min, tetra(ethylene glycol) thiol (EG_4-SH) (224 mg, 0.1 mmol) was added to the above mixture and dissolved by stirring for 5 min. $NaBH_4$ (75 mg, 2.0 mmol) was dissolved in Millipore water and added drop-wise to the solution with rapid stirring. The reaction mixture turned deep-brown immediately, and the reaction was allowed to continue for 2 h. MeOH was evaporated, and the NPs were purified and collected by several washings with MeOH (4×), followed by dissolution in water and storage in aqueous solution.

1,17-bis-Adamantyl-tri(ethylene glycol) urea (3)

To a solution of 1-adamantyl isocyanate (710 mg, 4 mmol) in CH_2Cl_2 a solution of 2-{2-[2-(2-amino-ethoxy)-ethoxy]-ethoxy}-ethylamine[65] (250 mg, 1.3 mmol) in CH_2Cl_2 was slowly added. The mixture was stirred at room temperature overnight. The solvent was evaporated under reduced pressure. The residue was purified by precipitation from ether to give the product **3** as white solid. Yield: 80 %; ^{1}H NMR (300 MHz, $CDCl_3$): δ 1.60 (s, 12H), 2.0 (s, 12H), 2.1 (s, 6H), 3.4 (m, 4H), 3.6-3.7 (m, 12H), 5.0 (s, 2H), 5.3 (t, 2H); ^{13}C NMR (400 MHz, $CDCl_3$): δ 157.5, 70.5, 69.7, 69.2, 50.6, 42.4, 39.2, 36.4, 29.6; MALDI-MS: m/z calcd for $[M+H]^+$ 547.0; found 546.9.

Thermogravimetric analysis

TGA was performed with a Setsys 16 SERATAM device, on dried CD Au NPs **1a** (29 mg), under air flow (50 ml/min) at a heating rate of 1 °C/min from 22-600 °C.

Transmission electron microscopy (TEM)

TEM images were collected on a Philips CM 30 Twin STEM fitted Kevex delta plus X-ray disperse electron spectroscopy (EDX) and Gatan model 666 PEELs operating at 300 kV. Samples for imaging were deposited onto a 200 mesh copper grid, and the liquid was allowed to dry in air at room temperature.

UV-vis spectroscopy

UV-vis spectra were recorded at room temperature on a Hewlett Packard HP 8452 UV-vis spectrophotometer in the range of 200-800 nm. UV-vis studies were performed on a quartz cuvette filled with 0.6 ml of different concentrations of CD Au NPs **1a** in phosphate buffer pH 5.7 and different concentrations of free native CD. Titrations were performed by gradual additions (of 1 to 10 μl, once per 5 min) of solutions of the guest molecules in phosphate buffer pH 5.7 and different concentrations of free native CD. After each addition, the UV-vis spectrum was recorded. Throughout this chapter, the

concentration of CD Au NPs **1a** and guest molecules is expressed as the concentration of functional groups. Modeling of the UV-vis spectra was performed by fitting a set of Gaussians to the spectra, in order to deconvolute the plasmon absorption band (used for determination of λ_{max} and the absorbance A at 530 nm) of the Au NPs. The deconvolution of the absorbance is needed particularly in the case of the experiments with the dendrimers (Figures 4.3D and 4.5D) because scattering of the light, caused by severe aggregation, led to an apparent increase of the overall absorbance. All solutions were prepared in phosphate buffer pH 5.7 with a constant excess of free CD in both solutions.

Isothermal calorimetry (ITC) titrations

Calorimetric titrations were performed at 25 °C using a Microcal VP-ITC titration microcalorimeter. Sample solutions were prepared in Millipore water. Titrations were performed by adding aliquots of **2** (5 mM) to the CD Au NPs **1a** solution (2.6 mg/ml).

4.5 References and Notes

1. Mammen, M.; Choi, S. K.; Whitesides, G. M. *Angew. Chem. Int. Ed.* **1998**, *37*, 2755-2794.
2. Kiessling, L. L.; Gestwicki, J. E.; Strong, L. E. *Curr. Opin. Chem. Biol.* **2000**, *4*, 696-703.
3. Akai, S.; Kajihara, Y.; Nagashima, Y.; Kamei, M.; Arai, J.; Bito, M.; Sato, K. *J. Carbohydr. Chem.* **2001**, *20*, 121-143.
4. Dam, T. K.; Roy, R.; Das, S. K.; Oscarson, S.; Brewer, C. F. *J. Biol. Chem*. **2000**, *275*, 14223-14933.
5. Kanai, M.; Mortell, K. H.; Kiessling, L. L. *J. Am. Chem. Soc.* **1997**, *119*, 9931-9932.
6. Cairo, C. W.; Gestwicki, J. E.; Kanai, M.; Kiessling, L. L. *J. Am. Chem. Soc.* **2002**, *124*, 1615-1619.
7. Gestwicki, J. E.; Cairo, C. W.; Strong, L. E.; Oetjen, K. A.; Kiessling, L. L. *J. Am. Chem. Soc.* **2002**, *124*, 14922-14933.
8. Kitov, P. I.; Shimizu, H.; Homans, S. W.; Bundle, D. R. *J. Am. Chem. Soc.* **2003**, *125*, 3284-3294.
9. Choi, S. K.; Mammen, M.; Whitesides, G. M. *J. Am. Chem. Soc.* **1997**, *119*, 4103-4111.
10. Roy, R.; Pagé, D.; Perez, S. F.; Bencomo, V. V. *Glycoconjugate J.* **1998**, *15*, 251-263.

11. Niemeyer, C. M. *Angew. Chem. Int. Ed.* **2001**, *40*, 4128-4158.
12. Barrientos, A. G.; De La Fuente, J. M.; Rojas, T. C.; Fernández, A.; Penadés, S. *Chem. Eur. J.* **2003**, *9*, 1909-1921.
13. Gu, H. W.; Ho, P. L.; Tong, E.; Wang, L.; Xu, B. *Nano Lett.* **2003**, *3*, 1261-1263.
14. Lin, C. C.; Yeh, Y. C.; Yang, C. Y.; Chen, G. F.; Chen, Y. C.; Wu, Y. C.; Chen, C. C. *Chem. Commun.* **2003**, 2920-2921.
15. Lin, C. C.; Yeh, Y. C.; Yang, C. Y.; Chen, C. L.; Chen, G. F.; Chen, C. C.; Wu, Y. C. *J. Am. Chem. Soc.* **2002**, *124*, 3508-3509.
16. Sun, X. L.; Kanie, Y.; Guo, C. T.; Kanie, O.; Suzuki, Y.; Wong, C. H. *Eur. J. Org. Chem.* **2000**, 2643-2653.
17. Kingerywood, J. E.; Williams, K. W.; Sigal, G. B.; Whitesides, G. M. *J. Am. Chem. Soc.* **1992**, *114*, 7303-7305.
18. Particularly well-characterized aggregating systems can be found in: (a) Olsen, L. R.; Dessen, A.; Gupta, D.; Sabesan, S.; Sacchettini, J. C. *Biochemistry* **1997**, *36*, 15073-15080. (b) Dimick, S. A.; Powell, S. C.; McMahon, S. A.; Moothoo, D. N.; Naismisth, J. H.; Toone, E. J. *J. Am. Chem. Soc*. **1999**, *121*, 10286-10296.
19. Doyle, E. L.; Hunter, C. A.; Phillips, H. C.; Webb, S. J.; Williams, N. H. *J. Am. Chem. Soc.* **2003**, *125*, 4593-4599.
20. Yang, T. L.; Baryshnikova, O. K.; Mao, H. B.; Holden, M. A.; Cremer, P. S. *J. Am. Chem. Soc.* **2003**, *125*, 4779-4784.
21. Mann, D. A.; Kanai, M.; Maly, D. J.; Kiessling, L. L. *J. Am. Chem. Soc.* **1998**, *120*, 10575-10582.
22. Smith, E. A.; Thomas, W. D.; Kiessling, L. L.; Corn, R. M. *J. Am. Chem. Soc.* **2003**, *125*, 6140-6148.
23. Gestwicki, J. E.; Kiessling, L. L. *Nature* **2002**, *415*, 81-84.
24. Beulen, M. W. J.; Bügler, J.; De Jong, M. R.; Lammerink, B.; Huskens, J.; Schönherr, H.; Vancso, G. J.; Boukamp, B. A.; Wieder, H.; Offenhauser, A.; Knoll, W.; Van Veggel, F. C. J. M.; Reinhoudt, D. N. *Chem. Eur. J.* **2000**, *6*, 1176-1183.
25. Onclin, S.; Mulder, A.; Huskens, J.; Ravoo, B. J.; Reinhoudt, D. N. *Langmuir* **2004**, *20*, 5460-5466.
26. Huskens, J.; Deij, M. A.; Reinhoudt, D. N. *Angew. Chem. Int. Ed.* **2002**, *41*, 4467-4471.
27. Auletta, T.; Dordi, B.; Mulder, A.; Sartori, A.; Onclin, S.; Bruinink, C. M.; Péter, M.; Nijhuis, C. A.; Beijleveld, H.; Schönherr, H.; Vancso, G. J.; Casnati, A.; Ungaro, R.; Ravoo, B. J.; Huskens, J.; Reinhoudt, D. N. *Angew. Chem. Int. Ed.* **2004** , *43*, 369-373.

28. Drechsler, U.; Erdogan, B.; Rotello, V. M. *Chem. Eur. J.* **2004**, *10*, 5570-5579.
29. Kumar, A.; Whitesides, G. M. *Apply Physical Letters* **1993**, *63*, 2002-2004.
30. Boyen, H. G.; Kästle, G.; Weigl, F.; Koslowski, B.; Dietrich, C.; Ziemann, P.; Spatz, J. P.; Riethmuller, S.; Hartmann, C.; Möller, M.; Schmid, G.; Garnier, M. G.; Oelhafen, P. *Science* **2002**, *297*, 1533-1536.
31. Brust, M.; Kiely, C. J.; Bethell, D.; Schiffrin, D. J. *J. Am. Chem. Soc.* **1998**, *120*, 12367-12368.
32. Wang, G. L.; Murray, R. W. *Nano Lett.* **2004**, *4*, 95-101.
33. Mucic, R. C.; Storhoff, J. J.; Mirkin, C. A.; Letsinger, R. L. *J. Am. Chem. Soc.* **1998**, *120*, 12674-12675.
34. Liu, J.; Mendoza, S.; Román, E.; Lynn, M. J.; Xu, R. L.; Kaifer, A. E. *J. Am. Chem. Soc.* **1999**, *121*, 4304-4305.
35. Liu, J.; Álvarez, J.; Ong, W.; Kaifer, A. E. *Nano Lett.* **2001**, *1*, 57-60.
36. Frankamp, B. L.; Boal, A. K.; Rotello, V. M. *J. Am. Chem. Soc.* **2002**, *124*, 15146-15147.
37. Boal, A. K.; Ilhan, F.; Derouchey, J. E.; Thurn-Albrecht, T.; Russell, T. P.; Rotello, V. M. *Nature* **2000**, *404*, 746-748.
38. Galow, T. H.; Boal, A. K.; Rotello, V. M. *Adv. Mater.* **2000**, *12*, 576-579.
39. Norsten, T. B.; Frankamp, B. L.; Rotello, V. M. *Nano Lett.* **2002**, *2*, 1345-1348.
40. Carroll, J. B.; Frankamp, B. L.; Rotello, V. M. *Chem. Commun.* **2002**, 1892-1893.
41. Boal, A. K.; Galow, T. H.; Ilhan, F.; Rotello, V. M. *Adv. Funct. Mater.* **2001**, *11*, 461-465.
42. Thibault, R. J.; Galow, T. H.; Turnberg, E. J.; Gray, M.; Hotchkiss, P. J.; Rotello, V. M. *J. Am. Chem. Soc.* **2002**, *124*, 15249-15254.
43. Thibault, R. J.; Hotchkiss, P. J.; Gray, M.; Rotello, V. M. *J. Am. Chem. Soc.* **2003**, *125*, 11249-11252.
44. Frankamp, B. L.; Uzun, O.; Ilhan, F.; Boal, A. K.; Rotello, V. M. *J. Am. Chem. Soc.* **2002**, *124*, 892-893.
45. Ryan, D.; Rao, S. N.; Rensmo, H.; Fitzmaurice, D.; Preece, J. A.; Wenger, S.; Stoddart, J. F.; Zaccheroni, N. *J. Am. Chem. Soc.* **2000**, *122*, 6252-6257.
46. Fullam, S.; Rao, S. N.; Fitzmaurice, D. *J. Phys. Chem. B* **2000**, *104*, 6164-6173.
47. Aherne, D.; Rao, S. N.; Fitzmaurice, D. *J. Phys. Chem. B* **1999**, *103*, 1821-1825.
48. Connolly, S.; Fitzmaurice, D. *Adv. Mater.* **1999**, *11*, 1202-1205.
49. Liu, J.; Xu, R. L.; Kaifer, A. E. *Langmuir* **1998**, *14*, 7337-7339.
50. (a) For a general review on cyclodextrins, see: *Chem. Rev*. **1998**, *98*, volume 5. (b) For a list with possible guest molecules, see: Rekharsky, M. V.; Inoue, Y. *Chem. Rev*. **1998**, *98*,

1880-1901.

51. Liu, J.; Ong, W.; Román, E.; Lynn, M. J.; Kaifer, A. E. *Langmuir* **2000**, *16*, 3000-3002.
52. Liu, J.; Álvarez, J.; Kaifer, A. E. *Adv. Mater.* **2000**, *12*, 1381-1383.
53. Brust, M.; Fink, J.; Bethell, D.; Schiffrin, D. J.; Kiely, C. *Chem. Commun.* **1995**, 1655-1656.
54. Zheng, M.; Davidson, F.; Huang, X. Y. *J. Am. Chem. Soc.* **2003**, *125*, 7790-7791.
55. Zheng, M.; Li, Z. G.; Huang, X. Y. *Langmuir* **2004**, *20*, 4226-4235.
56. Malinsky, M. D.; Kelly, K. L.; Schatz, G. C.; Van Duyne, R. P. *J. Am. Chem. Soc.* **2001**, *123*, 1471-1482.
57. Hunter, R. J. *Zeta Potential in Colloid Science*, Academic Press, New York & London, **1981.**
58. Baars, M. W. P. L.; Karlsson, A. J.; Sorokin, V.; De Waal, B. F. W.; Meijer, E. W. *Angew. Chem. Int. Ed.* **2000**, *39*, 4262-4265.
59. Michels, J. J.; Baars, M. W. P. L.; Meijer, E. W.; Huskens, J.; Reinhoudt, D. N. *J. Chem. Soc., Perkin Trans. 2* **2000**, 1914-1918.
60. Huskens, J.; Mulder, A.; Auletta, T.; Nijhuis, C. A.; Ludden, M. J. W.; Reinhoudt, D. N. *J. Am. Chem. Soc.* **2004**, *126*, 6784-6797.
61. Nijhuis, C. A.; Huskens, J.; Reinhoudt, D. N. *J. Am. Chem. Soc.* **2004**, *126*, 12266-12267.
62. Concentration of **1b** (0.62 mg/ml) was similar in weight to the concentration of **1a** (0.52 mg/ml) used for the UV-vis titrations.
63. Perrin, D. D.; Armarego, W. F. L. *Purification of Laboratory Chemicals*, 3rd ed., Pergamon, Oxford, UK, **1989**.
64. Rojas, M. T.; Königer, R.; Stoddart, J. F.; Kaifer, A. E. *J. Am. Chem. Soc.* **1995**, *117*, 336-343.
65. Ciuffarin, E.; Isola, M.; Leoni, P. *J. Org. Chem.* **1981**, *46*, 3064-3070.

Chapter 5

Supramolecular Layer-by-Layer Assembly: Alternating Adsorptions of Guest- and Host-Functionalized Molecules and Particles Using Multivalent Supramolecular Interactions*

The stepwise construction of a novel kind of self-assembled organic/inorganic multilayers based on multivalent supramolecular interactions between guest-functionalized dendrimers and host-modified gold nanoparticles has been developed, yielding supramolecular layer-by-layer assembly. The deposition process was monitored by surface plasmon resonance spectroscopy. Further characterization of the multilayer films was performed by means of UV/vis absorption spectroscopy, which showed a linear increase in absorption with the number of bilayers. The growth of the gold nanoparticle plasmon absorption band corresponded to approx. a dense monolayer of gold nanoparticles per bilayer. Ellipsometry and AFM scratching experiments were used to measure the development of the film thickness with the number of bilayers, confirming linear growth and a thickness increase of approximately 2 nm/bilayer

---

* Part of this chapter has been published in: Crespo-Biel, O.; Dordi, B.; Reinhoudt, D. N.; Huskens, J. *J. Am. Chem. Soc.* **2005**, *127*, 7594-7600.

5.1 Introduction

The huge interest in nanomaterials has become an important line of research in nanotechnology for the generation of functional molecular assemblies.[1] A prerequisite for the construction of molecule-based functional devices is the development of methods for integrating those molecular components into well-ordered assemblies with a well-defined supramolecular architecture.[2] Such devices require control of molecular orientation and organization at the nanometer scale, and therefore it is essential to study and develop methods for the controlled assembly of multicomponent nanostructures. Numerous examples of supramolecular systems have been previously studied, mainly comprising of organized monomolecular films on surfaces.[3] However, the extension of this approach to multilayer films can enhance the properties of monomolecular films, and create at the same time a new class of materials possessing functional groups at controlled sites in three-dimensional arrangements.

Initially, the molecularly controlled fabrication of nanostructured films was dominated by the Langmuir-Blodgett (LB) technique, by which monolayers are formed on an air-water interface and then transferred to a solid support.[4,5] However, the LB technique requires special equipment and has limitations with respect to substrate size and topology, as well as film quality and stability. Later on, self-assembly techniques[6-9] were developed as an alternative to LB films.

In recent years, layer-by-layer (LBL) assembly[10,11] has emerged as a promising method for fabricating structured and functional thin films on solid substrates. The LBL method allows one to construct a film atop a substrate of almost any composition or topology by alternating its exposure to solutions containing species of complementary affinities.[9,12-14] LBL assembly is mostly achieved by exploiting attractive forces, and by alternating immersions the multilayer films are attained.[15,16]This method, initially developed to prepare multilayer assemblies electrostatically,[16,17] has been successfully extended to various other driving forces such as hydrogen-bonding,[18] charge transfer,[19,20] acid-base pairs,[21] metal-ion coordination,[22] inter- and/or intramolecular interactions in the dried state,[23] covalent bonds,[24] biospecific interactions (*e.g.* sugar-lectin interactions),[25] and host-guest interactions between cyclodextrin dimers and positively charged

ferrocene-appended poly(allylamine) polymers.[26] LBL assembly has been performed with a large number of materials including polymers,[17] inorganic nanoparticles,[27] clay,[28] organic components,[29] carbon nanotubes,[30] dendrimers[31] and biological macromolecules such as proteins[32] and DNA.[33]

β-cyclodextrin (CD) self-assembled monolayers (SAMs) on gold[34] and silicon oxide[35] surfaces have been prepared onto which stable positioning and patterning of molecules has been achieved by means of multiple supramolecular interactions. Therefore, these CD SAMs constitute a molecular printboard for the positioning of thermodynamically and kinetically stable assemblies of multivalent systems, for example, dendrimers.[36,37]

It has been shown that an analogous ferrocene-terminated dendrimer (generation 5, containing 64 ferrocene end groups) binds to CD SAMs on gold with approximately seven interactions to the surface,[38] leaving multiple guest groups exposed to the solution available for complexation of hosts from solution. Moreover, it has been demonstrated that these molecules bind to the CD printboards with different numbers of interactions depending on the number of functional groups present in the dendrimer, thus thermodynamically and kinetically stable assemblies can be achieved.[36,39]

In Chapter 4, the complexation-induced aggregation in solution of CD-modified gold nanoparticles (CD Au NPs) and adamantyl-functionalized dendrimers was studied. The addition of such a dendrimer to a solution containing CD Au NPs led to pronounced and irreversible precipitation of the dendrimer/CD Au NP aggregates.

In this chapter, the stepwise construction of a novel kind of self-assembled organic/metal NP multilayers based on multivalent supramolecular host-guest interactions between dendritic guest molecules and host-modified Au NPs will be described. Surface plasmon resonance (SPR), ellipsometry, UV/vis, and AFM have been used for film thickness determination and for monitoring and quantifying the growth process.

5.2 Results and Discussion

5.2.1 Synthesis of the building blocks

Multilayer thin films composed of CD Au NPs and adamantyl-terminated dendrimers (generation 5, containing 64 adamantyl end groups, **1**; see Chart 5.1) have been prepared on CD SAMs using a supramolecular approach. CD SAMs were prepared on gold[34] and on silicon oxide[35] surfaces (Chart 5.1) following literature procedures. The binding of multivalent guest molecules onto these surfaces has shown that the binding properties of these printboards are practically identical.[35,37,40,41]

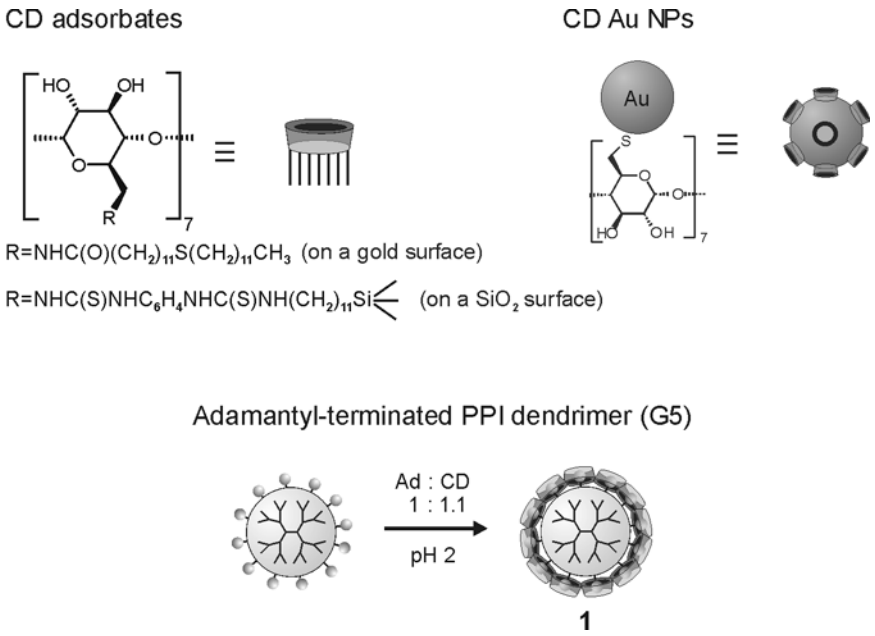

Chart 5.1: *Chemical structures of the host adsorbates, the CD Au NPs, and adamantyl-terminated PPI dendrimers* ***(1)*** *used in this study.*

CD-coated Au NPs (Chart 5.1) were synthesized according to a literature procedure[42] by reduction of $AuCl_4^-$ in DMSO solution containing perthiolated β-CD[43] (see Chapter 4). This one-phase procedure is similar to that reported by Brust and co-workers.[44] Using TEM, a mean particle size of 2.8 ± 0.6 nm was found. We chose to use

adamantyl-terminated poly(propylene imine) dendrimers, since the CD-adamantyl interaction is one of the strongest,[45] the number of adamantyl units (ranging from 4 - 64) can be easily varied, and the spherical shape of the dendrimers allows the multivalent display of these guest functionalities. Dendrimer **1** (Chart 5.1) has 64 adamantyl groups and the complexation with CD in solution has been described before.[46]

5.2.2 Supramolecular layer-by-layer assembly

The LBL assembly of dendrimer **1** and CD Au NPs is shown in Scheme 5.1. It is emphasized that the idealized layer order in this scheme does not reflect a possible intermixing of the layers after adsorption, but that it merely reflects the sequential adsorption steps. Throughout this chapter, the concentration of the two components is expressed as the concentration of functional substituents, *i.e.* of CD and adamantyl groups. The multilayers were deposited onto CD SAMs on gold[34] and on SiO_2.[35]

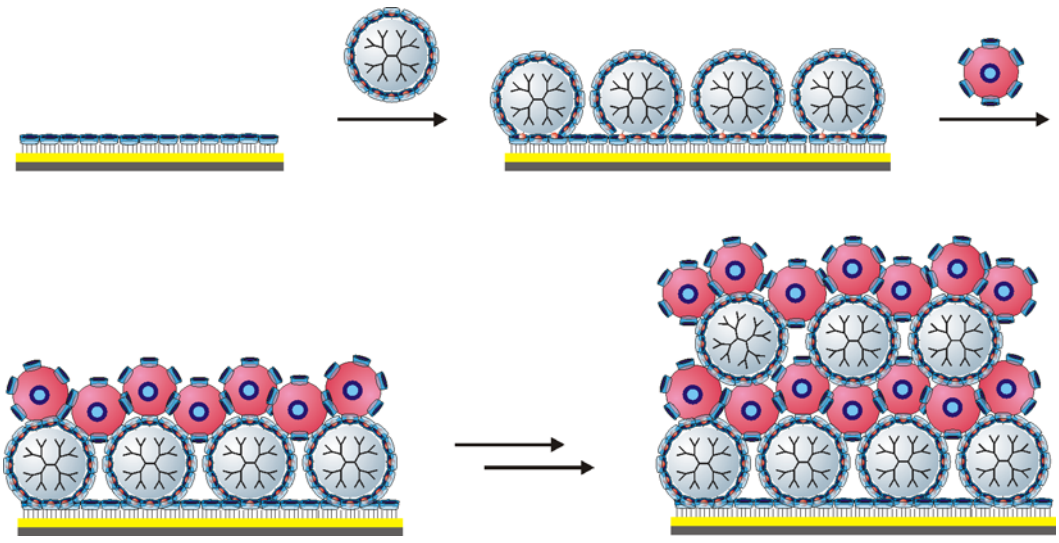

Scheme 5.1: *LBL assembly scheme for the alternating adsorption of adamantyl-terminated PPI dendrimer* ***1*** *and CD Au NPs onto CD SAMs.*

Adamantyl-terminated PPI dendrimers were insoluble in water, but by complexation of the adamantyl endgroups by slight excess of cyclodextrin and by the

protonation of the dendrimer core amine functionalities, they could be brought into aqueous solution (pH = 2).[46] However, at pH > 7 precipitation of the generations 3-5 of these PPI dendrimers occurs. Conversely, CD Au NPs are not stable in acidic solution. Therefore the LBL assembly was typically accomplished by alternately dipping the substrate into a solution of **1** in aqueous acidic 1 mM CD (pH = 2) solution, followed by rinsing the substrate with the same 1 mM CD (pH = 2) solution, and into an aqueous CD Au NPs solution, followed by rinsing with water. The delivery of the dendrimers from solution-phase CD complexes to the CD SAMs makes use of the competition between the solution and the surface host sites, as well as the multivalency of the surface host sites emerging from the surface immobilization.[36,37]

5.2.3 Characterization of the layer-by-layer assembly

The supramolecular LBL film formation was studied in situ by SPR spectroscopy. SPR titrations were performed in the presence of water or 1 mM CD pH 2 as the background, depending on which of the two components was added (see above). The formation of one bilayer is illustrated in Figure 5.1, where the SPR reflectivity changes upon injection of an aqueous solution of **1** (A1; vs. a background (a1) of 1 mM CD pH 2) and CD Au NPs (B1; vs. a background (b) of water), are shown. After the injection of each component, the adsorption was followed for 20 – 25 min followed by rinsing of the cell with the corresponding backgrounds 1 mM CD pH 2 (a1) after A1 and water (b) after B1, in order to remove non-specifically adsorbed material. In the SPR experiments, the background is switched before the actual injection of the other component (b before B1 and a1 before A1) in order to allow quantitative comparison of both adsorption steps with subsequent bilayer formation steps.

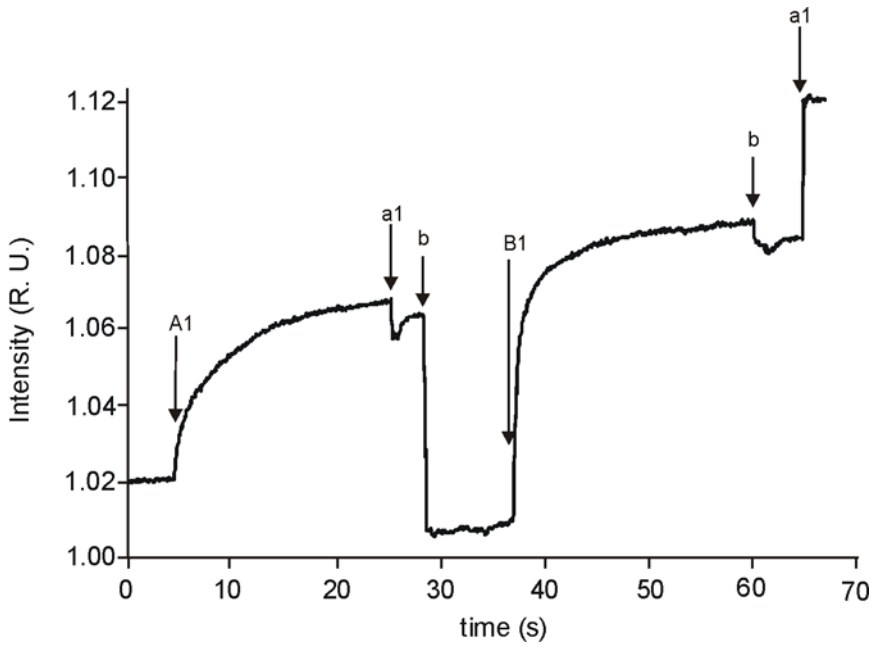

Figure 5.1: *SPR spectroscopy time traces for the adsorption of one bilayer of* ***1*** *(0.01 mM in hydrophobic moieties in a 1 mM CD solution, pH 2) and CD Au NPs (5.8 μM in CD moieties in water) onto a CD SAM on gold; solutions: A1:* ***1****; B1: CD Au NPs; a1: 1 mM CD, pH 2; b1: water.*

The SPR-monitored multilayer formation is shown in Figure 5.2, where 6-7 bilayers were successfully accomplished. SPR titrations were performed at different concentrations of the components (shown in Figure 5.2: left: 0.1 mM in hydrophobic moieties for **1** and 58 μM in CD moieties for CD Au NPs; and right: 0.01 mM **1** and 5.8 μM CD Au NPs) with the aim to find the right conditions for the supramolecular LBL assembly. The top graphs show the SPR sensograms, while the bottom graphs show the reflectivities as a function of the number of bilayers.

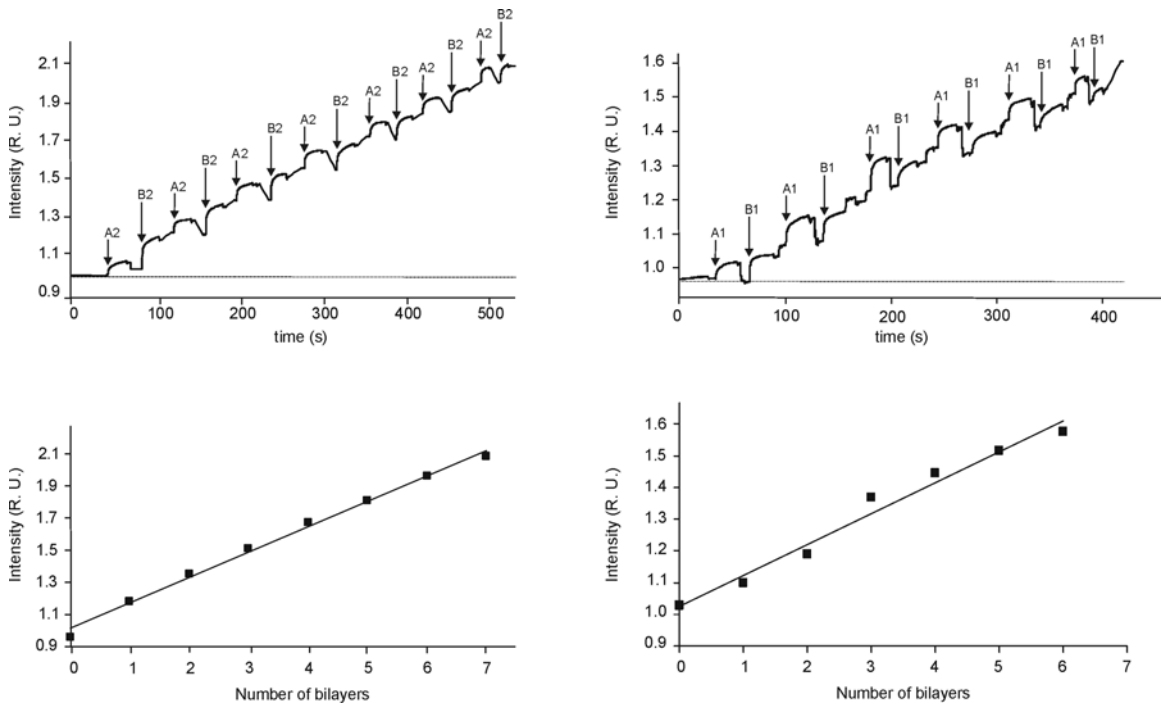

Figure 5.2: *Top: SPR time traces for the LBL assembly process of **1** (left, A2: 0.1 mM; right, A1: 0.01 mM, in a 1 mM CD pH 2 solution) and CD Au NPs (left, B2: 58 μM; right, B1: 5.8 μM, in water) onto CD SAMs on gold. Bottom: SPR reflectivity changes as a function of the number of bilayers of **1** and CD Au NPs on CD SAMs on gold.*

As shown in Figure 5.2, the adsorption behavior was observed to be similar at these concentrations. The bottom graphs show that the growth is linear with the number of bilayers deposited onto the CD SAMs for both concentrations. The slopes of the lines indicate that 10 times higher concentrations of both dendrimers and CD Au NPs leads to only about 1.5 times more adsorption, clearly confirming the supramolecular specificity of binding. For even higher concentrations, physisorption of in particular the CD Au NPs appeared to be more severe, while for lower concentrations adsorption of the dendrimer appeared to become too slow due to severe diffusion limitation.

Titrations performed with **1** (0.01 mM) on an oligo(ethylene glycol)[47] SAM (lacking the host sites) showed non-specific adsorption of **1**, which could be reversed by copious rinsing with concentrated CD solutions (Figure 5.3, left). As illustrated in Figure 5.3 (right), the adsorption of a low concentration of CD Au NPs (5.8 μM) (B1) onto a CD

SAM showed a small refractive index effect on the SPR signal, which could be instantaneously restored by rinsing with water. However, injection of a higher concentration of CD Au NPs (58 μM) (B2) showed non-specific adsorption, and extensive rinsing of the cell with water and salt solutions did not completely restore the signal. Even after rinsing with monovalent guests, sodium 1-adamantylcarboxylate (C) and 1-adamantylamine (D), more than 50% of the CD Au NPs remained on the surface. However, as has been observed in Figure 5.2, the LBL assembly for both CD Au NPs concentrations gave comparable SPR reflectivity changes, thus indicating that both concentrations are suitable for the LBL assembly. Apparently, the nonspecific adsorption of the CD Au NPs on a layer of already adsorbed Au CD NPs is significantly less severe than on a bare CD SAM.

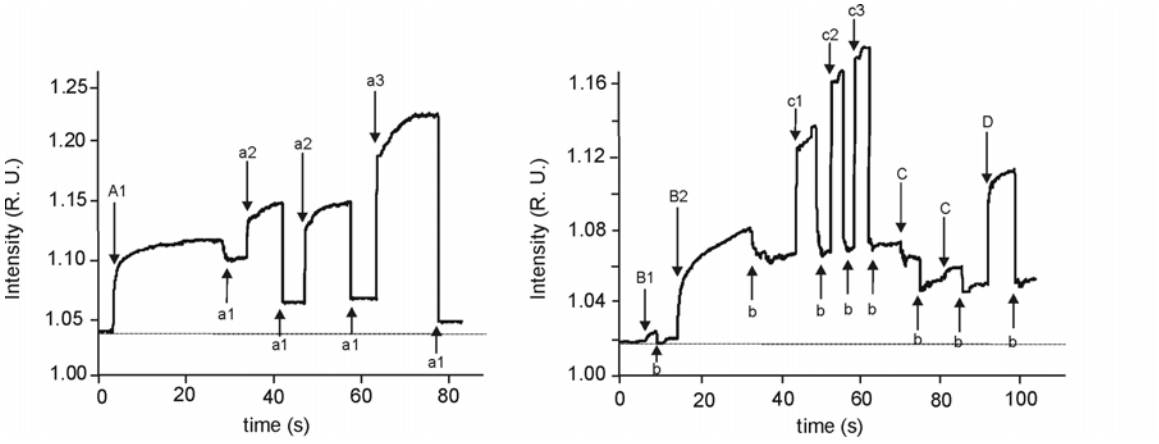

Figure 5.3: *(left) SPR time traces of the adsorption and attempted desorption of* ***1*** *(0.01 mM) onto an oligo(ethylene glycol) SAM; solutions: A1: 0.01 mM* ***1****; a1: 1 mM CD pH 2; a2: 5 mM CD pH 2; a3: 10 mM CD pH 2; (right) SPR time traces of the adsorption and attempted desorption of CD Au NPs onto a CD SAM; solutions: B1: 5.8 μM CD Au NPs; B2: 58 μM CD Au NPs; b: H_2O; c1: 50 mM NaCl; c2: 100 mM NaCl; c3: 1 M NaCl; C: 1 mM sodium 1-adamantylcarboxylate; D: 5 mM 1-adamantylamine.*

Information on the absolute film thickness increase with the number of bilayers was obtained from ellipsometry, using CD SAMs on SiO_2. Figure 5.4 shows the ellipsometric thickness as a function of the number of deposited bilayers. The starting 3

nm for the CD SAM confirms our earlier data.[35] The thickness of the multilayer film (using an estimated a refractive index of 1.500 for the organic/metal layers and 1.457 for the underlying native oxide) follows a linear behavior with the number of bilayers, in accordance with the SPR results. The line fit indicates a thickness increase of about 2 nm/bilayer. The exact value of the real part of the multilayer refractive index is not known, hence higher accuracies cannot be obtained.

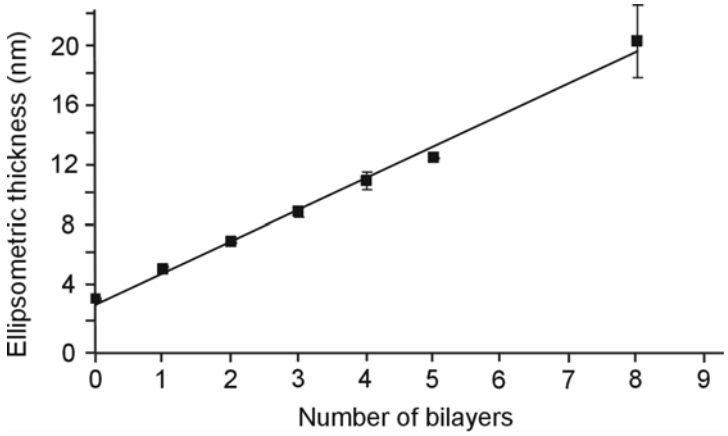

Figure 5.4: *Ellipsometric thicknesses as a function of the number of bilayers of* ***1*** *(0.1 mM in a 1 mM CD solution, pH 2) and CD Au NPs (58 μM in water) onto a CD SAM on silicon oxide.*

UV/vis spectroscopy was used to monitor the supramolecular assembly of the CD Au NPs on a glass surface. Dendrimer adsorption was not visible in the visible region. When CD Au NPs were adsorbed onto the film, the CD Au NPs plasmon absorption band in the visible region emerged at around 525 nm similar to the CD Au NPs in solution (see Chapter 4). Figure 5.5 (left) shows the UV/vis absorption spectra of the multilayer **1**/CD Au NPs films for different numbers of bilayers on a CD SAM. The increase in absorption at 525 nm as a function of the number of bilayers deposited on the CD surface is shown in Figure 5.5 (right). An essentially linear dependence was found, confirming the SPR and ellipsometry data. The linearity was shown to last up to 18 bilayers, which is a strong indication of a well-defined deposition process.[10,48]

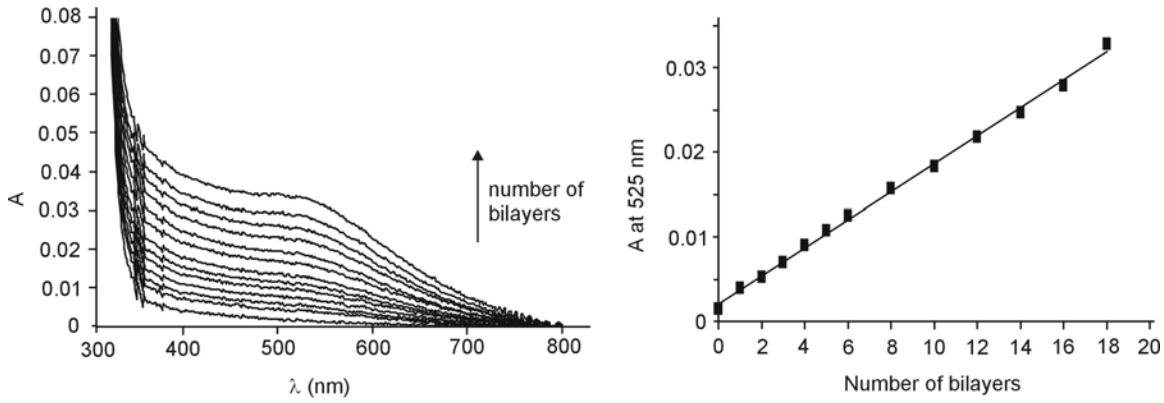

Figure 5.5: *UV/vis absorption spectra (left) and absorbance at 525 nm (right) as a function of the number of bilayers of* ***1*** *(0.1 mM in a 1 mM CD solution, pH 2) and CD Au NPs (58 μM in water) onto a CD SAM on glass.*

UV/vis spectroscopy can give a quantitative estimate of the amount of material deposited after each cycle, when it is assumed that the plasmon band extinction coefficients are identical in solution and in the multilayer architecture. Based on previous results (see Chapter 4) on aggregation of these CD Au NPs with dendrimers in solution, this assumption seems justified. From the absorption at 525 nm of a solution of 0.29 $mg \cdot cm^{-3}$ (58 μM in CD moieties) CD Au NPs, the extinction coefficient, ε, was calculated to be 0.586 $cm^2 \cdot mg^{-1}$ using the Lambert-Beer law. From the slope (0.001607) of Figure 5.5 (right) the surface coverage for one layer of CD Au NPs was calculated to be 3.1 $\mu g \cdot cm^{-2}$. A theoretical value of 1.7 $\mu g \cdot cm^{-2}$ was estimated based on the formation of a monolayer of CD Au NPs in a hexagonal packing with a lattice periodicity of a gold NP core summed with twice the CD cavity height,[49] and taking into account that the gold core contributes 62% the total weight of the Au NPs (see Chapter 4). Thus, the experimental value is a factor 1.8 larger than the crude theoretical estimate obtained assuming a hexagonal packing of monodisperse particles. Most of this difference can probably be attributed to the slight physisorption of the CD Au NPs at the relatively high concentration employed in the UV/vis experiments (compare to SPR results shown in Figure 5.2 and discussed above). Nevertheless, the fair comparison between the

experimental and the theoretical values clearly indicates that close to a monolayer of Au NPs is deposited after each deposition cycle.

AFM was used for a direct determination of the thickness of the multilayer thin film.[50] The LBL assembly was achieved by the alternating immersion of a CD SAM on an annealed gold substrate into the dendrimer and CD Au NPs solutions (0.01 mM for **1** and 5.8 μM for CD Au NPs) with rinsing steps in between. The AFM tip was used to create a scratch down to the gold, and the thickness was determined by scanning across the scratch with the AFM tip. The thickness was determined on different samples with 1-6 bilayers. The multilayer thickness as a function of the number of deposited bilayers is shown in Figure 5.6, demonstrating that the thickness of the film is linearly related to the number of deposited bilayers, thus corroborating the previous results. An estimate of the multilayer thickness of 2 nm/bilayer was obtained in congruence with the ellipsometry results.

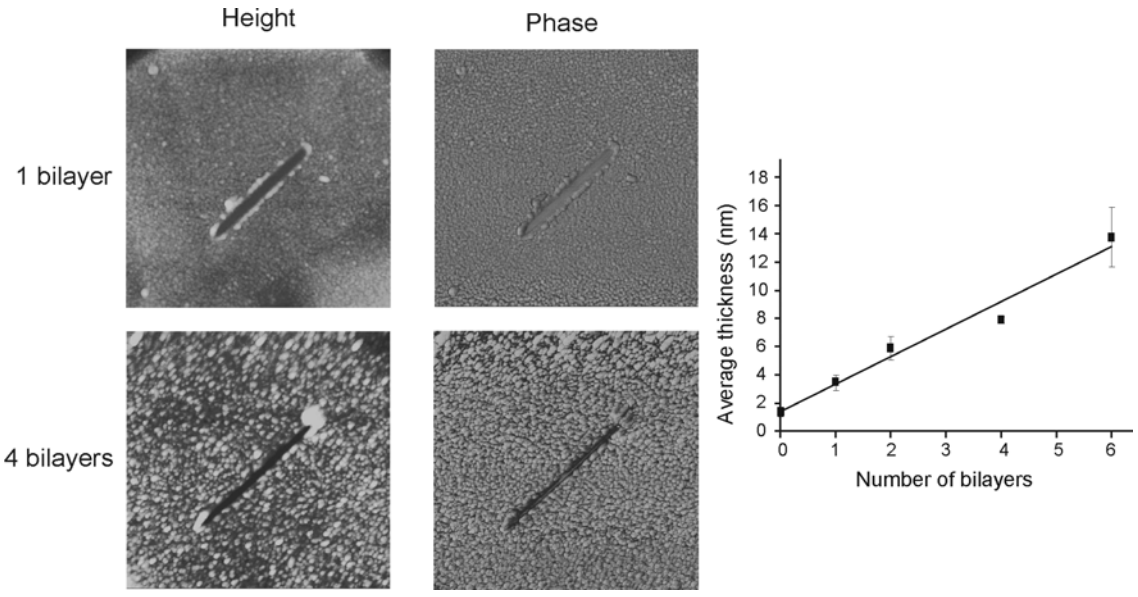

Figure 5.6: *TM-AFM height (top left, z range 20.0 nm; bottom left, z range 10.0 nm) and phase (top center, z range 50.0 °; bottom center, z range 80.0 °) images (1.2 × 1.2 μm^2) in air of 1 bilayer (top) and 4 bilayers (bottom) on a CD SAM after LBL assembly (**1**, 0.01 mM in hydrophobic moieties in a 1 mM CD pH 2 solution, and CD Au NPs, 5.8 μM in water). Graphic on the right: Multilayer thickness as a function of the number of bilayers measured with AFM scratching experiments.*

5.3 Conclusions

A supramolecular procedure was introduced for the stepwise construction of multilayer thin films. The procedure, based on the LBL assembly of guest-functionalized dendrimers and CD Au NPs, was demonstrated to yield multilayer thin films with thickness control at the nm level. Characterization by means of SPR, UV/vis spectroscopy, ellipsometry and AFM showed a well-defined multilayer formation, an accurate thickness control, and the need of specific host-guest interactions.

Such protocols as described in this chapter, can potentially be used for obtaining various structures, whose assembly is driven by multiple supramolecular interactions. This constitutes a general nanofabrication paradigm for the integration of organic, inorganic, metallic, and biomolecular components while retaining the interfacing supramolecular specificity. The ultimate *z* control, when combined with top-down surface patterning strategies such as soft lithography[16] for *x*,*y* control, can lead to 3D nanofabrication schemes.

5.4 Experimental Section

Materials

Chemicals were obtained from commercial sources and used as such. β-cyclodextrin (CD) was dried in vacuum at 80 °C in the presence of P_2O_5 for at least 5 h before use. Solvents were purified according to standard laboratory methods.[51] Perthiolated β-CD[43] and per-6-amino-β-cyclodextrin[52] were synthesized according to literature procedures. Millipore water with a resistance larger than 18 MΩ·cm was used in all our experiments. Generation 5 adamantyl-terminated poly(propylene imine) (PPI) dendrimer (with 64 adamantyl groups) (**1**) was synthesized as reported before.[53] Synthesis of the CD heptathioether adsorbate was reported previously.[34] 1-Mercaptoundec-11-yl-tetra(ethylene glycol) was synthesized according to a literature procedure.[47] CD-coated Au NPs were synthesized according to literature procedure,[42] by the reduction of $HAuCl_4$

in DMSO by $NaBH_4$ in the presence of per-6-thio-cyclodextrin.[43] The CD Au NPs were characterized by UV/vis spectroscopy, ^1H NMR, transmission electron microscopy (TEM), and thermogravimetric analysis (TGA). Using TEM, a mean particle size of 2.8 ± 0.6 nm was found (see Chapter 4). NMR spectra were recorded on Varian AC300 and AMX400 spectrometers. FAB-MS spectra were recorded with a Finnigan MAT 90 spectrometer using m-NBA as the matrix.

Substrate and monolayer preparation

All glassware used to prepare monolayers was immersed in piraña (conc. H_2SO_4 and 33% H_2O_2 in a 3:1 ratio). (Warning! piraña should be handled with caution; it has detonated unexpectedly). The glassware was rinsed with large amounts of Millipore water. All solvents used in monolayer preparation were of p.a. grade. All adsorbate solutions were prepared freshly prior to use. Round glass-supported gold substrates for SPR (2.54 cm diameter; 47.5 nm Au) and gold substrates for AFM (20 nm of gold on a glass substrate) were obtained from Ssens BV (Hengelo, The Netherlands). Gold substrates were cleaned by immersing the substrates in piraña for 5 s and leaving the substrates for 5 min in absolute EtOH.[54] Gold substrates used in the AFM scratching experiments were flame-annealed in a H_2 flame (200 nm on quartz, Metallhandel Schroer GmbH., Lienen, Germany). The substrates were subsequently immersed into a 0.1 mM CD heptathioether adsorbate solution in EtOH and $CHCl_3$ (1:2 v/v) for 16 h at 60 °C. SAMs of 1-Mercaptoundec-11-yl-tetra(ethylene glycol) were adsorbed from EtOH at r.t. for 24 h. The samples were removed from the solution and rinsed with substantial amounts of chloroform, ethanol, and Millipore water. Silicon oxide substrates were exposed to a cooled (3-7 °C) 0.1 vol % solution of 1-cyano-11-trichlorosilylundecane (purchased from Gelest Inc.) in freshly distilled toluene for 35 min under N_2. Following monolayer formation,[35] the substrates were rinsed with toluene to remove any excess of silanes and subsequently dried in a stream of nitrogen. The cyano-terminated SAMs were reduced to amines, and transformation of the amine-terminated SAMs to isothiocyanate-bearing layers was accomplished by exposure to a solution of 1,4-phenylene diisothiocyanate.

CD-terminated SAMs were finally obtained by reaction of the isothiocyanate-terminated monolayer with per-6-amino-β-cyclodextrin.[52]

Multilayer formation

The CD SAM substrates were immersed into the solution of dendrimer **1** for 10 min, followed by rinsing with 1 mM CD at pH 2. The films were then immersed in the CD Au NPs solution for 10 min, followed by rinsing with water. A multilayer structure was formed by repeating both adsorption steps in an alternating manner. For SPR measurements, titrations were performed starting with a buffer solution (a1, 1 mM CD pH 2) in the cell which was replaced by a solution of dendrimer **1**. After addition of **1**, the cell was thoroughly rinsed with 1 mM CD pH 2 followed by rinsing with water. After stabilization of the SPR signal, the cell solution was replaced by a CD Au NPs solution followed by extensive rinsing with water, and then switching back to the original CD solution (a1). The same procedure was repeated until the required number of bilayers was achieved.

Surface plasmon resonance (SPR) spectroscopy

The SPR setup was obtained from Resonant Probes GmbH.[55] A laser beam from the HeNe laser (JDS Uniphase, 10mW, λ = 632.8 nm) passes through a chopper that is connected to a lock-in amplifier (EG&G, 7256). The modulated beam then passes through two polarizers (Owis), by which the intensity and the plane of polarization of the laser can be adjusted. The modulated beam passes a beam-expanding unit (spatial filter) with a pinhole (25 μm) for spectral cleaning of the wave fronts. The light is coupled via a high index prism (Scott, LaSFN9) in this Kretschmann configuration to the (Au) metal-coated substrate which is index-matched to the prism in contact with a Teflon cell having O-rings for a liquid-tight seal. The sample cell is mounted on top of a θ-2θ goniometer with the detector measuring the reflectivity changes as a function of the angle of incidence of the p-polarized incoming laser beam. The incoming s/p laser beam passes through a beam splitter, which splits the p- and the s-polarized light. The s-polarized light

is conducted to a reference detector. The p-polarized light passes a beam-expanding unit (spatial filter) with a pinhole (25 μm) for spectral cleaning and control of the intensity of p-polarized light and is collected into a photodiode detector. The multilayer formation was measured in real time by recording the changes in the reflectivity in the fixed angle mode (55.2°).

UV/vis spectroscopy

Multilayers were deposited on a CD-modified glass substrate. UV/vis spectra were recorded on a Varian Cary 300 Bio instrument in double-beam mode, using an uncovered glass slide as a reference. The glass slide was placed perpendicular to the beam in order to maintain the same positioning during each measurement.

Ellipsometry

Ellipsometric measurements were performed on a Plasmon ellipsometer (λ = 633 nm) assuming a refractive index of 1.500 for the organic/metal multilayers and 1.457 for the underlying native oxide. The thickness of the SiO_2 layer was measured separately on an unmodified part of the same wafer and subtracted from the total layer thickness determined for the monolayer-covered silicon substrate. Optical measurements were performed after deposition of every bilayer on the same substrate, without changing the parameters of the ellipsometer.[56]

Atomic force microscopy (AFM)

AFM measurements were carried out on multilayer structures adsorbed on CD SAMs on flame-annealed gold substrates in tapping mode with a Nanoscope III multimode AFM (Digital Instrument, Santa Barbara, CA, USA) using silicon cantilever/tip (Nanosensor, Wetzlar, Germany; cantilever resonance frequency f_0= 280-320 kHz). A sample area of 500 × 500 nm was scanned by a silicon tip with a radius in the range of 5–10 nm, with a frequency of 1.5 Hz. The furrow was produced with the slow scanning motion disabled by gradually increasing the tip–sample interaction in steps of 0.5 V of the amplitude

setpoint, after each four scanning cycles. To easily locate the furrow and produce a better resolution, the scan size was increased and the scan direction was set to 45°. The samples were prepared on annealed gold.

5.5 References and Notes

1. See for example: a) Tredgold, R. H., *Order in Organic Films*, Cambridge University Press, Cambridge, UK, **1994**. b) Parikh, A. N.; Liedberg, B.; Atre, S. V.; Ho, M.; Allara, D. L. *J. Phys. Chem.* **1995**, *99*, 9996-10008. c) Finklea, H. O. in *Electroanalytical Chemistry*, Vol 19 (Eds: Bard, A. J.; Rubinstein, I.), Marcel Dekker, New York, U.S.A., **1996**.
2. Lehn, J.- M. *Supramolecular Chemistry*; VCH Press: New York, U.S.A., **1995**.
3. Ulman, A. *Chem. Rev.* **1996**, *96*, 1533-1554.
4. Blodgett, K. B. *J. Am. Chem. Soc.* **1934**, *56*, 495-495.
5. Blodgett, K. B.; Langmuir, I. *Phys. Rev.* **1937**, *51*, 964-982.
6. Whitesides, G. M. *Chimia* **1990**, *44*, 310-311.
7. Fendler, J. H.; Meldrum, F. C. *Adv. Mater.* **1995**, *7*, 607-632.
8. Colvin, V. L.; Goldstein, A. N.; Alivisatos, A. P. *J. Am. Chem. Soc.* **1992**, *114*, 5221-5230.
9. For self-assembled monolayers on gold surfaces: a) Nuzzo, R. G.; Allara, D. L. *J. Am. Chem. Soc.* **1983**, *105*, 4481-4483. b) Rubinstein, I.; Steinberg, S.; Tor, Y.; Shanzer, A.; Sagiv, J. *Nature* **1988**, *332*, 426-429. For self-assembled monolayers on silicon oxide: d) Maoz, R.; Sagiv, J. *Langmuir* **1987**, *3*, 1045-1051. e) Maoz, R.; Sagiv, J. *Langmuir* **1987**, *3*, 1034-1044. f) Wasserman, S. R.; Tao, Y.; Whitesides, G. M. *Langmuir* **1989**, *5*, 1074-1087. g) Onclin, S.; Ravoo, B. J.; Reinhoudt, D. N. *Angew. Chem. Int. Ed.* **2005**, *44*, 6282-6304.
10. Decher, G.; Hong, J. D. *Makromol. Chem., Macromol. Symp.* **1991**, *46*, 321-327.
11. Decher, G. *Science* **1997**, *277*, 1232-1237.
12. Hammond, P. T. *Curr. Opin. Colloid Interface Sci.* **1999**, *4*, 430-442.
13. Schönhoff, M. *Curr. Opin. Colloid Interface Sci.* **2003**, *8*, 86-95.
14. Decher, G.; Schlenoff, J. B., *Multilayer thin films*; Eds. Wiley: Weinheim, Germany, **2003**.
15. Decher, G.; Hong, J. D.; Schmitt, J. *Thin Solid Films* **1992**, *210*, 831-835.
16. For a review on electrostatic LBL assembly: Hammond, P. T. *Adv. Mater.* **2004**, *16*, 1271-1293.
17. For some examples: a) Sukhorukov, G. B.; Möhwald, H.; Decher, G.; Lvov, Y. M. *Thin*

Solid Films **1996**, *285*, 220-223. b) Cheung, J. H.; Stockton, W. B.; Rubner, M. F. *Macromolecules* **1997**, *30*, 2712-2716. c) Laurent D.; Schlenoff, J. B. *Langmuir*, **1997**, *13*, 1552-1557. d) Caruso, F.; Niikura, K.; Furlong, D. N.; Okahata, Y. *Langmuir* **1997**, *13*, 3422-3426. e) Hempenius, M. A.; Péter, M.; Robins, N. S.; Kooij, E. S.; Vancso, G. J. *Langmuir* **2002**, *18*, 7629-7634. f) Cho, J.; Quinn, J. F.; Caruso, F. *J. Am. Chem. Soc*. **2004**, *126*, 2270-2271. g) Vázquez, E.; Dewitt, D. M.; Hammond, P. T.; Lynn, D. M. *J. Am. Chem. Soc*. **2002**, *124*, 13992-13993. h) Tian, S.; Baba, A.; Liu, J.; Wang, Z.; Knoll, W.; Park, M.-K.; Advincula, R. *Adv. Funct. Mater*. **2003**, *13*, 473-479.

18. For some examples: a) Stockton, W. B.; Rubner, M. F. *Macromolecules* **1997**, *30*, 2717-2725. b) Yang, S. Y.; Rubner, M. F. *J. Am. Chem. Soc*. **2002**, *124*, 2100-2101. c) Bai, S.; Wang, Z.; Zhang, X. *Langmuir* **2004**, *20*, 11828-11832. d) Delongchamp, D. M.; Hammond, P. T. *Langmuir* **2004**, *20*, 5403-5411.
19. Shimazaki, Y.; Mitsuishi, M.; Ito, S.; Yamamoto, M. *Langmuir* **1997**, *13*, 1385-1387.
20. Wang, X. Q.; Naka, K.; Itoh, H.; Uemura, T.; Chujo, Y. *Macromolecules* **2003**, *36*, 533-535.
21. Li, D.; Jiang, Y. D.; Wu, Z. M.; Chen, X. D.; Li, Y. R. *Thin Solid Films* **2000**, *360*, 24-27.
22. a) Moav, T.; Hatzor, A.; Cohen, H.; Libman, J.; Rubinstein, I.; Shanzer, A. *Chem. Eur. J.* **1998**, *4*, 502-507. b) Hatzor, A.; Moav, T.; Cohen, H.; Matlis, S.; Libman, J.; Vaskevich, A.; Shanzer, A.; Rubinstein, I. *J. Am. Chem. Soc*. **1998**, *120*, 13469-13477. c) Hatzor, A.; Van der Boom-Moav, T.; Yochelis, S.; Vaskevich, A.; Shanzer, A.; Rubinstein, I. *Langmuir* **2000**, *16*, 4420-4423.
23. Serizawa, T.; Hashiguchi, S.; Akashi, M. *Langmuir* **1999**, *15*, 5363-5368.
24. Kohli, P.; Blanchard, G. J. *Langmuir* **2000**, *16*, 8518-8524.
25. a) Lvov, Y.; Ariga, K.; Ichinose, I.; Kunitake, T. *J. Chem. Soc., Chem. Commun.* **1995**, 2313-2314. b) Anzai, J.; Kobayashi, Y.; Nakamura, N.; Nishimura, M.; Hoshi, T. *Langmuir* **2000**, *16*, 2851-2856.
26. Suzuki, I.; Egawa, Y.; Mizukawa, Y.; Hoshi, T.; Anzai, J. *Chem. Commun.* **2002**, 164-165.
27. a) Lvov, Y.; Ariga, K.; Onda, M.; Ichinose, I.; Kunitake, T. *Langmuir* **1997**, *13*, 6195-6203. b) Cassagneau, T.; Mallouk, T. E.; Fendler, J. H. *J. Am. Chem. Soc.* **1998**, *120*, 7848-7859. c) Sun, Y.; Hao, E.; Zhang, X.; Yang, B.; Shen, J.; Chi, L.; Fuchs, H. *Langmuir* **1997**, *13*, 5168-5174. d) Khopade, A. J.; Caruso, F. *Langmuir* **2003**, *19*, 6219-6225. e) Crisp, M. T.; Kotov, N. A. *Nano Lett*. **2003**, *3*, 173-177. f) Jiang, C.; Markutsya, S.; Tsukruk, V. V. *Langmuir* **2004**, *20*, 882-890. g) Tian, S.; Liu, J.; Knoll, W. *Chem. Mater*. **2004**, *16*, 4103-4108. h) Schneider, G.; Decher, G. *Nano Lett.* **2004**, *4*, 1833-1839.

28. a) Glinel, K.; Laschewsky, A.; Jonas, A. M. *Macromolecules* **2001**, *34*, 5267-5274. b) Zhou, Y. L.; Li, Z.; Hu, N. F.; Zeng, Y. H.; Rusling, J. F. *Langmuir* **2002**, *18*, 8573-8579.
29. a) Shen, Y.; Liu, J. Y.; Jiang, J. G.; Liu, B. F.; Dong, S. J. *J. Phys. Chem. B* **2003**, *107*, 9744-9748. b) Place, I.; Penner, T. L.; McBranch, D. W.; Whitten, D. G. *J. Phys. Chem. A* **2003**, *107*, 3169-3177.
30. a) Mamedov, A. A.; Kotov, N. A.; Prato, M.; Guldi, D. M.; Wicksted, J. P.; Hirsch, A. *Nature Mater.* **2002**, *1*, 190-194. b) Olek, M.; Ostrander, J.; Jurga, S.; Möhwald, H.; Kotov, M.; Kempa, K.; Giersig, M. *Nano Lett.* **2004**, *4*, 1889-1895. c) Lahav, M.; Sehayek, T.; Vaskevich, A.; Rubinstein, I. *Angew. Chem. Int. Ed.* **2003**, *42*, 5576-5579.
31. a) Tsukruk, V. V.; Rinderspacher, F.; Bliznyuk, V. N. *Langmuir* **1997**, *13*, 2171-2176. b) Dan, N. *Nano Lett.* **2003**, *3*, 823-827. c) Khopade, A. J.; Caruso, F. *Nano Lett.* **2002**, *2*, 415-418.
32. a) Lvov, Y.; Ariga, K.; Ichinose, I.; Kunitake, T. *J. Am. Chem. Soc.* **1995**, *117*, 6117-6123. b) Caruso, F.; Möhwald, H. *J. Am. Chem. Soc.* **1999**, *121*, 6039-6046. c) Panchagnula, V.; Kumar, C. V.; Rusling, J. F. *J. Am. Chem. Soc.* **2002**, *124*, 12515-12521.
33. a) Zhou, L. P.; Yang, J.; Estavillo, C.; Stuart, J. D.; Schenkman, J. B.; Rusling, J. F. *J. Am. Chem. Soc.* **2003**, *125*, 1431-1436. b) Zhou, Y.; Li, Y. *Langmuir* **2004**, *20*, 7208-7214.
34. De Jong, M. R.; Huskens, J.; Reinhoudt, D. N. *Chem. Eur. J.* **2001**, *7*, 4164-4170.
35. Onclin, S.; Mulder, A.; Huskens, J.; Ravoo, B. J.; Reinhoudt, D. N. *Langmuir* **2004**, *20*, 5460-5466.
36. Huskens, J.; Deij, M. A.; Reinhoudt, D. N. *Angew. Chem. Int. Ed.* **2002**, *41*, 4467-4471.
37. Auletta, T.; Dordi, B.; Mulder, A.; Sartori, A.; Onclin, S.; Bruinink, C. M.; Péter, M.; Nijhuis, C. A.; Beijleveld, H.; Schönherr, H.; Vancso, G. J.; Casnati, A.; Ungaro, R.; Ravoo, B. J.; Huskens, J.; Reinhoudt, D. N. *Angew. Chem. Int. Ed.* **2004**, *43*, 369-373.
38. Nijhuis, C. A.; Huskens, J.; Reinhoudt, D. N. *J. Am. Chem. Soc.* **2004**, *126*, 12266-12267.
39. Nijhuis, C. A.; Yu, F.; Knoll, W.; Huskens, J.; Reinhoudt, D. N. *Langmuir* **2005**, *21*, 7866-7876.
40. Huskens, J.; Mulder, A.; Auletta, T.; Nijhuis, C. A.; Ludden, M. J. W.; Reinhoudt, D. N. *J. Am. Chem. Soc.* **2004**, *126*, 6784-6797.
41. Mulder, A.; Auletta, T.; Sartori, A.; Del Ciotto, S.; Casnati, A.; Ungaro, R.; Huskens, J.; Reinhoudt, D. N. *J. Am. Chem. Soc.* **2004**, *126*, 6627-6636.
42. Liu, J.; Ong, W.; Román, E.; Lynn, M. J.; Kaifer, A. E. *Langmuir* **2000**, *16*, 3000-3002.
43. Rojas, M. T.; Königer, R.; Stoddart, J. F.; Kaifer, A. E. *J. Am. Chem. Soc.* **1995**, *117*, 336-343.

44. Brust, M.; Fink, J.; Bethell, D.; Schiffrin, D. J.; Kiely, C. *Chem. Commun.* **1995**, 1655-1656.

45. (a) For a general review on cyclodextrins, see: *Chem. Rev*. **1998**, *98*, volume 5. (b) For a list with typical guest molecules, see: Rekharsky, M. V.; Inoue, Y. *Chem. Rev*. **1998**, *98*, 1880-1901.

46. Michels, J. J.; Baars, M. W. P. L.; Meijer, E. W.; Huskens, J.; Reinhoudt, D. N. *J. Chem. Soc., Perkin Trans. 2* **2000**, 1914-1918.

47. Palegrosdemange, C.; Simon, E. S.; Prime, K. L.; Whitesides, G. M. *J. Am. Chem. Soc.* **1991**, *113*, 12-20.

48. Decher, G.; Schlenoff, J. B., *Multilayer thin films*; Eds. Wiley: Weinheim, Germany, **2003**.

49. The lattice constant was calculated assuming monodisperse CD Au NPs of 2.8 nm in core diameter, adding twice the cyclodextrin cavity height of 0.8 nm. The total weight of the CD Au NPs is constituted of gold (62%), cyclodextrin(25%), and water (13%) (see Chapter 4). The hexagonal packing on the surface gives the maximal surface coverage possible for a well-packed self-assembled monolayer of a monodisperse sample of nanoparticles, assuming the formation of specific interactions only.

50. Lobo, R. F. M.; Pereira-Da-Silva, M. A.; Raposo, M.; Faria, R. M.; Oliveira, O. N. *Nanotechnology* **1999**, *10*, 389-393.

51. Perrin, D. D.; Armarego, W. F. L. *Purification of Laboratory Chemicals*, 3rd ed., Pergamon, Oxford, UK, **1989**.

52. Ashton, P. R.; Koniger, R.; Stoddart, J. F.; Alker, D.; Harding, V. D. *J. Org. Chem.* **1996**, *61*, 903-908.

53. Baars, M. W. P. L. ; Karlsson, A. J.; Sorokin, V.; De Waal, B. F. W.; Meijer, E. W. *Angew. Chem. Int. Ed.* **2000**, *39*, 4262-4265.

54. Ron, H.; Rubinstein, I. *Langmuir* **1994**, *10*, 4566-4573.

55. Aust, E. F.; Ito, S.; Sawondny, M.; Knoll, W. *Trends Polym. Sci.* **1994**, *2*, 313-323.

56. Boukamp, B. A. *Solid State Ionics* **1986**, *20*, 31-44.

Chapter 6

Patterned, Hybrid, Multilayer 3D Nanostructures Based on Multivalent Supramolecular Interactions*

Various patterning strategies have been developed to create hybrid nanostructures of dendrimers and gold nanoparticles on cyclodextrin self-assembled monolayers (CD SAMs) based on multiple supramolecular interactions using a layer-by-layer (LBL) approach. A lack of specificity of the adsorption of the dendrimer prevented the use of LBL assembly on chemically patterned SAMs, which were prepared by microcontact printing (μCP) or nanoimprint lithography (NIL). Nanotransfer printing (nTP) and nanoimprint lithography (NIL) solved that problem and resulted in patterned LBL assemblies on the CD SAMs. nTP was achieved by LBL assembly on a PDMS stamp followed by transfer onto a full CD SAM. NIL-prepared PMMA patterns provided patterned CD SAMs and functioned as a physical mask for LBL assembly. Furthermore, the latter led to truly 3D nanostructures with aspect ratios approaching 1.

---

* Part of this chapter have been submitted for publication: a) Crespo-Biel, O.; Dordi, B.; Maury, P.; Péter, M.; Reinhoudt, D. N.; Huskens, J. *Chem. Mater.*

6.1 Introduction

Nanotechnology requires new methodologies for the assembly of molecular- to micrometer-scale objects onto substrates in predetermined arrangements for the productivity of sensors, electrical and optical devices, MEMS, and photonic systems.[1] The ability to achieve control over the lateral dimensions, to deposit films of different compositions onto a surface, and to construct 3D devices is important for such methodologies.[2,3]

Layer-by-layer (LBL) assembly[4,5] is a simple and elegant method for fabricating structured and functional thin films on solid substrates. The technique is based on the sequential adsorption of species with complementary affinities on a substrate of arbitrary composition or topology. It allows to build up films with nanometer thickness control.[5-8] LBL structures can contain various structural entities from conducting and dielectric layers to functional organic and inorganic nanoparticles. LBL assembly is therefore emerging as an inexpensive and versatile technique to create electro-optical,[9-11] conducting,[12,13] and luminescent[14,15] thin films and to provide functional systems for photovoltaics,[16,17] cell templating,[18-20] and drug delivery.[21]

Achieving high spatial resolution while retaining the interfacial properties and specificity of the components is a key issue. Hammond *et al.* have introduced a route to pattern polymeric films by using chemically patterned surfaces as templates for electrostatic LBL assembly.[22,23] Patterning of full multilayers using UV or thermal crosslinking followed by dissolution of the non-crosslinked areas has been developed as well, but it requires the introduction of a photo-crosslinkable monomer into the LBL assembly.[24,25] Cui *et al.* have described a metal mask and lift-off approach to pattern LBL assemblies of two different types of nanoparticles.[26] Polymer-on-polymer stamping (POPS)[27] has been used to create a pattern of a single layer of a chemical functionality on top of an existing multilayer. Additionally, Hammond *et al.* have performed LBL assembly on a PDMS relief stamp, which allowed subsequent transfer of the LBL structures onto a substrate in the contact areas.[28] This approach resembles nanotransfer printing (nTP), which has been developed by Rogers *et al.*[29]

In Chapter 5 LBL assembly on full β-cyclodextrin (CD) self-assembled monolayers (SAMs) of hybrid organic/metal nanoparticle multilayers using multivalent supramolecular interactions between dendritic guest molecules and CD-modified gold nanoparticles was described. These multilayers showed a well-defined thickness control of 2 nm per bilayer.

In this chapter, various methods to create patterns of these supramolecular LBL assemblies are compared. Microcontact printing (μCP) and nanoimprint lithography (NIL) have been used to create patterned SAMs to obtain directed LBL assembly, nTP has been employed to transfer complete LBL assemblies, and NIL has provided topographical masks for LBL assembly. Emphasis lies on the interfacial supramolecular specificity and on the layer growth characteristics.

6.2 Results and Discussion

6.2.1 Supramolecular layer-by-layer assembly

Multilayer thin films composed of CD-modified gold nanoparticles (CD Au NPs) and adamantyl-terminated dendrimers (generation 5 with 64 adamantyl end groups, see Chart 6.1) have been patterned on CD SAMs using several lithographic techniques such as μCP[30,31] and NIL.[32] CD SAMs were prepared both on gold[33] and on silicon oxide surfaces.[34] These layers display similar binding properties towards multivalent guest molecules.[34-37] The alternating adsorption of the adamantyl-terminated dendrimers and the CD Au NPs, was performed using LBL assembly as described in Chapter 5.

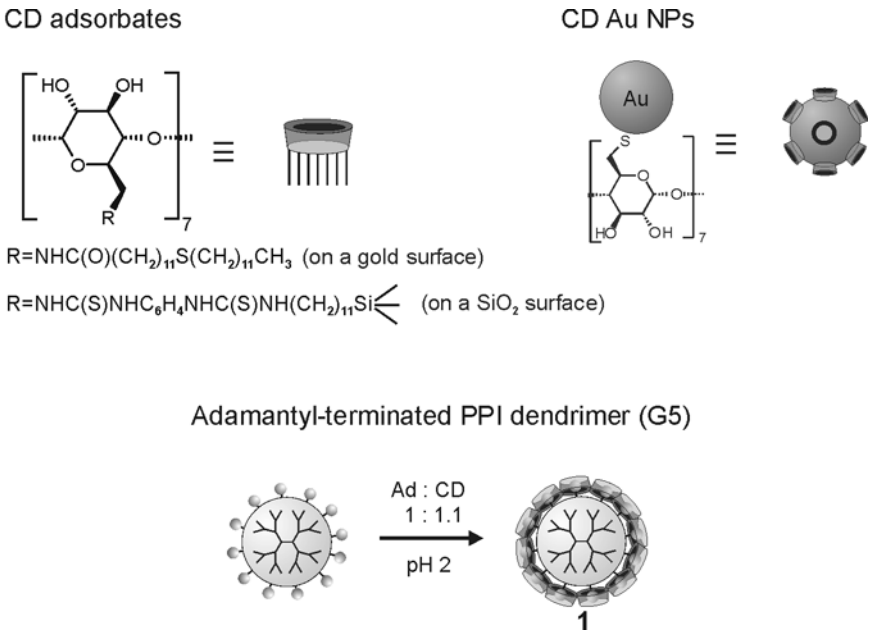

Chart 6.1: *Chemical structures of the host adsorbates, the CD Au NPs, and the adamantyl-terminated PPI dendrimers* ***1*** *used in this study.*

6.2.2 LBL assembly on μCP- and NIL-patterned SAMs

The first approach for patterning supramolecular LBL assemblies utilized the concept of selective deposition on chemically patterned surfaces as a template for multilayer deposition, that was introduced by Hammond's group.[22,23,38] A schematic representation of the method is shown in Scheme 6.1. The goal is to create patterned SAMs, of which one type of area consists of CD SAMs suitable for the LBL assembly, while the remaining areas resist adsorption of both LBL components. μCP- and NIL-patterned CD SAMs were used to achieve selective LBL deposition, with various adsorption-resisting SAMs in between to prevent nonspecific LBL assembly in these areas. μCP-patterned CD SAMs on gold (Scheme 6.1A) were prepared by μCP of mercapto-oligo(ethyleneglycol) (EG)[39] or 11-mercaptoundecanol (OH), followed by CD SAM formation from solution on the other (bare) regions.[33] NIL-patterned CD SAMs (Scheme 6.1B) were obtained by metal evaporation of a layer of 20 nm gold on PMMA-imprinted silicon oxide substrates followed by metal lift-off.[40] Various inert silanes

(amino-terminated, PEG-terminated, or none) were deposited from the gas phase onto the bare silicon oxide areas. CD heptathioether assembly was performed onto the NIL-patterned gold regions as described in literature.[33]

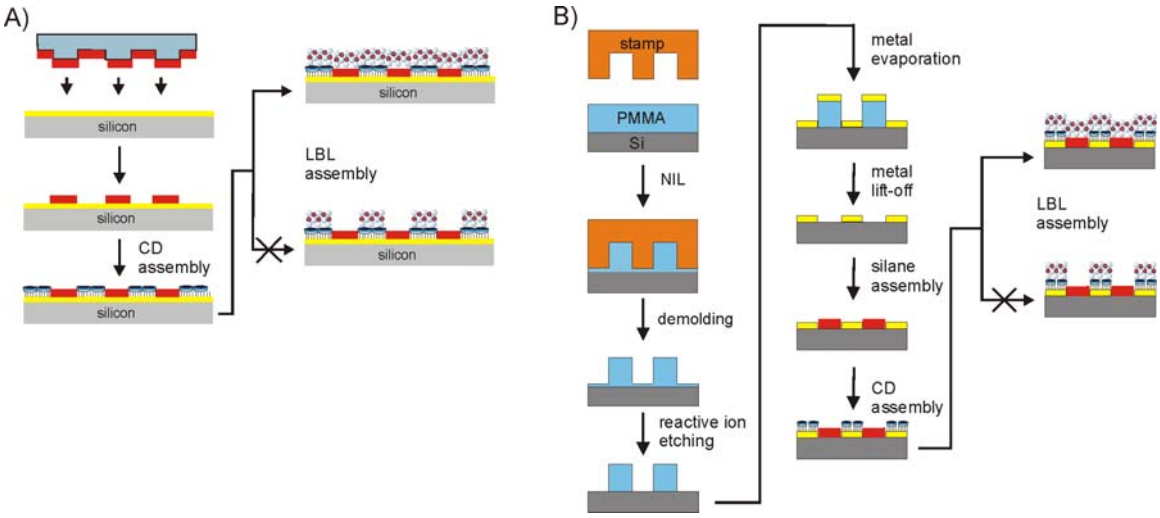

Scheme 6.1*: Preparation of patterned LBL assemblies on chemically patterned SAMs. (A) Microcontact printing of an inert SAM followed by CD assembly, and LBL assembly. (B) Nanoimprint lithography (left); metal evaporation and lift-off, formation of an inert silane SAM, and CD assembly (center); LBL assembly (right).*

Patterned SAMs created by μCP or NIL, were alternately immersed into solutions of the adamantyl-terminated dendrimer and of CD Au NPs (0.01 mM for the dendrimer and 5.8 μM for the CD Au NPs, in supramolecular functionalities). After each adsorption step the samples were rinsed with a concentrated CD solution and water. AFM was used to characterize the chemically patterned surfaces before and after the LBL assembly. AFM images (data not shown) indicated that the LBL assembly was nonspecific, *i.e.* not only on the CD regions, but also on the (intentionally resistant) silane regions. The lack of specificity for the LBL assembly is attributed to strong hydrophobic interactions caused by the dendrimer deposition and to the relatively low solubility of these dendrimers. These results led to investigate different methodologies for patterning these hybrid supramolecular LBL assemblies.

6.2.3 Nanotransfer printing of LBL assemblies

A schematic representation of the nTP[28,29] method is shown in Scheme 6.2. PDMS stamps with 10 μm lines and dots were oxidized by a UV/ozone (UVO) treatment, resulting in a negatively charged surface.[41] Subsequently, the slightly negatively charged stamps were immersed in an aqueous solution of the dendrimer (1 mM in adamantyl functionalities) to allow adsorption of one layer of dendrimers onto the stamp based on electrostatic interactions. Hereafter, alternating adsorptions of CD Au NPs and dendrimer (5.8 μM in cyclodextrin functionalities and 0.01 mM in adamantyl functionalities, respectively) with rinsing steps in between yielded a complete multilayer on the stamp surface, both on the protruding and recessed stamp areas. As the last layer, a dendrimer layer was deposited, thus promoting host-guest interactions between the multilayer stack on the stamp and the CD SAM on the substrate. The patterned PDMS stamp with the multilayer thin film, was put into contact with the CD substrate for 5 min. After removal of the stamp, the substrate was thoroughly rinsed with aqueous 1 mM CD (pH = 2) and water, and dried under a flow of N_2.

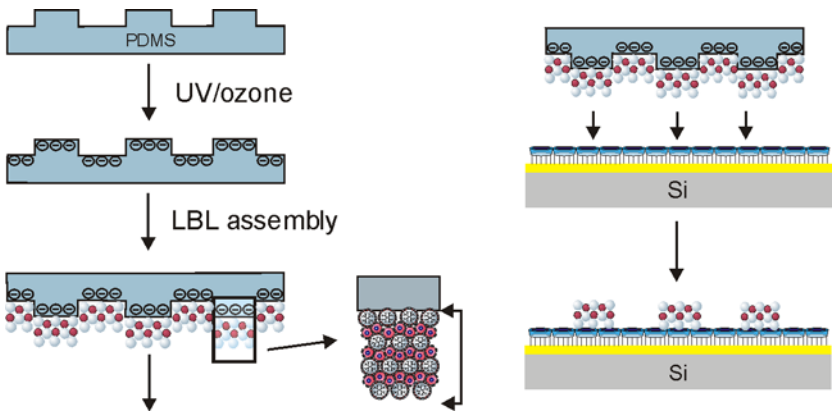

Scheme 6.2: *Preparation of patterned LBL assemblies by nanotransfer printing, which consists of oxidation of the PDMS surface, LBL assembly on the PDMS stamp, and contacting it with a CD SAM.*

Transfer of the multilayer stacks was visualized by atomic force microscopy (AFM) imaging as shown in Figure 6.1 (top).[42] Apparently, the electrostatic interactions

between the PDMS stamp and the first dendrimer layer are weaker than the host-guest interactions between the last dendrimer layer and the CD SAM.

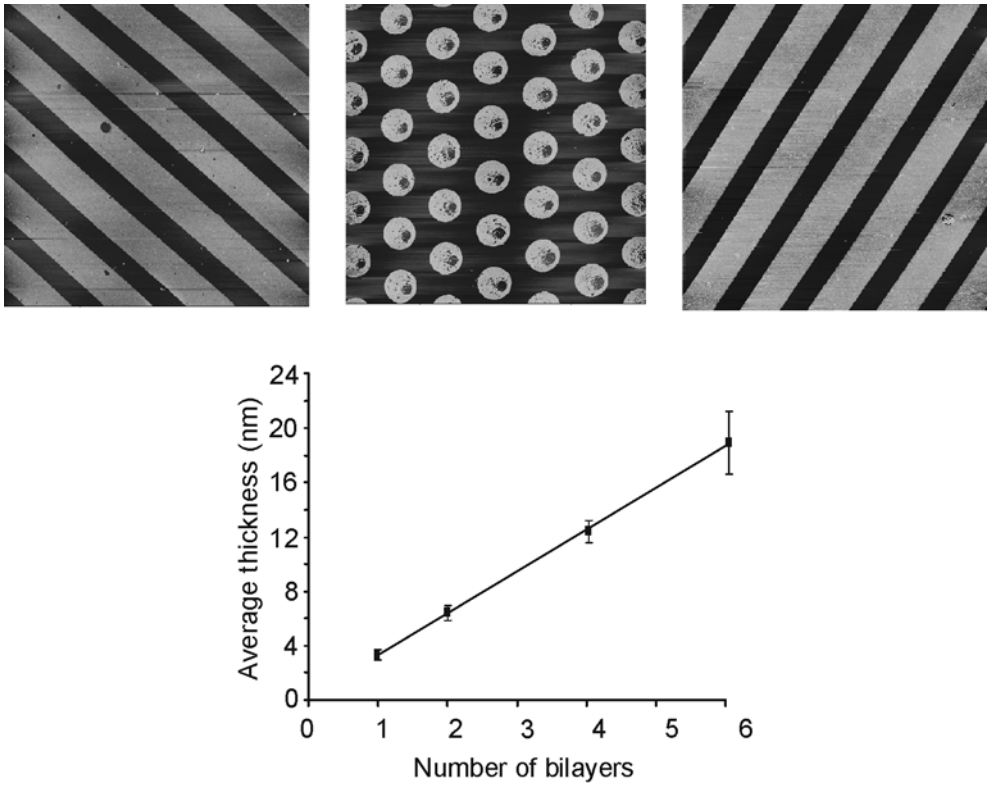

Figure 6.1: *(top) Contact mode AFM height images (80 × 80 μm², z range 30 nm) of lines of 2 bilayers (left), dots of 4 bilayers (center) of dendrimer/CD Au NPs, each with an additional dendrimer layer on top (see Scheme 6.2), after nanotransfer printing onto a CD SAM, and 4 bilayers (right) of dendrimer/CD Au NPs after nTP with a CD Au NPs-terminated PDMS stamp to a a dendrimer-covered CD SAM. (Bottom) Multilayer thickness after nTP as a function of the number of bilayers assembled onto the CD SAM as measured by AFM.*

The transferred multilayer thickness as a function of the number of deposited bilayers is shown in Figure 6.1 (bottom), indicating a linear thickness increase of approx. 3 nm per bilayer. This is somewhat higher than the thickness increase observed on unpatterned substrates (2 nm per bilayer, see Chapter 5). Nevertheless, it can be concluded that the nTP of the complete multilayer stacks was accomplished successfully. In a similar manner, the nTP can also be accomplished faithfully (Figure 6.1, top right)

when a LBL assembly ending in CD Au NPs on the stamp is contacted with a dendrimer-covered CD SAM (adsorbed from solution using a 0.01 mM solution in adamantyl functionalities).

The supramolecular specificity of the multilayer transfer was tested by two control experiments. In the first, a dendrimer layer (0.01 mM in adamantyl functionalities) was adsorbed on the CD SAM prior to nTP. The dendrimer-covered CD SAM substrate was thoroughly rinsed with 1 mM CD and water before the multilayer transfer. LBL assembly was performed onto the PDMS stamp as described above, ending in a dendrimer layer as well. Subsequently, the stamp was placed on the dendrimer-covered CD SAM applying contact for 5 min. Transfer of the LBL assembly was observed, as illustrated by AFM (Figure 6.2, A).

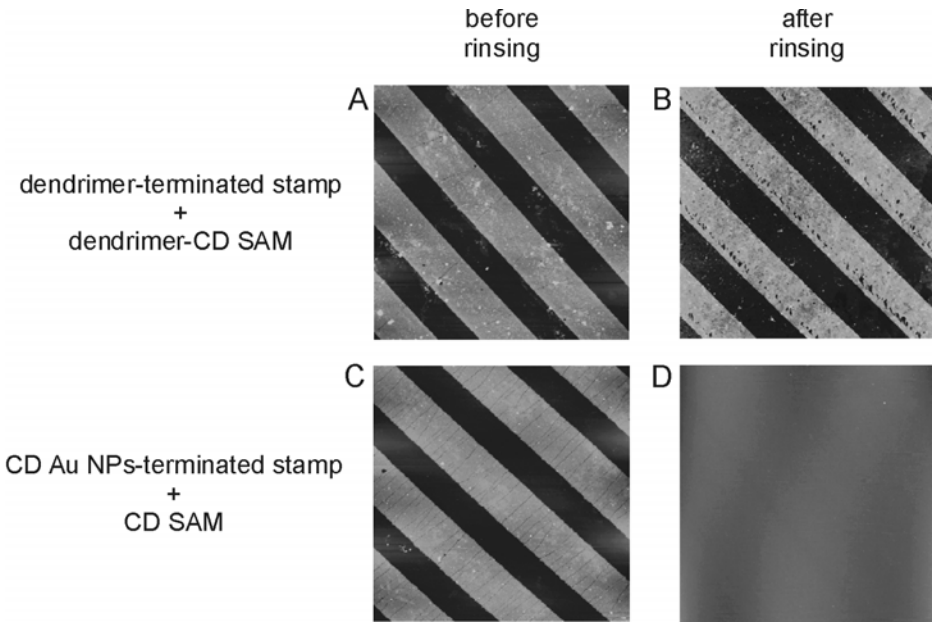

Figure 6.2: *Contact mode AFM height images (50 × 50 μm^2, z range 60 nm for A, B, and z range 40 nm for C, D) before (A, C) and after (B, D) rinsing (with 1 mM CD and water) of CD SAM substrates with 4 bilayers (A, C) and 6 bilayers (B, D) nTP LBL assemblies, using a dendrimer-terminated stamp on a dendrimer-covered CD SAM (A, B) or a CD Au NPs-terminated stamp on an (empty) CD SAM (C, D).*

Transfer of 4 bilayers showed a thickness of 16 nm, comparable to the results given above. After thorough rinsing with 1 mM CD and water, the multilayer structures remained (Figure 6.2, B). Apparently, nonspecific, hydrophobic interactions are in this case strong enough to retain the LBL assemblies on the substrate. In a second control experiment, a layer of CD Au NPs was deposited at the end of the multilayer stack on the stamp, which was put in contact with an (empty) CD SAM. AFM showed that the multilayer stack was transferred (Figure 6.2, C). However, after rinsing the substrate extensively with aqueous 1 mM CD followed by water, the multilayer pattern was removed completely from the CD substrate, indicating, in this case, the need for specific supramolecular interactions for maintaining stable LBL assemblies on the substrates (Figure 6.2, D).

6.2.4 LBL assembly on NIL-patterned PMMA templates

To pattern multilayer thin films, a third multistep process was developed, which involves the combination of NIL and LBL assembly. Possible advantages of the integration of LBL with NIL are: (i) the high resolution,[32] and (ii) the possibility to remove nonspecifically adsorbed material by lift-off from the PMMA substrates. The integrated scheme of the two multistep processes is shown in Scheme 6.3. The left part shows the NIL process, resulting in patterned PMMA structures with native silicon oxide areas in between. The center part shows the process to fabricate the CD SAMs on the silicon oxide areas, employing the PMMA structures as a physical barrier for the CD pattern.[34] The right part shows the LBL assembly on the NIL-patterned substrates and the polymer removal, resulting in patterned LBL structures.

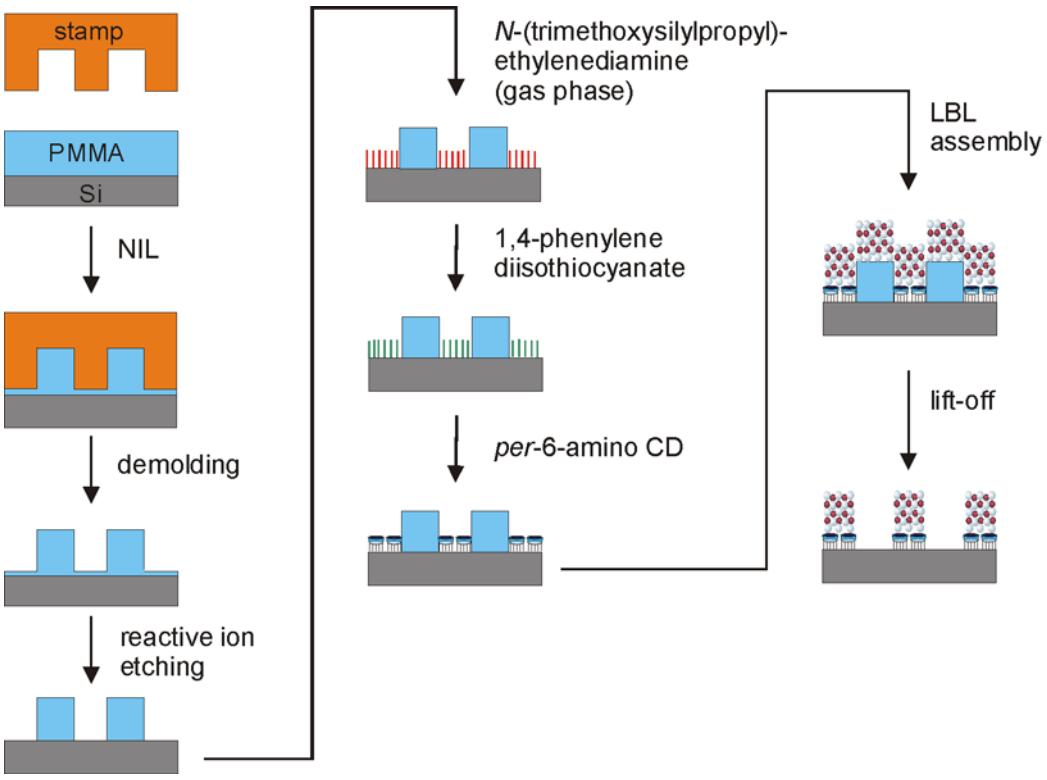

Scheme 6.3: *Preparation of NIL-patterned LBL assemblies using NIL (left), CD monolayer formation (center), and LBL assembly and lift-off (right).*

Patterned substrates containing various micrometer structures were prepared using spin-coated PMMA layers of 400 nm thickness, followed by NIL (T = 180 °C, p = 40 bar). The residual PMMA layer was removed by acetone/ultrasound treatment. The silicon oxide areas in between were further functionalized in a three-step process resulting in patterned CD monolayers on silicon oxide using a methodology previously described.[34] AFM confirmed the expected layer thickness of 2.8 nm for a CD-patterned sample which was subjected to acetone and ultrasound prior to AFM imaging in order to remove the PMMA. These results were similar to the ones obtained for a full CD SAM.[34] LBL assembly was performed on the NIL-patterned substrates as described above. Since the LBL assembly was performed in aqueous solution, damaging or dissolution of the PMMA structures does not occur. Multilayer deposition took place in the CD regions as well as on the PMMA. Hereafter, the PMMA structures, with the nonspecifically adsorbed LBL material, were removed in acetone using ultrasonication

Figure 6.3 (top) shows various NIL-patterned LBL structures with different numbers of bilayers. A thickness increase per bilayer of only about 1.1 nm was observed (Figure 6.3, bottom). LBL assembly on full substrates, subjected to the same lift-off procedure, yielded comparable thicknesses (as witnessed by AFM scratching experiments) before and after the treatment. Also, acetone treatment on nTP-patterned substrates did not result in a decrease of feature height of these LBL assemblies. Thus, it was concluded that the lower thickness values for NIL patterning, compared to LBL assembly on full layers and nanotransfer printed assemblies, do not result from the lift-off procedure, but possibly from different wetting and mass transport limitations of the LBL components on the PMMA-structured substrates. Nevertheless, the linear growth observed in this case as well (Figure 6.3, bottom) shows the potential of NIL for structuring LBL assemblies.

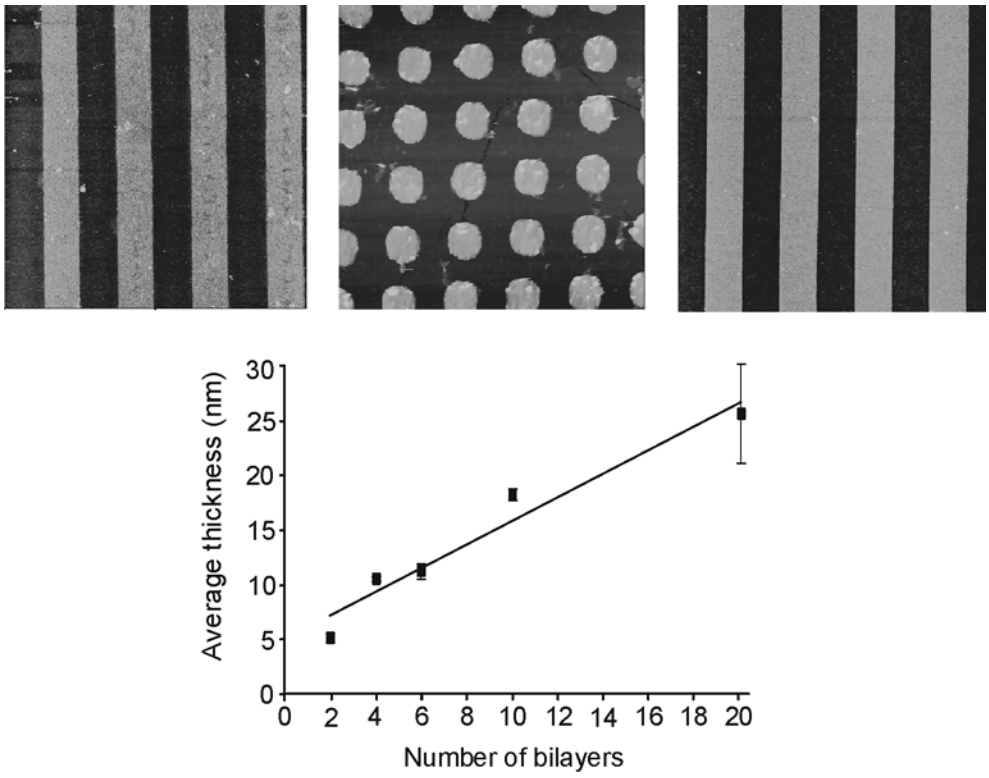

Figure 6.3: *(top) Contact mode AFM height images of LBL assemblies on NIL-patterned PMMA-CD SAM structures after PMMA removal. AFM images show micrometer lines and dots of 4 bilayers (left; 40 × 40 μm^2, z range 30 nm), 10 bilayers (center; 10 × 10 μm^2, z range 40 nm), and*

20 bilayers (right; 40 × 40 μm^2, z range 60 nm). (Bottom) Multilayer thickness after NIL patterning, LBL, and lift-off (see Scheme 6.3) as a function of the number of bilayers assembled onto the CD SAM as measured by AFM.

The same process was used to obtain 3D nanostructures, where LBL assembly was patterned at nanometer-scale. This was visualized by AFM (Figure 6.4), where submicron patterned LBL assemblies were obtained by the integration of NIL and LBL assembly.

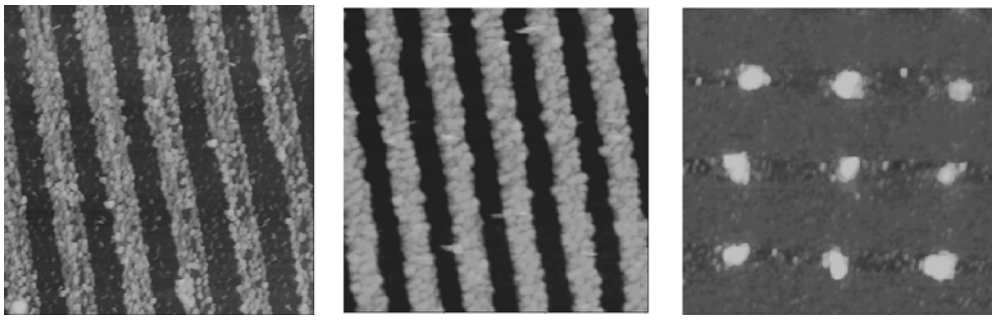

Figure 6.4: *Contact mode AFM height images of LBL assemblies on sub-micron NIL-patterned PMMA-CD SAM structures after PMMA removal. AFM images show nanometer lines and dots of 10 bilayers (left; 3 × 3 μm^2, z range 40 nm, height 9 nm), 20 bilayers (center; 3 × 3 μm^2, z range 60 nm, height 21 nm), and sub-100 nm structures of 15 bilayers (right; 1.5 × 1.5 μm^2, z range 30 nm, height 18 nm).*

It was observed that for submicron patterned LBL assemblies with bilayer numbers larger than 10, smaller layer thicknesses were obtained. This was, for example, visualized for the multilayer structures prepared in the 50 nm wide holes, which after deposition of 15 bilayers showed an average height of only 20 nm. The lower than expected growth at small feature sizes could be attributed to different sources. Mass transport limitation due to the physical confinement of the adsorbate solution within the PMMA structures, and a possible rupture of the hybrid nanostructures in the lift-off stage due to a nonspecific adhesion of the LBL on the PMMA structures could affect the multilayer thickness. These two problems can potentially be solved by changing the deposition conditions (concentration, temperature) and by changing the polymeric

material. Nevertheless, submicron patterned LBL structures could be obtained with feature sizes down to 50 nm with and 20 nm height. Thus, the formation of truly 3D nanostructures with aspect ratios approaching 1 was achieved.

6.3 Conclusions

Various patterning strategies have been applied to create 3D structures of supramolecular LBL assemblies on CD molecular printboards. μCP and NIL, followed by metal evaporation and lift-off, have been performed in order to obtain chemically patterned SAMs to attempt directed LBL assembly, relying on the chemical specificity. These two approaches did not lead to patterned LBL assemblies. The observed indiscriminate LBL adsorption was attributed to non-specific adsorption of the dendrimer. In contrast, patterned LBL assemblies were obtained faithfully by nTP. They showed good stability against rinsing, even with a monovalent competitive host in solution, and against acetone/ultrasound treatment. Supramolecular specificity was observed, but was not perfect, again due to nonspecific interactions induced by the dendrimer. Dendrimers with a higher solubility[43] may suppress these nonspecific interactions. Patterned LBL assemblies by NIL, LBL assembly, and lift-off have been obtained using PMMA as a physical barrier for the multilayer deposition. Differences in the multilayer heights as a function of the number of bilayers have been observed for the various methods, which are partly explained by wetting differences. Moreover, high resolution 3D nanostructures with aspect ratios on the order of 1 were obtained combining LBL assembly and NIL.

Combining top-down and bottom-up approaches, hybrid organic/metal NPs nanostructures have been obtained with control over all three dimensions, *x, y* by the top-down methods and *z* by the LBL assembly. These methodologies can in principle be used in other nanofabrication schemes and may lead to well-defined, high-resolution 3D nanostructures of a large variety of materials.

6.4 Experimental Section

Materials

Chemicals were obtained from commercial sources and used as such. β-Cyclodextrin (CD) was dried in vacuum at 80 °C in the presence of P_2O_5 for at least 5 h before use. Solvents were purified according to standard laboratory methods.[44] *Per*-6-thio-β-cyclodextrin[45] and *per*-6-amino-β-cyclodextrin[46] were synthesized according to literature procedures. Millipore water with a resistivity > 18 MΩ·cm was used in all experiments. Generation 5 adamantyl-terminated poly(propylene imine) (PPI) dendrimers (with 64 adamantyl groups) were synthesized as reported before.[47] Synthesis of the CD heptathioether adsorbate was reported previously.[33] 1-Mercapto-11-undecyl-tetra(ethylene glycol) (HS-$(CH_2)_{11}$-$(EG)_4$OH) was synthesized according to a literature procedure.[39] CD-functionalized gold nanoparticles were synthesized according to a literature procedure,[48] by the reduction of $HAuCl_4$ in DMSO by $NaBH_4$ in the presence of *per*-6-thio-cyclodextrin. Using TEM, a mean particle size of 2.8 ± 0.6 nm was found (see Chapter 4).

Substrate preparation

All glassware used to prepare monolayers was immersed in piraña (conc. H_2SO_4 and 33% H_2O_2 in a 3:1 ratio). (Warning! piraña should be handled with caution; it has detonated unexpectedly). The glassware was rinsed with large amounts of Milli-Q water. All adsorbate solutions were prepared freshly prior to use. Gold substrates for AFM (20 nm of gold on a glass substrate) were obtained from Ssens BV (Hengelo, The Netherlands). Prior to use the substrates were cut to the preferred shape and size.

Microcontact printing (μCP)

Gold substrates were cleaned by immersing the substrates in piraña for 5 s and leaving the substrates for 5 min in absolute EtOH.[49] Stamps were fabricated by casting a 10:1 (v/v) mixture of PDMS and curing agent (Sylgard 184, Dow Corning) against a

photolithographically patterned silicon master, cured for 1 h at 60 °C and released at this curing temperature. PDMS stamps were left in the oven at 60 °C for at least 18 h to ensure complete curing. For the μCP-patterned SAMs, μCP of an inert SAM (1-mercaptoundec-11-yl-tetra(ethylene glycol) or 11-mercaptoundecanol) onto a gold surface was performed by inking the PDMS stamps with a 1 mM adsorbate in solution ethanol for 15 min. After removal from the solution and drying under a flow of nitrogen, the stamps were applied by hand for 1-2 min onto the clean gold substrate. The substrates were rinsed with Millipore water and dried under a flow of nitrogen. The patterned substrates were subsequently immersed into a 0.1 mM β-CD heptathioether adsorbate solution in EtOH and $CHCl_3$ (1:2 v/v) for 16 h at 60 °C. For nTP, substrates were subsequently immersed into a 0.1 mM CD heptathioether adsorbate solution in EtOH and $CHCl_3$ (1:2 v/v) for 16 h at 60 °C. The samples were removed from the solution and rinsed with substantial amounts of chloroform, ethanol, and Millipore water. Oxidation of the PDMS stamps was carried out in a commercial UV/ozone plasma reactor (UltraViolets Product Inc., model PR-100) for 30 min. The surface of the PDMS stamps were kept hydrophilic by immersing the stamps in an aqueous ink solution immediately after UVO treatment. After multilayer formation, the stamps were applied by hand for 5 min onto the CD SAM. At last, the substrates were thoroughly rinsed with large amounts of an aqueous solution of 10 mM native CD followed by Millipore water. Substrates were dried under a flow of nitrogen.

Nanoimprint lithography (NIL)

Stamps for NIL were made by photolithography followed by reactive ion etching (RIE, Elektrotech Twin system PF 340). 1H,1H,2H,2H-perfluorodecyltrichlorosilane was used as an anti-adherent layer to facilitate the stamp-imprint separation. Silicon oxide substrates were first oxidized by immersion in piraña solution for 15 min and then covered with a 400 nm thick layer of PMMA by spin-coating. Stamp and substrate were put in contact and a pressure of 40 bar was applied at a temperature of 180 °C using a hydraulic press (Specac). The residual layer was removed by dipping the samples in acetone during 60 s.[40] For the NIL-patterned SAMs, a 20 nm layer of gold was

evaporated using a metal evaporator BAK 600 at a vacuum of 1×10^{-6} mbar. The metal lift-off was achieved using acetone and ultrasonication. After metal lift-off, assembly of an inert SAM (*n*-(3-trimethoxysilylpropyl)-ethylenediamine or 2-[methoxypoly (ethyleneoxy)-propyl]trimethoxysilane (6 to 9 ethylene glycol units per molecule) onto the silicon oxide surface was performed by gas-phase evaporation as described before,[40] or the silicon oxide surface was left unfunctionalized. The NIL-patterned substrates were subsequently immersed into a 0.1 mM CD heptathioether adsorbate solution in EtOH and $CHCl_3$ (1:2 v/v) for 16 h at 60 °C. NIL-patterned CD monolayers in PMMA structures were prepared following a procedure similar to the one described by Onclin *et al.*,[34] although some changes were done in order to maintain the PMMA structures. After aminoalkyl SAM formation from the gas phase, the diisocyanate was reacted in ethanol (40 °C, 2 h), and the CD heptamine was subsequently reacted in water (40 °C, 2 h).

Layer-by-layer (LBL) assembly

μCP-patterned CD SAMs, NIL-patterned CD SAMs and NIL-patterned CD SAMs in PMMA structures were immersed into a solution of dendrimer **1** (0.01 mM in adamantyl functionalities) for 10 min, followed by rinsing with 1 mM CD at pH = 2. The films were then immersed in a solution of CD Au NPs (5.8 μM in CD functionalities) for 10 min, followed by rinsing with water. A multilayer structure was formed by alternating these adsorption steps. For the nTP process, oxidized PDMS stamps were inked by immersion into the dendrimer solution (1 mM in adamantyl functionalities) for 15 min. After removal from the solution, the stamps were immersed in a CD Au NPs solution (5.8 μM in CD functionalities) for 10 min, followed by rinsing with water. Further LBL assembly was performed as described above.

Atomic force microscopy (AFM)

AFM experiments were carried out with a NanoScope IIIa Multimode AFM (Digital Instruments, Veeco Metrology Group, USA) in contact mode using V-shaped Si_3N_4 cantilevers (Nanoprobes, Veeco) with a nominal spring constant of 0.12 $N \cdot m^{-1}$. The AFM

was equipped with a J scanner. To ensure maximum sensitivity for lateral force images, the sample was scanned at an angle of 90° with respect to the long axis of the cantiliver. Images were captured in ambient atmosphere (ca. 40 – 50 % relative humidity, 25 °C) unless mentioned otherwise.

6.5 References and Notes

1. General introduction to microfabrication: (a) Menz, W.; Mohr, J.; Paul, O. *Microsystem Technology*, 2nd ed., Wiley-VCH, Weinheim, Germany, **2001**. (b) Madou, M. J. *Fundamentals of Microfabrication: The Science of Miniaturization*, 2nd ed., CRC Press, Boca Raton, U.S.A., **2001**.
2. For a general review on nanofabrication see: Gates, B. D.; Xu, Q.; Stewart, M.; Ryan, D.; Willson, C. G.; Whitesides, G. M. *Chem. Rev*. **2005**, *105*, 1171-1196.
3. Hammond, P. T. *Adv. Mater.* **2004**, *16*, 1271-1293.
4. Decher, G.; Hong, J. D. *Makromol. Chem., Macromol. Symp.* **1991**, *46*, 321-327.
5. Decher, G. *Science* **1997**, *277*, 1232-1237.
6. Hammond, P. T. *Curr. Opin. Colloid Interface Sci.* **1999**, *4*, 430-442.
7. Schönhoff, M. *Curr. Opin. Colloid Interface Sci.* **2003**, *8*, 86-95.
8. Decher, G.; Schlenoff, J. B., *Multilayer thin films*; Eds. Wiley: Weinheim, Germany, **2003**.
9. Schrof, W.; Rozouvan, S.; Van Keuren, E.; Horn, D.; Schmitt, J.; Decher, G. *Adv. Mater.* **1998**, *10*, 338-341.
10. Cutler, C. A.; Bouguettaya, M.; Kang, T. S.; Reynolds, J. R. *Macromolecules* **2005**, *38*, 3068-3074.
11. Delongchamp, D. M.; Hammond, P. T. *Langmuir* **2004**, *20*, 5403-5411.
12. Fou, A. C.; Rubner, M. F. *Macromolecules* **1995**, *28*, 7115-7120.
13. Delongchamp, D. M.; Hammond, P. T. *Chem. Mater.* **2003**, *15*, 1165-1173.
14. Wang, Y.; Tang, Z. Y.; Correa-Duarte, M. A.; Liz-Marzan, L. M.; Kotov, N. A. *J. Am. Chem. Soc.* **2003**, *125*, 2830-2831.
15. Clark, S. L.; Handy, E. S.; Rubner, M. F.; Hammond, P. T. *Adv. Mater.* **1999**, *11*, 1031-1035.
16. Tokuhisa, H.; Hammond, P. T. *Adv. Funct. Mater.* **2003**, *13*, 831-839.
17. He, J. A.; Mosurkal, R.; Samuelson, L. A.; Li, L.; Kumar, J. *Langmuir* **2003**, *19*, 2169-

2174.

18. Donath, E.; Moya, S.; Neu, B.; Sukhorukov, G. B.; Georgieva, R.; Voigt, A.; Baumler, H.; Kiesewetter, H.; Mohwald, H. *Chem. Eur. J.* **2002**, *8*, 5481-5485.
19. Berg, M. C.; Yang, S. Y.; Hammond, P. T.; Rubner, M. F. *Langmuir* **2004**, *20*, 1362-1368.
20. Kim, H.; Doh, J.; Irvine, D. J.; Cohen, R. E.; Hammond, P. T. *Biomacromolecules* **2004**, *5*, 822-827.
21. Khopade, A. J.; Caruso, F. *Biomacromolecules* **2002**, *3*, 1154-1162.
22. Clark, S. L.; Montague, M.; Hammond, P. T. *Supramol. Sci.* **1997**, *4*, 141-146.
23. Clark, S. L.; Hammond, P. T. *Adv. Mater.* **1998**, *10*, 1515-1519.
24. Yang, S. Y.; Rubner, M. F. *J. Am. Chem. Soc.* **2002**, *124*, 2100-2101.
25. Lu, C. H.; Wu, N. Z.; Wei, F.; Zhao, X. S.; Jiao, X. M.; Xu, J.; Luo, C. Q.; Cao, W. X. *Adv. Funct. Mater.* **2003**, *13*, 548-552.
26. Hua, F.; Shi, J.; Lvov, Y.; Cui, T. *Nano Lett.* **2002**, *2*, 1219-1222.
27. Jiang, X. P.; Hammond, P. T. *Langmuir* **2000**, *16*, 8501-8509.
28. Park, J.; Hammond, P. T. *Adv. Mater.* **2004**, *16*, 520-525.
29. Loo, Y. L.; Willett, R. L.; Baldwin, K. W.; Rogers, J. A. *J. Am. Chem. Soc.* **2002**, *124*, 7654-7655.
30. Kumar, A.; Biebuyck, H. A.; Whitesides, G. M. *Langmuir* **1994**, *10*, 1498-1511.
31. Yan, L.; Zhao, X. M.; Whitesides, G. M. *J. Am. Chem. Soc.* **1998**, *120*, 6179-6180.
32. Guo, L. J. *J. Phys. D: Appl. Phys.* **2004**, *37*, R123-R141.
33. De Jong, M. R.; Huskens, J.; Reinhoudt, D. N. *Chem. Eur. J.* **2001**, *7*, 4164-4170.
34. Onclin, S.; Mulder, A.; Huskens, J.; Ravoo, B. J.; Reinhoudt, D. N. *Langmuir* **2004**, *20*, 5460-5466.
35. Auletta, T.; Dordi, B.; Mulder, A.; Sartori, A.; Onclin, S.; Bruinink, C. M.; Péter, M.; Nijhuis, C. A.; Beijleveld, H.; Schönherr, H.; Vancso, G. J.; Casnati, A.; Ungaro, R.; Ravoo, B. J.; Huskens, J.; Reinhoudt, D. N. *Angew. Chem. Int. Ed.* **2004** , *43*, 369-373.
36. Huskens, J.; Mulder, A.; Auletta, T.; Nijhuis, C. A.; Ludden, M. J. W.; Reinhoudt, D. N. *J. Am. Chem. Soc.* **2004**, *126*, 6784-6797.
37. Mulder, A.; Auletta, T.; Sartori, A.; Del Ciotto, S.; Casnati, A.; Ungaro, R.; Huskens, J.; Reinhoudt, D. N. *J. Am. Chem. Soc.* **2004**, *126*, 6627-6636.
38. Jiang, X. P.; Clark, S. L.; Hammond, P. T. *Adv. Mater.* **2001**, *13*, 1669-1673.
39. Palegrosdemange, C.; Simon, E. S.; Prime, K. L.; Whitesides, G. M. *J. Am. Chem. Soc.* **1991**, *113*, 12-20.
40. Maury, P.; Péter, M.; Mahalingam, V.; Reinhoudt, D. N.; Huskens, J. *Adv. Funct. Mater.*

2005, *15*, 451-457.

41. Efimenko, K.; Wallace, W. E.; Genzer, G. *J. Colloid Interface Sci.* **2002**, *254*, 306-315.
42. Note that the "holes" present on the dot structures are due to a stamp artifact.
43. Nijhuis, C. A.; Yu, F.; Knoll, W.; Huskens, J.; Reinhoudt, D. N. *Langmuir* **2005**, *21*, 7866-7876.
44. Perrin, D. D.; Armarego, W. F. L. *Purification of Laboratory Chemicals*, 3rd ed., Pergamon, Oxford, UK, **1989**.
45. Rojas, M. T.; Königer, R.; Stoddart, J. F.; Kaifer, A. E. *J. Am. Chem. Soc.* **1995**, *117*, 336-343.
46. Ashton, P. R.; Koniger, R.; Stoddart, J. F.; Alker, D.; Harding, V. D. *J. Org. Chem.* **1996**, *61*, 903-908.
47. Baars, M. W. P. L.; Karlsson, A. J.; Sorokin, V.; De Waal, B. F. W.; Meijer, E. W. *Angew. Chem. Int. Ed.* **2000**, *39*, 4262-4265.
48. Liu, J.; Ong, W.; Román, E.; Lynn, M. J.; Kaifer, A. E. *Langmuir* **2000**, *16*, 3000-3002.
49. Ron, H.; Rubinstein, I. *Langmuir* **1994**, *10*, 4566-4573.

Chapter 7

Enhancement of Supramolecular Complexes at Interfaces by Multivalent, Orthogonal Interaction Motifs

The multivalent binding of a supramolecular complex at a multivalent host surface by combining the orthogonal β-cyclodextrin (CD) host-guest and metal ion-ethylenediamine coordination motifs is described. As a heterotropic, divalent linker an adamantyl-functionalized ethylenediamine derivative was used. This was complexed with Cu(II) or Ni(II). The binding of the complexes to a CD self-assembled monolayer (SAM) was studied as a function of pH by means of surface plasmon resonance (SPR) spectroscopy. The Cu(II) complex showed divalent binding to the CD surface with an enhancement factor higher than 100. A heterotropic, multivalent binding model at interfaces was used to quantify the multivalent enhancement at the surface. Similar behavior was observed for the Ni(II) system. Although the Ni(II) system could potentially be trivalent, only divalent binding was observed at the CD SAMs, which was confirmed by desorption experiments.

7.1 Introduction

Multivalent interactions involve the simultaneous interaction between multiple (two or more) functionalities on one entity and complementary functionalities on another.[1] Multivalent interactions are involved in a variety of biological processes such as cell signaling, pathogen identification, and inflammatory response.[1,2] Multivalent binding events have unique collective properties that are qualitatively and quantitatively different from the properties displayed by their monovalent constituents. For example, multivalent interactions can achieve higher binding affinities and can afford larger contact areas between surfaces.[3-5]

For mechanistic studies of multivalent interactions, receptors anchored on a surface offer a number of advantages over receptors in solution. One of the main advantages is the relative ease of preparation of the building blocks, because a monovalent receptor becomes multivalent upon immobilization. A second important advantage is that the binding strength is enhanced in multivalent complexes compared to the corresponding monovalent parent. This effect can commonly be ascribed to an effective concentration (C_{eff}) term. It represents a probability of interaction between two reactive or complementary interlinked entities and symbolizes a "physically real" concentration of one of the reacting or interacting functionalities as experienced by its complementary counterpart.[6,7] To this aim, different template substrates have been synthesized to serve as model systems for cell membranes, such as self-assembled monolayers (SAMs),[8-13] nanoparticles,[14-16] and vesicles.[17,18]

The development of functional surfaces and supramolecular structures built upon them by the assembly of molecular building blocks is an important issue in nanotechnology.[19] Furthermore, supramolecular interactions have been employed for the immobilization of molecules at surfaces, achieving characteristic features such as high specificity, tunable affinity, and reversibility of immobilization.[20-25] The use of multiple, intrinsically weak interactions can lead to complexes that are thermodynamically and/or kinetically stable, where the overall strength can be fine-tuned by controlling the number of interactions and the strength of the intrinsic interaction.[7]

Metal-ligand interactions have already been successfully used to generate complex molecular architectures with specific topology, high stability, and original properties.[26,27] Special interest has been focused on the *N*-nitrilotriacetic acid (NTA)-histidine-tag (His_6-tag) chelator system. This approach utilizes the NTA chelator to coordinate divalent metal cations (Cu^{2+}, Ni^{2+}, Zn^{2+}, Co^{2+}) leaving coordination sites of the chelator-metal complex free for the ligation of the His_6-tag. The group of Tampé has used NTA-functionalized lipids[28-30] and SAMs[31,32] to immobilize proteins through multivalent interactions. Evidence for multivalent interactions between the His_6-tag and the NTA groups was found in experiments involving immobilization of His_6-tagged proteins on chelating lipid membranes with chelators at different surface concentrations.[28] In a similar approach, Hunter and co-workers studied the cooperative binding of Cu^{2+} ions to a membrane-bound synthetic receptor, with a dansyl-ethylenediamine conjugate as the head group and cholesterol as the membrane anchor.[33] This model system allowed to quantify the membrane environment and therefore to investigate the relationship between receptor concentration and the cooperativity of multicomponent assembly processes at the membrane surface.

Heterotropic, orthogonal recognition motifs are intermolecular interactions that operate independently of each other so that no crossover or interference occurs.[34,35] They can lead to higher stoichiometries, better specificities, and more complex architectures than when only one single interaction motif is employed. Supramolecular chemistry has profited greatly from the simultaneous binding of several orthogonal recognition motifs for the construction of elaborate multicomponent superarchitectures.[35,36] The ultimate example of this is DNA for which every pair of matching single strands is orthogonal to other pairs. This approach has been used to obtain DNA nanostructures.[37,38]

In this chapter, multivalent binding of a supramolecular complex at a multivalent host surface by combining the orthogonal cyclodextrin host-guest and metal ion-ethylenediamine coordination interaction motifs is described. Divalent binding of the metal complex formed between adamantyl-functionalized ethylenediamine and divalent metal cations is central in this study. Complexation of the complex to a β-cyclodextrin (CD) host SAM was studied as a function of pH by means of surface plasmon resonance (SPR) spectroscopy. Quantitative analysis of the different species present in solution and

at the surface was performed using a thermodynamic model.[7] The aim of this study was to compare the relative concentrations of the divalent complex in solution and at the surface in order to investigate a possible surface enhancement effect. Binding of a divalent Cu(II) complex to the CD SAM was compared to the complexation of a potentially trivalent Ni(II) complex.

7.2. Results and Discussion

A schematic picture of surface enhancement at CD SAMs by a multivalent receptor surface is represented in Figure 7.1. In this study multivalent building blocks consisting of a single binding motif (CD SAMs and M^{2+} ions) and a divalent linker with complementary units of both motifs were employed. The two interaction motifs (CD-adamantyl (Ad) and M^{2+}-ethylenediamine (en)) are considered to be orthogonal.

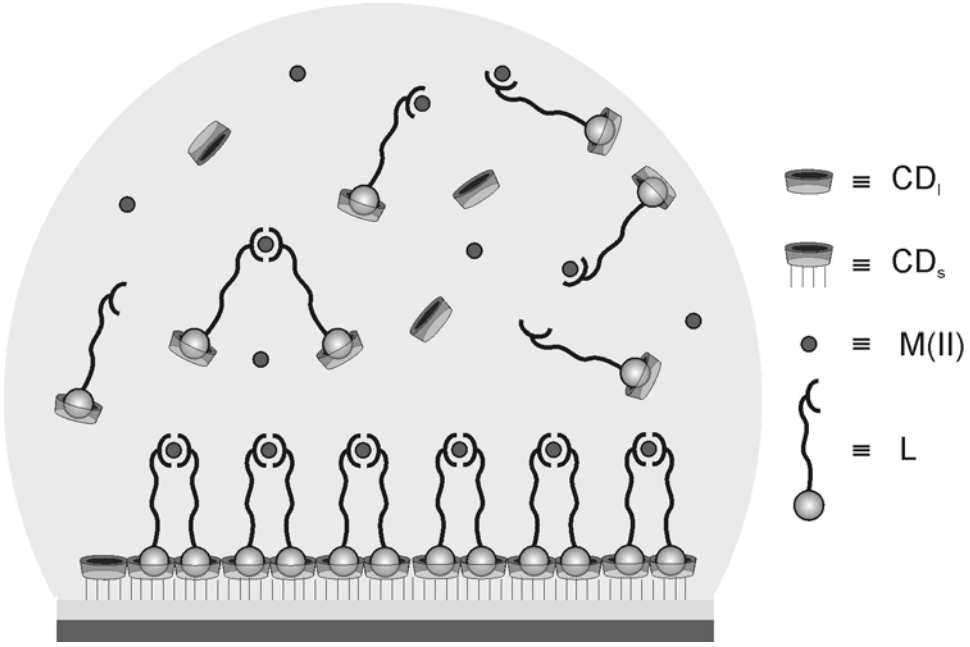

Figure 7.1*: Schematic representation of the multivalent enhancement concept at CD SAMs induced by metal complexation of Cu(II) by L.*

7.2.1 A model system for multivalent, orthogonal interactions at surfaces

As a model system to study multivalent, orthogonal complexes at SAMs, three building blocks were employed. As the metal-ligand coordination motif the Cu(II)-en and Ni(II)-en interaction pairs was used, and thus Cu(II) as a divalent building block and Ni(II) as (potentially) trivalent. CD SAMs on gold[39] (CD_s, host) were chosen as the monotropic multivalent display for the CD host-guest interaction motif. As a heterotropic, divalent linker, the Ad-functionalized en derivative ligand L was used (Chart 7.1).

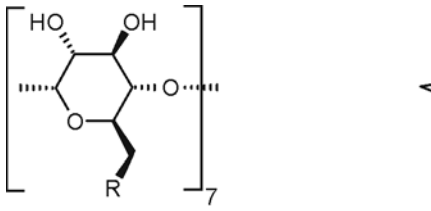

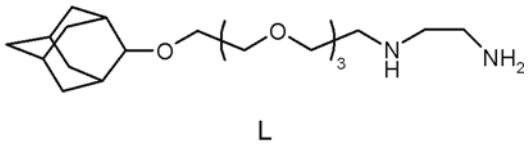

L

CD_l : R=OH

CD_s : R=NHC(O)$(CH_2)_{11}$S$(CH_2)_{11}CH_3$

Chart 7.1*: Guest and host compounds used in this study: CD host in solution (CD_l) and at the surface (CD_s), and adamantyl-functionalized en (L).*

The synthesis of L was performed in three steps (see Scheme 7.1). Nucleophilic substitution of 1-bromo-adamantane with tetraethylene glycol in the presence of triethylamine gave the monoadamantyl-functionalized tetraethylene glycol.[6] Subsequent conversion of the remaining hydroxyl functionality to bromide, using PBr_3 in toluene,[40] followed by nucleophilic substitution on the bromide with an excess of ethylenediamine gave L.

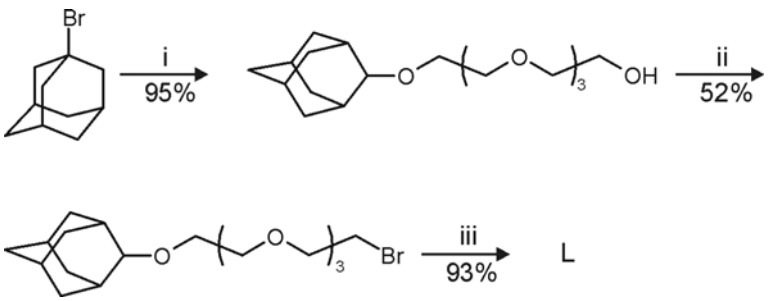

Scheme 7.1*: Synthesis of the adamantyl-functionalized en guest L: (i) Et_3N, tetraethylene glycol, 180 °C, overnight; (ii) PBr_3, toluene, RT, overnight; (iii) ethylenediamine, 80 °C, overnight.*

As a multivalent host platform the heptathioether-modified CD SAM of CD_s on gold[39] was chosen. This type of host with long alkyl chains is especially suitable for this study because it forms densely packed, well-ordered SAMs.[41] These CD SAMs allow a fundamental understanding of multivalent binding at the surface, which has been correlated previously, to binding studies in solution.[6] The hexagonal packing of these SAMs has been observed with high-resolution AFM.[42] The center-to-center distance between the CDs is approximately 2.1 nm. Molecule L was designed: (i) to interact with CD (in solution and at CD SAMs) through the adamantyl moiety, (ii) to coordinate to divalent metals (Cu(II), Ni(II)) with different coordination numbers through the en group as a bidentate ligand[43], and (iii) to provide a sufficiently long linker to allow multivalent host-guest binding to the CD SAMs when multiple ligands are coordinated to the M(II) center.

The basicity of the amino groups makes the complexation to metal cations pH dependent. In principle, it is assumed that all guest species present - protonated, unprotonated or metal-complexed - are able to bind CD. The oligo(ethylene glycol) chain is used to provide enough length and flexibility for binding the CD SAM in a multivalent fashion, while retaining water solubility and preventing non-specific interactions. All solution species of L, resulting from protonation, metal complexation, and CD_l complexation are given in Scheme 7.2.[44] When full orthogonality is assumed, all intrinsic stability constants for CD_l complexation of any species of L are equal, but this is to be verified experimentally (see below).

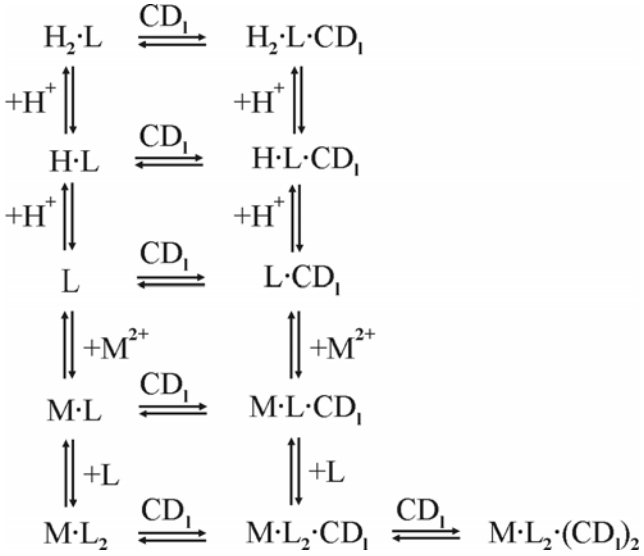

Scheme 7.2: *Equilibria for all solution species of L, in the absence and presence of M(II) and CD_l (charges are omitted for clarity).*

At a CD SAM surface, all species containing one molecule of L will behave as monovalent guests, binding a single surface CD in a similar manner as in solution. In contrast, the divalent ML_2 is expected to show the equilibria give in Scheme 7.3. This behavior is expected for M = Cu(II), while Ni(II) can potentially be trivalent, *i.e.* give NiL_3 complexes (see Section 7.2.5). From previous studies, it is known that the formation of $M{\cdot}L_2{\cdot}(CD_s)_2$ is governed by an effective concentration (C_{eff}) term, which is the driving force for the preferential formation of such multivalent species at the multivalent CD SAMs.[6,7]

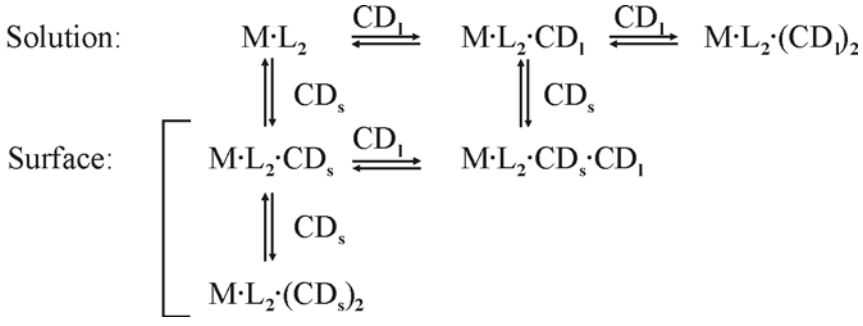

Scheme 7.3: *Equilibria for solution and surface species of ML_2.*

The first metal ion chosen for this study was Cu(II) which forms divalent ($Cu{\cdot}en_2$) complexes with a square-planar geometry.[45] The *cis*- and *trans*- configurations (see Chart 7.2) are likely to behave similarly in our studies since (i) the total lengths of the linkers between the Ad groups (2.9 and 3.2 nm) are larger than the lattice periodicity of the CD SAMs (2.1 nm) and (ii) differences in length and flexibility of the oligo(ethylene glycol) chain are not expected to lead to significant differences in effective concentration.[6,7] Preparation of the metal complex was achieved by mixing a solution of L and $CuCl_2$ in a 2:1 molar ratio.

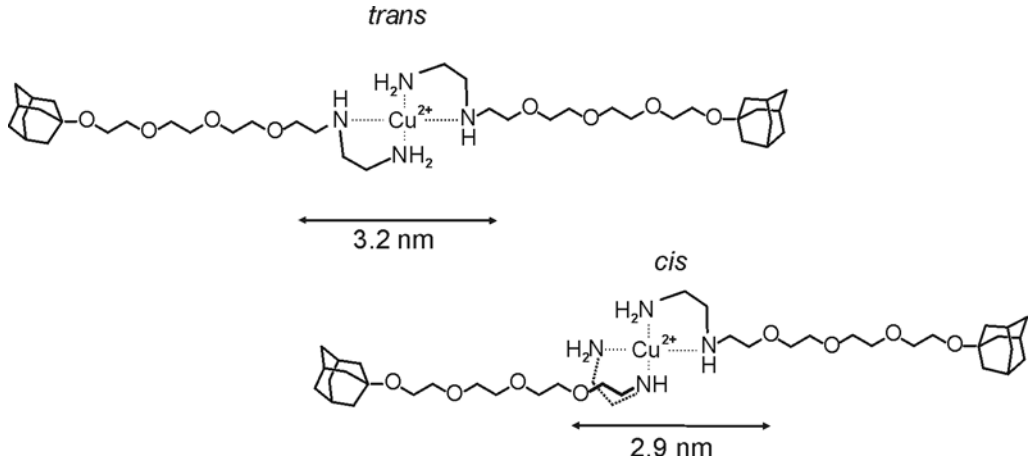

***Chart 7.2**: Distances of the adamantyl moieties in the most extended (cis- and trans-) conformations of CuL_2 derived from CPK models.*

The metal-ligand motif was not studied in detail. It is known that the additional substitution at the en moiety with *N*-alkyl groups does not influence considerably the protonation constants,[46] however, it strongly reduces the metal complex formation constants.[47] Therefore protonation[46] and metal complex formation[47] constants corresponding to *N*-*n*-butylethylenediamine were used in this study for L. These values lead to an expected pH dependence of the speciation of L in the absence and presence of Cu(II) as shown in Figure 7.2.

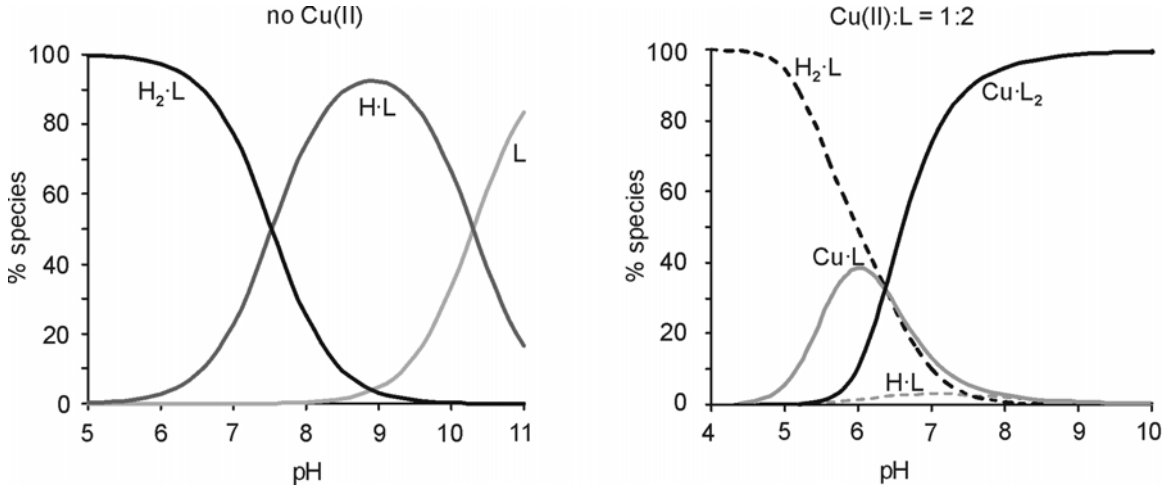

***Figure 7.2**: Speciation of the different species of L present in solution as a function of pH in the absence (left) and presence (right) of Cu(II) (total concentration of L: 1 mM; with Cu(II): total concentration of Cu(II): 0.5 mM). In the presence of Cu(II) (right) solid lines represent Cu(II) complexes and dashed lines represent species without Cu(II).*

In the absence of Cu(II), H_2L is the main species in the pH range of 4-7.5, whereas between 7.5 and 10.5 HL is the major one. Only at a pH higher than 10.5, L starts to become the main species. However, when Cu(II) is present in the solution at a 1:2 M:L ratio, the uncomplexed H_2L is present for more than 50% only at a pH lower than 6, while HL and L are present less than 10% at any pH. As can be observed from Figure 7.2, a pH above 6.5 favors the formation of CuL_2, whereas CuL is significant only in the narrow pH range between pH 5.5 to 6.5.

7.2.2 Binding studies in solution for Cu(II) complexes

To verify the orthogonality of the Cu-en CD-Ad binding motifs, binding studies of L, with or without Cu(II) at various pH, with CD_l were performed in aqueous solution using isothermal titration calorimetry (ITC). Figure 7.3 depicts the exothermic heat profiles obtained from the calorimetric titration of L (left) and a 1:2 Cu^{2+}:L mixture (right) with CD at pH 7.

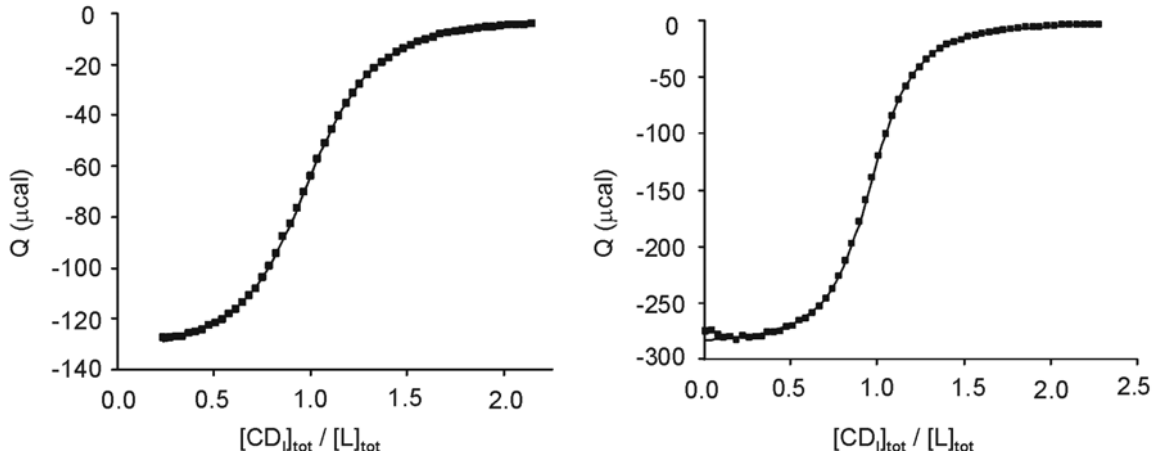

***Figure 7.3**: Heat involved per injection plotted against the molar ratio (markers) and fits (solid lines) for the calorimetric titrations of L (5 mM) to CD_l (0.5 mM) (left) and of CD_l (10 mM) to $CuCl_2$ (0.5 mM) and L (1 mM) (right) in water (pH = 7) at 298 K.*

The inflection point in the titration curve obtained for the binding of L with CD_l indicates a 1:1 (host-guest) complex (Figure 7.3, left). The titration curve was fitted to a 1:1 model taking the association constant (K) and the binding enthalpy ($\Delta H°$) as independent fitting parameters. The thermodynamic parameters obtained at different pH are listed in Table 7.1.

***Table 7.1:** Thermodynamic parameters of the complexation of CD_l with L in the presence and absence of Cu(II), as determined by ITC at 298 K.*

Guest	pH	Stoichiometry (host-guest)	$K_{i,l}$ (M^{-1})	$\Delta H°$ kcal·mol^{-1}	$T\Delta S°$ kcal·mol^{-1}
L	2	1:1	6.1×10^4	-6.0	-0.2
	7	1:1	6.4×10^4	-5.9	-0.1
	9	1:1	5.5×10^4	-5.2	0.6
Cu(II):L (1:2)	7	1:2	6.2×10^4	-5.7	1.2
	9	1:2	9.6×10^4	-5.2	2.0

As it can be seen from Table 7.1 no significant pH (pH 2-9) effect on the host-guest complexation was observed. The binding constant (K = (6.0 ± 0.4) × 10^4 M^{-1}) averaged for the different pH values and the enthalpy of binding ($\Delta H°$ = -5.7 ± 0.4 kcal·mol^{-1}) are typical of a 1:1 CD-adamantane inclusion interaction.[48]

In the presence of Cu(II) (Cu:L = 1:2), the titration curve for the complexation of L with CD_l (Figure 7.3, right) shows an inflection point at a molar ratio of 1 also suggesting a 1:1 host-guest complex where each adamantyl group is complexed by CD_l. At pH 7, however, CuL_2 is expected to be the major species (in the absence of CD). Therefore, the experimental curve was fitted to a 2:1 binding model considering the two adamantyl groups as two identical, independent binding sites.[49] The observed 1:1 stoichiometry and the quality of the fit (Figure 7.3, right) confirm that both adamantyl groups bind CD in an independent manner. The thermodynamic parameters are listed in Table 7.1, and it is clearly observed that no significant pH effect on the host-guest complexation was observed. The average intrinsic binding constant (K_i = 7.9 × 10^4 M^{-1}) and the enthalpy of binding ($\Delta H°$ = –5.4 kcal·mol^{-1}) are similar to the thermodynamic parameters obtained for the complexation of L with CD_l in the absence of Cu(II), and in the same manner the pH (pH 7-9) did not significantly affect the Ad-CD inclusion interaction (see Table 7.1). Also, additional heat effects, *e.g.* of metal complex dissociation or ligand (de)protonation were totally absent in the enthalpograms. These observations led to the conclusion that the CD host-guest and the metal ion-ethylenediamine coordination motifs are fully orthogonal, and that there is no influence of pH on the complexation.

7.2.3 Binding of the Cu(II)-L system at CD SAMs.

The binding of L (in the presence and absence of 0.5 equiv. of Cu(II)) at a CD SAM (CD_s) was studied as a function of pH by means of SPR spectroscopy. SPR titrations were performed in the presence of 1 mM buffer concentration and 1 mM CD_l concentration, in order to have thermodynamic equilibrium.

Figure 7.4 shows the SPR titration of L at a CD SAM at pH 6. The SPR curve was obtained by exposing the CD SAM to increasing concentrations of L. Addition of L

resulted in an increase of reflectivity, indicative of adsorption of the guest molecule at the host SAM. The adsorption was followed for 5 min until equilibrium was reached. Extensive rinsing of the cell with buffer and 10 mM CD_l led to restoration of the original SPR signal, which indicates the complete desorption of L from the surface. Thorough rinsing of the cell with 10 mM CD_l was needed in order to obtain a complete restoration of the base line. The SPR curve was fitted to a Langmuir isotherm (1:1 model) taking the binding constant to the surface ($K_{Langmuir}$) and the maximum Intensity change (I_{max}) as independent parameters. The binding constant obtained (1.3 x 10^5 M^{-1}) is typical of a monovalent CD-adamantane inclusion interaction.[48]

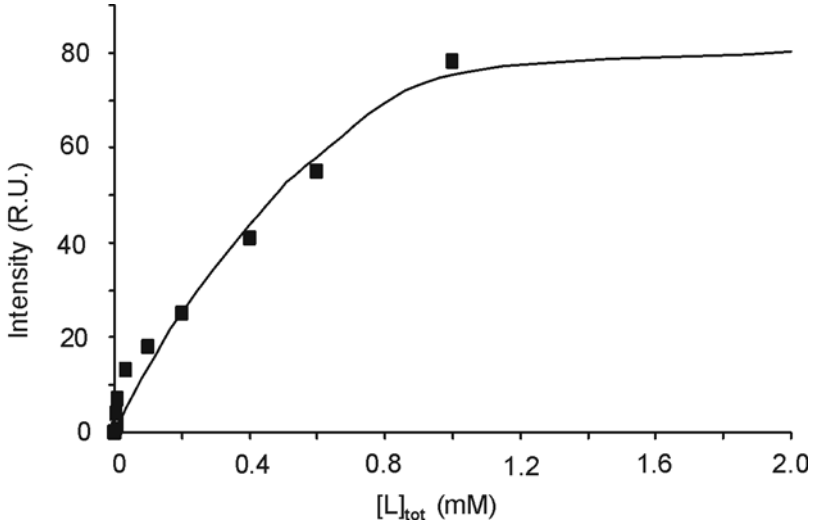

Figure 7.4: *SPR titrations (data points) and the corresponding fit to a Langmuir isotherm (solid line) for the titration of L at a CD SAM (1 mM MES buffer pH 6, 1 mM CD_l)*

The interaction of L in the presence of Cu(II) (Cu(II):L = 1:2) with CD SAMs was studied at different pH by using several buffers. A background of 1 mM CD_l concentration in the solutions was needed in order to obtain reliable binding constants. The SPR titration curves are shown in Figure 7.5 and were fitted to a sequential binding model (see Section 7.2.5). All experiments led, within experimental error, to the same I_{max}, which suggests that similar surface coverages are reached. For easy comparison, therefore, these are joined in a normalized graph (Fig. 7.5, bottom right).

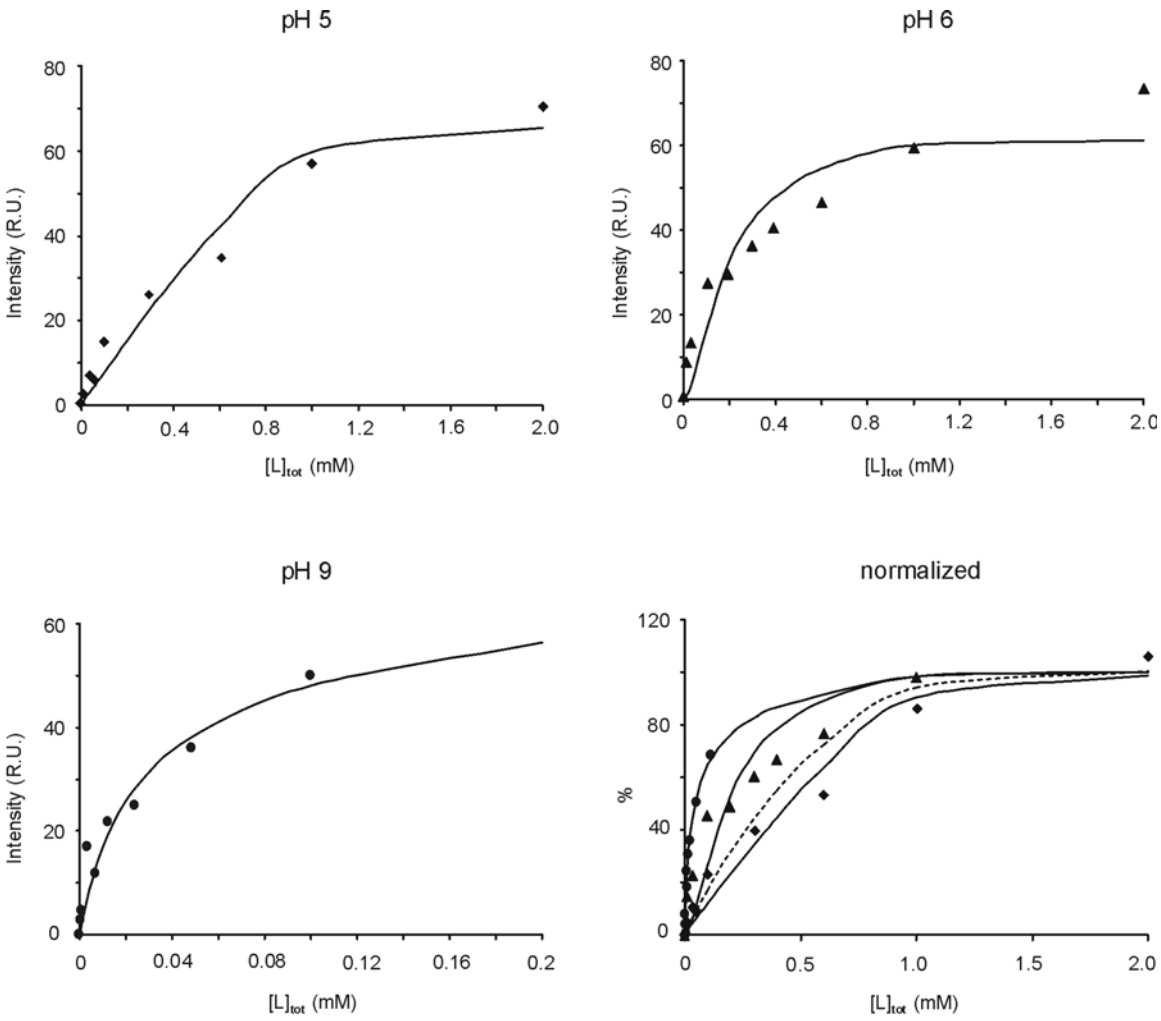

Figure 7.5: *SPR titrations (data points) and the corresponding fits to the multivalent, heterotropic, sequential binding model (solid lines) for titrations of L in the presence of Cu(II) (Cu(II):L = 1:2) to CD SAMs at various pH (◆ = pH 5, 1 mM acetate buffer and 1 mM CD; ▲ = pH 6, 1 mM MES buffer and 1 mM CD; ● = pH 9, 1 mM bicarbonate buffer and 1 mM CD). The graph at the bottom right shows the normalized SPR data points and the corresponding fits (solid lines) for the different titrations of L in the presence of Cu(II) (Cu(II):L = 1:2) to the CD SAMs,where the dashed line corresponds to the normalized fit of the adsorption of L to the CD SAM (Fig. 7.4).*

As can be observed in Figure 7.5, the titration of Cu^{2+}:L at pH 9 showed strong adsorption at low concentrations when compared to lower pH, which is an indication for divalent binding to the surface in the former case. The speciation diagram (Figure 7.2) for

the species in the presence of Cu(II) showed that, at pH 9, the major species in solution is CuL_2. Thus, divalent CuL_2 is also expected to be the major species at the surface. The titration curves at pH 5 showed a behavior similar to the titration of L in the absence of Cu(II), as can be most easily observed in the normalized graph (Figure 7.5, bottom right). In both cases, therefore, the binding is interpreted as monovalent binding. The speciation diagram (Figure 7.2) showed as major ligand species CuL and H_2L in solution at pH 5, and no divalent species, thus corroborating monovalent binding.

However, a different behavior is observed at pH 6. From the normalized graph the binding at the surface appears intermediate between pH 5 and pH 9, thus indicating, apart from monovalent binding, also a significant contribution from divalent binding. However, the speciation diagram showed only 10% CuL_2 in solution at pH 6, and 40% of the monovalent CuL complex and 50% of H_2L. These differences in behavior in solution and at the surface can be attributed to the effective concentration. For species where self-assembly is involved to obtain multivalent entities, which is here the case, the high effective concentration at the surface leads to enhancement of such entities at the interface.

The thermodynamic parameters obtained from the SPR titration curves fitted to a Langmuir and multivalent binding model (see below), respectively, are listed in Table 7.2. The SPR titration curves were fitted to Langmuir isotherms assuming monovalent binding only. The resulting and calculated binding constants, $K_{Langmuir}$, are listed in Table 7.2. At pH 9, $K_{Langmuir}$ (2.3×10^6 M^{-1}) is two orders of magnitude higher than for a monovalent adamantyl-cyclodextrin interaction.[48] This supports divalent binding at pH 9. However, at pH 5, $K_{Langmuir}$ (1.4×10^5 M^{-1}) is almost equal to $K_{Langmuir}$ (1.3×10^5 M^{-1}) obtained for the binding of L (in the absence of Cu(II)) to the CD SAM. This can be explained from the speciation diagram in solution (Figure 7.2) where at pH 5 the major ligand species is H_2L, thus supporting monovalent binding in this case. On the other hand, pH 6 gave an intermediate value (2.7×10^5 M^{-1}) suggesting both divalent and monovalent binding.

Table 7.2: *Stability constants $K_{Langmuir}$ and $K_{i,s}$ of the complexation of L in the presence and absence of Cu(II) to a CD SAM, as fitted to a Langmuir isotherm and to the heterotropic multivalency model, respectively.*

guest	pH	$K_{Langmuir}$ (M^{-1})	$K_{i,s}$ (M^{-1})	I_{max}
L	6	1.3×10^5	_	0.76
Cu(II):L (1:2)	5	1.4×10^5	8.7×10^4	0.68
	6	2.7×10^5	7.8×10^4	0.63
	9	2.3×10^6	2.1×10^4	0.72

Titrations performed with L in the presence of Cu(II) (1 mM MES buffer pH 6 and 1 mM CD) on 11-mercapto-1-undecanol reference SAMs only exhibited a small refractive index effect on the SPR signal, which could be instantaneously restored by rinsing the SAMs with the buffer solution at a 1 mM CD concentration. Therefore, it was concluded that the adsorption of L, in the absence or presence of Cu(II), to the CD SAM is a result of specific host-guest interactions.

7.2.4 The heterotropic multivalency model at interfaces

The SPR titration curves could be fitted to a model where the multivalent binding of CuL_2 to the CD surface is represented as two sequential binding events, using the effective concentration term (C_{eff}).[6,7] The equilibria involved are shown in Scheme 7.3. All equilibria with CDs can be expressed in terms of intrinsic binding constants, taken separately for binding to a solution host ($K_{i,l}$) and a surface host ($K_{i,s}$). For $K_{i,l}$ the value was determined before using ITC for the binding of L and CD in solution (6.0×10^4 M^{-1}). The maximal C_{eff} ($C_{eff,max}$) which applies to low surface coverages,[7] was determined from the linker length, which was based on the extended conformation of CuL_2.[6,7] In our case, $C_{eff,max}$ for the divalent complex CuL_2 was calculated to be 0.2 M, consistent with previous work.[6] SPR curves were fitted to the sequential binding model in a least squares optimization routine using $K_{i,s}$ and the I_{max} as variables and fixed values for $K_{i,l}$ (6.0×10^4

M^{-1}) and $C_{eff,max}$ (0.2 M). In the model, the protonation[46] and metal-complex formation[47] constants of *N*-*n*-butylethylenediamine were used.

Results obtained by fitting the SPR curves using the sequential binding model are given in Table 7.2. The values obtained for $K_{i,s}$ at the different pH values are within the same order of magnitude and are in good agreement with the binding constant obtained for the interaction of L (in absence and presence of Cu(II)) in solution, and also comparable to the interaction of L at a CD SAM. These observations support the conclusion that (i) the binding motifs behave orthogonal, also at the CD SAM interface, and that (ii) the binding enhancement can be attributed solely to the effective concentration effect, and thus heterotropic multivalency without the need for introducing cooperativity effects.

Multivalent enhancement at the CD surface is evident from a detailed analysis of the different species present in solution and at the surface at the different pH values. These results were obtained from the fitted SPR curves. Figure 7.6 depicts the results obtained for the concentration of the different species present at the CD surface. Concentrations of the species in solution are represented in the speciation (Figure 7.2).

As can be observed in Figure 7.6, at the highest pH (bottom, right) the divalent CuL_2 is the predominant species at the surface, as it is also in solution (see speciation diagram Figure 7.2, right). Moreover, at the lowest pH (5) the inverse situation is observed, where the monovalent species of L are the major species at the surface as well as in solution. However, at pH 6, the situations in solution and at the surface differ. As mentioned before, the major species in solution is the monovalent complex CuL (80%), while the divalent form CuL_2 accounts for less than 10%. Conversely, at the surface, the concentration of the divalent CuL_2 is 4 times higher than the monovalent one (Figure 7.6, bottom left), showing the preferential formation of CuL_2 at the CD over CuL in almost the entire concentration range at this pH.[50]

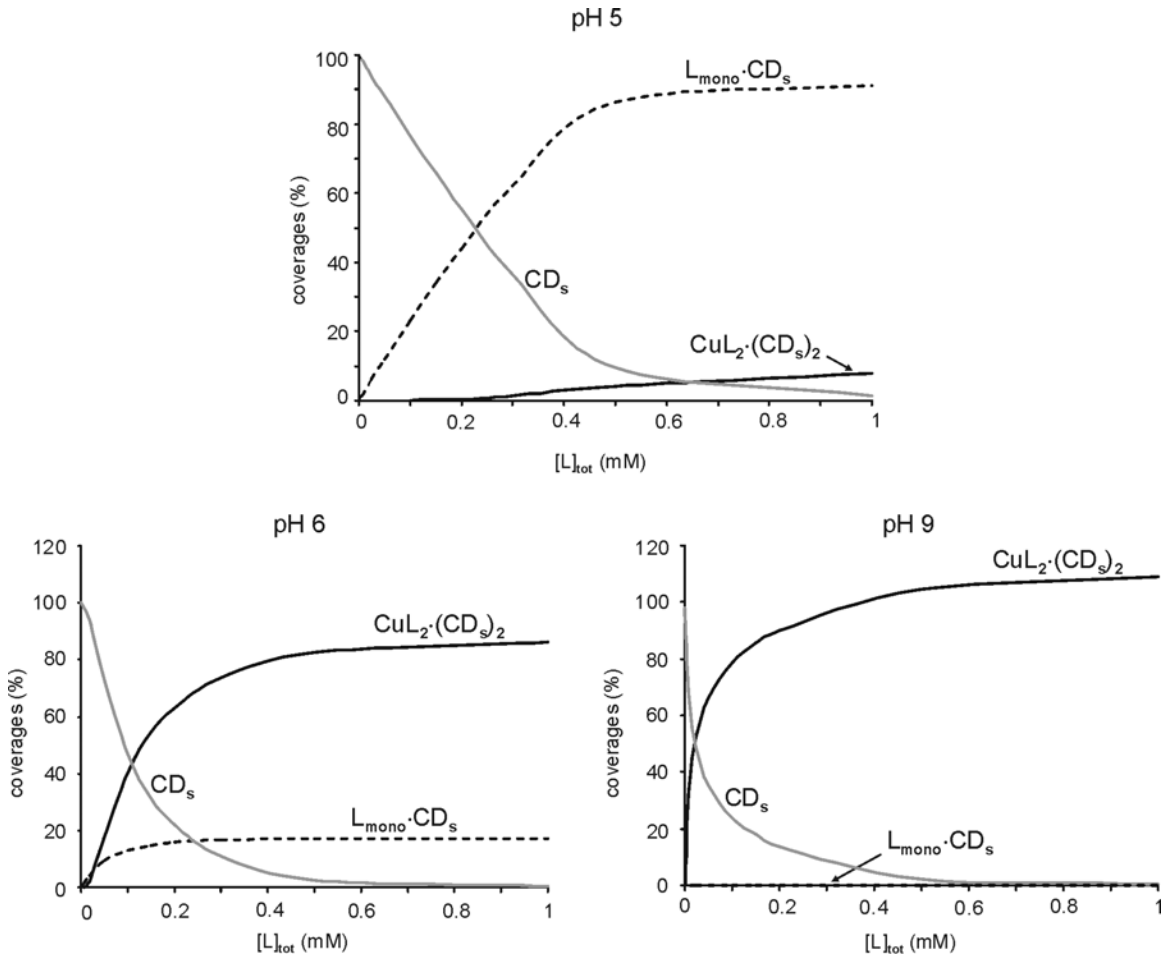

Figure 7.6: *Surface coverages of monovalently bound L (sum of concentrations of adsorbed H_2L, HL, L, CuL, and monovalently bound CuL_2) (dashed lines), the divalently bound CuL_2 (black solid lines), and uncomplexed CD_s present at a CD SAM at different pH as a function of L_{tot} (with $Cu(II)_{tot}$:L_{tot} = 1:2).*

These observations lead to a surface multivalency enhancement, which can be quantified by an enhancement factor (*EF*) (Equation 1, *f* = molar fraction), which is > 200 at lower concentrations and which gradually decreases at higher concentrations (Figure 7.7).

$$EF = \left(\frac{f_{s,div}}{f_{s,mono}}\right) / \frac{(f_{l,div})}{(f_{l,mono})} \qquad (1)$$

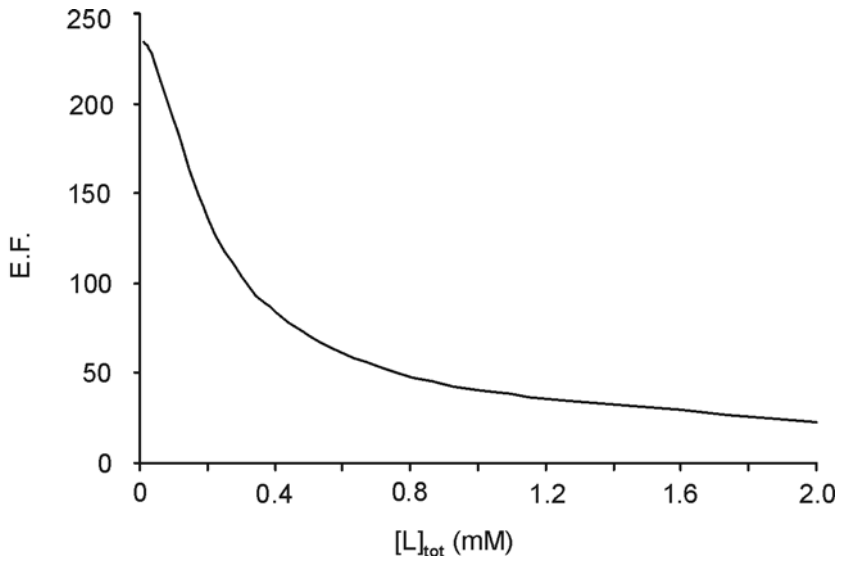

***Figure 7.7**: EF for the divalent species (CuL_2) present at the CD SAM at pH 6 as a function of the total concentration of L (with $Cu(II)_{tot}:L_{tot}$ = 1:2).*

Thus, it can be concluded that the multivalent host surface (CD SAM) favors the formation of divalent (multivalent) species (see Figure 7.2), and that this surface enhancement can be as large as a factor of 100.

7.2.5 Binding studies of the Ni(II)-L system at CD SAMs.

To increase our understanding of heterotropic multivalency at the CD surface, we also prepared a metal complex using Ni(II) as the metal ion. This divalent cation with a coordination number of six forms complexes with an octahedral geometry. Ethylenediamine (en), for example, is known to give a trivalent $Ni(en)_3$ complex.[43] All solution species of L due to protonation, metal and CD_l complexation are given in Scheme 7.4.

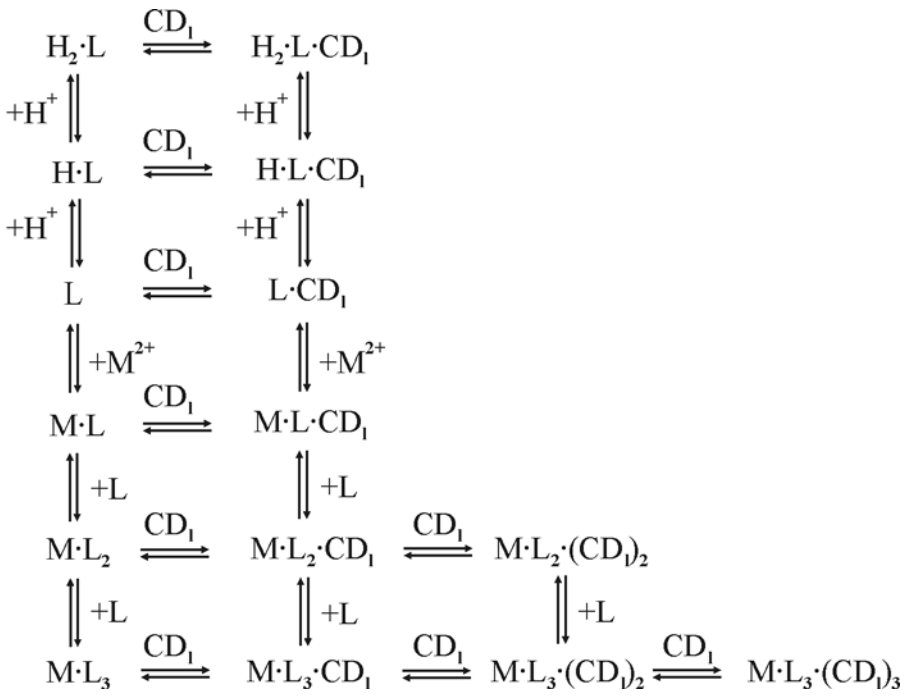

Scheme 7.4: *Equilibria for all solution species of L, in the absence and presence of Ni(II) and* CD_l *(charges are omitted for clarity).*

Similar to the case of Cu(II), when full orthogonality is assumed, all intrinsic stability constants for CD_l complexation of any species of L are equal. At a CD SAM surface, all species containing one molecule of L will behave as monovalent guests, binding a single surface CD in a similar manner as in solution. The divalent NiL_2 is expected to show the surface equilibria similar to CuL_2 give in Scheme 7.3, whereas the surface equilibria for the trivalent NiL_3 are given in Scheme 7.5. A priori, $ML_3(CD_s)_3$ is expected as the major surface species for ML_3 because of the high effective concentration at the CD SAM.

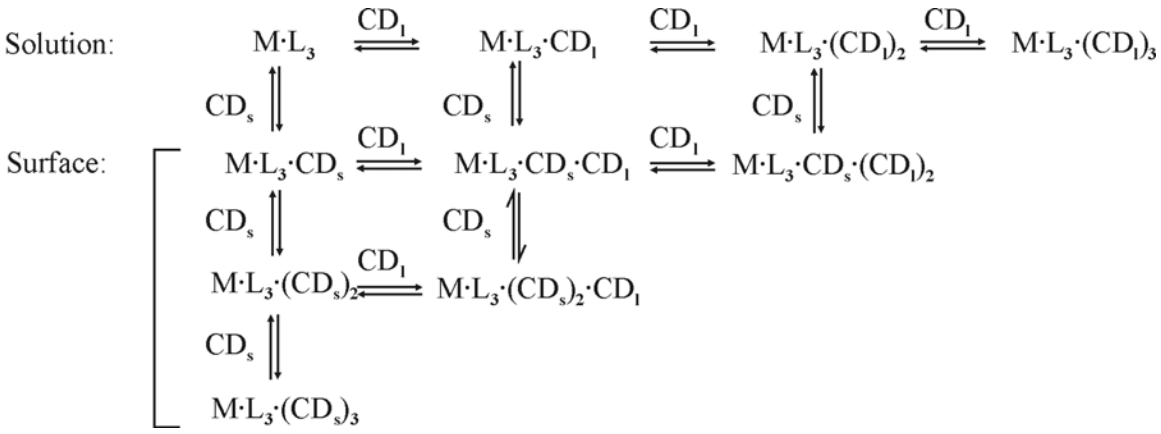

Scheme 7.5: *Equilibria for solution and surface species of NiL_3.*

The metal complex was prepared by mixing a solution of $NiCl_2$ and L in a 1:3 molar ratio. A geometric analysis of the most extended configuration of NiL_3 derived from CPK models (taking into account the two possible structural isomers) showed that the three adamantyl moieties are separated by about 3.0 nm. Considering the CD lattice periodicity of 2.1 nm, it is sterically feasible that all three adamantyl groups in the NiL_3 complex can interact with the CD SAM.

The protonation[46] and metal complex formation[47] constants corresponding to *N*-*n*-butylethylenediamine were used for the Ni(II) system as well. Similar to the Cu(II) complexes, the additional substitution at the en moiety with *N*-alkyl groups strongly reduces the metal complex formation constants.[47] These values lead to an expected pH dependence of the speciation of L in the presence of Ni(II) as shown in Figure 7.8.

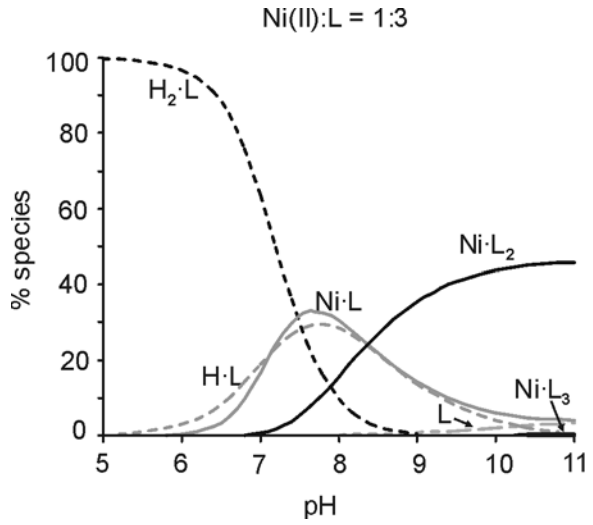

Figure 7.8: *Speciation of the different species of L present in solution as a function of pH in the presence of Ni(II) (total concentration of L: 1 mM). Solid lines represent Ni(II) complexes and dashed lines represent species without Ni(II).*

The speciation diagram in the absence of Ni(II) is identical to the one described before (Figure 7.2, left). When Ni(II) is present in solution, uncomplexed H_2L is present for more than 50% only at a pH below 7. At intermediate pH (7-8.5), NiL is the major species and HL a minor one. At higher pH (pH > 8.5) NiL_2 becomes dominant. Conversely, the trivalent NiL_3 is hardly expected (less than 5% at pH 11). This effect is due to K_{ML3} which is relatively small compared to K_{ML} and K_{ML2}, in particular for substituted en derivatives (such as *N*-*n*-butylethylendiamine) compared to en.[47]

SPR titrations were performed at pH 9 (1 mM $NaHCO_3$ and 1 mM CD_l) in order to ensure the maximum coordination number. SPR curves were fitted to the heterotropic multivalency model. Analogous to the thermodynamic model for the Cu(II) complex, $K_{i,s}$ and the I_{max} were variables, while $K_{i,l}$ (6.0×10^4 M^{-1}) and C_{eff} (0.2 M) were fixed.

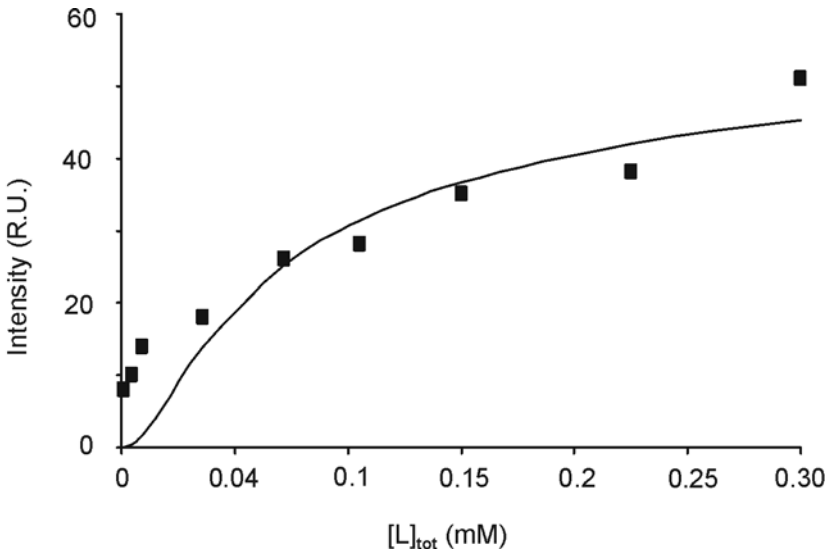

Figure 7.9: *SPR titration (data points) and the corresponding fit for a trivalent sequential binding model (solid lines) for the titration of L in the presence of Ni(II) (Ni(II):L = 1:3) to CD SAMs (1 mM bicarbonate buffer pH 9, 1 mM CD$_l$).*

The results obtained by fitting the SPR curves to a trivalent model gave a $K_{i,s}$ (3.4×10^4 M^{-1}) corresponding to an intrinsic adamantyl-cyclodextrin interaction[48] similar to the results obtained in solution. However, fitting the same SPR curve to a divalent model assuming that two adamantyls bind the CD surface, gave an intrinsic binding constant, $K_{i,s}$, (3.4×10^4 M^{-1}), equal to the binding constant found when all three guest moieties are used in the complexation to the surface. Finally, fitting assuming monovalent binding gave a binding constant (5.7×10^5 M^{-1}) that is much higher than the K obtained in solution for an adamantyl-cyclodextrin interaction.[48] These results established that the binding is multivalent but that the thermodynamic model could not discriminate between trivalent and divalent binding.

In order to determine whether the Ni(II) complex adsorbing to the CD SAM is divalent or trivalent, desorption experiments were performed. SPR titrations were performed in the presence of 1 mM Na_2CO_3 buffer (pH 11) and 5 mM CD. Addition of a solution of Ni^{2+}:L ($[Ni^{2+}]_{tot}$ = 0.5 mM; $[L]_{tot}$ = 1.5 mM) or Cu^{2+}:L ($[Cu^{2+}]_{tot}$ = 0.5 mM; $[L]_{tot}$ = 1.0 mM), respectively, to the CD SAM resulted in an increase of the SPR signal, which levelled off after 10 min. Rinsing of the surface with 1 mM Na_2CO_3 buffer (pH 11)

and 5 mM CD was monitored for 30 min, until all guest had been completely removed. Similar desorption kinetics were observed for the Ni(II) and Cu(II) complexes. Since divalent binding was determined for the Cu(II) complex, the desorption experiments indicate also divalent binding for the Ni(II) complex, since multivalency is known to have a strong kinetic effect and a trivalent complex would desorb much slower than a divalent complex.[7,10]

In order to find a possible explanation for the apparent divalency of the Ni(II) complex, the concentrations of the different species, $[L]_{free}$, [NiL], $[NiL_2]$, $[NiL_3]$ were analyzed by using the sequential binding model with three interactions to the CD surface. Figure 7.10 shows the different species that are present in solution and at the CD surface at pH 9 and 1 mM CD_l concentration.

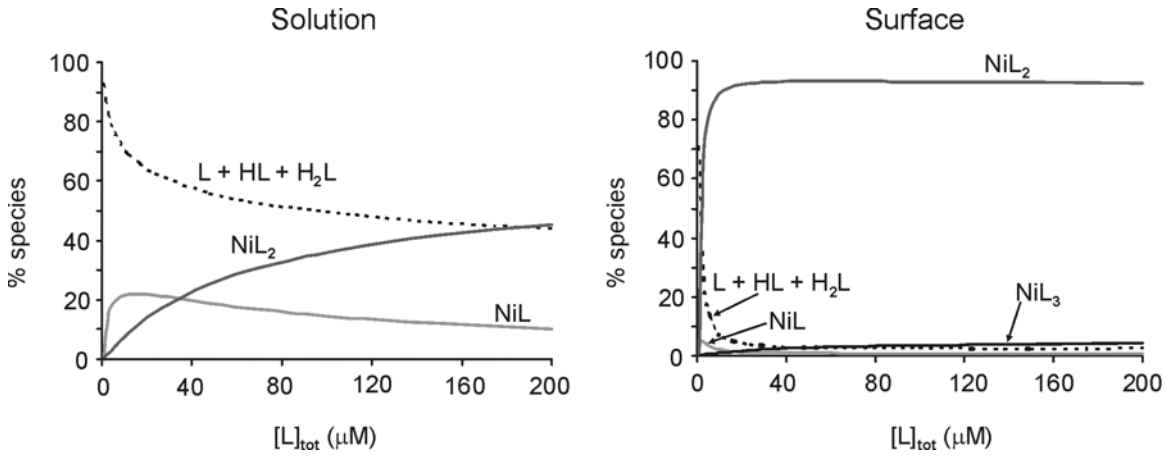

Figure 7.10: *Concentrations of uncomplexed L (L, HL, H_2L) (dashed lines), NiL (solid line, light gray), NiL_2 (solid line, gray), and NiL_3 (solid lines, black) present in solution (left) and at the CD SAM (right) at pH 9 (1 mM $NaHCO_3$, 1 mM CD_l) employing the sequential binding model for trivalent interactions.*

It can be observed that, in solution, uncomplexed L is always dominant, while NiL and NiL_2 are observed as well. NiL_3 is not observed at all. In contrast, at the surface, NiL_2 is essentially the only species, reaching complete coverage even at very low Ni^{2+} concentrations. At the surface, the trivalent NiL_3 reached up to 5%, but this is too low to be detected experimentally. Thus, a surface enhancement of the divalent NiL_2 is observed

with an *EF* of ~ 100. The divalent species NiL_2, which is in minority in solution, is dominant at the surface. On the other hand, the monovalent species (L, HL, H_2L) and NiL, which are dominant in solution, are non-existent at the surface. The *EF* for the trivalent NiL_3 is expected by the model to be about 10^4, but this is apparently still not enough to make it verifiable experimentally.

7.3 Conclusions

The binding of a host-guest metal-ligand complex formed between an adamantyl-functionalized ethylenediamine (L**)** and Cu(II) at CD SAMs results from multivalency of the guest molecules. Binding constants of the host-guest binding of the Cu(II) complex in solution and at the surface are of the same order of magnitude. Quantitative analysis of the different species present in solution and at the surface was performed as a function of pH. At high pH the metal complex adsorption on the surface led to the preferred formation of the divalent form (CuL_2), while the monovalent species (CuL) was only present in minority. The same behavior was observed in solution. Upon decrease of the pH, a different situation was observed. At pH 6 the multivalent surface clearly enhanced the presence of the divalent CuL_2 complex at its interface, whereas the monovalent CuL was the majority species in solution. This behavior is attributed to the high C_{eff} of cyclodextrin sites present at the surface and the close-to-optimal linker lengths between the two adamantyl groups relative to the periodicity of the CD lattice (ca. 2 nm).[42] At lower pH (5), the monovalent form CuL was predominant both in solution and at the surface [7]

The Ni(II) complex was studied at pH 9 and compared to the Cu(II) complex. The sequential multivalent, heterotropic binding model, although successful in explaining the divalent binding of the CuL_2 complex, could not discriminate between two or three interactions for the Ni(II) system. Desorption experiments, performed at equal concentrations, showed a similar behavior for both the Ni(II) and Cu(II) complexes, which is an indication of divalent binding for both complexes. Quantitative analysis of the different species of the Ni(II) complexes, showed that the divalent form is hardly

present in solution but multivalency enhanced its presence at the surface with an *EF* > 100.

This new concept of surface-enhanced multivalency using two types of orthogonal noncovalent interactions (host-guest and metal-ligand coordination) can be used in nanofabrication schemes towards the formation of large molecular assemblies where assembly is driven by multiple interactions.

7.4 Experimental Section

Materials

Chemicals were obtained from commercial sources and used as such. β-cyclodextrin (CD) was dried in vacuum at 80 °C in the presence of P_2O_5 for at least 5 h before use. Solvents were purified according to standard laboratory methods. Millipore water with a resistivity larger than 18 MΩ·cm was used in all our experiments. Synthesis of the CD heptathioether adsorbate was reported previously.[39] NMR spectra were recorded on Varian AC300 and AMX400 spectrometers. FAB-MS spectra were recorded with a Finnigan MAT 90 spectrometer using *m*-nitrobenzylalcohol as the matrix.

N-[2-(2-{2-[2-(Adamantan-1-yloxy)ethoxy]ethoxy}ethoxy)ethyl]ethane-1,2-diamine (**L**)

A stirred solution of triethylene glycol bromoethyl adamantyl ether[40] (0.65 g, 1.6 mmol) in an excess of ethylenediamine (20 ml) was heated to 80 °C overnight under a nitrogen atmosphere. The reaction mixture was cooled down to room temperature and evaporated under reduced pressure. The crude product was separated by flash column chromatography (CH_2Cl_2: EtOH: NH_4OH, 1:1:0.1-1:4:0.4, v/v) to afford the compound as a yellow oil (0.58 g, 93%). ^{1}H NMR (300 MHz, $CDCl_3$): δ (ppm) 3.67 -3.58 (m, 12H, AdOCH_2 and (CH_2OCH_2)$_3$), 2.81 (t, J = 5.7 Hz, 2H, CH_2CH_2NH), 2.80 (t, J = 5.3 Hz, 2H, NHCH_2CH_2), 2.70 (t, J = 5.4 Hz, 2H, $CH_2CH_2NH_2$), 2.13 (m, 3H, CH_2CHCH_2[Ad]), 1.96 (m, 6H, CHCH_2C[Ad]), 1.73-1.74 (m, 6H, CHCH_2CH[Ad]); ^{13}C NMR (75 MHz,

$CDCl_3$): δ (ppm) 72.4, 71.5, 70.8-70.5, 59.5, 52.3, 49.2, 41.7, 36.7, 30.7. MS (MALDI-TOF): m/z calcd for $C_{20}H_{38}N_2O_4$ 370.2; found 371.1 $[M+H]^+$; Elemental analysis: H 10.34, C 64.83, N 7.56, calcd for $C_{20}H_{38}N_2O_4$; found: H 10.38, C 62.87, N 7.07.

Preparation of the metal complex form of L with Cu(II) and Ni(II)

The metal complexes of Cu(II) and Ni(II) with L were prepared by mixing aliquots of a concentrated solution of $CuCl_2$ and $NiCl_2$ in distilled water (Millipore) to a solution of L. The molar ratio of metal and L was maintained at exactly 1:2 (Cu(II)) and 1:3 (Ni(II)) in order to prevent the formation of metal hydroxides. After addition of the metal salts the solutions were brought to the corresponding buffer solution (1 mM) and the CD concentration (1 mM).

Substrate and monolayer preparation

All glassware used to prepare monolayers was immersed in piraña (conc. H_2SO_4 and 33% H_2O_2 in a 3:1 ratio). (Warning! piraña should be handled with caution; it has detonated unexpectedly). The glassware was rinsed with large amounts of high purity water (Millipore). All solvents used in monolayer preparation were of p.a. grade. All adsorbate solutions were prepared freshly prior to use. Round glass-supported gold substrates for SPR (2.54 cm diameter; 47.5 nm Au) were obtained from Ssens BV (Hengelo, The Netherlands). Gold substrates were cleaned by immersing the substrates in piraña for 5 s and leaving the substrates for 5 min in absolute EtOH.[51] The substrates were subsequently immersed into a 0.1 mM CD heptathioether adsorbate solution in EtOH and $CHCl_3$ (1:2 v/v) for 16 h at 60 °C. SAMs of 11-mercaptoundecanol were adsorbed from EtOH at r.t. for 24 h. The samples were removed from the solution and rinsed with substantial amounts of chloroform, ethanol, and Millipore water.

Calorimetric titrations

Calorimetric measurements were performed at 25 °C using a Microcal VP-ITC instrument with a cell volume of 1.4115 ml. Sample solutions were prepared in Millipore

water. For studying the complexation of L to native CD at different pH (2, 7, 9, 11), 5 μl aliquots of a 5 mM solution of L were added to a 0.5 mM solution of CD in the calorimetric cell, monitoring the heat effect after each addition. For studying the complexation of L in the presence of Cu(II) (Cu(II):L = 1:2) to CD at different pH (7, 9), 5 μl aliquots of a 10 mM solution of CD were added to a solution of 0.5 mM $CuCl_2$ and 1 mM L. Dilution experiments showed that at the experimental concentrations employed in these experiments, none of the three species showed any detectable aggregation in water.

Surface plasmon resonance (SPR) spectroscopy

The SPR setup was obtained from Resonant Probes GmbH.[52] A light beam from the HeNe laser (JDS Uniphase, 10mW, λ = 632.8 nm) passes through a chopper that is connected to a lock-in amplifier (EG&G, 7256). The modulated beam then passes through two polarizers (Owis), by which the intensity and the plane of polarization of the laser can be adjusted. The modulated beam passes a beam-expanding unit (spatial filter) with a pinhole (25 μm) for spectral cleaning of the wave fronts. The light is coupled via a high index prism (Scott, LaSFN9) in this Kretschmann configuration to the (Au) metal-coated substrate which is index-matched to the prism in contact with a Teflon cell having O-rings for a liquid-tight seal. The sample cell is mounted on top of a θ-2θ goniometer with the detector measuring the reflectivity changes as a function of the angle of incidence of the p-polarized incoming laser beam. The incoming s/p laser beam passes through a beam splitter, which splits the p- and the s-polarized light. The s-polarized light is conducted to a reference detector. The p-polarized light passes a beam-expanding unit (spatial filter) with a pinhole (25 μm) for spectral cleaning and control of the intensity of p-polarized light and is collected into a photodiode detector. Titrations were measured in real time by recording the changes in the reflectivity in the fixed angle mode (55.2°). Titrations were performed starting with a buffer solution in the cell which was replaced by increasing concentrations of the analyte (L in the absence and presence of Cu(II) (Cu(II):L = 1:2). After addition of the analyte and stabilization of the SPR signal, the cell was thoroughly rinsed with 10 mM CD (in the corresponding buffer) followed by rinsing

with buffer solution. The same procedure was repeated until complete restoration of the CD surface.

Modelling

The thermodynamic model was implemented in Excel (Microsoft Excel 2000). For a more detailed description and the equations corresponding to the equilibrium constants and the mass balances see Appendix 7.5.

7.5 Appendix: The Heterotropic Multivalency Model at Interfaces

7.5.1 Heterotropic divalent model at interfaces

A general description is given for the divalent binding of a heterotropic supramolecular complex at a multivalent host surface by combining the orthogonal CD host-guest and metal ion-en coordination interaction motifs. All solution and surface species of L, due to protonation, metal complexation, and CD_l/CD_s complexation are in Scheme 7.6. Since full orthogonality has been shown (see before in this chapter), all intrinsic stability constants for CD_l or CD_s complexation of any species of L are equal.

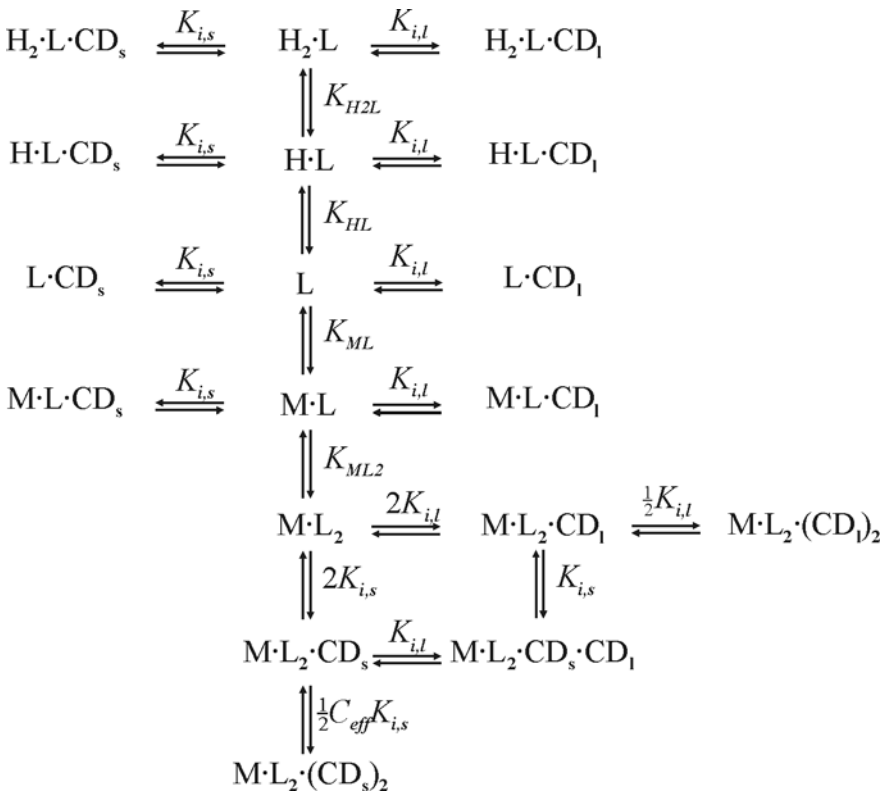

***Scheme 7.6**: Equilibria for all (solution and surface) species of L, in the absence and presence of M(II) and CD_l and/or CD_s (charges are omitted for clarity).*

As described before,[6,7] the SPR titrations performed for the binding to the CD SAMs are fitted yielding $K_{i,s}$ values, whereas the $K_{i,l}$ value is fixed to the value determined from solution data. These values are expected to be the same,[39] but this is used here as a verification for the correctness of the model[6,7] and/or of the stoichiometry.[13]

Since all measurements are done at a constant and known pH, the ratios between the protonated forms are fixed and determined by the protonation constants. Their equilibria with CD_l and CD_s do not shift these ratios since the binding constants of the protonated forms are identical (full orthogonality). Therefore, the concentration of free, uncomplexed L, $[L_f]$ is defined as:

$$[L]_f = [L] + [H{\cdot}L] + [H_2{\cdot}L] \qquad (2)$$

while the CD-complexed species (for both CD_l and CD_s) are given by:

$$[L_f{\cdot}CD] = [L{\cdot}CD] + [H{\cdot}L{\cdot}CD] + [H_2{\cdot}L{\cdot}CD] \quad (3)$$

Thus, the (simplified) mass balances for L, M(II), CD_l, and CD_s are given by:

$$[L]_{tot} = [L_f] + [M{\cdot}L] + 2[M{\cdot}L_2] + [L_f{\cdot}CD_l] + [M{\cdot}L{\cdot}CD_l] + 2[M{\cdot}L_2{\cdot}CD_l] + 2[M{\cdot}L_2{\cdot}(CD_l)_2] + [L_f{\cdot}CD_s] + [M{\cdot}L{\cdot}CD_s] + 2[M{\cdot}L_2{\cdot}CD_s] + 2[M{\cdot}L_2{\cdot}CD_s{\cdot}CD_l] + 2[M{\cdot}L_2{\cdot}(CD_s)_2] \quad (4)$$

$$[M]_{tot} = [M] + [M{\cdot}L] + [M{\cdot}L_2] + [M{\cdot}L{\cdot}CD_l] + [M{\cdot}L_2{\cdot}CD_l] + [M{\cdot}L_2{\cdot}(CD_l)_2] + [M{\cdot}L{\cdot}CD_s] [M{\cdot}L_2{\cdot}CD_s] + [M{\cdot}L_2{\cdot}CD_s{\cdot}CD_l] + [M{\cdot}L_2{\cdot}(CD_s)_2] \quad (5)$$

$$[CD_l]_{tot} = [CD_l] + [L_f{\cdot}CD_l] + [M{\cdot}L{\cdot}CD_l] + [M{\cdot}L_2{\cdot}CD_l] + 2[M{\cdot}L_2{\cdot}(CD_l)_2] + [M{\cdot}L_2{\cdot}CD_s{\cdot}CD_l] \quad (6)$$

$$[CD_s]_{tot} = [CD_s] + [L_f{\cdot}CD_s] + [M{\cdot}L{\cdot}CD_s] + [M{\cdot}L_2{\cdot}CD_s] + [M{\cdot}L_2{\cdot}CD_s{\cdot}CD_l] + 2[M{\cdot}L_2{\cdot}(CD_s)_2] \quad (7)$$

The protonation and metal complexation constants of L are given by:

$$K_{HL} = \frac{[H \cdot L]}{[H][L]} \quad (8) \qquad K_{H2L} = \frac{[H_2 \cdot L]}{[H \cdot L][H]} \quad (9)$$

$$K_{ML} = \frac{[M \cdot L]}{[M][L]} \quad (10) \qquad K_{ML2} = \frac{[M \cdot L_2]}{[M \cdot L][L]} \quad (11)$$

For all monovalent species X (X = L, HL, H_2L, ML) the stability constants for CD complexation are given by:

$$K_{i,l} = \frac{[X \cdot CD_l]}{[X][CD_l]} \quad (12) \qquad K_{i,s} = \frac{[X \cdot CD_s]}{[X][CD_s]} \quad (13)$$

Species involving CD_s are expressed in volume concentrations employing the total sample volume.[6,7]

For the divalent ML_2, binding to CD_l involves statistical factors (see Scheme 7.6) arising from the probabilities for binding relative to the monovalent species.

Similarly, the first binding constant of ML_2 with the CD SAM is defined by:

$$\frac{[M \cdot L_2 \cdot CD_s]}{[M \cdot L_2][CD_s]} = 2K_{i,s} \tag{14}$$

The second, intramolecular binding event at the surface, *i.e.* the formation of $ML(CD_s)_2$, is accompanied by an effective concentration term.[6,7]

$$\frac{[M \cdot L_2 \cdot (CD_s)_2]}{[M \cdot L_2 \cdot CD_s][CD_s]} = \frac{1}{2} C_{eff} K_{i,s} \tag{15}$$

The effective concentration, C_{eff}, is given by multiplying the maximum effective concentration, $C_{eff,max}$, which is the number of accessible host sites in the probing volume,[6,7] with the fraction of the free host sites at the surface:

$$C_{eff} = C_{eff,\max} \frac{[CD_s]}{[CD_s]_{tot}} \tag{16}$$

Substitution of the equilibrium constant definitions into the mass balances for $[L]_{tot}$, $[M]_{tot}$, $[CD_l]_{tot}$, and $[CD_s]_{tot}$ provide a set of numerically solvable species with [L], [M], $[CD_l]$, and $[CD_s]$ as the variables.

Starting from an initial estimate for $K_{i,s}$, using fixed values for $C_{eff,max}$ and all other stability constants, this set of equations is solved numerically using a Simplex algorithm in a spreadsheet approach.[53] When fitting SPR data, $K_{i,s}$ is optimized in a least-squares optimization routine, assuming that the SPR response (Intensity) is linearly dependent on the total amount of L adsorbed to the CD SAM regardless of the type of species. The maximum I_{max} is then optimized as an independent fitting parameter as well.

For calculating the surface enhancement factor, EF, the ratios of divalent to monovalent species, both in solution and at the surface, are compared. In solution, the total concentration of monovalent species, $[L]_{mono}$, is given by:

$$[L]_{l,mono} = [L_f] + [M{\cdot}L] + [L_f{\cdot}CD_l] + [M{\cdot}L{\cdot}CD_l] \quad (17)$$

whereas the total concentration of divalent species, $[L]_{l,div}$, is given by:

$$[L]_{l,div} = [M{\cdot}L_2] + 2[M{\cdot}L_2{\cdot}CD_l] + 2[M{\cdot}L_2{\cdot}(CD_l)_2] \quad (18)$$

At the surface, the corresponding concentrations, $[L]_{s,mono}$ and $[L]_{s,div}$, are given by:

$$[L]_{s,mono} = [L_f{\cdot}CD_s] + [M{\cdot}L{\cdot}CD_s] + 2[M{\cdot}L_2{\cdot}CD_s] + 2[M{\cdot}L_2{\cdot}CD_s{\cdot}CD_l] \quad (19)$$

$$[L]_{s,div} = 2[M{\cdot}L_2{\cdot}(CD_s)_2] \quad (20)$$

Thus, *EF* is given by (see also Equation 1):

$$EF = \left(\frac{[L]_{s,div}}{[L]_{s,mono}}\right)/\left(\frac{[L]_{l,div}}{[L]_{l,mono}}\right) = \frac{[L]_{s,div}\cdot[L]_{l,mono}}{[L]_{s,mono}\cdot[L]_{l,div}} \quad (21)$$

For the Cu-L system, the following parameters were used: K_{HL} = 2.00 × 10^{10} M^{-1},[46] K_{HL2} = 3.39 × 10^{7} M^{-1},[46] K_{CuL} = 8.71 × 10^{9} M^{-1},[47] K_{CuL2} = 1.89 × 10^{8} M^{-1},[47] $K_{i,l}$ = 6.0 × 10^{4} M^{-1} (see above) and $C_{eff,max}$ = 0.20 M.

7.5.2 Heterotropic trivalent model at interfaces

The heterotropic trivalent model, for fitting the Ni-L system, was built in the same manner as described above, now also introducing the NiL_3. A schematic diagram

representing the new equilibria (besides the ones shown in Scheme 7.6, above) involved is shown in Scheme 7.7.

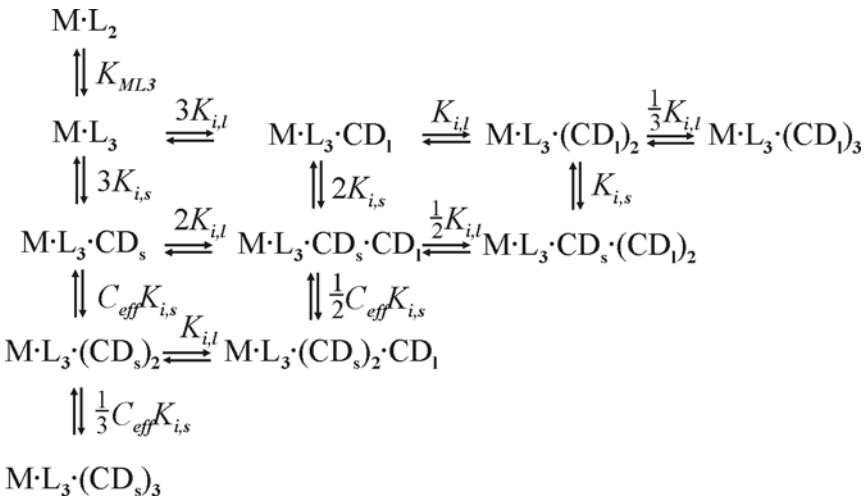

Scheme 7.7*: Equilibria for (solution and surface) species of ML_3, in the absence and presence of M(II) and CD_l and/or CD_s (charges are omitted for clarity).*

All additional stability constant equations and additional terms to the mass balance equations are logical extensions of the divalent model described above, and are therefore not given here explicity. The stepwise adsorption of ML_3 to the CD SAM involves now an intermolecular and two intramolecular steps (the latter of which both involve the C_{eff} parameter), to yield finally the trivalent $ML_3(CD_s)_3$ complex. The numerical routine as well as the optimization routine for $K_{i,s}$ and I_{max} are identical to the procedures described above. For the Ni-L systems, the following parameters were used: $K_{HL} = 2.00 \times 10^{10}$ M^{-1},[46] $K_{HL2} = 3.39 \times 10^{7}$ M^{-1},[46] $K_{NiL} = 5.37 \times 10^{6}$ M^{-1},[47] $K_{NiL2} = 3.63 \times 10^{5}$ M^{-1},[47] $K_{NiL3} = 1.58 \times 10^{2}$ M^{-1},[47] $K_{i,l} = 6.0 \times 10^{4}$ M^{-1} (see above) and $C_{eff,max} = 0.20$ M.

7.6 References and Notes

1. Sigal, G. B.; Mammen, M.; Dahmann, G.; Whitesides, G. M. *J. Am. Chem. Soc.* **1996**, *118*, 3789-3800.
2. Spaltenstein, A.; Whitesides, G. M. *J. Am. Chem. Soc.* **1991**, *113*, 686-687.

3. Mammen, M.; Choi, S. K.; Whitesides, G. M. *Angew. Chem. Int. Ed.* **1998**, *37*, 2755-2794.
4. Lundquist, J. J.; Toone, E. J. *Chem. Rev.* **2002**, *102*, 555-578.
5. Varki, A. *Glycobiology* **1993**, *3*, 97-130.
6. Mulder, A.; Auletta, T.; Sartori, A.; Del Ciotto, S.; Casnati, A.; Ungaro, R.; Huskens, J.; Reinhoudt, D. N. *J. Am. Chem. Soc.* **2004**, *126*, 6627-6636.
7. Huskens, J.; Mulder, A.; Auletta, T.; Nijhuis, C. A.; Ludden, M. J. W.; Reinhoudt, D. N. *J. Am. Chem. Soc.* **2004**, *126*, 6784-6797.
8. Mann, D. A.; Kanai, M.; Maly, D. J.; Kiessling, L. L. *J. Am. Chem. Soc.* **1998**, *120*, 10575-10582.
9. Rao, J. H.; Yan, L.; Xu, B.; Whitesides, G. M. *J. Am. Chem. Soc.* **1999**, *121*, 2629-2630.
10. Metallo, S. J.; Kane, R. S.; Holmlin, R. E.; Whitesides, G. M. *J. Am. Chem. Soc.* **2003**, *125*, 4534-4540.
11. Smith, E. A.; Thomas, W. D.; Kiessling, L. L.; Corn, R. M. *J. Am. Chem. Soc.* **2003**, *125*, 6140-6148.
12. Crespo-Biel, O.; Péter, M.; Bruinink, C. M.; Ravoo, B. J.; Reinhoudt, D. N.; Huskens, J. *Chem. Eur. J.* **2005**, *11*, 2426-2432.
13. Nijhuis, C. A.; Yu, F.; Knoll, W.; Huskens, J.; Reinhoudt, D. N. *Langmuir* **2005**, *21*, 7866-7876.
14. Fantuzzi, G.; Pengo, P.; Gomila, R.; Ballester, P.; Hunter, C. A.; Pasquato, L.; Scrimin, P. *Chem. Commun.* **2003**, 1004-1005.
15. Barrientos, A. G.; De La Fuente, J. M.; Rojas, T. C.; Fernández, A.; Penadés, S. *Chem. Eur. J.* **2003**, *9*, 1909-1921.
16. Lin, C. C.; Yeh, Y. C.; Yang, C. Y.; Chen, G. F.; Chen, Y. C.; Wu, Y. C.; Chen, C. C. *Chem. Commun.* **2003**, 2920-2921.
17. Thibault, R. J.; Galow, T. H.; Turnberg, E. J.; Gray, M.; Hotchkiss, P. J.; Rotello, V. M. *J. Am. Chem. Soc.* **2002**, *124*, 15249-15254.
18. Lim, C. W.; Ravoo, B. J.; Reinhoudt, D. N. *Chem. Commun.* **2005**, in press.
19. Whitesides, G. M. *Small* **2005**, *1*, 172-179.
20. Sanyal, A.; Norsten, T. B.; Uzun, O.; Rotello, V. M. *Langmuir* **2004**, *20*, 5958-5964.
21. Park, J. S.; Lee, G. S.; Lee, Y. J.; Park, Y. S.; Yoon, K. B. *J. Am. Chem. Soc.* **2002**, *124*, 13366-13367.
22. Chen, Y. F.; Banerjee, I. A.; Yu, L.; Djalali, R.; Matsui, H. *Langmuir* **2004**, *20*, 8409-8413.
23. Huskens, J.; Deij, M. A.; Reinhoudt, D. N. *Angew. Chem. Int. Ed.* **2002**, *41*, 4467-4471.
24. Fragoso, A.; Caballero, J.; Almirall, E.; Villalonga, R.; Cao, R. *Langmuir* **2002**, *18*, 5051-

5054.

25. Zhang, S.; Palkar, A.; Fragoso, A.; Prados, P.; De Mendoza, J.; Echegoyen, L. *Chem. Mater.* **2005**, *17*, 2063-2068.
26. Holliday, B. J.; Mirkin, C. A. *Angew. Chem. Int. Ed.* **2001**, *40*, 2022-2043.
27. Cotton, F. A.; Lin, C.; Murillo, C. A. *Proc. Natl. Acad. Sci. U. S. A.* **2002**, *99*, 4810-4813.
28. Dorn, I. T.; Eschrich, R.; Seemuller, E.; Guckenberger, R.; Tampé, R. *J. Mol. Biol.* **1999**, *288*, 1027-1036.
29. Radler, U.; Mack, J.; Persike, N.; Jung, G.; Tampé, R. *Biophys. J.* **2000**, *79*, 3144-3152.
30. Thess, A.; Hutschenreiter, S.; Hofmann, M.; Tampé, R.; Baumeister, W.; Guckenberger, R. *J. Biol. Chem.* **2002**, *277*, 36321-36328.
31. Gamsjaeger, R.; Wimmer, B.; Kahr, H.; Tinazli, A.; Picuric, S.; Lata, S.; Tampé, R.; Maulet, Y.; Gruber, H. J.; Hinterdorfer, P.; Romanin, C. *Langmuir* **2004**, *20*, 5885-5890.
32. Tinazli, A.; Tang, J. L.; Valiokas, R.; Picuric, S.; Lata, S.; Piehler, J.; Liedberg, B.; Tampé, R. *Chem. Eur. J.* **2005**, *11*, 5249-5259.
33. Doyle, E. L.; Hunter, C. A.; Phillips, H. C.; Webb, S. J.; Williams, N. H. *J. Am. Chem. Soc.* **2003**, *125*, 4593-4599.
34. Fyfe, M. C. T.; Stoddart, J. F. *Coord. Chem. Rev.* **1999**, *183*, 139-155.
35. Hofmeier, H.; Schubert, U. S. *Chem. Commun.* **2005**, 2423-2432.
36. Some examples can be found: (a) Thalladi, V. R.; Goud, B. S.; Hoy, V. J.; Allen, F. H.; Howard, J. A. K.; Desiraju, G. R. *Chem. Comm.* **1996**, 401-402; (b) Funeriu, D. P.; Lehn, J. M.; Baum, G.; Fenske, D. *Chem. Eur. J.* **1997**, *3*, 99-104.
37. Rosi, N. L.; Mirkin, C. A. *Chem. Rev.* **2005**, *105*, 1547-1562.
38. Samori, B.; Zuccheri, G. *Angew. Chem. Int. Ed.* **2005**, *44*, 1166-1181.
39. De Jong, M. R.; Huskens, J.; Reinhoudt, D. N. *Chem. Eur. J.* **2001**, *7*, 4164-4170.
40. Mulder, A.; Onclin, S.; Péter, M.; Hoogenboom, J. P.; Beijleveld, H.; Ter Maat, J.; García-Parajó, M. F.; Ravoo, B. J.; Huskens, J.; Van Hulst, N. F.; Reinhoudt, D. N. *Small* **2005**, *1*, 242-253.
41. Ulman, A. *An Introduction to Ultrathin Organic Films: From Langmuir-Blodgett to Self-Assembly*; Academic Press: Boston, U.S.A., **1991**.
42. Schönherr, H.; Beulen, M. W. J.; Bügler, J.; Huskens, J.; Van Veggel, F. C. J. M.; Reinhoudt, D. N.; Vancso, G. J. *J. Am. Chem. Soc.* **2000**, *122*, 4963-4967.
43. Sillen, L.G.; Martell, A. E. *Stability Constants of Metal-Ion Complexes. Section 2: Organic Ligands;* The Chemical Society: London, UK, **1964**.
44. Charges are omitted for clarity.

45. Mellor, D. P. *Chem. Rev.* **1943**, *33*, 137-183.
46. Basolo, F.; Murmann, R. K. *J. Am. Chem. Soc.* **1952**, *74*, 2373-2374.
47. Basolo, F.; Murmann, R. K. *J. Am. Chem. Soc.* **1952**, *74*, 5239-5246.
48. Rekharsky, M. V.; Inoue, Y. *Chem. Rev.* **1998**, *98*, 1875-1917.
49. For two independent, sequential binding events this implies: $K_1 = 2K_i$, $K_2 = {}^1/_2K_i$, and $\Delta H_1^\circ = \Delta H_2^\circ = \Delta H_t^\circ$.
50. The cause of this observation is the equilibria in solution but not at the surface.
51. Ron, H.; Rubinstein, I. *Langmuir* **1994**, *10*, 4566-4573.
52. Aust, E. F.; Ito, S.; Sawondny, M.; Knoll, W. *Trends Polym. Sci.* **1994**, *2*, 313-323.
53. Huskens, J.; Van Bekkum, H.; Peters, J. A. *Comp. Chem.* **1995**, *19*, 409-416.

Summary

This thesis describes the use of multivalent host-guest interactions at interfaces for the construction of 2D and 3D nanostructures. Self-assembled monolayers (SAMs) on flat surfaces and nanoparticles have been employed to confine and organize such structures. The host-guest interactions between β-cyclodextrin (CD) and different guest derivatives are the focus of attention in this thesis. Host monolayers of CDs were prepared on flat gold and silicon oxide surfaces. These host monolayers have been utilized as molecular printboards for the recognition and positioning of molecules by means of multiple supramolecular interactions. Gold nanoparticles have also been modified with CD and the formation of large 3D aggregates in the presence of multivalent guest molecules was studied as a function of the number of hydrophobic endgroups of the guest molecule and its geometry. The combination of multiple interactions between adamantyl-terminated dendrimers and CD-modified gold nanoparticles (CD Au NPs) was employed to create organized 2D structures at surfaces generated by layer-by-layer assembly. The combination with lithographic techniques, by which such structures can be directed to specific target areas, led to the formation of 3D nanostructures.

New methodologies for the assembly of molecular- to micrometer-scale objects onto substrates in predetermined arrangements for the fabrication of 2D and 3D nanostructures are reviewed in Chapter 2. The positioning of molecules onto substrates has been achieved with noncovalent interactions, with special attention to multiple supramolecular interactions for the assembly. The first part of this chapter covers different systems and methodologies that have been used in order to attach molecules and nanoparticles to flat surfaces. Some examples of layer-by-layer systems are described as potential platforms for the construction of 3D systems, especially when combined with patterning methodologies. The second section is focused on various methodologies to create and control nanoparticle assembly into well-defined nanoarchitectures.

Chapter 3 describes the interaction between poly(isobutene-*alt*-maleic acid)s modified with *p*-*tert*-butylphenyl or adamantyl groups and CD SAMs. The binding of the hydrophobic guest-functionalized polymers to the CD SAMs takes place through multiple inclusions of the guest substituents of the polymers into the CD cavities. It was shown to be very strong and irreversible. In solution these polymers are known to be spherical with a hydrodynamic radius of about 10 nm. They have strong intramolecular hydrophobic interactions leading to reduce affinity for CD in solution. However, the polymer adsorption onto the CD SAMs led to very thin polymer films (0.5 nm) as shown by AFM scratching experiments. Apparently the polymer uses all or many of the hydrophobic groups, as was further supported by the absence of specific binding of CD Au NPs to the polymer surface assemblies. Variations of the nature and/or number of hydrophobic groups in the polymer, and of the polymer concentration in solution did not lead to significant differences in adsorption behavior. Competition experiments with monovalent host and guest, did not lead to measurable polymer desorption. This behavior was attributed to the large number of functional groups on the polymer and to the close-to-optimal linker lengths (1.6-5.4 nm) between the hydrophobic substituents, leading to high effective concentrations (0.25 M) and thus very high estimated binding constants ($K > 5 \times 10^{87}$ M^{-1}). Supramolecular microcontact printing (μCP) of the polymers onto the CD SAMs resulted in the assembly formation in the targeted areas of the substrate.

Chapter 4 shows that adamantyl-terminated guest molecules can mediate the aggregation of CD Au NPs in aqueous solution by employing strong and specific, multivalent host-guest interactions. Gold nanoparticles bearing surface-immobilized CD hosts were synthesized following a one-phase procedure and characterized by UV-vis spectroscopy, thermogravimetric analysis, ^{1}H NMR spectroscopy and TEM. The latter showed unaggregated particles and a relatively narrow particle size distribution of 2.8 ± 0.6 nm. The aggregation rate between the CD Au NPs and the guest molecules could be controlled taking into account several parameters such as, the number of interactions available for the assembly, the geometry of the molecules and the addition of a competitor in solution to prevent aggregation. Adamantyl-terminated dendrimers, owing to their globular shape and high number of interactions, led to the formation of insoluble nanoparticle aggregates without a long-range order, which is a strong indication of

intermolecular binding. Conversely, a bis-adamantyl molecule, with two interaction sites and a flexible linker did not show the formation of an insoluble complex, which was attributed to predominantly *intramolecular* binding. Addition of the monovalent adamantyl carboxylate to a solution of CD Au NPs did not induce precipitation and resulted in stable assemblies. The binding constant (2.31×10^4 M^{-1}) could be determined by isothermal titration calorimetry (ITC). In contrast to the experiments using CD Au NPs, the addition of adamantyl-terminated dendrimers to a solution of oligo(ethylene glycol)-functionalized Au NPs did not lead to precipitation nor to changes of the plasmon absorption band. Furthermore, by adding a monovalent competitor in solution, the aggregation process of the bis-adamantyl guest molecule could be controlled.

Chapter 5 describes a new supramolecular procedure for the stepwise construction of a novel kind of self-assembled organic/inorganic multilayer thin films. The procedure is based on the layer-by-layer (LBL) assembly of guest-functionalized dendrimers and CD Au NPs deposited onto CD SAMs on gold or on SiO_2. This type of supramolecular LBL assembly was demonstrated to yield multilayer thin films with a thickness control at the nm level. Different techniques were used to monitor the assembly. Surface plasmon resonance spectroscopy (SPR) was used to monitor in situ the LBL assembly at different concentrations of the components. The adsorption behavior was observed to be similar at the studied range of concentrations, showing a linear growth with the number of bilayers deposited onto the CD SAMs. Blank experiments lacking the host SAM or the guest molecule did not show any specific or controllable LBL assembly. Information about the absolute thickness increase with the number of bilayers was obtained from ellipsometry and AFM. An estimate of the multilayer thickness of 2 nm/bilayer was obtained in both cases. Furthermore, UV/vis spectroscopy was used to monitor the supramolecular assembly on a glass surface. The linear increase in absorption at 525 nm as a function of the number of bilayers (for 1-18 bilayers) was again a strong indication of a well-defined deposition process. Additionally, UV/vis spectroscopy gave a quantitative estimation of the amount of material deposited after each cycle assuming a hexagonal packing of monodisperse particles. Comparison between the experimental and the theoretical values clearly indicates that close to a monolayer of CD Au NPs was deposited after each assembly cycle.

Chapter 6 introduces various patterning strategies to create 3D hybrid nanostructures of dendrimers and CD Au NPs on CD SAMs based on multiple supramolecular interactions using the LBL approach described in Chapter 5. Initially, μCP and nanoimprint lithography (NIL), followed by metal evaporation and lift-off, have been performed in order to obtain chemically patterned SAMs to attempt directed LBL assembly, relying on the supramolecular specificity. However, these two approaches did not result in patterned LBL assemblies, and indiscriminate multilayer deposition was observed attributed to nonspecific adsorption of the dendrimers. In contrast, nanotransfer printing (nTP) and NIL resulted in patterned LBL assemblies on the CD SAMs. nTP was achieved by LBL assembly on an oxidized PDMS stamp followed by transfer onto a full CD SAM. The structures showed good stability against rinsing, even with a monovalent, competitive host in solution, and against acetone/ultrasound treatment. nTP-patterned LBL assemblies showed a linear thickness increase of approx. 3 nm per bilayer. The supramolecular specificity observed was not perfect which could again be attributed to nonspecific interactions of the dendrimers. Furthermore, LBL assemblies patterned by NIL, LBL assembly, and lift-off have been obtained using PMMA as a physical barrier for the multilayer deposition. Thus, patterned LBL assemblies showed a linear thickness increase, in this case of only about 1.1 nm per bilayer. These differences in the multilayer heights as a function of the number of bilayers can possibly be explained by wetting problems. Nevertheless, high resolution 3D nanostructures with aspect ratios on the order of 1 were obtained combining LBL assembly and NIL.

Chapter 7 introduces a new concept for nanofabrication which involves multivalent, heterotropic, orthogonal interactions. The binding of a host-guest metal-ligand complex formed between adamantyl-functionalized ethylenediamine (L) and Cu(II) or Ni(II) at CD SAMs was shown to result from multivalency of the guest molecules. To verify the orthogonality of the metal-ethylenediamine and CD-adamantyl binding motifs, binding studies of L, with or without Cu(II) at various pH, with CD were performed in aqueous solution using ITC. The binding constants with ($K = 7.9 \times 10^4$ M^{-1}) and without ($K = 6.0 \times 10^4$ M^{-1}) Cu(II) are typical for a 1:1 CD-adamantyl inclusion interaction and showed no influence of pH on the complexation, thus proving full orthogonality. Binding constants at CD SAMs were of the same order of magnitude as in

solution. Quantitative analysis of the different species present in solution and at the surface was performed as a function of pH by using a sequential, multivalent, heterotropic binding model. At high pH the metal complex adsorption on the surface led to the preferred formation of the divalent form (CuL_2), while at pH 5 mainly the monovalent species were present. The same behavior was observed in solution. Conversely, at pH 6 the multivalent surface clearly enhanced the presence of the divalent CuL_2 complex at its interface with an enhancement factor (*EF*) higher than 100, whereas monovalent species were predominant in solution. This behavior is attributed to the high effective concentration of CD sites present at the surface and the close-to-optimal linker lengths between the two adamantyl groups relative to the periodicity of the CD lattice (ca. 2 nm). In the case of the Ni(II) complex, the sequential multivalent, heterotropic binding model could not discriminate between divalent or trivalent binding. Desorption experiments, performed at equal concentrations, showed comparable desorption rates for both Ni(II) and Cu(II) complexes, which is a strong indication of divalent binding at the surface in both cases. Quantitative analysis of the different species of the Ni(II) complexes showed that the divalent form was hardly present in solution but multivalency enhanced its presence at the surface, again with $EF > 100$.

The results presented in this thesis illustrate the versatility of self-assembly and multivalency to create 2D and 3D nanostructures and to apply such protocols in more complex nanofabrication schemes. The work on the different supramolecular assemblies on flat surfaces and nanoparticles demonstrates that different nanoarchitectures can be obtained by combining the supramolecular specificity and stability of multiple interactions. Combination with lithographic techniques, such as μCP and NIL, opens new approaches for the supramolecular patterning of interfaces and for the construction of well-defined 3D nanostructures.

Samenvatting

Dit proefschrift beschrijft het gebruik van multivalente (meervoudige) receptor-ligand-interacties aan grensvlakken voor de constructie van 2D- en 3D-nanostructuren. Voor het organiseren en begrenzen van dergelijke structuren is gebruik gemaakt van zelf-geassembleerde monolagen (*self-assembled monolayers*, *SAMs*) op vlakke oppervlakken en op nanodeeltjes. In dit proefschrift wordt de nadruk gelegd op receptor-ligand-interacties tussen β-cyclodextrine (CD) en verschillende gastderivaten. Monolagen met receptoren bestaande uit CD zijn gemaakt op vlakke goud- en siliciumoxide-oppervlakken. Deze receptor-monolagen zijn toegepast als moleculaire printplaten voor de herkenning en rangschikking van moleculen door middel van multivalente supramoleculaire interacties. Naast deze monolagen zijn ook goud-nanodeeltjes (*nanoparticles, NPs*) gefunctionaliseerd met CD en is de vorming van grote 3D-aggregaten in de aanwezigheid van multivalente gastmoleculen bestudeerd als functie van het aantal hydrofobe eindgroepen van de gastmoleculen en hun geometrie. De combinatie van multivalente interacties tussen adamantyl-getermineerde dendrimeren en CD-gemodificeerde goud-nanodeeltjes is gebruikt om georganiseerde 2D-structuren op oppervlakken te maken door middel van laagsgewijze assemblage (*layer-by-layer assembly*). Met behulp van lithografische technieken, waarbij deze structuren op specifieke delen van het substraat opgebouwd kunnen worden, zijn vervolgens 3D-nanostructuren verkregen.

Nieuwe methodologieën voor de assemblage van objecten, van molecuul- tot micrometerschaal, op substraten in van te voren vastgestelde patronen voor het vervaardigen van 2D- en 3D-nanostructuren zijn besproken in Hoofdstuk 2. Het rangschikken van de moleculen op substraten geschiedt door middel van niet-covalente interacties, waarbij speciale aandacht is geschonken aan het gebruik van multivalente supramoleculaire interacties in de assemblage. Het eerste gedeelte van dit hoofdstuk omvat verscheidene systemen en methodologieën die zijn gebruikt om moleculen en nanodeeltjes te bevestigen op vlakke oppervlakken. Enkele voorbeelden van gelaagde

systemen zijn beschreven als potentieel platform voor het maken van 3D-systemen, in het bijzonder wanneer deze gecombineerd worden met technieken om patronen te maken. Het tweede gedeelte richt zich op verscheidene methoden om nanodeeltjes te maken en op het controleren van de assemblage van nanodeeltjes in goed gedefinieerde nanoarchitecturen.

Hoofdstuk 3 beschrijft de interactie tussen CD-SAMs en poly(isobuteen-*alt*-maleïnezuur) gefunctionaliseerd met *p-tert*-butylphenyl- of adamantylgroepen. De binding van deze hydrofobe gast-gefunctionaliseerde polymeren op de CD-SAMs vindt plaats door de meervoudige insluiting van de gastsubstituenten van de polymeren in de CD-holten. De binding van de gefunctionaliseerde poly(isobuteen-*alt*-maleïnezuur)-derivaten is zeer sterk en irreversibel. Het is bekend dat deze polymeren in oplossing bolvormig zijn met een hydrodynamische straal van ongeveer 10 nm. Ze vertonen sterke intramoleculaire hydrofobe interacties die leiden tot een vermindering in affiniteit voor CD in oplossing. Met behulp van AFM-experimenten is aangetoond dat de adsorptie van polymeren op de CD-SAMs zeer dunne polymeerfilms (0.5 nm) oplevert. Het is aannemelijk dat alle - of tenminste zeer vele - van de hydrofobe gastgroepen van het polymeer deelnemen in het bindingsproces. Deze hypothese wordt ondersteund door de afwezigheid van specifieke binding van CD-gefunctionaliseerde goud-nanodeeltjes nadat deze zijn toegevoegd aan de polymeer-oppervlakte-assemblages. Variaties van het soort en aantal hydrofobe groepen in het polymeer alsmede de polymeerconcentratie in oplossing leidden niet tot significante veranderingen in adsorptiegedrag. Eveneens werd bij competitieëxperimenten met monovalente receptoren en liganden geen meetbare polymeerdesorptie waargenomen. Dit gedrag is toegeschreven aan het grote aantal functionele groepen die aanwezig zijn in het polymeer en aan de bijna optimale lengtes van de linkers (1.6-5.4 nm) tussen de hydrofobe substituenten, hetgeen leidt tot hoge effectieve concentraties (0.25 M) en daardoor zeer hoge geschatte bindingsconstanten ($K > 5 \times 10^{87}$ M^{-1}). Assemblage op specifieke gebieden van het substraat kon tenslotte worden aangetoond door middel van het supramoleculaire microcontact-printen (μCP) van de polymeren op de SAMs.

Hoofdstuk 4 toont aan dat adamantyl-getermineerde gastmoleculen de aggregatie van CD-gefunctionaliseerde goud-nanodeeltjes (CD-Au-NPs) in waterige oplossing

kunnen sturen door middel van sterke en specifieke, multivalente receptor-ligand-interacties. Goud-nanodeeltjes met oppervlakte-geïmmobiliseerde CD-receptoren zijn gesynthetiseerd volgens een éénstapsprocedure en gekarakteriseerd met behulp van UV/vis-spectroscopie, thermogravimetrische analyse, ^{1}H-NMR-spectroscopie en electrontransmissiemicroscopie. Met behulp van de laatstgenoemde techniek zijn niet-geaggregeerde deeltjes aangetoond met een relatief smalle deeltjesgrootteverdeling van 2.8 ± 0.6 nm. De aggregatiesnelheid van de CD-Au-NPs met de gastmoleculen kan worden gestuurd door middel van het variëren van een aantal parameters zoals het aantal beschikbare interacties voor assemblage, de geometrie van de moleculen en het toevoegen van een competitief agens in oplossing om aggregatie te voorkomen. Adamantyl-getermineerde dendrimeren geven, als gevolg van hun bolvorm en het grote aantal interacties, onoplosbare aggregaten van nanodeeltjes zonder lange-afstandsordening, hetgeen een sterke aanwijzing is voor *intermoleculaire* binding. Daarentegen vormt een bis-adamantyl-molecuul met twee interactieplaatsen en een flexibele linker geen onoplosbaar complex, hetgeen kan worden toegeschreven aan overwegend *intramoleculaire* binding. Toevoeging van het monovalente adamantylcarboxylaat aan een oplossing van CD-Au-NPs veroorzaakt geen neerslag en resulteert in stabiele assemblages. De bindingsconstante (2.31×10^4 M^{-1}) is vastgesteld door middel van isothermische microcalorimetrische titraties (ITC). In tegenstelling tot de experimenten waarbij gebruik gemaakt werd van CD-Au-NPs, leidde de toevoeging van adamantyl-getermineerde dendrimeren aan een oplossing van oligo(ethyleenglycol)-gefunctionaliseerde goud-nanodeeltjes niet tot neerslag noch tot veranderingen in de plasmon-absorptieband. Verder kan door toevoeging van een monovalent competitief agens in oplossing het aggregatieproces van het bis-adamantyl-gastmolecuul worden gestuurd.

Hoofdstuk 5 beschrijft een nieuwe supramoleculaire procedure voor de stapsgewijze constructie van een nieuw soort zelfgeassembleerde organische/anorganische multilagen. De procedure is gebaseerd op laagsgewijze assemblage van gast-gefunctionaliseerde dendrimeren en CD-Au-NPs die zijn gedeponeerd op CD-SAMs op goud of op siliciumoxide. Het is aangetoond dat dit soort supramoleculaire laagsgewijze assemblage dunne multilagen geeft waarvan de dikte op

nm-schaal gestuurd kan worden. Verscheidene technieken zijn gebruikt om de assemblage te bestuderen. Oppervlakte-plasmonresonantie-spectroscopie (SPR) is gebruikt om *in situ* de laagsgewijze assemblage te bestuderen bij verschillende concentraties van de componenten. Het adsorptiegedrag was vergelijkbaar in het bereik van de gebruikte concentraties, en vertoonde een lineaire verloop van de laagdikte als functie van het aantal bilagen die zijn gedeponeerd op de CD-SAMs. Blanco-experimenten in de afwezigheid van de receptormoleculen in de monolagen of van de gastmoleculen vertoonden geen specifieke of controleerbare laagsgewijze assemblage. Informatie over de toename van de absolute dikte als functie van het aantal bilagen is verkregen met behulp van ellipsometrie en AFM. In beide gevallen is bij benadering een multilaagdikte van 2 nm per bilaag verkregen. Verder was het mogelijk de supramoleculaire assemblage op een glasoppervlakte te bestuderen met UV/vis-spectroscopie. De lineaire toename van de absorptie bij 525 nm als functie van het aantal bilagen (voor 1-18 bilagen) was wederom een sterke indicatie voor een nauwkeurig depositieproces. Bovendien geeft UV/vis-spectroscopie, wanneer een hexagonale pakking van monodisperse deeltjes wordt aangenomen, een goede schatting van de hoeveelheid materiaal die gedeponeerd wordt na iedere cyclus. Vergelijking tussen de experimentele en theoretische waarden gaf duidelijk aan dat bij benadering een monolaag van CD-Au-NPs is gedeponeerd na iedere assemblage-cyclus.

Hoofdstuk 6 introduceert verscheidene strategieën om patronen te maken met het doel hybride 3D-nanostructuren van dendrimeren en CD-Au-NPs op CD-SAMs te verkrijgen die gebaseerd zijn op meervoudige supramoleculaire interacties waarbij gebruik gemaakt wordt van het laagsgewijze assemblageproces zoals beschreven in Hoofdstuk 5. Aanvankelijk is gebruik gemaakt van μCP en nanoimprint-lithografie (NIL), en vervolgens van het opdampen van metaal en *lift-off* om chemisch gepatroneerde SAMs te verkrijgen om zo te proberen de laagsgewijze assemblage te sturen, welke dan afhankelijk is van de supramoleculaire specificiteit. Deze twee methoden resulteerden echter niet in gepatroneerde laagsgewijze assemblage maar in een willekeurige multilaag-depositie die wordt toegeschreven aan niet-specifieke adsorptie van de dendrimeren. Daarentegen was het mogelijk gepatroneerde multilagen op de CD-SAMs te verkrijgen met behulp van *nanotransfer printing* (nTP) en NIL. nTP was

mogelijk door laagsgewijze assemblage op een geoxideerde PDMS-stempel gevolgd door overdracht op een volledige CD SAM. De structuren vertoonden een goede stabiliteit tegen wasprocedures, zelfs wanneer gebruik werd gemaakt van een monovalente competitieve receptor in oplossing of van een aceton/ultrasoon-behandeling. nTP-gepatroneerde multilagen vertoonde een lineaire toename van de laagdikte van ongeveer 3 nm per bilaag. De niet optimale supramoleculaire specificiteit die werd waargenomen kon wederom worden toegekend aan niet-specifieke interacties van de dendrimeren. Verder zijn multilagen, gepatroneerd met behulp van NIL, laagsgewijze assemblage en *lift-off*, verkregen door gebruik te maken van NIL-gepatroneerd PMMA als een fysieke barrière voor multilaagdepositie. De aldus gepatroneerde multilagen vertonen een lineaire toename van de dikte van, in dit geval, slechts 1.1 nm per bilaag. Deze verschillen in de multilaaghoogten als een functie van het aantal bilagen kan mogelijk worden verklaard door bevochtigingsproblemen. Desalniettemin zijn hoge-resolutie-3D-nanostructuren met hoogte-breedte-verhoudingen in de ordegrootte van 1 verkregen door middel van het combineren van laagsgewijze assemblage en NIL.

Hoofdstuk 7 introduceert een nieuw concept voor het vervaardigen van structuren op nanoschaal waarbij multivalente heterotrope orthogonale interacties betrokken zijn. Het is aangetoond dat de binding van een metaal-ligand-complex (gast), gevormd tussen adamantyl-gefunctionaliseerd ethyleendiamine (L) en Cu(II) of Ni(II), aan CD-SAMs plaats vindt door middel van multivalente binding door de gastmoleculen. Om de orthogonaliteit van de metaal-ethyleendiamine- en CD-adamantyl-bindingsmotieven na te gaan zijn bindingsstudies verricht met L in waterige oplossingen - met en zonder Cu(II), en bij verschillende pH-waarden - met behulp van ITC. De bindingsconstanten verkregen in aanwezigheid ($K = 7.9 \times 10^4$ M^{-1}) en afwezigheid ($K = 6.0 \times 10^4$ M^{-1}) van Cu(II) waren kenmerkend voor een 1:1 CD-adamantyl-interactie en vertoonden geen invloed van de pH op de complexering, hetgeen volledige orthogonaliteit bewijst. De bindingsconstanten met CD-SAMs zijn van dezelfde ordegrootte vergeleken met die gevonden in oplossing. Quantitatieve analyse van de verschillende deeltjes die aanwezig zijn in oplossing en aan het oppervlak is uitgevoerd als functie van de pH door gebruik te maken van een sequentieel, multivalent, heterotroop bindingsmodel. Bij hoge pH-waarden leidde de adsorptie van metaal-ligand-complex aan het oppervlak tot de vorming van het divalente

complex (CuL_2), terwijl bij pH 5 voornamelijk monovalente deeltjes aanwezig waren. Hetzelfde gedrag werd waargenomen in oplossing. Daarentegen versterkte de multivalentie van het oppervlak bij pH 6 de aanwezigheid van het divalente CuL_2-complex aan het grensvlak met een versterkingsfactor (*EF*) hoger dan 100, terwijl in oplossing voornamelijk monovalente deeltjes aanwezig waren. Dit gedrag wordt toegeschreven aan de hoge effectieve concentratie van CD-bindingsplaatsen die aanwezig zijn aan het oppervlak en de bijna optimale lengtes van de linkers tussen de beide adamantylgroepen ten opzichte van de periodiciteit van het CD-rooster (ca. 2 nm). In het geval van het Ni(II)-complex was het niet mogelijk een onderscheid te maken tussen divalente en trivalente binding. Desorptie-experimenten, uitgevoerd bij gelijke concentraties, vertoonden vergelijkbare desorptiesnelheden voor Ni(II) en Cu(II), hetgeen sterke aanwijzingen geeft voor divalente binding aan het oppervlak in beide gevallen. Quantitatieve analyse van de verschillende Ni(II)-complexen liet zien dat de divalente vorm nauwelijks aanwezig was in oplossing maar dat als gevolg van multivalentie de aanwezigheid van divalente deeltjes aan de oppervlakte wederom versterkt werd met *EF* > 100.

De resultaten die zijn weergegeven in dit proefschrift illustreren de veelzijdigheid van zelf-assemblage en multivalentie om 2D- en 3D-nanostructuren te maken en de toepassing van deze methoden voor het verkrijgen van meer complexe nanostructuren. Het werk aan de verschillende supramoleculaire structuren op vlakke oppervlakken en nanodeeltjes geeft aan dat verschillende nanoarchitecturen verkregen kunnen worden door het combineren van supramoleculaire specificiteit en stabiliteit van meervoudige interacties. De combinatie van lithografische technieken, zoals microcontact-printen en NIL, geeft nieuwe benaderingen voor het maken van supramoleculaire patronen op grensvlakken en voor het verkrijgen van goed-gedefinieerde 3D-nanostructuren.

Thanks

I belive that this “chapter” of this thesis is one of the most important. However, I have found these pages the most difficult ones to write because sometimes feelings are just too complex to express with simple words. During these four years many people have been next to me, both scientifically and personally, and now it is time to thank everybody to whom I owe a debt of gratitude.

First, I would like to express my gratitude and appreciation to my promotor Prof. David N. Reinhoudt. Thanks David for the opportunity you gave me to be part of this group, it has been a pleasure scientifically and also personally. I have really appreciated all the freedom you gave, trust and support during the whole PhD, and for being proud of what I have achieved. Bedankt voor alles David.

Prof. J. Huskens, my supervisor and promotor, there are not enough words of gratitude to thank you. You have been my absolute guide throughtout this whole thesis. I have always been impressed with your capacity of teaching and making things easy when they were not. Jurriaan, I just want to thank you for everything you have taught me, for all your patience and for the freedom you have given to me. It has been a pleasure for me having you first as supervisor and now as promotor. Van haarte bedankt Jurriaan!

I owe my gratitude to my other supervisor, Bart Jan Ravoo. Bart Jan, thanks for taking over part of my project and for having always time for me. You have given me lot of confidence, probably when I needed it the most. I really enjoyed our Dutch-Spanish lessons in the Sam Sam. Muchísimas gracias por las conversaciones de holandés-español; heel veel dank voor onze Nederlands/Spaans gesprekken.

My first trip to Enschede was as an Erasmus student. I would like to thank the group of Catalytic Processes and Materials: Prof. L. Lefferts, Dr. K. van Ommen, Dr. K. Seshan, Bert Geerdink, Karin Altena-Schildkamp, Marco Rip, Takeshi, Uli and Hycke.

During these four years I had the chance to collaborate with many people, the results of which are presented in this thesis. I owe my appreciation to Prof. Wolfgang Knoll and Fang Yu from the Max-Planck Institute for Polymer Research in Mainz, (Germany) for showing me how the SPR worked. I want to thank Mária Péter for her AFM contribution to Chapters 3 and 6 and for providing me with the AFM pictures when I asked for them. I would like to thank Christian Bruinink for introducing me in the world of microcontact printing and for his participation in Chapter 3. I thank Pascale Maury for her contribution to Chapter 6. Thanks as well to Steffen Onclin for showing me how to prepare cyclodextrin SAMs on silicon oxide. I would like to thank Christian Nijhuis (the dendrimer guy!) and Manon Ludden (thanks for all the advice about the SPR set-up). There are special words for some people that also helped me to achieve this thesis. Alart Mulder (Alarto) was always there for all the questions that I have asked, even if it was only a “small question”, van harte bedankt Alart!. Barbara Dordi was always willing to measure my samples, even if the results were not exactly like we really wanted; dendrimers stick everywhere! My appreciation also goes to Choon Woo Lim with whom I shared fruitful discussions over modeling and what was cooperativity or multivalency. Your help and advice during the last period of this thesis were essential, and the results are shown in Chapter 7. I am grateful to all my labmates from the lab 2906. Thank you all for providing me with a stimulating and pleasant environment and for all the nice moments we have shared.

I am deeply indebted to Amela Jukovič and Maria Karlsoon for their contributions on Chapter 4. Amela, your patience and hard work made Chapter 4 possible; Maria, it was nice having you as an Erasmus student!

Alart, Emiel and Tommaso, accepted to read and correct the concept thesis. Thank you for carefully checking and finding the “small” errors. I really appreciate your

constructive suggestions on this manuscipt. I hope that it was not too boring! Thanks Mattijs for translating the summary into samenvatting. Thanks also to Vincent and Manon for transforming the ideas about the cover into something real.

Thanks also to Marcel de Bruine for the technical support (always smiling even on Monday morning), Richard Egberink for the computer assistance (even with chocolate-computers), Tieme Stevens for the help provided in the analytical field, Izabel Katalanc and Marieke Slotman for the administrative work. Mark Smithers from the Analytical Material Laboratory of MESA$^+$ is also ascknowledged for his contribution on the TEM images.

During my PhD, I have had the opportunity to meet a lot of fantastic people, inside and outside SMCT. Special thanks to those who made these four years an unforgettable period for the rest of my life: Juanjo (y Floren), thanks for being there especially at the beginning, you have been an example to follow; Mattijs, always willing to help without asking anything back; Soco and Rob, my famous couple, thanks for the great dinners; Emiel and Monica, thanks for such wonderful moments; Barbara and Bas, unforgettable Beiaard times; Roberto, be careful with the double meanings in Spanish!; Marta, thanks for your Dutch translations; Francesca, la Corbe para los amigos!; Tommaso (and Jeanette) thanks for teaching me what a monolayer is and for a great time in Stockholm; Mónica and Marco, thanks for your help when I was an Erasmus student; Andrea, il mio studente di spagnolo; Irene, la mia amica romana favorita; Mercedes (Niels y el cacahuete!), I have really enjoyed being you, do you know what I mean?!; Deborah, grazie mille per venire alla mia promotion; Mirko, genio dello spagnolo; Henk and Marloes, my favourite Ducth couple, thanks for counting on us; Xing-Yi, the singer of the SMCT; Javier, gracias por soportarme durante dos años; Hans; Ruben; Menglin; Núria; Francesca; Roald; Kazu; Jessica; Paolo; Siggi; Aldrik; Laura; Charu; Francesca; Ana (Anita). Thank you all!

Part of these great moments I have shared with my girl-flatmates of Javastraat 173. I am deeply indebted to Lourdes Basabe, my best and unconditional friend during

these four years; always planning a hundred things at the same time! Thanks Lourdes for being my flatmate, my colleague and my friend. Rebecca Zimmerman, thanks for the long talks and wise advice, and for the Italian-Spanish discussions about olive oil! Itxaro Arratibel, a fast stay in Javastraat, sorry if I didn't make it too easy for you. Marina Gianotti with whom I have shared a lot of great moments in Javastraat. Marina, I am grateful for the year we had lived together.

Some people that day after day have been next to me, when I was laughing and when I was not, deserve special words. Muchísimas gracias Lourdes por haber estado siempre a mi lado, por los buenos y malos momentos que hemos compartido juntas, especialmente cuando mi humor no era el mejor; me alegro de ser tu amiga y espero seguir siéndolo. Fernando, mi madrileño favorito; gracias por hacerme reir y por darme apoyo cuando lo necesitaba. Gracias a los dos por ser mis paraninfs! Michel, siempre dispuesto a darte una mano; mis columnas tambien te dan las gracias! Marina, creo que mi vocabulario se ha expandido hacia la parte de las Americas! Gracias por haberme escuchado siempre.

A mis amigos a 1500 km de distancia: Javi (gracias por venir), Maria, Laura, Belén, Palmira (i a totes les altres encara que només ens veiéssim als matrimonis, ara haurem d'esperar fins al meu!), Carlos, Juan, Ferran, Jose, Escuder y Raúl, gracias a todos por haber estado siempre disponible cuando me dejaba ver por Sabadell y San Esteban, gracias por continuar la amistad.

Muchísimas gracias Tata por haber hecho el esfuerzo de venir a mi promotion así como en tantas otras ocasiones. Soy muy afortunada de tenerte como prima. Te quiero mucho.

Mamá, papá y Natalia, muchísimas gracias por lo que habeis hecho y todavía continuais haciendo por mí sin esperar nada a cambio. Gracias por haberme apoyado siempre en todas mis decisiones incluso cuando decidí marcharme a Holanda, mamá se que para tí no fue fácil. Estoy convencida de que sin vuestra incondicional ayuda todo esto hubiera sido mucho más difícil. Espero que esteis orgullosos de mi tanto como yo lo

estoy de vosotros. Os echo mucho de menos. Os quiero. Moltes gràcies David per venir a la meva promotion i per cuidar de la meva germana.

Alessio, mia anima gemella. Grazie per essermi stato sempre vicino condividendo gioie e dolori, per avermi sostenuta nei momenti difficili, per esserti preso cura di me con tanta dolcezza e per farmi sentire sempre cosí speciale. Tu mi hai insegnato ad apprezzare le cose e a vedere la vita con occhi diversi, mostrandome sempre il lato positivo de ogni cosa. Sono felice di poter condividere la mia vita con una persona come te. TQ.

Olga Crespo Biel

About the Author

Olga Crespo Biel was born on 14th February 1978 in Sabadell (Spain). She studied chemistry at the Universitat Autònoma de Barcelona (Spain) from 1996 until 2001. From October 2000 to March 2001 she obtained an Erasmus Grant and she joined the group of Catalytic Processes and Materials (CPM) at the University of Twente, where she worked under the supervision of Prof. L. Lefferts and Dr. J. van Ommen on the preparation of carbon nanotubes for catalyst support. In November 2001 she returned to the University of Twente and joined the Supramolecular Chemistry and Technology group directed by Prof. D. N. Reinhoudt, where she worked as a PhD student under the supervision of Prof. J. Huskens and Dr. B. J. Ravoo. The results of this research are described in this thesis. From January 2006 she is working as a postdoctoral researcher in department of Performance Materials Chemistry and Technology at DSM Research (Geleen, The Netherlands).